

COASTAL EVOLUTION OVER THE PAST 3000 YEARS AT CONRADS
BEACH, NOVA SCOTIA, CANADA: UNDERSTANDING THE DYNAMICS OF
TRANSGRESSIVE COASTS

by

Tanya C. Forde

Submitted in partial fulfilment of the requirements
for the degree of Master of Science

at

Dalhousie University
Halifax, Nova Scotia
June 2014

© Copyright by Tanya C. Forde, 2014

To my family: Winston, Leah, Jason, Laurie, and Granddad. Thank your for supporting all of my dreams and pursuits... no matter how far and how long they take me away from you.

TABLE OF CONTENTS

LIST OF TABLES	vi
LIST OF FIGURES	vii
ABSTRACT	ix
LIST OF ABBREVIATIONS USED	x
ACKNOWLEDGEMENTS	xi
CHAPTER 1: INTRODUCTION	1
1.1 Objectives	2
1.2 Organization of Thesis	3
1.3 Contributions of Author	3
CHAPTER 2: BACKGROUND	5
2.1 Geologic Setting	5
2.2 Coastal Evolution	6
2.2.1 Barriers	6
2.2.2 Beach ridges	10
2.2.3 Coastal sand dunes	12
2.3 Transgression	14
2.4 Regression	15
2.5 Landward Migration of Coastal Systems	16
2.5.1 Northeast Graham Island, British Columbia	16
2.6 Seaward Migration of Coastal Systems	18
2.6.1 On Transgressive Shorelines	18
2.6.1.1 <i>Bouctouche Spit, New Brunswick</i>	18
2.6.1.2 <i>North Padre Island, Gulf of Mexico, Texas</i>	19
2.6.2 On Regressive Shorelines	20
2.7 Coastal Sensitivity	21
2.8 Consequences of Sea-level Rise	25

CHAPTER 3: COASTAL EVOLUTION OVER THE PAST 3000 YEARS AT CONRADS BEACH, NOVA SCOTIA, CANADA: THE INFLUENCE OF LOCAL SEDIMENT SUPPLY ON A TRANSGRESSIVE SYSTEM.....	27
3.1 Abstract	27
3.2 Introduction	28
3.3 Field site and Geological Background	31
3.4 Methods and Data	35
3.4.1 Global Positioning Systems	35
3.4.2 Ground-penetrating Radar, Beach Profiles and LiDAR	36
3.4.3 Seismic Refraction	38
3.4.4 Vibracoring	40
3.4.5 Grain-size Analysis	41
3.4.6 Radiocarbon Dating	43
3.4.7 Aerial Photographs, Satellite Photographs, Maps and LiDAR	43
3.5 Results	44
3.5.1 GPR and Seismic Results	44
3.5.2 Core Results	51
3.5.2.1 <i>Lithofacies Results</i>	51
3.5.2.2 <i>Grain-size Analysis Results</i>	56
3.5.3 Radiocarbon Dating Results	59
3.5.4 Historical Evidence for Geomorphological Change	62
3.5.4.1 <i>Photographs, Maps and LiDAR</i>	62
3.5.4.2 <i>Beach Profiles</i>	67
3.6 Discussion.....	71
3.7 Conclusions	79
3.8 Acknowledgments	80
CHAPTER 4: DISCUSSION	82
4.1 Comparison to Other Sites in Atlantic Canada	82
4.1.1 Carters Beach, NS	84
4.1.2 Pomquet Beach, NS	87

4.1.3 Point Deroche Beach, PEI	89
4.1.4 Brackely Beach, PEI	92
4.1.5 Greenwich Beach, PEI	93
4.1.6 Reconnaissance Beach Summary	95
4.2 Future work	97
CHAPTER 5: CONCLUSIONS	99
REFERENCES	103
APPENDIX 1: GPR and GPS methodology.....	117
APPENDIX 2: Vibracore Log Sheets	125
APPENDIX 3: GRADISTAT Grain-size Analysis Statistics	164
APPENDIX 4: Beta Analytic Inc. Radiocarbon Dating Report	187

LIST OF TABLES

Table 2.1 Ranking of coastal Sensitivity Index values.....	24
Table 3.1 Photograph and map sources.....	45
Table 3.2 Refraction seismic results	51
Table 3.3 Facies characteristics	53
Table 3.4 Radiocarbon dating results.....	61
Table 3.5 Natural and anthropogenic events affecting Conrads Beach.....	63
Table 4.1 Study site environments.	83
Table 4.2 Features of coastal dune study sites	84

LIST OF FIGURES

Figure 2.1 Regional bedrock geology and study site	5
Figure 2.2 Global distribution of wide beach ridges, coastal dunes and extensive barrier islands	6
Figure 2.3 Barrier systems.	7
Figure 2.4 Lawrencetown Beach.....	11
Figure 2.5 Transgression versus regression	15
Figure 2.6 Northeast Graham Island, British Columbia	17
Figure 2.7 Bouctouche Spit, New Brunswick.....	19
Figure 2.8 Padre Island, Gulf of Mexico, Texas.....	20
Figure 2.9 North coast of Rio Grande do Norte, northeastern Brazil.	22
Figure 2.10 Study site and the coastal Sensitivity Index.....	23
Figure 2.11 Barrier genesis, destruction, and re-establishment in response to..... rising relative sea-levels on the paraglacial coast of Nova Scotia	26
Figure 3.1 Study area, geomorphic setting and field sites	32
Figure 3.2 Examples of Conrads Beach radargrams and facies acquired using 100 MHz antenna.	49
Figure 3.3 Radargrams (30 m wide by 5 m deep) showing detailed structure..... associated with dated cores	50
Figure 3.4 Facies distribution and sediment types for Conrads Beach vibracores	54
Figure 3.5 Dated vibracores and associated radargrams	55
Figure 3.6 Comparison of grain-size date (Phi [negative log ₂] scale) to Friedman's (1961) partitions.....	58

Figure 3.7 Topographic changes at Conrads Beach since 1779.	64
Figure 3.8 Conrads Beach seaward limit of vegetation	67
Figure 3.9 Selected profiles along three Conrads Beach transects.....	70
Figure 3.10 Comparison of results to Scott et al. (1995)	78
Figure 4.1 Sensitivity Index and locations of additional study sites	82
Figure 4.2 Carters Beach reconnaissance GPR/GPS lines and sample	
radargrams	86
Figure 4.3 Pomquet Beach reconnaissance GPR/GPS lines and sample	
radargram.....	88
Figure 4.4 Point Deroche Beach reconnaissance GPR/GPS lines and sample	
radargrams	90
Figure 4.5 Brackley Beach reconnaissance GPR/GPS lines and sample	
radargram.....	93
Figure 4.6 Greenwich Beach reconnaissance GPR/GPS lines and sample	
radargrams	96

ABSTRACT

Although many modern coastlines are retreating as a result of global sea-level rise, periods of stability and progradation may result from time-varying sediment supply. In formerly glaciated regions, where sediment is derived primarily from finite glaciogenic sources, sediment input may support progradation for a time, but decline when the source deposit becomes exhausted. For Conrads Beach on the Atlantic coast of Nova Scotia, georectified maps based on aerial photographs, satellite photographs, maps and LiDAR data, coupled with beach profiles and historic records, show that the shoreline has retreated overall during the past ~230 years. The western and eastern shorelines have also experienced stasis and progradation, respectively, over intervals of years to decades, as well as rapid erosion and accretion over periods of days to months, largely as a result of powerful storms. In the 1960s, a tidal inlet formed and filled within a few decades, migrating ~60 m laterally during this time.

To investigate timescales of centuries to millennia, ground-penetrating radar profiles which imaged to depths of 6-8 m were linked to 13 vibracores that penetrated up to 4.2 m, and supplemented by refraction seismic data to 23.5 m depth. Grain-size parameters were used to support facies identification for sand samples. An age profile based on radiocarbon dating suggests that the area was open-marine or littoral at about 2800 calendar years BP. Locally increased sediment supply caused rapid buildup and progradation of beach ridges along the eastern beach from ~600-150 years BP. Landward of the beach-ridge area, cores from a lagoon and marsh connected to the ocean by tidal inlets yield dates that correspond to the period of beach-ridge formation. As the coast retreated, erosion of drumlins provided large sediment pulses over a period of centuries, temporarily building out the coast and creating a lagoon. The results support previous models for the Atlantic coast of short-term progradation in response to intermittent sediment supply from discrete sources, superimposed on prevailing coastal retreat. Conrads Beach may serve as a model for the behaviour of other high-sensitivity coasts with local sediment sources.

To test the Conrads Beach model, comparably detailed studies at other sites would be required. To check whether such studies are feasible, reconnaissance ground-penetrating radar/global positioning system data were collected at five additional Atlantic Canada study sites. These sites represent three distinctive environments of coastal evolution (Atlantic Ocean, Northumberland Strait and Gulf of St. Lawrence) located in areas of both moderate and high coastal sensitivity. Radargram facies similar to Conrads Beach were identified, study site features were compared and sediment sources evaluated. Aerial photographs, satellite photographs, maps and LiDAR were also located for some of these sites. The abundance of aerial/map data and encouraging preliminary ground-penetrating radar results suggest that the Conrads Beach model could be tested at those locations.

LIST OF ABBREVIATIONS USED

°C	Degrees Celsius
¹⁴ C	Carbon 14
3D	Three-dimensional
BP	Before Present
CGVD28	Canadian Geodetic Vertical Datum of 1928
CVI	Coastal Vulnerability Index
CMP	Common mid-point
DEM	Digital Elevation Model
E	East
Fig.	Figure
g	Grams
GPR	Ground-Penetrating Radar
GPS	Global Positioning System
GSC	Geological Survey of Canada
HHWLT	Higher High Water at Large Tide
LiDAR	Light Detection And Ranging
m	Metre
mm	Millimetre
MHz	Megahertz
MSL	Mean Sea Level
MTL	Mean Tide Level
NAD83	North American Datum 1983
nm/s	Nanometer per second
N	North
NE	Northeast
NS	Nova Scotia
NW	Northwest
PEI	Prince Edward Island
RSL	Relative Sea-Level
SE	Southeast
SI	Sensitivity Index
SW	Southwest
USA	United States of America
μ	Micron
W	West
WGS-84	World Geodectic System 1984

ACKNOWLEDGEMENTS

This work would not have been possible without the contributions from a wide range of people. Thank you to my co-supervisors Dr. Martin R. Gibling and Dr. Mladen R. Nedimović for finding the perfect project for me to work on and providing support and encouragement when needed. Thank you thesis committee member Dr. Donald L. Forbes for your invaluable insights. Thank you former thesis committee member Dr. Daniel J. Utting for insight into the bigger picture and providing Pomquet Beach LiDAR data. Thanks to 2010 ground penetrating radar/global positioning systems field assistants Darragh O'Connor and Peter Regan; the Earth Sciences 2270 (Introduction to Applied Geophysics) classes of 2007, 2010, 2011, 2012 and 2013; and the 2012 and 2013 field assistants Aaron Farkas (vibracoring), Darragh O'Connor (vibracoring), Fred Walsh (vibracoring and common midpoint gathers), Bertha Louis (vibracoring), Kyle Landry (vibracoring), Harold Kuehn (vibracoring and common midpoint gathers, and John Evangelatos (common midpoint gathers). Without your assistance, I wouldn't have such a large quantity of high quality data. Thanks to nearby landowners Mr. and Mrs. Welch and Mr. Hood for your cooperation during Conrads Beach data acquisition. Thank you John Thibodeau for providing both field work and technical assistance for the ground penetrating radar/global position systems and vibracoring and for data analysis and visualization assistance. I know you spent a lot of time to make the 2011 data the best it could be. Thank you Thomas Duffett for technical assistance and field work during the ground penetrating radar / global positioning systems, vibracoring and grain-size analysis phases. Mr. Bob Taylor and Mr. Dave Frobel... thank you for sharing your wealth of information regarding Conrads Beach. Mr. Owen Brown... thank you for providing technical assistance regarding grain-size analysis. Dr. Phillip MacAulay... thank you for the assistance with sea-level conversions.

CHAPTER 1: INTRODUCTION

Conrads Beach is a coastal barrier system along Nova Scotia's Atlantic shoreline and faces dramatic changes due to rising sea levels. Such coastal systems, which include barriers, beaches, beach ridges, dunes, tidal channels and lagoons, are dynamic natural environments, the longevity of which may range from a few short years to centuries or millennia. They protect inland areas from high-water events (Trenhaile 1997), are critical for maintaining biodiversity and organism habitats (Defeo et al. 2009), and store water in their aquifers (Defeo et al. 2009). Large coastal areas will be affected by changing barrier and related ecosystems and these areas must be managed to maintain their health. Conrads Beach includes a variety of landforms, is along a shoreline which is highly sensitive to geomorphological change resulting from sea-level rise and is near to an area with a high-resolution sea-level record. The Boyd et al. (1987) model for coastal barrier evolution in response to rising relative sea-level was tested. Ground penetrating radar (GPR) and refraction seismic surveys can be used to image the internal structure of coastal sediments. Combining these data with vibracores provides insight into sediment history with radiocarbon dating suggesting the timeframe, and grain-size analysis suggesting the quantity and quality of sediment. Examination of aerial photographs, satellite photographs, maps, light detection and ranging (LiDAR) data, topographic data and historical archives suggests changing coastal geomorphology. Understanding coastal evolution will provide insight into how these important systems may change in the future.

1.1 Objectives

Several short-term goals (to be completed within the scope of the M.Sc.) have been identified for the study at Conrads Beach:

1) Determine the geometry and spatial relations of radar facies to assess evidence for patterns of coastal development and migration in relation to other aspects of the barrier system and overall transgression or regression.

a) Use GPR surveying to identify erosional surfaces and depositional units in the stratigraphic record and conduct radar-facies analysis for the study site.

b) Characterize the composition of radar facies using sedimentological data from vibracores.

2) Document the evolution of coastal geomorphic elements over time and identify major changes at the study site.

a) Conduct radiocarbon dating (if suitable samples are obtained) to link erosional surfaces and depositional units to events in coastal development.

b) Create a timeline for coastal evolution by integrating the GPR data with archival information and radiocarbon data.

c) Compare the timeline with known weather and other historical events that affected the coastal area.

1.2 Organization of Thesis

Chapter 2 provides the necessary geologic background information regarding the development and migration of coastal components, transgression, regression, coastal sensitivity and the effects of sea-level rise. The manuscript entitled “Coastal Evolution Over the Past 3000 Years at Conrads Beach, Nova Scotia, Canada: The Influence of Local Sediment Supply on a Transgressive System” by Forde, Nedimović, Gibling and Forbes forms the body of the thesis and is presented as Chapter 3. It will be submitted to *Estuarine, Coastal and Shelf Science* and provides a comprehensive account of Conrads Beach evolution during the past 3000 years. Chapter 4 is a broader discussion of the results, considering other open-ended questions. Chapter 5 presents the conclusions of this thesis. Appendix 1 describes GPR and global positioning system (GPS) methodology, and Appendices 2 and 3 contain the hand-written vibracore log sheets and grain-size analysis sample statistics, respectively.

1.3 Contributions of Author

This study is the result of six field seasons (spring/summer 2007, 2010, 2011 and 2012, fall 2012 and spring/summer 2013). During the first field season the undergraduate students of EARTH 2270 (Introduction to Applied Geophysics) acquired refraction seismic data. Ground penetrating radar data were acquired during the second field season. The author began her study in May 2010. Subsequently the author and two field assistants (D. O'Connor and P. Regan) spent six weeks (May 26-July 3, 2010) acquiring GPR data at Conrads Beach,

Carters Beach, Pomquet Beach, Point Deroche Beach, Brackley Beach and Greenwich Beach. Dr. M. Nedivmović provided supervision and assistance during this field season. After a decision was taken to restrict the study to Conrads Beach, the primary focus of the third field season (April 2011) was to acquire a GPR data grid in the vicinity of a buried channel fill at Conrads Beach. Dr. M. Nedivmović supervised the ERTH 2270 field assistants during two days of data acquisition. The author supervised the ERTH 2270 field assistants during the fourth season (April 2012). Additional GPR data were acquired to fill gaps in the previous years' data acquisition. Vibracore data were collected at Conrads Beach during the fifth field season (Oct 2012). The author directed the field crews during four days of data acquisition. T. Duffet provided technical support and Dr. M. Gibling supervised. The final field season (spring/summer 2013) was used to acquire GPR common-midpoint data. The author directed the ERTH 2270 field crew for three days in April and the graduate student field crew for an additional three days in May. J. Thibodeau provided in-field GPS support during all five field seasons. He also corrected the 2011 GPS data by interpolating missing values. All subsequent GPR/GPS data processing and interpretation, vibracore core logging, grain-size analysis, and manuscript preparation were performed by the author. T. Duffet and O. Brown provided advice during grain-size analysis. Dr. M.R. Gibling, Dr. M. Nedivmović and Dr. D. Forbes provided advice and editing.

CHAPTER 2: BACKGROUND

2.1 Geologic Setting

Conrads Beach is located 25 km east of Halifax, Nova Scotia (NS), in the Meguma Terrane (Fig. 2.1). Here the bedrock is Halifax Formation and Goldenville Formation of Cambrian to Early Ordovician age (White 2002). A key event in the Quaternary history of the area was the Wisconsinan glaciation during which, at the glacial maximum, sea-level was 110-120 m lower than present mean sea-level (Stea et al. 1994). During parts of the glacial history, Hartlen Till and then Lawrencetown Till were deposited on the bedrock (Stea et al. 1998). These till deposits survive as drumlins up to 30 m thick located west, north and east of Conrads Beach and as a locally present till veneer less than 5 m thick (Utting 2011). The modern and sub-modern sediments at Conrads Beach are marine littoral in nature, with an estimated thickness of 1-5 m (Utting 2011).

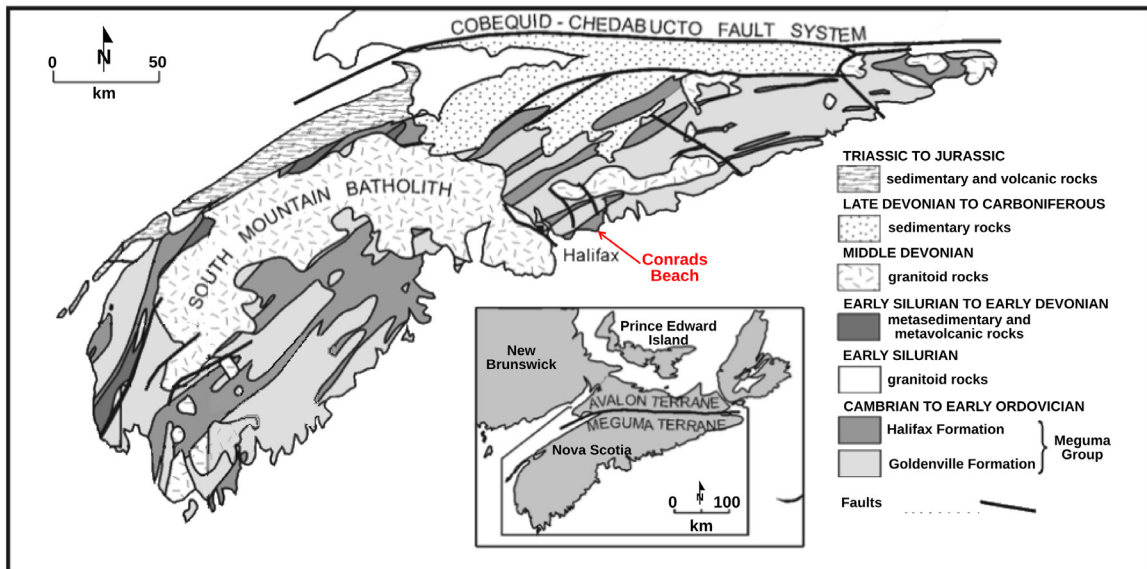


Figure 2.1. Regional bedrock geology and study site. Adapted from White (2002).

2.2 Coastal Evolution

2.2.1 Barriers

Conrads Beach is a coastal barrier system. Barriers are depositional landforms separated from the mainland coast by lagoons, bays and/or marshes (Trenhaile 1997; Davidson-Arnott 2010). They make up more than 10% of the world's coastlines (Davidson-Arnott 2010) and are distributed globally with extensive systems located in North and South America, Europe, Asia and Africa (Fig. 2.2). Many coastal barriers are the result of shoreward sweeping of beach sediments during and since the Late Quaternary marine transgression (Bird 2000).

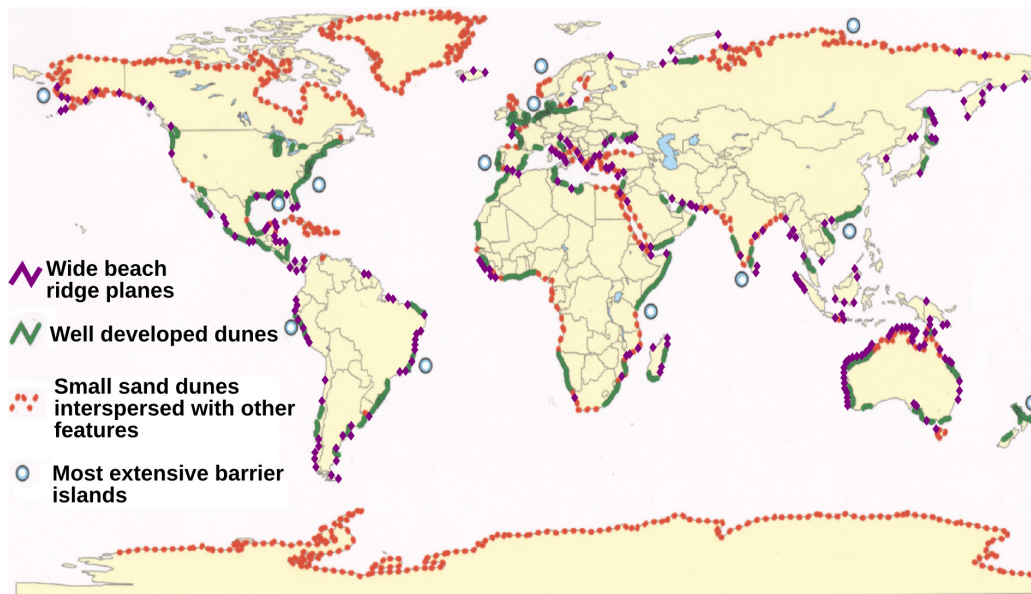


Figure 2.2 Global distribution of wide beach ridge plains, coastal dunes and extensive barrier islands. Adapted from Martinez et al. (2008) and Scheffers et al. (2011).

Most barriers share the following six components: 1) the mainland coast,

2) the lagoon, 3) the subaerial barrier including the beach, dune and backbarrier deposits, 4) the subaqueous sediment platform, 5) the shoreface extending offshore from the exposed beach and 6) inlets and tidal deltas (Davidson-Arnott 2010). Variations in barrier morphology are the result of the interactions between the basic environmental controls of sediment supply, relative sea-level change, terrestrial basement settings and wave climate (Orford et al. 1996). Barriers may be classified according to how many free ends they have (Fig. 2.3).

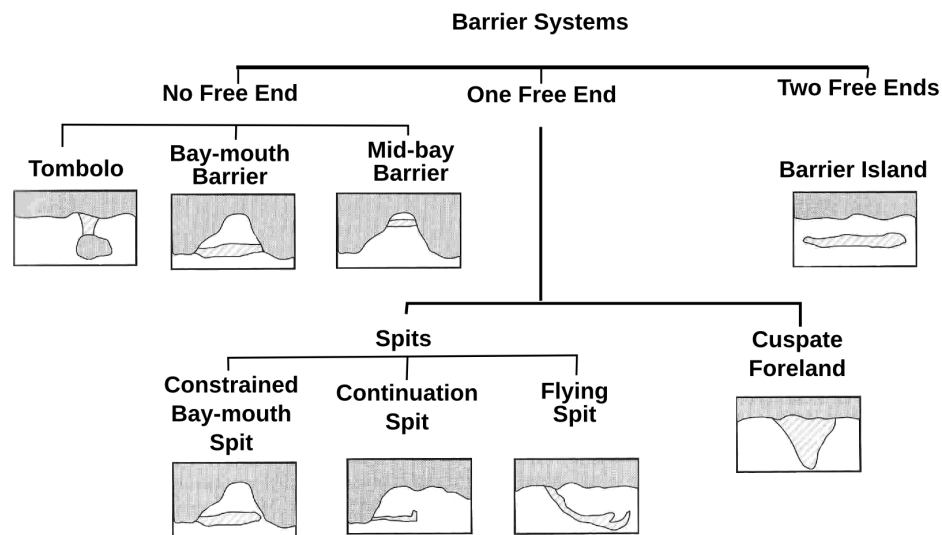


Figure 2.3 Barrier systems. Adapted from Davidson-Arnott 2010.

Tombolos develop on the lee sides of islands where wave refraction and diffraction cause longshore currents to converge (Trenhaile 1997; Davidson-Arnott 2010). This results in sediment deposition and may occur under conditions of relative sea-level rise, fall or stability (Trenhaile 1997). One of the key factors that determines tombolo evolution and direction of growth is the sediment source (the island, the mainland or a combination of the two) (Trenhaile

1997). Bay-mouth barriers and mid-bay barriers form at the entrance, or along the sides of, a bay respectively, and are the result of littoral sediment transport (Davidson-Arnott 2010). Littoral transport may be from one or both ends of the barrier.

Barrier spits develop where sediment moving alongshore is deposited at the mouth of estuaries and other places where there is an abrupt change in the direction of the coast (Trenhaile 1997). While barriers tend to develop on coasts with a small tidal range, barrier islands form where the tidal range generates strong ebb and flow currents which maintain gaps between them, thereby preventing wave action from depositing sand or shingle to seal the intervening inlets (Bird 2000). Cuspate forelands develop either where longshore transport is mainly from one direction or is from two opposite directions, or where coastlines are reoriented to face the dominant waves (Trenhaile 1997).

Barrier islands enclose estuaries, embayments or narrow lagoons, which are connected to the open sea by channels or tidal inlets between islands (Trenhaile 1997). They also consist of long, narrow sand bodies that separate offshore muddy sediments from lagoonal muddy sediments (Reinson 1992).

There are three main hypotheses for the origin of barrier islands: 1) the aggradation and emergence of submarine bars, 2) spit progradation parallel to the coast and segmentation of the spit by channels, and 3) isolation of beach and beach-dune complexes due to coastal submergence (Hoyt 1967; Reinson 1992). The controversy remains largely unresolved because most of the evidence pertaining to their origin has usually been destroyed by subsequent modification

(Hoyt 1967; Reinson 1992).

Barrier island chains contain three main geomorphological elements: sandy barrier islands, the enclosed lagoon or estuaries behind the barriers and the tidal channels that cut through the barriers, and connect the lagoons to the open sea (Reinson 1992). Each of these environments is made up of a number of subenvironments which in turn are characterized by distinct lithofacies (Reinson 1992). Barrier beach, channel and delta environments result in sand and gravel facies whereas the lagoon environment produces mud and sand deposits, and tidal channels and tidal deltas produce sand bodies that are oriented perpendicular or oblique to the barrier complex (Reinson 1992).

Barriers may also be classified according to their alignment. Swash-aligned barriers are parallel to the crest of the incoming waves and form where there is no net longshore transport (Trenhaile 1997). Drift-aligned barriers result when a significant amount of sediment is transported by longshore currents and deposited alongshore (Trenhaile 1997). Drift-aligned barriers are maintained when the sediment supply persists and may be transformed into swash-aligned barriers if the sediment supply decreases and/or the wave conditions change (Trenhaile 1997).

Microtidal barrier islands tend to be long and narrow, with abundant storm overwash features, well-developed tidal channels and associated tidal deltas (Reinson 1992). There are few channels, so storm surges tend to overtop the barrier forming extensive overwash conduits (Reinson 1992). In the case where tidal channels develop and then are abandoned, the vertical succession should

consist largely of mud which caps thin active channel sands, as opposed to the thicker channel sands that result from lateral barrier inlet migration (Reinson 1992)

Lawrencetown Lake (east of Conrads Beach) is a barrier beach anchored to two drumlin headlands (Boyd and Honig 1992). The marine littoral nature of Conrads Beach's modern sediments (Utting 2011) and the fact that it is anchored to the drumlin immediately to the west of the beach, suggest that this beach is a constrained bay-mouth spit.

2.2.2 Beach ridges

Conrads Beach includes beach ridges and dunes. The pattern of beach ridges and dunes can be used to decipher the history of barrier evolution (Bird 2000). Each beach ridge represents a previous shoreline with a series of beach ridges recording the evolutionary stages of an accretionary feature (Trenhaile 1997). Beach ridges are wave-formed deposits and commonly form during either high wave conditions and/or high water events on low energy beaches (Hesp et al. 2005). They can also be formed by the successive addition of spits that have grown parallel to the coast (Bird 2000). There are two requirements for the formation of beach ridges: a high rate of sediment supply and a low offshore gradient (Johnston et al. 2007). Beach ridges are primarily formed of sand and/or gravel and are swash-aligned (Hesp et al. 2005). They become beach ridges when they are separated from the active shoreline by progradation (Johnston et al. 2007). Their internal sedimentary structure consists of sigmoidal packages and they are usually located above the spring high-tide level (Hesp et

al. 2005). Beach ridge longevity depends upon overall progradation of the coastline and the separation of new beach ridges from older beach ridges by swales (Bird 2000).

The beach ridge system at nearby Lawrencetown Beach (Fig. 2.4) was initiated ~ 700 years BP and is the result of marine reworking of drumlin sediments during transgression (Hoskin 1983; Boyd and Honig 1992). Hoskin (1983) identified a submerged boulder retreat shoal midway between Lawrencetown Head and Half Island Point that was interpreted as the drumlin sediment source for beach ridge development (Fig. 2.4). The eastern portion of Conrads Beach (closest to Lawrencetown Beach) is also a beach ridge system and the nearby drumlins have provided a large sediment supply (Taylor et al. 1985) for their development.



Figure 2.4 Lawrencetown Beach (Google Maps 2014 CNES/SPOT, Digital Globe). (Red lines) Approximate locations of beach ridges identified by Boyd and Honig (1992). (White oval) Approximate location of boulder retreat shoal identified by Hoskin (1983).

2.2.3 Coastal Sand Dunes

On sandy beaches the formation of successive parallel beach ridges is often accompanied by the evolution of successive foredunes (Bird 2000). Coastal sand dunes and associated landforms protect inland areas from high water events (extreme waves and tides), and provide the sediment store that is used to replenish beaches during and after storms (Trenhaile 1997). Dunes can be found worldwide (Fig. 2.2) and are the result of aeolian transportation of marine sand from beaches to the backshore (Carter 1988). Saltation (particle movement by jumping or leaping) is the primary method of sand transport from the beach to the dunes (Carter 1988). Saltating particles travel tens of centimeters from the ground surface and the saltation cloud is rarely larger than 1-2 m in total height (Trenhaile 1997). A wind speed of 5 m/s is required to initiate saltation and wind speeds from 4-5 m/s are required to continue the process (Pethick 1984). Saltation moves sand grain from 0.2 mm to 2mm in diameter (Pethick 1984). Surface creep moves sand grains > 2 mm in diameter and suspension moves grains < 0.2 mm in diameter, but saltation is responsible for moving 75% of dune sand from the beaches (Pethick 1984, Trenhaile 1997).

Coastal sand dunes are most common on dissipative coasts with strong onshore winds and a large supply of sand-sized material (Carter 1988). In many cases they originated when sea-level was lower and/or sediment supply was at a maximum (Carter 1988).

Hesp (2002) identified primary factors (vegetation, wind velocity, erosion, overwash incidence, wind direction) that govern the initiation of dunes. An

obstacle (such as vegetation) in the path of a saltating cloud of grains will result in a decreased wind velocity and sand grain deposition around and/or downwind of the obstacle. This embryo dune has the potential to become a more permanent landform (Pethick 1984; Carter 1988). While saltating grains passing over a soft sandy surface lose energy (resulting in deposition of sand grains), the same grains passing over a hard pebbly surface gain energy (resulting in erosion of loose sand grains on the surface) (Pethick 1984). If an embryo dune grows parallel to the shoreline, it may form a ridge on the order of 2 m in height, which is known as a fore-dune (Pethick 1984). Together, the embryo dunes and fore-dunes constitute the primary dune system (Davidson-Arnott 2010).

The secondary dune system includes all dunes located inland from the primary dune system (Davidson-Arnott 2010). The morphological development of established dunes is influenced by sand supply, vegetation cover, rates of sand supply in conjunction with accretion and erosion, frequency and magnitude of wind and wave forces, frequency and magnitude of storms and overwash, long-term beach state, water levels, and human impact (Hesp 2002). The key to dune formation and shape is the balance between the depositional/erosional forces of saltation and the responsiveness of the transport rate to this balance (Pethick 1984). Between dune-building phases, an unbalanced state exists in which there are either periods of relative stability, during which soils are formed (Carter 1988, Trenhaile 1997), or periods of erosion. Impeded dunes are stabilized by their vegetation, but transgressive dunes lack vegetation and are much more mobile (Davidson-Arnott 2010). There is a continuum of secondary

dune types according to vegetation cover (Davidson-Arnott 2010).

Conrads Beach is on a dissipative coast with strong onshore winds year round (Phillips 1990), and the geomorphology of the western beach includes sand dunes. These well vegetated primary dunes are 1-2 m in height and are oriented roughly parallel to the western beach.

2.3 Transgression

Relative sea-level change is one of the key factors in determining coastal barrier geomorphology (Orford et al. 1996). Transgression is the long-term inundation of the land by the sea (Fig. 2.5 A,B). In Atlantic Canada, long-term tide-gauge records at Halifax, Nova Scotia (NS) show relative sea-level rise of 0.32 m/century over the past 100 years (Forbes et al. 2004, 2009). Relative sea-level rise results from a combination of subsidence and regional sea-level rise (McCulloch et al. 2002, Webster and Forbes 2005; Daigle 2006). Migration of the marginal forebulge associated with the last glaciation has resulted in ~ 10,000 years of coastal subsidence in Atlantic Canada (Quinlan and Beaumont 1981; Daigle 2006) and GPS measurements in Dartmouth, NS, show a subsidence rate of 0.16 ± 0.05 m / century (Forbes et al. 2009).

Transgressive coasts receive sediment from rivers that reach the coast and/or wave processes that erode pre-existing deposits as the coast moves landward (Boyd 2010). In the case of Conrads Beach, the Eel River-West Marsh system north of the beach area is a tidal channel complex.

In Nova Scotia, the transgressive nature of the shoreline is the driving force for barrier change (Orford et al. 1996). In transgressive settings there is a spectrum of depositional settings ranging from 1) barrier islands that protect lagoons with few rivers flowing into the lagoons, 2) more extensive lagoons with several drowned river mouths, and 3) funnel-shaped drowned river valleys with few or no barriers at the estuary mouth (Reinson 1992).

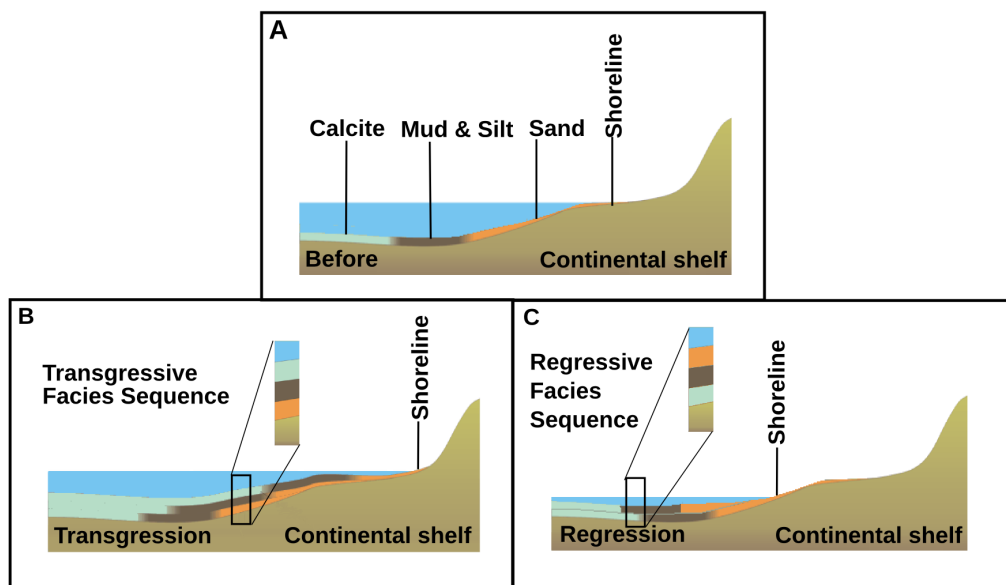


Figure 2.5 Transgression versus regression. (A) The shoreline at some initial condition. (B) Initial shoreline after transgression. (C) Initial shoreline after regression. Adapted from Harwood (2014).

2.4 Regression

Regression is the relative seaward motion of the shoreline (Fig 2.5 A, C) and also results from the dynamic interplay between coastal erosion/deposition and sea-level rise/fall (Boyd 2010). If the sediment supply is sufficiently large to build the shoreline seaward during times of sea-level rise, normal regression

occurs (Boyd 2010). In contrast, forced regression is the case where falling sea-level results in a seaward moving shoreline (Boyd 2010). A prograding shoreline results from regression; a normally prograded shoreline occurs during stationary or slowly rising sea-levels while a forced prograding shoreline results from falling sea-level (Lessa et al. 2000).

2.5 Landward Migration of Coastal Systems

Changing sea levels can cause coastal systems to migrate. Landward barrier migration has been observed in many parts of the world where the coastlines are transgressive (Dillenburg et al. 2006; Harvey 2006). Assuming a relatively stable initial state, an increase in mean sea level will initially cause erosion and redistribution of sediments (Dubois 1992; Costas et al. 2006). When a new equilibrium state has been reached, the overall result of the increased mean sea level is net landward migration (Dubois 1992, Costas et al. 2006). Walter's Law indicates that transgression results in shallow-water facies being overlain by deep-water facies (Dubois 1992) but, in a coastal setting, retreating barrier systems build up subaerial sediment accumulations.

2.5.1 Northeast Graham Island, British Columbia

Northeast Graham Island (Fig. 2.6) is located on the central coast of British Columbia which is highly sensitive to level change (Walker and Barrie 2004). Over the Holocene, sea level rose 166 m and the current sea level rise is 1.5 mm/year (Walker and Barrie 2004). The long-term trend of regional sea-level

rise suggests this shore is transgressive, so landward migration of the coastal system would be expected. The authors found the area had three distinct landscapes. The North Beach consists of prograding foredunes; Rose spit has reflective cusped cobble beaches with sandy low tide terraces; and East Beach has multiple barred beaches backed by migrating foredunes and parabolic dunes. The dissipative shores of North Beach are prograding at 0.3-0.6 m/year while the high energy East Beach is retreating by 1-3 m/year. Shoreline retreat at East Beach (the larger change) is the expected outcome of landward migration of a coastal system on a transgressive shore, but the sediment supply is sufficiently large for North Beach to prograde.

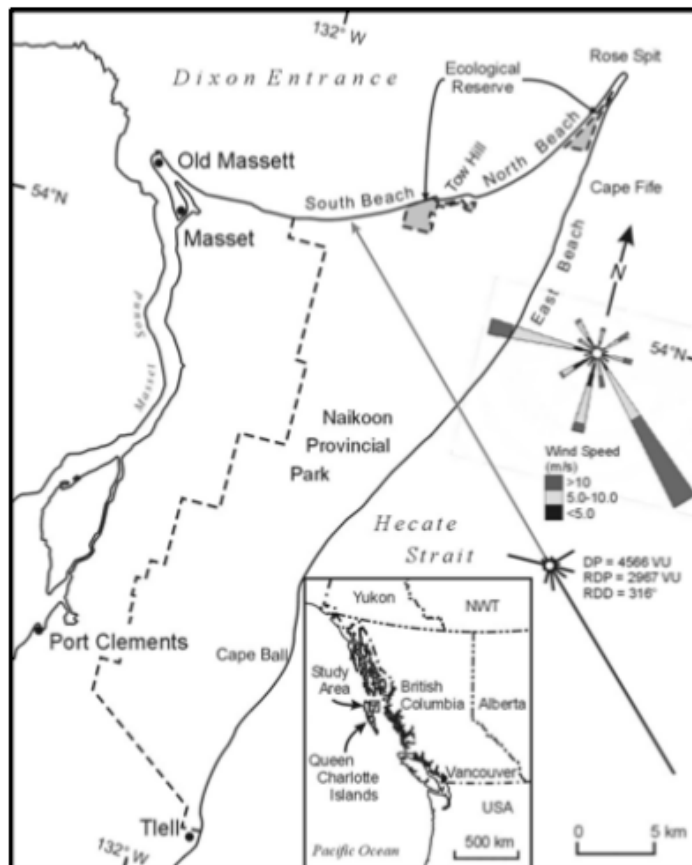


Figure 2.6 Northeast Graham Island, British Columbia (Walker and Barrie 2004). Wind rose and sand drift potential roses are shown.

2.6 Seaward Migration of Coastal Systems

Seaward barrier migration has been observed on both transgressive shorelines (Ollerhead and Davidson-Arnott 1995; Walker and Barrie 2004, Garrison et al. 2010) and regressive shorelines (Lessa et al. 2000; De Oliveira Caldas et al. 2006). The following are some case studies of the effects of seaward barrier migration on transgressive and regressive shores.

2.6.1 On Transgressive Shorelines

2.6.1.1. Bouctouche Spit, New Brunswick

Bouctouche Spit is a flying spit (Fig. 2.7) located along the north shore of New Brunswick, facing PEI (Ollerhead and Davidson-Arnott 1995). This is a mixed microtidal environment in a low energy coastal environment dominated by bedrock outcrops, sandy barrier systems and numerous drowned river valleys (Ollerhead and Davidson-Arnott 1995). These authors estimated that for the past 4000 years the average rate of relative sea-level rise at the west end of PEI was 90 cm / century. Long-term regional sea-level rise suggests this shore is transgressive, so landward migration of the coastal system is expected.

Between 1839 and 1988 the distal end of the spit advanced ~ 400 m seaward while the middle section of the spit narrowed. The center section of Bouctouche Spit has been migrating landward with rising sea level for at least the past 1100 years. Similarly the proximal end of the spit has likely been migrating landward at the rate of at least 3 m/year for at least the past 1000 years. The large advance of the distal end of the spit is an example of seaward migration of a

coastal system on a transgressive coast.

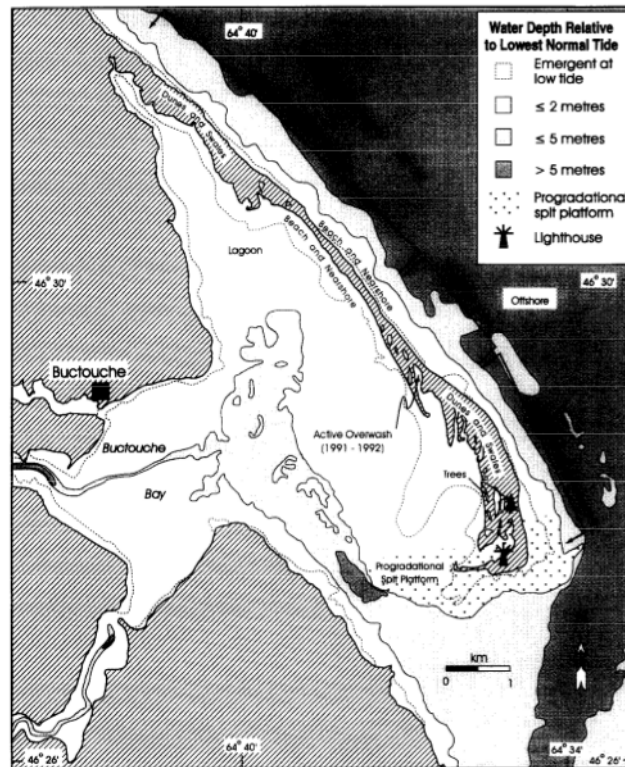


Figure 2.7 Bouctouche Spit, New Brunswick (Ollerhead and Davidson Arnott 1996).

2.6.1.2 North Padre Island, Gulf of Mexico, Texas

At 200 km long, up to 3 km wide and 10-15 m thick, Padre Island, Texas, is the widest and longest barrier island in the world (Garrison et al. 2010). This Gulf of Mexico barrier island (Fig. 2.8) is located in a microtidal environment with a tidal range < 0.5 m (Garrison et al. 2010). Holocene sea-level curves indicate lowstands 2400 years BP, 1100 years BP, and between 600 and 400 years BP (Tanner 1992; Balsillie and Donoghue 2004) and a highstand at ~ 2000 years BP

(Morton et al. 2000). Barrier island growth was initiated during the lowstand at 2400 years BP (Garrison et al. 2010). Regional sea-level has been rising since 2400 years BP suggesting the shoreline is transgressive. The island has been prograding seaward at a rate of 1 m /year as a result of longshore sediment transport (Garrison et al. 2010), which is an example of seaward migration on a transgressive shoreline.

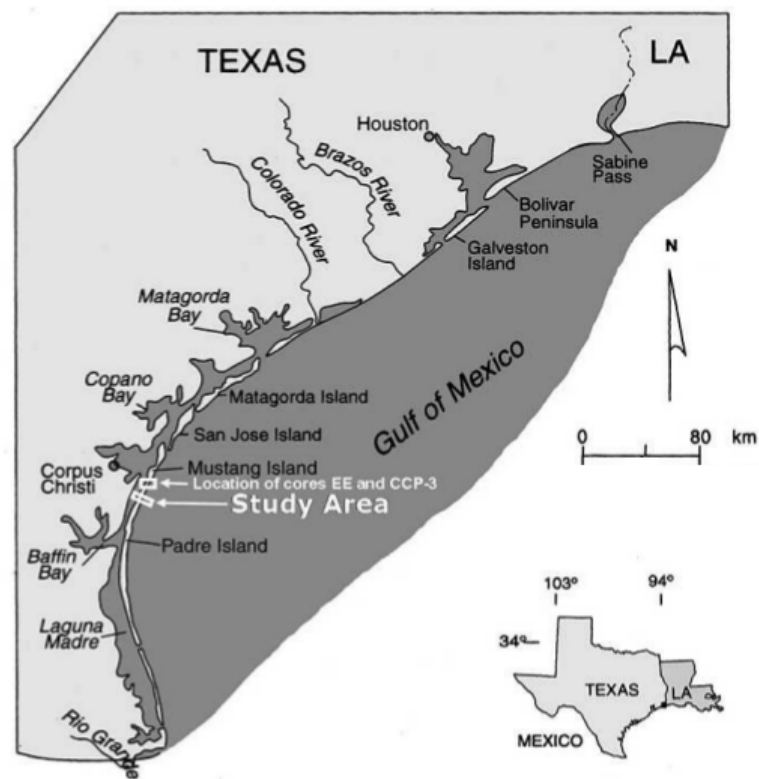


Figure 2.8 Padre Island, Gulf of Mexico, Texas (Garrison et al. 2010).

2.6.2 On Regressive Shorelines

Regressive barriers that are not near river mouths may be built from the reworking of inner shelf sediments during sea-level fall (De Oliveira Caldas et al.

2006). The north coast of Rio Grande do Norte State, in northeastern Brazil (Fig 2.9), is wave-dominated, with mean wave heights from 0.2 m to 1.4 m, depending upon location (De Oliveira Caldas et al. 2006). These authors found that ~ 6000 years BP sea-level was similar to modern sea level. At 4500 years BP, sea-level rose to 3 m above present mean sea level, and it has been falling ever since. This long-term history of regional sea-level fall suggests this shoreline is regressive. During sea-level fall a regressive barrier was deposited and has since been migrating seaward (De Oliveira Caldas et al. 2006). This is an example of seaward migration of a coastal system on a regressive shore.

2.7 Coastal Sensitivity

Another factor that influences shoreline evolution is coastal sensitivity. Coastal sensitivity is the degree to which a rise in sea-level would accelerate geomorphological change (Shaw et al. 1998). The sensitivity index (SI) is calculated using the following formula

$$SI = \sqrt{\frac{(a \times b \times c \times d \times e \times f \times g)}{7}} \quad [2.1]$$

where a = relief ranking, b = rock type ranking, c = coastal landform ranking, d = sea-level tendency ranking, e = shoreline displacement rate ranking, f = mean tidal range ranking and g = mean annual maximum significant wave height ranking (Shaw et al. 1998). Conrads Beach is in a region of high SI (Fig. 2.10), along with much of the Atlantic coast of NS and most of the PEI.

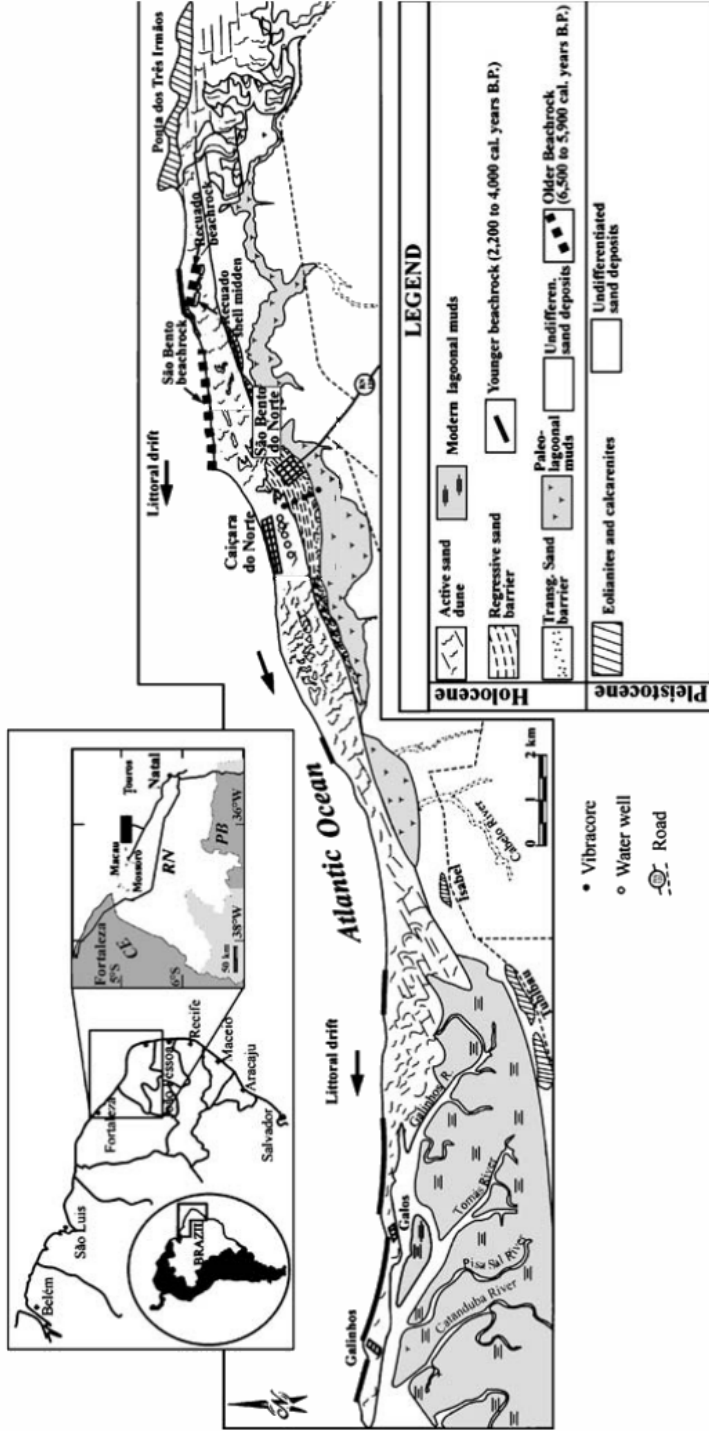


Figure 2.9 North coast of Rio Grande do Norte State, northeastern Brazil (De Oliveira Caldas et al. 2006).

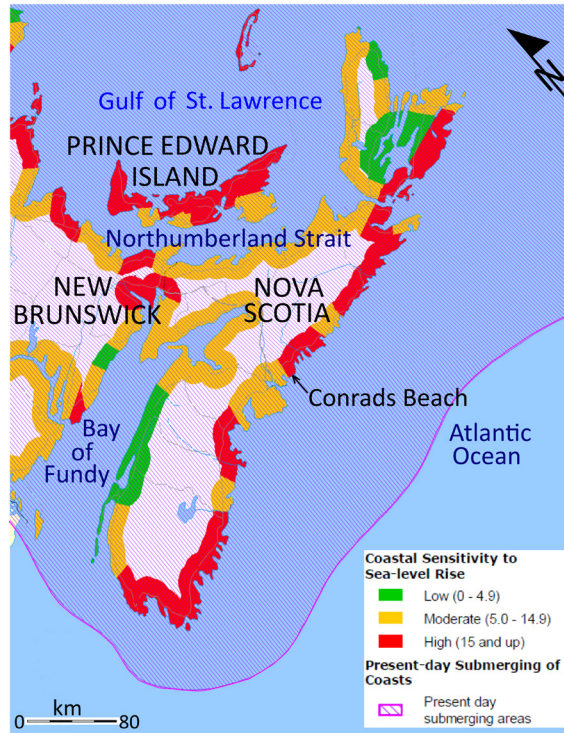


Figure 2.10 Study site and the coastal Sensitivity Index. Modified from Shaw et al. (1998).

Shaw et al. (1998) calculated the SI for shorelines along each 1:50,000 map sheet with locations being assigned a ranking from 1 to 5 for each of the seven SI variables (Shaw et al. 1998). The minimum and maximum values possible are 0.3 and 106 respectively, with SI of 0-4.9 considered low, 5-14.9 considered medium and 15 and larger considered high (Shaw et al. 1998). At Conrads Beach mixed semi-diurnal tides range from 1.8–2.1 m (Taylor and Frobel 2001), so the tidal range ranking is 2 (Table 2.1). Landforms include beaches and unconsolidated sediment (till) over bedrock, and barrier, salt marshes and peat. The average dune height is on the order of 2-3 m. A relative sea-level rise of 32 cm / century for the past 90 years (Parkes et al. 2002; Forbes et al. 2004, 2009) is also an indicator of a high SI. The till and marine littoral

sediments are easily erodible. Additionally, beaches and dunes are dynamic coastal landforms that respond to a variety of factors. The combination of regional subsidence and local sea-level rise results in a relative sea-level rise of ~32 cm / century (Forbes et al. 2009). A mean tidal range and maximum significant wave height of 1.8-2.1 m (Taylor and Frobel 2001) and 7-8 m (Boyd et al, 1987; Taylor and Frobel 2001), respectively, also contribute to Conrads Beach's high SI.

Table 2.1 Ranking of coastal Sensitivity Index variables (adapted from Shaw et al. 1998) for Conrads Beach (bolded).

	Ranking of Sensitivity Index				
	Very low	Low	Moderate	High	Very high
Variable	1	2	3	4	5
1. Relief (m)	>30	21-30	11-20	6-10	0-5
2. Rock type	Plutonic rocks, high-grade metamorphic & volcanic rocks	Metamorphic rocks	Most sedimentary rocks	Pooly consolidated sediments	Unconsolidated sediments, ice
3. Landform	Fjord, high rock cliffs, fiard	Moderate and low rock cliffs	Beach, unconsolidated sediment over bedrock	Barriers, bluffs, salt marsh, peat, mud flats, delta, spit, tomobolo	Ice-bonded sediments, ice-rich sediments, ice shelf, tidewater glacier
4. Sea-level change (cm/100 a)	>-50	-50 to -20	-19 to +20	21 to 40	>40
5. Shoreline displacement (m/a)	>+0.1 accreting	0 stable	-0.1 to -0.5 eroding	-0.6 to -1.0 eroding	>-1.0 eroding
6. Tidal range (m)	<0.50	0.5-1.9	2.0-4.0	4.1-6.0	>6.0
7. One year maximum wave height (m)	0-0.9	3.0-4.9	5.0-5.9	6.0-6.9	>6.9

2.8 Consequences of Sea-level Rise

The rate of eustatic sea-level rise is accelerating (Bindoff et al. 2007; Rahmstorf et al. 2007; Forbes et al. 2009). Transgression and regression are the result of the interaction between coastal erosion or deposition and relative sea-level changes (Boyd 2010). The two most common outcomes are transgression (shoreline erosion) and regression (shoreline deposition). Forced regression occurs when relative sea-level falls and normal regression occurs when the rate of deposition exceeds the rate of relative sea-level rise. In the case of transgression, shoreline erosion can cause rapid change over considerable distances. In Atlantic Canada, the anticipated results of sea-level rise include increased rates of bluff erosion, higher rates of beach erosion, more frequent overwashing of beaches and destabilization of coastal dunes (Shaw et al. 1998). Barrier systems on transgressive coasts go through a cycle of progradation, retreat and reestablishment (Boyd et al. 1987). Boyd et al. (1987) studied several barrier systems along the eastern shore of NS and created an evolutionary model for transgressive sedimentation (Fig. 2.11). In this model, deglaciation results in relative sea-level rise, estuary formation and the deposition of till and drumlins. As relative sea-level rises, the drumlins are eroded and the redistributed sediments form barriers which are anchored to the remaining drumlins. Hoskin (1983) and Boyd and Honig (1992) confirmed that the Lawrencetown Beach/Lawrencetown Lake system fits the model. It is not known whether this model applies to all drumlin-anchored barrier systems or which of the four barrier geomorphological controls (sediment supply, relative

sea-level change, terrestrial basement setting and wave climate (Orford et al. 1996)) is most important in determining coastal barrier morphology.

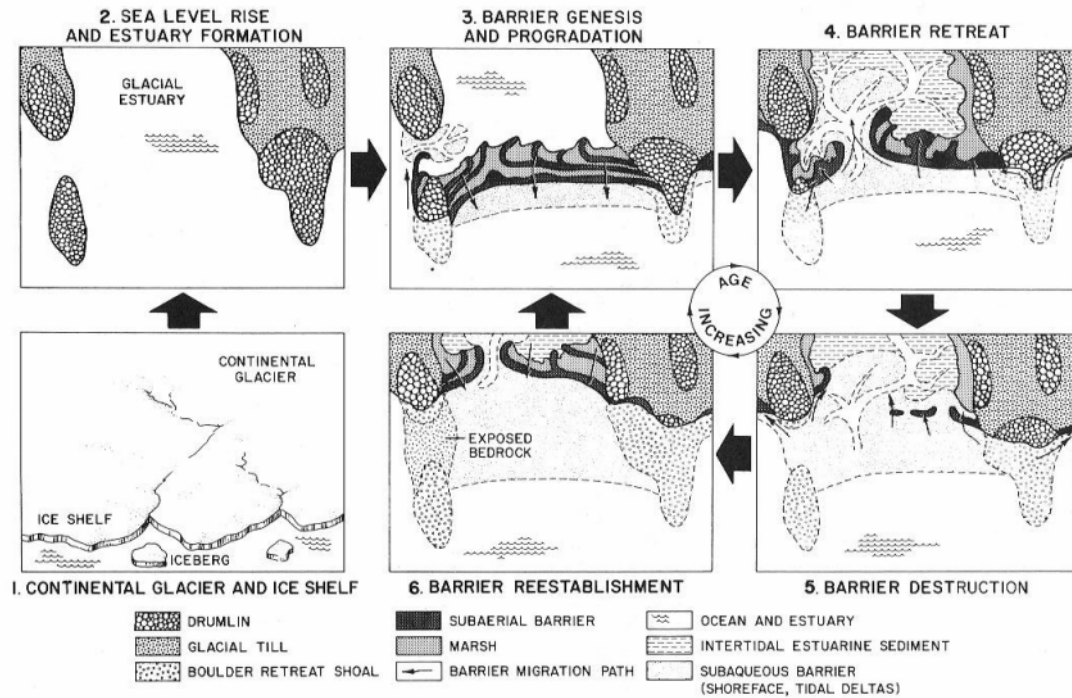


Figure 2.11 Barrier genesis, destruction, and re-establishment in response to rising relative sea-levels on the paraglacial coast of Nova Scotia (Boyd et al. 1987)

In order to answer these questions, a detailed study of Conrads Beach was conducted and reconnaissance GPR/GPS data were collected at five other locations. Detailed interpretations of the reconnaissance GPR/GPS results were outside the scope of this study, but may indicate how well the factors for Conrads Beach evolution fit with other locations and whether other factors play a greater role in determining the response of these coastal systems to sea-level rise.

CHAPTER 3: COASTAL EVOLUTION OVER THE PAST 3000 YEARS AT CONRADS BEACH, NOVA SCOTIA, CANADA: THE INFLUENCE OF LOCAL SEDIMENT SUPPLY ON A TRANSGRESSIVE SYSTEM

3.1 Abstract

Although many modern coastlines are retreating as a result of global sea-level rise, periods of stability and progradation may result from time-varying sediment supply. In formerly glaciated regions, where sediment is derived primarily from finite glaciogenic sources, sediment input may support progradation for a time, but decline when the source deposit becomes exhausted. For Conrads Beach on the Atlantic coast of Nova Scotia, georectified maps based on aerial photos, satellite photos, maps and LiDAR data, coupled with beach profiles and historic records, show that the shoreline has retreated overall during the past ~230 years. The shoreline has also experienced progradation and stasis over intervals of years to decades, as well as rapid erosion and accretion over periods of days to months, largely as a result of powerful storms. In the mid to late 1900s, a tidal inlet formed and filled within a few decades, migrating ~60 m laterally during this time.

To investigate timescales of centuries to millennia, ground-penetrating radar profiles which imaged to depths of 6-8 m were linked to 13 vibracores that penetrated up to 4.2 m, and supplemented by refraction-seismic data to 23.5 m depth. Grain-size parameters were used to support facies identification for sand samples. An age profile based on radiocarbon dating suggests that the area was open-marine or littoral at about 2800 calendar years BP but that locally increased

sediment supply caused rapid buildup and progradation of beach ridges from ~600-150 years BP. Landward of the beach-ridge area, cores from a lagoon and marsh connected to the ocean by tidal inlets yield dates that correspond to the period of beach-ridge formation. As the coast retreated, erosion of drumlins provided large sediment pulses over a period of centuries, temporarily building out the coast and creating a lagoon. The results support previous models for the Atlantic coast of short-term progradation in response to intermittent sediment supply from discrete sources, superimposed on prevailing coastal retreat. Conrads Beach may serve as a model for the behaviour of other high-sensitivity coasts with local sediment sources.

3.2. Introduction

Global sea level has risen 120 m over the last 21,000 years (Bindoff et al. 2007). The rate of global sea-level rise has been variable both in time and space, with an average for the 20th century of 1.7 ± 0.3 mm per year (Church and White 2006; Bindoff et al. 2007). Global sea-level rise has been accelerating (Scott et al. 1995; Church and White 2006) and satellite data from 1993-2006 show a sea-level rise of 3.3 ± 0.4 mm/year (Church and White 2006; Rahmstorf et al. 2007). Roughly 50% of the world's population lives within 200 km of the coastline, and 23% of the world's population lives less than 100 km from the coast and less than 100 m above sea-level (Creel 2003; Nicholls et al. 2007). As these percentages are expected to grow coastline changes will increasingly affect human populations.

Barrier islands and coastal dune systems are distributed globally under a variety of climates (Carter 1988; Martinez et al. 2008) and form vital, dynamic buffers that protect coastlines from high-water events. Sediments are supplied to coastal systems by the reworking of seafloor deposits, by longshore sediment transport and by rivers (a negligible contribution in Nova Scotia). Thus marine processes play an important role in shaping the coastal landforms through a dynamic interplay between geomorphic setting, climate, sediment transport, hydrodynamics and biogeochemistry (Reed et al. 2009). In the case of established dunes, factors that influence their morphological development include sand supply source and rate, sand remobilisation, vegetation cover, intensity of wind and wave forces, frequency and magnitude of storms and overwash, long-term beach state, water levels and human impacts (Hesp 2002). Rising sea-level affects wave forces and water levels from storms and overwash events, thus indirectly affecting coastal systems (McCann 1990).

The Atlantic coast of Nova Scotia has experienced an exceptionally rapid rate of Holocene relative sea-level rise with average increases of 2.5 m every 1000 years for the past 5000 years (Gehrels et al. 2004) and 3.2 ± 0.1 mm/year for the past century (Gehrels et al. 2005; Charman et al. 2010). Rising sea-level and associated increased storminess has led to retreating beaches, dune scarping, and loss of dune vegetation (Brown and McLachlan 2002). Shaw et al. (1998) used a set of criteria to rank the sensitivity of Canada's coastline to geomorphological change. They inferred that the presence of low-relief, unconsolidated or poorly consolidated sediments, beaches, barriers, salt

marshes, peat, and high rate of sea-level change contribute to Atlantic Canada's moderate and high coastal sensitivity.

The response of coastal areas to Holocene sea-level rise has been documented at several key sites along the Atlantic coast of Nova Scotia. Based on analysis of marsh-estuarine foraminifera in dated cores from Chezzetcook Inlet, sea-level curves were established by Scott (1977), Brown (1993), Scott et al. (1995) and Gehrels et al. (2005). At Conrads Beach and Lawrencetown Beach, beach-ridge formation and post-glacial transgressive sedimentation have been documented (Hoskin 1983; Boyd et al. 1987; Shaw et al. 1993), along with beach profiles and dynamics (Taylor et al. 1985), dune morphology (Hales 1992), and the late Holocene history of Lawrencetown Lake (Boyd and Honig 1992). Aerial video surveys covered both beaches (Taylor and Frobel 2001).

This study extends the historical account of the Lawrencetown Lake area (Boyd and Honig 1992) to a nearby barrier system at Conrads Beach. The purpose of this article is to establish the historical records of Conrads Beach, a broad coastal compartment between eroding drumlins.

Changes in sedimentation and geomorphic setting at Conrads Beach on the scale of decades to a few centuries (short-term) and millennia (long-term) are investigated. Extending previous research results, high-resolution surface and subsurface information were obtained from a collection of maps and aerial images, ground-penetrating radar profiles, seismic refraction data, facies analysis and dating of cores. The study site is located on a highly sensitive coast that is susceptible to rapid geomorphological change (Taylor et al. 1983; Boyd et al.

1987; Shaw et al. 1993). Other important factors include proximity to Chezzetcook Inlet, for which a high-resolution record of sea-level rise exists (Scott et al. 1995), and a lack of fluvial input, which makes it easier to isolate marine effects. Although the study site has experienced anthropogenic activities since European settlement, many of these activities are documented and modern anthropogenic effects have been minimized since the beach received protected status in 1984 (Bird 1984). The combination of these factors allows Conrads Beach to serve as a proxy for future global sea-level change on other sensitive coasts, both nationally and globally (e.g. Orford et al. 2000).

3.3. Field Site and Geological Background

Conrads Beach is located 25 km east of Halifax, Nova Scotia (Fig. 3.1A). The study area has 2.7 km of shoreline and an area of ~1.4 km². The bedrock consists of metasedimentary rocks of the Cambrian-Ordovician Goldenville and Halifax groups (White 2010). Large drumlins are located close to the beach, and a till veneer is present locally (Utting 2011). Eroding drumlin headlands west and east of the beach (Fig. 3.1A, Conrads Head and Lawrencetown Head, respectively) are undergoing erosion at the rate of 1 m/yr (up to 3 m/yr during severe storm seasons) (Boyd et al. 1987). Conrads Beach sediment is derived largely from Conrads Head and is predominantly sand with a pebble-cobble storm ridge or cobble berm in the western part. The eroded Egg Island-Fox Island drumlin complex was an important sediment source in the past (Boyd et al. 1987; Carter et al. 1990; Forbes 2012). Additional sediment sources include the

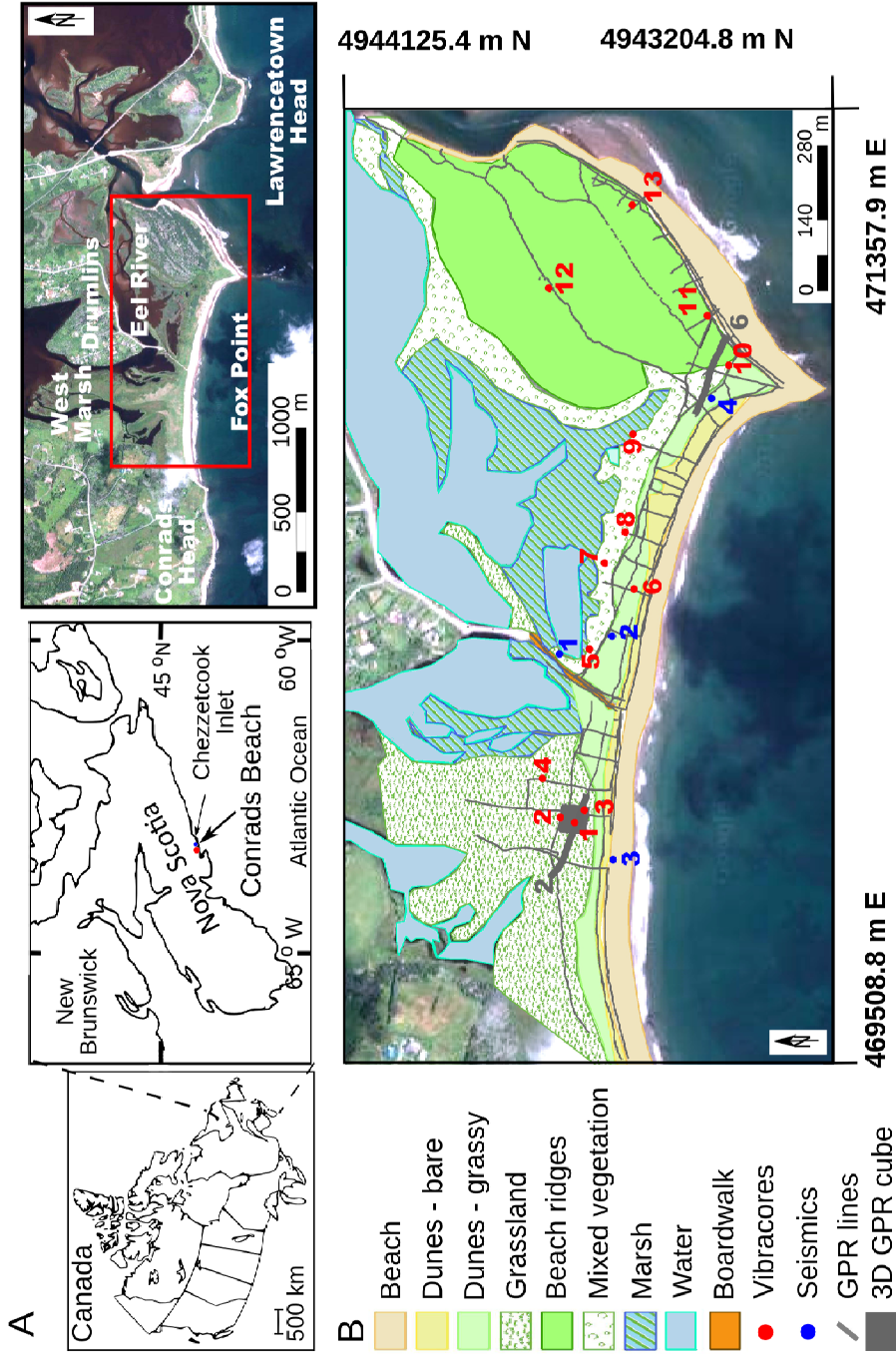


Figure 3.1 Study area, geomorphic setting and field sites. (A) Conrads Beach on the Eastern Shore of Nova Scotia. (B) Locations of GPR traverses, 3D GPR cube, vibracores, and centers of shallow seismic refraction spreads superimposed on the mapped geomorphological units at Conrads Beach. The radargram sections of GPR traverses 2 and 6 (Fig. 3.2) are indicated by thick gray lines.

eroding beach ridges and offshore areas. A gravel-cobble ridge is located west of Fox Point and appears to extend below the dunes on the western beach.

Several geomorphic elements are present (Fig. 3.1B). A sandy beach varies from 12 m wide at its northeasternmost point to 85 m wide at Fox Point, measured from the dune boundary to the shoreline in a 2012 aerial photograph. West of Fox Point, the beach passes gradually landward into dunes with crests 1-2 m high, but behind the beach east of the point the dunes are cut by a steep erosion surface and are greater than 2 m high. The dunes are vegetated, with grassland, mixed vegetation (grass and trees), and marsh bordering the lagoonal areas of West Marsh and Eel River. A large area of beach ridges with undulating topography and tree cover lies north and east of Fox Point.

The Labrador current flows southwest year-round along the Atlantic Coast of Nova Scotia, with ocean surface temperatures from 15-18 °C in the summer and 0–3 °C in the winter (Phillips 1990). During the summers, prevailing winds are toward the northeast with an average speed of 18-23 km/h, and offshore sands are deposited on the beaches by wave action. Storm tracks are oriented east-northeast and wave heights are less than 2 m, 90% of the time. During the winter, the prevailing winds are toward the southeast with an average speed of 32-37 km/h, and beach sands are carried out to sea. Storm tracks are oriented northeast or east-northeast and wave heights are above 6 m, 2-5 % of the time. The Nova Scotia coast is subject to high wave energy with deep-water wave heights of 7-8 m, wind waves generated on the Scotian Shelf, and a long-period, low-amplitude Atlantic swell (Boyd et al. 1987; Taylor and Frobel 2001). Maximum

wave power occurs from October to April (Boyd et al. 1987).

The seasonal variation in wind, wave and ice conditions (Taylor and Frobela 2001) influences deposition in the beach-dune system. Dune growth is directly related to wind regime, beach-dune sand transport rate, and vegetation cover (Davidson-Arnott 2010). Summer sand transport rates are low and plant growth rates are high, leading to minor deposition in the foredunes (Davidson-Arnott 2010). In the autumn increasing sand transport rates and decreasing vegetation cover result in the greatest rate of sand transport to the foredune crests (Davidson-Arnott 2010). In the winter freezing conditions reduce the availability of beach sediments and increased storminess results in beach-dune system erosion (Davidson-Arnott 2010). At Conrads Beach, winter erosion transports sand offshore in large enough quantities to reduce beach width, expose pebble-cobble gravel underlying the beach sand, and cut and steepen the foredunes. Increased beach deposition in the spring, summer and fall covers the cobbles with sand and increases dune heights. North of Conrads Beach, Eel River and West Marsh receive tidal water but have no fluvial input. Mixed semi-diurnal tides range from 1.8–2.1 m (Taylor and Frobela 2001).

During the Wisconsin glacial maximum, 22,000 years ago, glaciers extended as far south as the shelf edges of Atlantic Canada (Shaw et al. 2006). Migration and subsidence of the marginal forebulge over the past ~10,000 years (Quinlan and Beaumont 1981) and glacioeustatic sea-level rise have combined to cause long-term inundation of the coast (McCulloch et al. 2002; Webster and Forbes 2005; Diagle 2006). Nova Scotia is located in the peripheral forebulge

zone, which experienced a short period of relative sea-level fall prior to 7000 years BP and has been undergoing relative rise since then (Scott et al. 1987). In the Halifax area, the subsidence rate is 0.16 ± 0.05 m per century, and long-term tide-gauge records indicate a relative sea-level rise of 0.32 m per century over the past 90 years (Forbes et al. 2009).

3.4. Methods and Data

Ground-penetrating radar (GPR) with a differential global positioning system (GPS) was selected as the main method for subsurface analysis due to its ability to quickly, precisely, and in great detail image the subsurface and obtain positional information. GPR has been used successfully to image coastal dunes in a variety of global locations (Bristow et al. 2000; Neal and Roberts 2001; Buynevich et al. 2007; Garrison et al. 2010; Gonzalez-Villanueva et al. 2011). Seismic data were collected at several locations to determine the thickness of the unlithified sediments, which was not possible using the GPR due to its depth-penetration limitations. Vibracoring (a minimally invasive technique) was used at locations selected on the basis of GPR profiles. The cores provided materials for grain-size analysis and radiocarbon dating. Additional surface and elevation data were obtained from aerial photographs, satellite photographs, profiles, maps and LiDAR.

3.4.1 Global Positioning Systems

A Leica Geosystems GPS 1200™ differential GPS was used simultaneously

with the GPR to collect location and elevation data with a precision of ± 1.5 cm. In order to maintain positional accuracy the GPS base-station receiver was centered over the same position during each survey and the benchmark GSC-001 was surveyed. The World Geodetic System (WGS) 1984 Universal Transverse Mercator (UTM) Zone 20 North coordinate system was used with the WGS 1984 datum. The GPS calculated local sea-level by subtracting the local geoid model from the GPS ellipsoidal heights and in the value was 19.6 m above datum for Conrads Beach.

3.4.2 Ground-penetrating Radar, Beach Profiles and LiDAR

A Sensors and Software Inc. Smart Cart™ with 50 MHz, 100 MHz and 200 MHz antennas was used to collect common offset GPR traverses. Also collected were 14 common mid-point (CMP) vertical profiles at a frequency of 200 MHz and a step size of 0.2 m. Over three field seasons (spring/summer 2010, 2011 and 2012), 182 common offset traverses totalling 20.3 km were acquired. Most common offset traverses were collected either parallel or perpendicular to the shoreline (Fig. 1B) and all had near-zero common offset (0.5 m).

Reconnaissance traverses acquired in 2010 intersected a buried channel south of West Marsh, and a detailed 50 m by 50 m GPR grid (51 north/south lines and 51 east/west lines) was collected in 2011 using the 100 MHz antenna. The CMP traverses were acquired during the spring 2013 field season and were oriented parallel or oblique to the nearest common offset traverse.

The GPR data were processed using Sensors and Software EKKO_View

Deluxe (version 1 release 3)[™] and Paradigm's Focus 5.4[™] software. The dewow high pass filter was applied to remove the inductive low frequency component of the GPR data (Sensors and Software Inc. 2006). This was followed by application of a trapezoid bandpass filter with corner frequencies 20, 35, 80 and 100 MHz for the 2010 50 MHz data; 25, 40, 155 and 225 MHz for the 2010 100 MHz data; 37, 70, 140, 210 MHz for the 2011 100 MHz data cube; and 30, 65, 140, and 210 MHz for the 2012 100 MHz data. The 200 MHz data collected in 2010 were spatially undersampled and were not useable.

Precise and accurate topographic information is required in order to apply a topographic correction to the GPR data. The GPS rover occasionally lost contact with the base station resulting in a loss of vertical accuracy. In the case of six traverses, the vertical position was computed by interpolation and the GPS files were edited manually prior to applying the topography correction. During acquisition of the 2011 data cube, a GPR-GPS miscommunication resulted in GPS data being collected for ~1 in 10 traces. Bezier curves were used to interpolate the missing easting and northing values for each line. Elevation values were interpolated by first creating a Delauney Triangulation of the known elevations and then creating Bezier triangles. All GPR traverses were migrated using a velocity of 0.125 m/ns. A top-mute was applied in Paradigm's Focus 5.4[™] to remove migration noise arriving prior to the direct wave. Kingdom Suite 8.6[™] and Opendtect 4.4.0[™] software were utilized for GPR/GPS data visualization and ArcGIS 9.2[™] software was used for GPS data visualization.

Beach profiles acquired by the Geological Survey of Canada over many

years were surveyed using a variety of techniques that included graduated rods sighted on the horizon, conventional optical levelling and electronic total stations. For almost 20 years, real-time kinematic GPS has been employed (Taylor et al. 2014). Surveys were tied to fixed monuments (typically T-bars or rebar with numbered caps) and eventually to WGS-84, NAD83, and the CGVD28 (Canadian Geodetic Vertical Datum of 1928) vertical datum.

LiDAR data were acquired by the Halifax Regional Municipality in partnership with the Geological Survey of Canada, the Province of Nova Scotia and others in 2008 (Forbes et al. 2009). They covered about 1384 km² centred on Halifax Harbour but extended some distance east along the Eastern Shore, including the present study area. The data made available for this project were from a 'bare-Earth' (buildings and vegetation removed) digital elevation model (DEM), adjusted to the CGVD28 vertical datum, with a vertical resolution of ± 15 cm, and gridded horizontally at 2 m.

3.4.3 Seismic Refraction

Seismic refraction data were collected during the springs of 2007, 2011, and 2012 using the Geode/ES-3000 Seismic System™ with a laptop computer as controller. At each of the investigated locations (Fig. 3.1B) two spreads with 24 vertical geophones spaced 5 m and 1 m apart and planted on the surface were employed. The long, 120 m spread was used to determine the sediment thickness and velocity, as well as the velocity of the crystalline basement. The short, 24 m spread was used to determine the thickness and velocity of the

uppermost layer of surficial material characterized by slow P-wave velocity. The source for the long spread was a buffalo shotgun (12 gauge steel shot) triggered at 0.5-1 m depth to generate a strong signal with deep penetration. For the short spread, a sledgehammer was struck at the surface to generate critical refractions at the shallow boundary between the sediment layers characterized by slow and fast P-wave velocities. Head waves at this boundary could not be generated using the shotgun source, which is triggered below this interface. The shotgun and sledgehammer were triggered at both ends of the spreads, 5 m and 1 m from the last geophone, respectively. A hand auger was used to excavate to a depth of 0.5-1 m; the shotgun was inserted into the hole and water poured into the hole to improve coupling. The sledge hammer was struck six times on a 2.5 cm-thick steel plate at both ends of the spread. To improve the signal to noise ratio, shot gathers for both shotgun and sledgehammer source were formed by stacking 5 and 30 records, respectively.

Data analysis was carried out using RefractTM software (Burger et al. 2006), which is based on the method of Aadachi (1954). First arrivals, picked on amplitude balanced and bandpass filtered shot gathers, were first input into the software. A starting subsurface model, constrained by the picked first arrivals and containing an arbitrary number of layers separated by planar interfaces, was then formed. These initial conditions allow RefractTM software to calculate the first arrival times for the starting model and to adjust the subsurface model to minimize the root mean square misfit between the modeled and the picked traveltimes.

3.4.4 Vibracoring

Vibracoring was carried out in the Fall 2012 field season, following GPR data analysis which identified many potential subsurface targets. A Wink Vibracore System™ was employed to collect core samples at 13 locations (Fig. 3.1B) for which the elevation was precisely determined using the differential GPS.

Aluminum pipes 10 cm in diameter with 5 mm wall thickness were used to collect the cores. The vibrations that allowed the tube to penetrate into the ground also caused the sediments inside the core tube to compact. Before extracting the cores, measurements were taken from the top of the tube to the ground surface outside the tube and to the topmost sediment inside the tube. The difference between the two values reflects the vertical extent of sediment compaction during coring. Compaction measurements range from 59 cm to 243 cm. The tubes were extracted and transported to Dalhousie University for analysis. The sediment cores ranged in length from 124 cm to 353 cm. A Ridgid™ battery powered, reciprocating saw was used to cut the tubes into 150 cm lengths and in half longitudinally. A length of wire was moved along the cut tube from bottom to top in order to aid sediment separation when the tube halves were opened. Each halved core segment was covered with clingfilm, bagged and labelled. One segment was archived and the other was used for logging and analysis.

Each working segment was photographed in colour at scales of ~ 1:2 and 1:7 and sketched on core log sheets with a scale of 1:5. A Munsell™ colour chart was used for sediment colour identification and a grain-size chart and hand lens were used to visually estimate grain size, roundness and sphericity. The

presence of organic material (roots, grass, wood fragments) and shell fragments was also noted.

In order to obtain accurate depths of core penetration, a unitless linear stretching factor was calculated for each core ((core length + compaction) / core length) and ranged from 1.17 to 2.71. For example core 1 was 124 cm long, has 134 cm of compaction, a stretching factor of 2.08, and penetrated to a depth of 258 cm (core length * stretching factor). Almost all of the core material is sand so the stretching factors were applied uniformly to all cores except Core 4, which contained a non-compactable cobble (long axis 85 mm); the remaining sediment was stretched by an additional factor to generate the original core length. Cores 5 and 9 each had a 2-3 cm gap in a sandy layer with roots and grass in the top 50 cm. These gaps are artefacts of core splitting and the stretching factor was not applied to them. The stretched logs range in length from 241 cm to 422 cm and SedLog (version 3.0) software (Zervas et al. 2009) was used to generate visual columns.

3.4.5 Grain-size Analysis

Cores were selected from each modern setting (tidal channel, dunes, marsh, beach ridges). Although predominantly sandy, the samples contained varied proportions of gravel, sand and mud, requiring an analytical protocol to assess these components separately. This was carried out at the Bedford Institute of Oceanography (Geological Survey of Canada). Eighteen sand-rich samples and five mud-rich samples ranged in mass from 87 g to 112 g and 2 g to 28 g,

respectively. The samples were weighed, wet-washed through a 63 μ filter to remove the mud fraction, dried, and re-weighed to determine the mud fraction. The sand-rich samples contained less than 2% mud, which was discarded. The mud fractions from the mud-rich samples were centrifuged and decanted to remove excess water.

The mud-rich samples contained organic material in both their sand and mud fractions, and this was removed using a 35% hydrogen peroxide solution. The mixture was heated to 60 °C to activate the hydrogen peroxide and complete digestion (an exothermic reaction generating bubbles) and then to 100 °C to deactivate the hydrogen peroxide, rinsed to remove any remaining hydrogen peroxide, and dried.

The gravel and sand fractions were hand-sieved through -3.0 phi (8 mm) to -1.0 phi (2 mm) at 1/4 phi intervals (phi = $-\log_2$ (particle diameter / reference diameter of 1 mm)) to measure and separate the gravel. Finer material (less than 1.0 phi or 2 mm) was analyzed using a Beckman Coulter LS230™ Laser Diffraction Analyzer (long bench unit) with a variable-speed fluid module. This system requires an obscuration of 8-10% for optimum results. The sand and mud fractions were split to remove any bias in grain size, and small quantities (~1 g) were added to the analyzer until the optimum obscuration range was reached. Sample sizes from 3-9 g were needed. The weighted percentages of the gravel, sand, and mud fractions were entered into GRADISTAT software (Blott and Pye 2001) and the sample statistics were calculated. Grain-size parameters were calculated using the Method of Moments (Folk and Ward 1957; Friedman 1961).

3.4.6 Radiocarbon Dating

Some cores contained woody material, shell fragments and peat in sufficiently large quantities for radiocarbon dating. The materials were removed using tweezers. After being air-dried and weighed, seven samples were submitted to BETA Analytic Inc. for dating. Due to the small sample size, accelerator mass spectrometry ^{14}C dating was performed. The shell fragments were pretreated using acid etching. Woody samples and locally charred plant materials that were extracted from the peat were pre-treated using a standard acid/alkali/acid method. INTCAL13 and MARINE13 databases were used to calibrate the radiocarbon dates (Reimer et al. 2013).

3.4.7 Aerial Photographs, Satellite Photos, Maps and LiDAR

The recent evolution of Conrads Beach was established by analyzing maps from 1776, 1865, 1906, 1981, and 1992; vertical aerial photographs from 1945, 1954, 1960, 1973 (Nova Scotia Land Registry Service), 1974, 1992, 1997 and 2003, satellite photos from 2002, 2008, 2010, 2012, and 2013; and 2008 LiDAR data. See Table 3.1 for map and photo sources. The 1845, 1964, 1974, 1992, 1997 and 2002 air photos were scanned at 800 dpi and the 1960 and 1973 air photos were scanned at 1200 dpi. The 2008 satellite photo digital file was referenced to the North American Datum 1983 Canadian Spatial Reference System Universal Trans-mercator Zone 20 N reference system and covered the largest surface area. This satellite photo, and three benchmarks were used in ArcGIS 9.1™ to georectify the other maps (except for the maps whose areal

extent was too small for georectification) and photographs. The benchmarks were Geological Survey of Canada benchmark 001, the center of the western gate post and the center of the southernmost landing (where the GPS base station was located for the majority of the surveys). Table 3.1 gives total root mean square (RMS) error for each georectified image. To calculate errors for retreat rates of vegetation lines, the RMS errors for selected images were squared, the values were added, and the square root was divided by the number of years between the images. Subsequently, the georectified images, LiDAR and GPS field data were all displayed in ArcGIS 9.1™.

3.5. Results

3.5.1 GPR and Seismic Results

The GPR 100 MHz antennas provided useful images of the subsurface to depths of 6-8 m, estimated using an average near-surface velocity of 0.11 m/ns from the common-midpoint survey. Using this velocity, the depth resolution was ~0.3 m (based on the $\frac{1}{4}$ of the dominant wavelength rule: Widess 1973, Annan 2009), and the lateral resolution at a depth of 8 m was ~2 m (based on the radius of the first Fresnel zone; Annan 2009). Imaged subsurface reflectors were variably continuous or discontinuous, horizontal, dipping and/or sigmoidal, and chaotic. Four radar facies were identified.

Figure 3.2 shows sample radargrams with numbered facies, providing a geomorphic context for facies analysis. Line 2 (Fig. 3.2A) runs just inland from the modern beach in the western part of the study area (Fig. 3.1B). The

alternating bands at the top of the line mirror the topography and represent the ground wave. At greater depth from position 42-22 m, a U-shaped reflector is visible and is bordered by a series of sigmoidal reflectors that dip southeastward from 90-42 m (Fig. 3.2A, D). This body of sediment represents a tidal channel that migrated approximately 60 m to the southeast before it was filled and buried.

Table 3.1 Photograph and map sources

Date	Material	Scale	Total RMS Error	Source
1779	Map	1:80000	N/A	Taylor et al. 1985
1865	Map	1:11880	15.6	Church 1865, Nova Scotia Public Archives
1906	Map	1:63360	26.4	Faribault 1906
July 1945	Air photo	1:15000	4.04	National Air Photo Library
1951	Map	1:80000	N/A	Taylor et al. 1985
1954	Map	1:60000	N/A	Taylor et al. 1985
July 1954	Air photo	1:15840	5.55	National Air Photo Library
1960	Air photo	1:25400	3.55	National Air Photo Library
1973	Air photo	1:33000	5.10	Nova Scotia Land Registry Service
8-11-1974	Air photo	1:10880	5.40	Nova Scotia Land Registry Service
1974	Map	1:60000	N/A	Taylor et al. 1985
1981	Map	1:10000	N/A	Taylor et al. 1985
7-25-1992	Air photo	1:10000	3.75	Nova Scotia Provincial Photos
10-25-1997	Air photo	1:10000	5.45	Nova Scotia Provincial Photos
Aug 2002	Air photo	1:10000	4.54	Nova Scotia Provincial Photos
Oct/Nov 2003	Digital air photo	1:24000	1.07	Department of Natural Resources
2008	LiDAR survey	N/A	N/A	Halifax Regional Municipality
2008	Digital satellite photo	N/A	1.07	Halifax Regional Municipality
2010	Satellite photo	1:20000	2.47	Google Map Imagery 2010 CNES/SPOT, Digital Globe
2012	Satellite photo	1:20000	1.89	Google Map Imagery 2012 CNES/SPOT, Digital Globe
2013	Satellite photo	1:20000	5.35	Google Map Imagery 2013 CNES/SPOT, Digital Globe
Dec 2013	Satellite photo	1:20000	2.76	Google Map Imagery 2013 CNES/SPOT, Digital Globe

The dipping reflectors represent the progressively advancing accretionary bank

of the channel, and their sigmoidal form indicates near-complete preservation of the bank sediments, yielding a vertical extent of about 2 m that approximates the original channel depth. Below and southeast of the channel body are closely spaced sub-parallel reflectors, possibly beach sediment associated with the tidal channel.

Line 6 (Fig. 3.2B) in the eastern part of the study area crosses vegetated dunes and runs southeastward across vegetated beach ridges (Fig. 3.1B). The top reflectors follow the surface. The series of sigmoidal, dipping reflectors with associated scours from 125-42 m represent seaward-prograding beach ridges (Fig. 3.2B, E). From the northwestern end of the line to position 125 m, reflectors that dip approximately northwestward may represent dune foresets, seen tangentially.

Radar facies 1 has continuous, planar to sinuous, parallel to subparallel reflectors, and has a sheet to sheet-drape configuration. This facies includes the air wave/ground wave, which mirrors the topography and generates widely spaced reflectors. Facies 1 also appears at depth with closely spaced reflectors (Fig. 3.2A, B, C, and F), and probably represents several geomorphic settings. In trenches at Conrads Beach and elsewhere along the Nova Scotia coast, the modern foreshore shows well stratified sand and gravel and the modern lagoonal fringe shows interbedded planar units of organic-rich mud and sand-gravel, the latter interpreted as washover deposits associated with storms.

Radar facies 2 (Fig. 3.2A, D) has planar to sigmoidal, dipping, subparallel, moderately continuous reflectors. The upper contact tends to have a toplap or

erosional boundary whereas the lower surface tends to have a downlapping and commonly erosional signature. This facies is not present at surface but was observed locally in the shallow sub-surface with dips of inclined surfaces approximately parallel to the coast, as indicated from 3D reconstructions using closely spaced traverses from the GPR cube (Fig. 3.1B). The facies is interpreted as tidal-channel deposits laid down in a channel that originally connected the lagoons of West Marsh and Eel River to the ocean.

Radar facies 3 (Fig. 3.2B, E) has sinuous, horizontal to dipping, parallel reflectors that are moderately continuous. The upper boundaries are concordant whereas the lower boundaries exhibit erosion. Inclined surfaces dip approximately toward the offshore. This facies is best developed below the beach ridges, with local scours at depth. In some areas, dipping reflectors of radar facies 3 underlie dunes and are interpreted as dune foresets.

Radar facies 4 (Fig. 3.2F), a minor component, has low-amplitude, discontinuous reflectors that are locally associated with radar facies 3. The facies is interpreted as poorly stratified material within extensive dunes and smaller dune areas associated with beach ridges.

Figure 3.3 shows radargram-core intersections for five cores. GPR traverse X4 (Fig. 3.3A) was located west of the beach entrance and core 3 intersects the tidal channel illustrated in Figure 3.2A, terminating slightly above the “U”-shaped scour at the channel base. GPR Traverse 45 (Fig. 3.3B) was located south of the marsh and position 41 m (from the beginning of the traverse) was 14 m southwest of core 5. GPR traverse 60 (Fig. 3.3C) was located near the east end

of the marsh and core 9 intersected it a position 6.5 m. Cores 5 and 9, adjacent to the Eel River marsh, intersect horizontally stratified layers of radar facies 1 (Figs. 3.3 B, C). GPR traverse 68 (Fig. 3.3D) was located near the tip of Fox Point and core 10 was located ~ 15 m east of position 140 m. GPR traverse 78 (Fig. 3.3E) was located east of Fox Point and core 11 intersected it at position 66 m. Cores 10 and 11 in an area of beach ridges near Fox Point intersect dipping strata of radar facies 3, representing beach-ridge cross-sections (Figs. 3.3 D, E).

At all four seismic locations (Fig. 3.1B), the top sediment layer was thin (0.5-1.5 m) and composed of dry sand and soil, as inferred from hand drilling at shotgun source locations and slow P-wave velocities. This surface unit was underlain by a layer of unconsolidated sediment that we infer to be wet sand based on drilling and its higher acoustic velocities (Table 3.2). The depth to basement (interpreted as top of Ordovician metasediments) at the four investigated locations, was ~20 m for all locations except at the West Beach where it was ~10 m (Table 3.2). These results indicate that the GPR profiles imaged most of the sediment package at West Beach (Fig. 3.1B, seismic location 3) and the upper one-third of the unconsolidated sedimentary package elsewhere. Utting (2011) estimated the marine littoral sediments in the Conrads Beach and Lawrencetown Beach area to be 1-5 m thick. The refraction seismic results suggest a greater thickness of unconsolidated material.

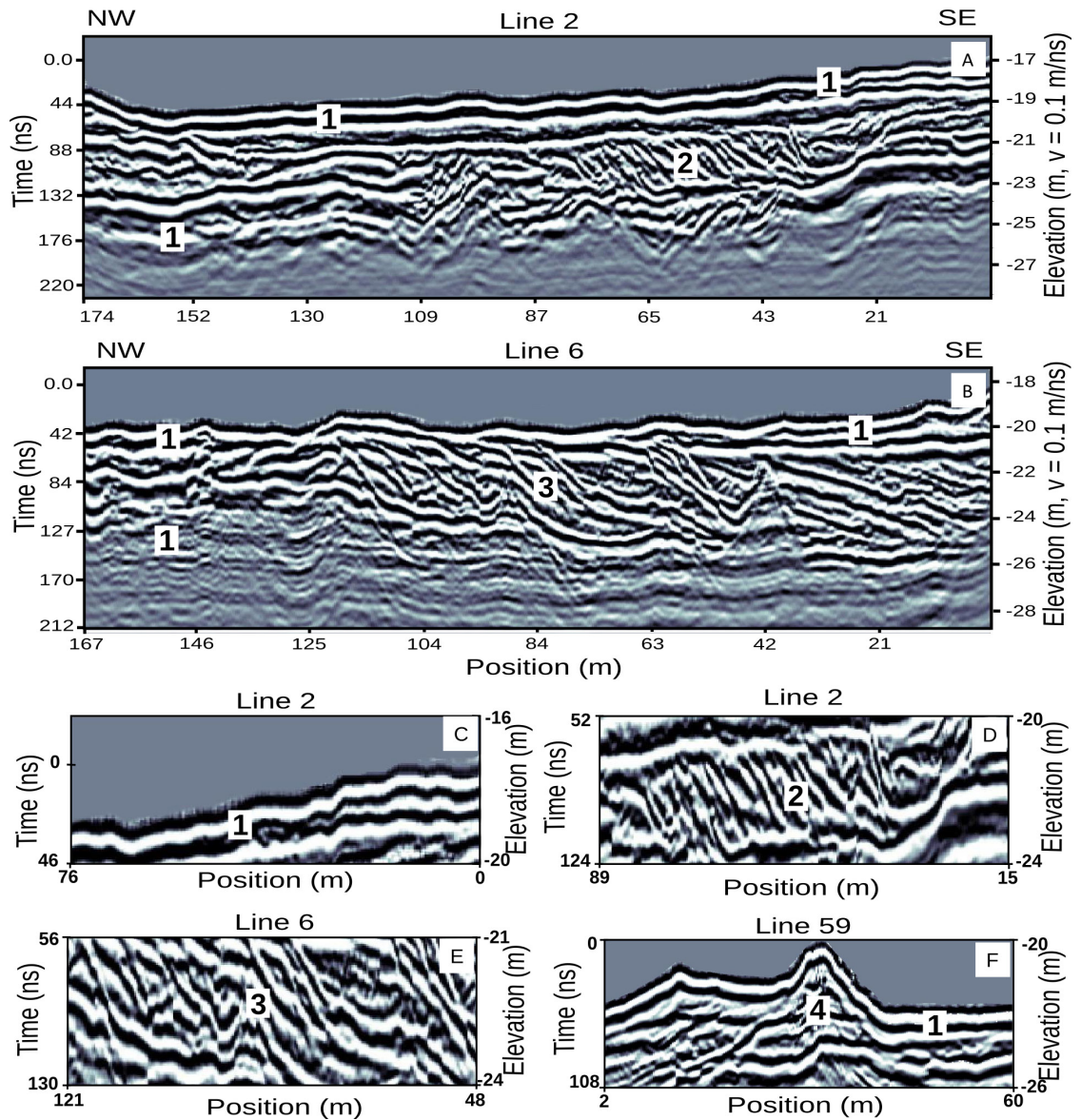


Figure 3.2 Examples of Conrads Beach radargrams and facies acquired using 100 MHz antenna. (A) and (B) show the entire traverses (located in Fig. 3.1B) with a vertical exaggeration of 4. (A) Traverse 2 located west of the main beach access and intersecting a buried channel. (B) Traverse 6 located east of Fox Point and intersecting beach ridges. (C) Close-up of radar facies 1 from traverse 2. (D) Close-up of radar facies 2 from traverse 2. (E) Close-up of radar facies 3 from traverse 6. (F) Close-up of traverse 59 showing radar facies 1 and 4.

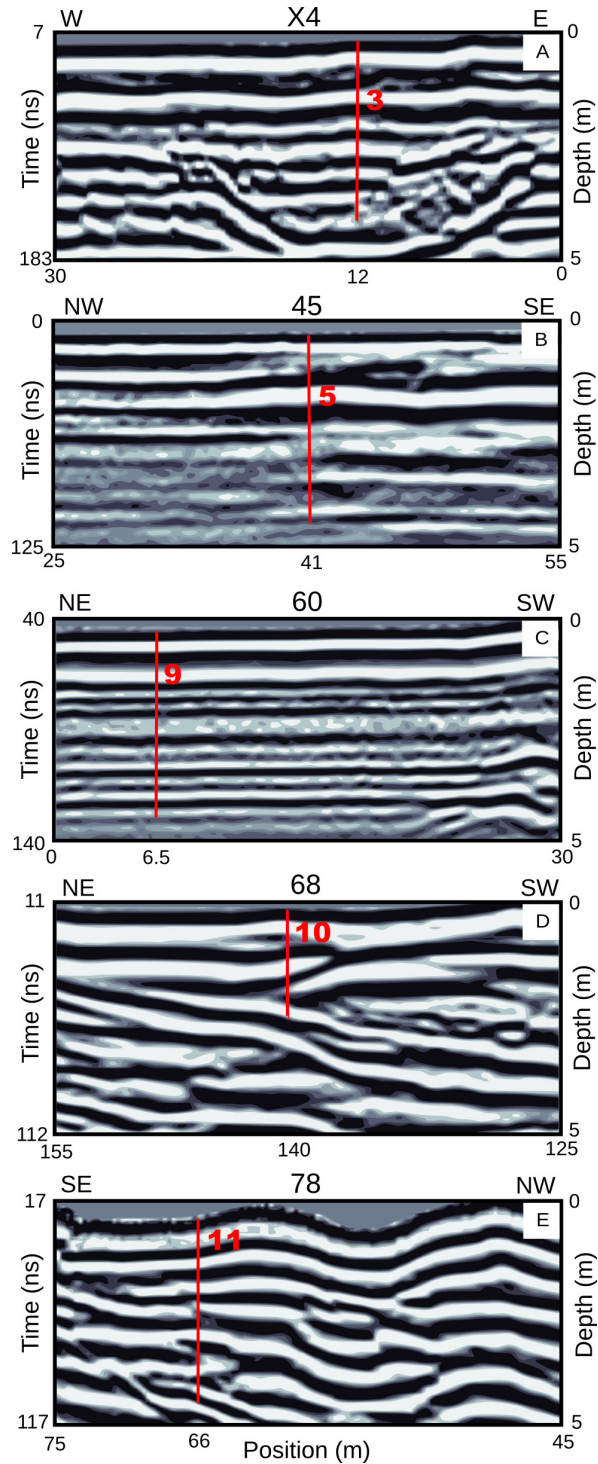


Figure 3.3 Radargrams (30 m wide by 5 m deep) showing detailed structure associated with dated cores. The GPR traverses were acquired using 100 MHz antenna. The nearest vibracore locations are indicated in red and the core lengths are shown to scale. See Fig. 3.1B. for vibracore locations. (A) GPR traverse X4 and core 3. (B) GPR traverse 45 and core 6. (C) GPR traverse 60 and core 9. (D) GPR traverse 68 and core 10. (E) GPR traverse 78 and core 11.

Table 3.2 Refraction seismic results.

Location	Layer	Thickness (m)	Velocity (m/s)
1) 2007 Boardwalk	1	0.5	300
	2	18.5	1800
	3		4300
2) 2007 Center Beach	1	1.0	300
	2	21.5	1500
	3		3300
3) 2011 West Beach	1	1.0	300
	2	9.5	1500
	3		4700
4) 2012 Fox Point	1	1.5	300
	2	22.0	1500
	3		3100

3.5.2 Core Results

3.5.2.1 Lithofacies Results

Eight lithofacies were identified based on sediment size and texture, colour and the presence or absence of shell fragments and organic material (Table 3.3). Figure 3.4 shows the core sections and facies positioned with respect to their elevations relative to mean sea level.

Facies 1-3 form thin sheets of relatively coarse material that constitutes ~13% of the cores, mainly in the western part of the study area (Fig. 3.4). Based on the geomorphic settings of the cores and correlation with GPR profiles, these facies represent tidal channel, beach and washover deposits. Facies 1 comprises cobbles and pebbles to coarse sand with numerous shell fragments and fine roots near the tops of some cores. Gravel is a component of the facies at depth in tidal channel deposits in cores 2 and 3 and at a low level in core 4, drilled

through dunes. Coarse-grained sand is present at depth in cores 1-4, at the top of cores 5 and 8 on the marsh fringe, where it is interpreted as coarse washover deposits, and near the bottom of core 11 drilled through beach ridges, where it may represent an underlying foreshore. Gravel at the base of core 6 is also interpreted as a coarse washover deposit.

Facies 2 comprises coarse- to medium-grained sand, and Facies 3 comprises slightly finer sand on average. These facies are prominent in tidal-channel deposits, within dune deposits, and in the topmost parts of marsh deposits; in the latter two settings, they probably represent washover layers.

Facies 4-7 (fine- to very fine-grained sand with some silt) constitute the bulk of sediment in all cores (~85%) in units up to 3 m thick, especially through the beach ridges, dunes and bordering the marsh. Roots and grass are common in Facies 4 in near-surface sites, and the facies also contains a few shell fragments, which were not noted in other facies. The finer facies 7 is present only in the lower part of the tidal-channel fill in core 3.

Facies 8 is peat and constitutes less than 2% of the cores. Peat occurs in layers less than 0.2 m thick just below the surface in four cores (5, 7, 8, 9) drilled through the marsh

Figure 3.5 compares the dated vibracores and their associated radargrams (see Fig. 3.3 for the full radargrams). The 3 m wide radargram slices are shown at the same vertical scale as their associated core logs. The correlation between the radargram slices and the vibracore lithofacies is poor. Some core lithofacies are not detected by the GPR, and some of the GPR interfaces do not correspond

Table 3.3 Facies characteristics. Grain size and colour ranges were determined using a grain-size chart and Munsell Colour Chart, respectively. Twenty-three grain-size samples were collected and analyzed using laser diffraction. The modal phi and mean phi values represent unimodal samples or unimodal sample ranges, respectively (see Fig. 3.8 for bimodal and polymodal outliers). Unit thicknesses and percentage of the core assemblage were calculated after the cores were stretched to account for compaction.

Facies	1	2	3	4	5	6	7	8
Grain size	Cobble to coarse sand	Coarse to medium sand	Medium to fine sand	Fine to very fine sand	Fine to very fine sand	Fine to very fine sand	Very fine sand to silt	Peat
Colour	Dark brown to dark gray & dark grayish brown	Gray to dark brown	Light to dark grayish brown	Light grayish brown to brown	Dark gray to very dark grayish brown	Brownish yellow to dark yellowish brown	Dark grayish brown to black	Very dark grayish brown to black
Shell fragments	Locally present				Not noted			
Organic material	Fine roots near tops of some cores	Roots in top of 1 core	Roots at top of 1 core; at depth in a 2nd	Roots & grass near tops of most cores	Organic fragments / roots in 4 cores	Roots / organic fragments in 2 cores	Wood fragments at depth in 1 core	Peat
Modal Phi	2.3	2.0-2.4	2.0	1.8-2.3	2.0-2.6	1.9	2.2-2.4	N/A
Mean Phi	2.0	1.7-2.3	1.7	1.9-2.2	1.7-2.7	1.4	2.0-3.7	N/A
Unit Thickness	<4 m	< 0.3 m	<0.4 m	<2 m	<3 m	<0.6 m	<1 m	<0.2 m
Inferred Environment	Tidal channel, beach, washover			Tidal channel, ridge, marsh, beach, dunes	Tidal channel, beach		Tidal channel	Marsh
Place in sequence	Variable depths in 8 cores	Variable depths in 3 cores	Variable depths in 7 cores	Variable depth; in all cores	Variable depth; in all cores	Below 1 m in 5 cores; top unit in tidal channel core	Below 2.3 m in buried channel	Upper meter in marsh
% of cores	7.7%	1.8%	3.9%	45.5%	33.2%	3.7%	2.8%	1.4%

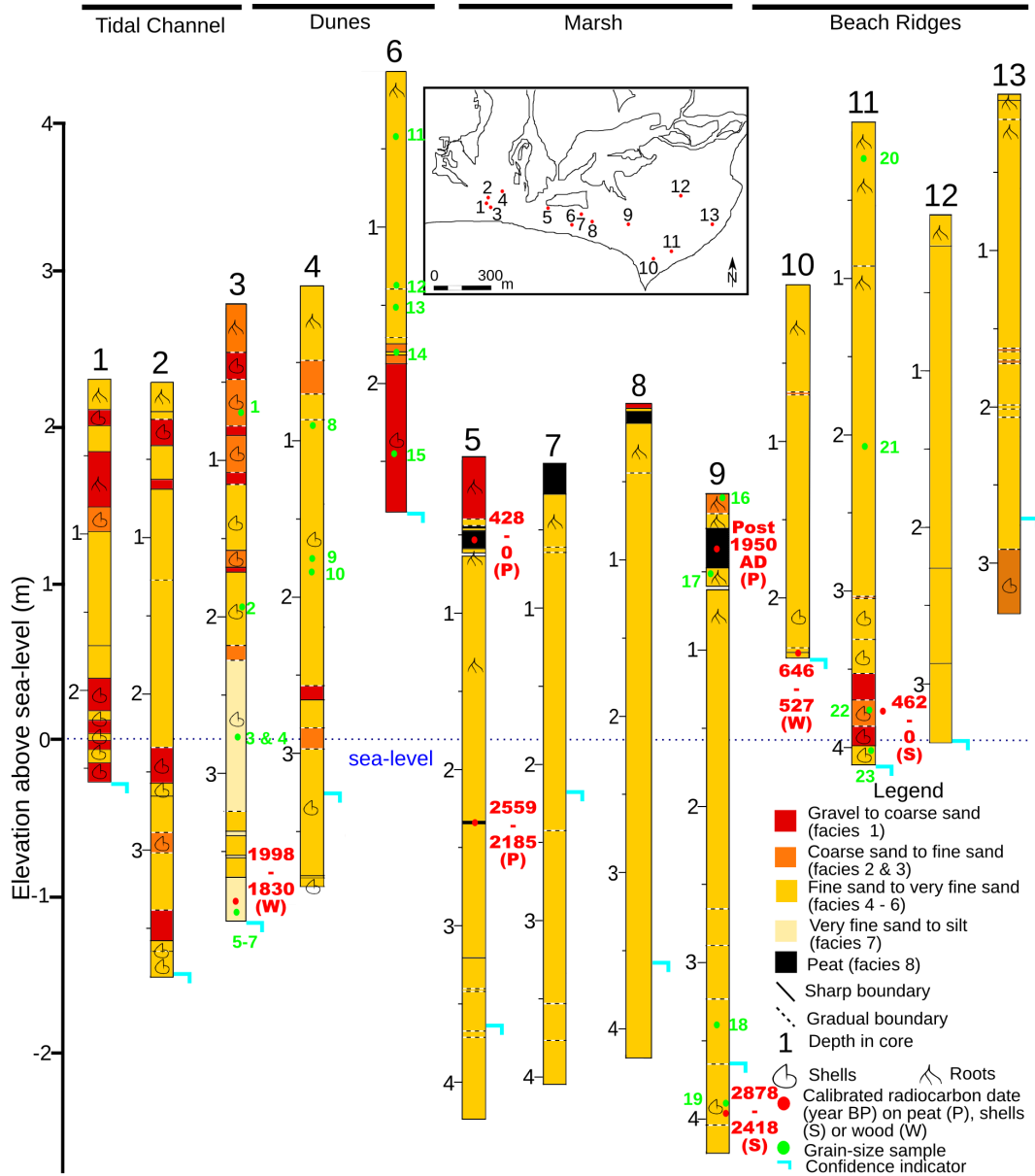


Figure 3.4 Facies distribution and sediment types for Conrads Beach vibracores (see Table 3.3 and text for facies descriptions). Inset shows the location of the vibracores. The confidence indicators were determined by comparing the vibracore cores to their associated radargrams and marking the lowest depth in the radargram where the data are considered reliable.

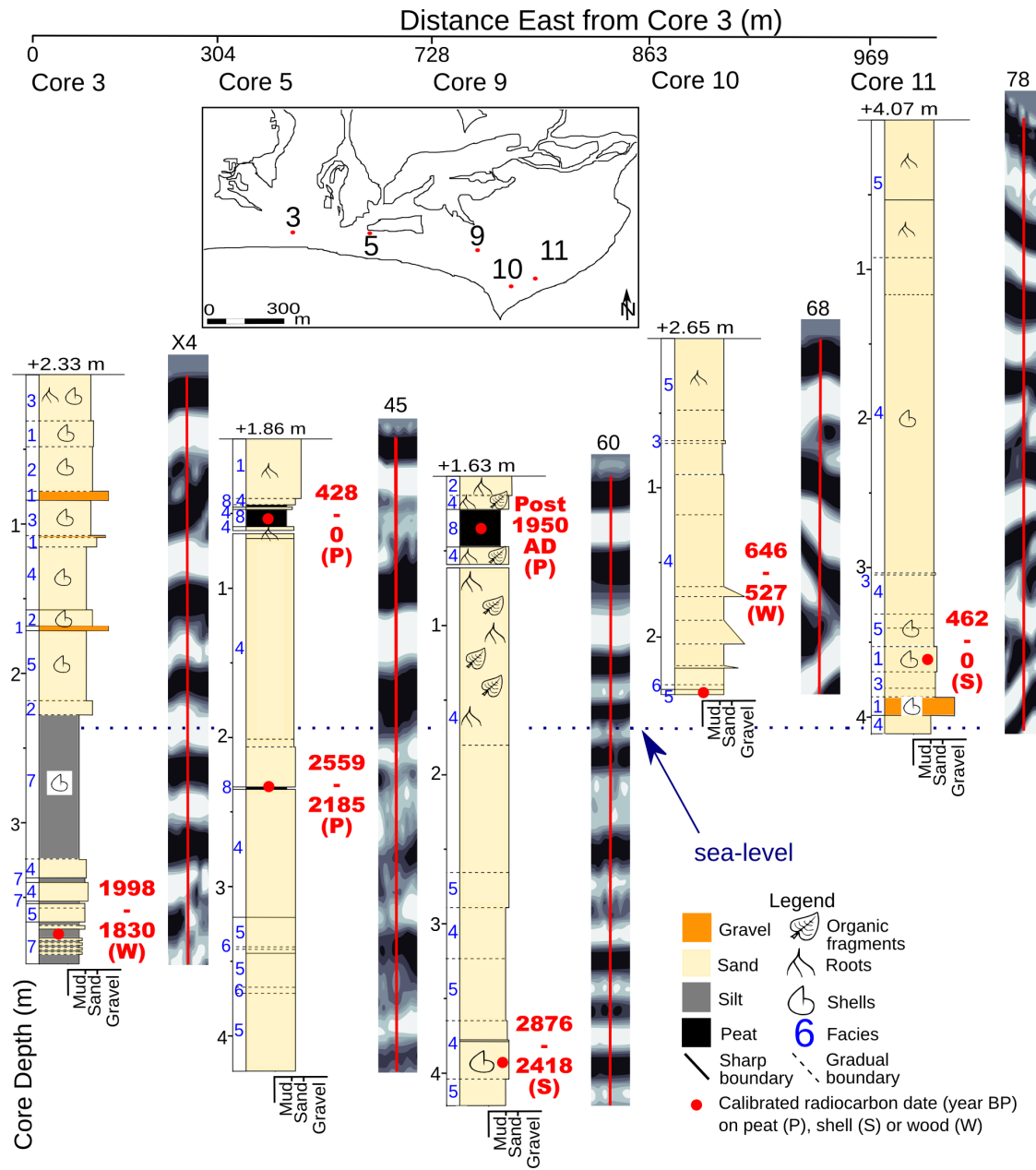


Figure 3.5 Dated vibracores and associated radargrams. Five vibracores contained material suitable for radiocarbon dating using accelerated mass spectrometry. Corresponding sections of GPR traverses 3 m long, centered at vibracores 3, 9, and 11 and closest to vibracores 6 and 10 are shown to vertical scale, with the vibracore locations shown in the inset. See Fig. 3.3 for extended GPR images that include these radargrams.

to lithofacies changes in the cores. Several factors may have contributed to this. Firstly, the compaction during coring was likely non-linear and the stretching factor may not have put the core lithofacies in the correct vertical positions. Secondly, the GPR may have detected variations in sediment composition, orientation, shape, size and packing that are not reflected in the eight core lithofacies. Thirdly, some thin core lithofacies may be too thin for the GPR to detect. Using more core lithofacies and a higher GPR antenna frequency may have improved the correlation. The majority of the core assemblage (82.4%) is composed of fine to very fine sand (Table 3.3), but creating meaningful subdivisions for facies 4 (45.5%) and 5 (33.3 %) proved difficult. While using a higher antenna frequency would have increased the GPR resolution, it would also have decreased the penetration depth (Neal 2004). The confidence indicators (Fig. 3.4) are near the bottom of most vibracore cores, suggesting the GPR penetration depths are an appropriate match with most vibracore penetration depths.

3.5.2.2 Grain-size Analysis Results

In view of the predominance of Facies 4-7 in cores in all geomorphic settings, grain-size analysis was conducted to provide additional insight regarding depositional environment based on plots of grain-size parameters (Folk and Ward 1957; Friedman 1961; Blott and Pye 2001). Sample positions are shown in Fig. 3.4. Samples 3, 4, 12, and 13 have bimodal distributions and sample 23 has a polymodal distribution. All other samples have a unimodal distribution.

Figure 3.6 shows the Conrads Beach grain-size parameters classified by their inferred depositional setting based on geomorphic setting and correlation with GPR profiles, in relation to Friedman's (1961) divisions. For Figure 3.6A, Friedman's (1961) data indicate that beach sand generally has negative skewness and that dune sand has positive skewness. The Conrads Beach core samples are broadly distributed across Friedman's beach and dune fields, with most inferred beach-ridge samples plotting in the beach field but with greater scatter in inferred dune samples.

Friedman's (1961) data indicate that dune sands are better sorted than river sands but with a large region of overlap and poor discrimination. The Conrads Beach core samples are poorly discriminated on this plot (Fig. 3.6B), but tidal-channel deposits show moderate to poor sorting and mainly plot in the river field.

Friedman's (1961) data indicate that river sands have a higher standard deviation and generally more positive skewness than beach sands. The Conrads Beach core samples are generally poorly discriminated (Fig. 3.6C), but tidal-channel deposits mainly plot within the river field.

In summary, grain-size parameters provide some confirmation that the core samples have been correctly attributed to depositional settings, although the level of discrimination is modest. It is probable that, with such a short transport distance of sand from the foreshore to bordering dunes and beach ridges, textural changes would have been slight, militating against the use of these parameters for discrimination. However, some similarity of river and tidal-channel processes might be expected, and this appears to be the case.

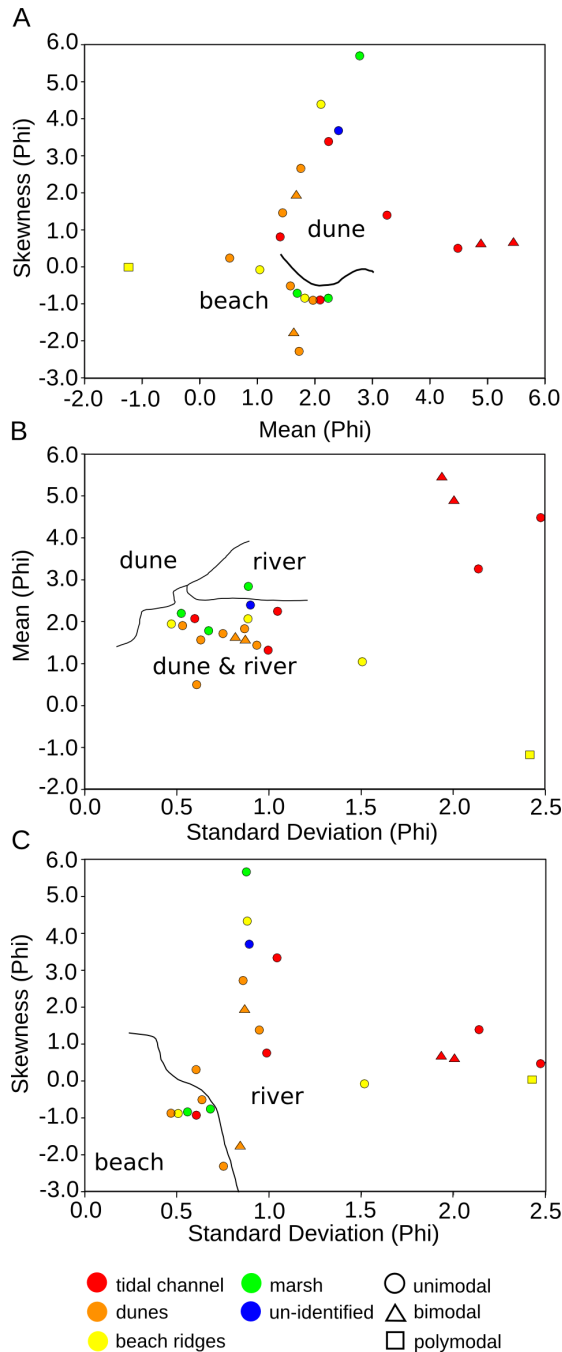


Figure 3.6 Comparison of grain-size data (phi [negative \log_2] scale) to Friedman's (1961) partitions. Mean, standard deviation and skewness were calculated using the method of moments. (A) Skewness vs. mean. (B) Mean vs. standard deviation (sorting). (C) Skewness vs. standard deviation (sorting). The dataset includes 18 unimodal, 4 bimodal and 1 polymodal sample. Modern environment of deposition is indicated by colour ('un-identified' refers to samples at too great a depth to identify the environment). The black lines represent Friedman's (1961) divisions between beach, dune and river sands.

3.5.3 Radiocarbon Dating Results

The dated cores were drilled in four geomorphological settings: tidal channel, marsh, beach ridge, and mixed vegetation on dunes (Fig. 3.1B). The dated material was collected from five vibracores (Table 3.4). Shallower samples are reliably attributed to environments based on correlation with GPR profiles, but the sample from depth in core 9 lies below the level of reliable returns from the associated GPR profile and its setting is uncertain. The measured radiocarbon age (Table 3.4) is the measured age in radiocarbon years before present (AD 1950) whereas the conventional age is the measured radiocarbon age corrected for isotopic fractionation and is calculated using $\delta^{13}\text{C}$. The 2 sigma calibrated age is the conventional radiocarbon age calibrated using Calib7.0. The 2 sigma calibrated ages will be used for discussion purposes.

Samples 343156 and 343157 were collected low in beach ridge cores 10 and 11, 106 m apart (Fig. 3.5, Table 3.4). Given their similar elevations above sea-level, close proximity and geomorphology, it is reasonable to expect these sample ages to be within error. The samples returned calibrated dates of less than 650 years BP.

Samples 343159 and 343161 were from peat in the tops of cores 5 and 9, bordering the marsh and 424 m apart. They have similar elevations with respect to sea-level (Fig. 3.4, Table 3.4) and returned young calibrated dates of less than 428 years BP and post 1950 AD, respectively. Differences in the dates, despite the similarity in setting and depth in the cores, may be related to their differing geomorphologic setting (marsh versus mixed vegetation), their distance apart,

and local events such as washovers that may locally have terminated peat accumulation.

Samples 343158, 343160 and 343162 are below sea-level (Fig. 3.4, Table 3.4) and were taken from cores 5 and 9 bordering the modern marsh and from the basal sediments of the tidal channel in core 3. They cumulatively show a range of calibrated ages from 2876 to 1830 BP. The deepest sample at about 2 m below sea level in core 9 (343160) is the oldest, and the tidal-channel sample (343158) at a mid elevation is the youngest, possibly due to preservation of tidal-channel sediments cut into older sediments. As discussed below, the tidal-channel deposits may be composite because a relatively old radiocarbon date was obtained for the lower part whereas the upper part is known from historical records to have been abandoned recently.

Mean rates of deposition were calculated based on the central value for each 2 Sigma Calibrated age and the corresponding depth in the. These accumulation rates have a high degree of uncertainty, because they assume uniform depositional rates. In reality depositional events are likely to have been episodic. In the beach-ridge area, accumulation rates from the dated level to the core top were relatively rapid: ~3.6 mm/year for core 10 and ~13 mm/year for core 11. For cores in the marsh area, slower accumulation is indicated. Core 5 yielded ~1.9 mm/year for the top 235 cm and ~0.8 mm/year between the two dated samples. Core 9 yielded a rate of ~1.4 mm/year for the top 386 cm and 1.3 mm/year between the two dated samples. Core 3 through the tidal-channel fill yielded an average rate of 1.9 mm/year.

Table 3.4 Radiocarbon dating results. Calibrations used the INTCAL13 and MARINE13 calibration databases. See Fig. 3.5 for radiocarbon sample locations.

Lab Sample Number	343156	343157	343158	343159	343160	343161	343162
Core	10	11	3	9	9	5	5
Depth in Core	237 cm	370 cm	374 cm	36 cm	386 cm	55 cm	235 cm
Elevation above sea-level	+42 cm	+37 cm	-141 cm	+127 cm	-223 cm	+131 cm	-49 cm
Material	wood	shell	wood	peat	shell	peat	peat
Geomorphic setting	Beach ridge	Beach ridge	Tidal Channel	Marsh	Marsh	Mixed vegetation	Mixed vegetation
Facies	5	1	7	8	4	8	8
Inferred Environment	Tidal channel, beach or dune	Wash-over	Tidal channel	Marsh	Marsh or beach	Marsh	Marsh
Measured ¹⁴ C age	580±30 BP	180±30 BP	1990±30 BP	60±30 BP	2450±30 BP	250±30 BP	2770±30 BP
¹³ C/ ¹² C ratio	-25.9 ‰	+0.4 ‰	-26.6 ‰	-24.8 ‰	+1.0 ‰	-25.3 ‰	-22.4 ‰
Conventional ¹⁴ C age	570±30 BP	600±30 BP	1960±30 BP	60±30 BP	2880±30 BP	250±30 BP	2310±30 BP
2 Sigma Calibrated age	646-527 BP	462-0 BP	1998-1830 BP	Post 1950 AD	2876-2418 BP	428-0 BP	2559-2185 BP

3.5.4 Historical Evidence for Geomorphological Change

Both natural and anthropogenic events (Table 3.5) may have contributed to changes at Conrads Beach. Agriculture was a key industry when Europeans first settled in the area and marsh reclamation may have taken place as early as 1750.

3.5.4.1 Photographs, Maps and LiDAR

The earliest map (1779) (Taylor et al. 1985) with a sufficiently large scale to show Conrads Beach (Fig. 3.7A) shows that the southernmost tip of was a peninsula ~500 m long. The western shore was oriented northwest-southeast, the eastern shore was oriented approximately north-south, and the channel between Conrads Beach and Lawrencetown Beach was approximately 500 m wide. By 1865 (Fig. 7B) (Church 1865), Egg Island and Eel River had been named, Fox Point appears shorter and wider, and Eel River cuts southwest. Although not shown in the 1865 map (Church 1865), the British began construction of a dyke across the mouth of Eel River in 1830 (Degen 1976) and this feature is visible on a 1906 map (Faribault 1906). Prior to the early 1900s, Egg Island was a forested island ~ 800 m south of the tip of Fox Point (Degen 1976). Lawrencetown Dyke (across Eel River) was deliberately destroyed in 1917 and a wharf was constructed on Fox Island in 1920 (Degen 1976).

By 1954 (Fig. 3.7C) (National Air Photo Library), Conrads Beach had attained its modern shape. Notable features include increased deposition east of Fox Point, a shoreline retreat at Fox Point and Fox Island, increased marsh west of Fox Point, and a decreased beach width adjacent to the West Marsh. A

Table 3.5 Natural and anthropogenic events affecting Conrads Beach

Date	Event
Just prior to 1752	The Acadians, the first European settlers, may have built an aboiteau (dyke with bridge) at the entrance to West Marsh (Degen 1976).
1754	British settled at Lawrencetown, close to West Marsh (Degen 1976).
1798 – 1857	Seven major storms known to have damaged the Halifax area (Degen 1976, Delure 1983)
1881	521 residents of Lawrencetown practice farming, fishing, and trades with 412 acres of cultivated land and 375 acres of reclaimed marsh (Degen 1976).
Early 1900s	A heavy storm subdivides Egg Island (subsequently all soil washed away) (Degen 1976).
June 19, 1918	Siberian Prince struck a shoal near Egg Island (Degen 1976)
Sept 11, 1954	Hurricane Edna impacts the Halifax area (Delure 1983).
Dec 30, 1956	Severe wind storm knocks down 1000 trees in Point Pleasant Park and tosses barges on shore in Dartmouth (Delure 1983)
1962	Opening of a tidal channel along the western shore of Conrads Beach (Taylor et al. 1985).
Aug 16, 1971	Hurricane Beth causes record rainfall and flooding in Halifax (Delure 1983)
Sept 29, 2003	Hurricane Juan damages Lawrencetown Beach, destroying boardwalks, cutting back dunes by 5.5 m, and scouring upper beach, resulting in loss of the cobbles that had accumulated since Feb 1998 (NRCan 2011)
Nov 3-4, 2007	Post-tropical Storm Noel damages Conrads Beach by flooding and scouring the boardwalk, and eroding and lowering the upper beach (Taylor et al. 2008).
Aug 22-23, 2009	Hurricane Bill causes flooding at Conrads Beach (NRCan 2011).
Sept 4, 2010	Hurricane Earl (NRCan 2011) Halifax Harbour had a storm surge of 1.15 m that coincided with low tide. The maximum total water level was 1.83 m. Wave heights of 10.1 m with a peak of 25.1 m. Upper beach and dunes along the south-facing beach at Conrads Beach were trimmed, exposing the cobble substrate. East of Fox Point the dunes were severely cut. Small landward extent of overwash. "Smearing" of a sand ridge and transfer of large sediment volume to sea at Lawrencetown Beach.
Dec 2010	Four storms damaged Conrads Beach (Taylor et al. 2013). The pedestrian bridge and backshore were flooded. On the western beach, furrows were etched into the embryo dunes and the beach was lowered to expose the pebble-cobble dune base. Waves from the Dec 27 th storm washed 53 m inland at the buried channel. On the central beach the beach was lowered and the dunes cut back by 5 m. Along the eastern beach, total dune retreat was 9.1 m.

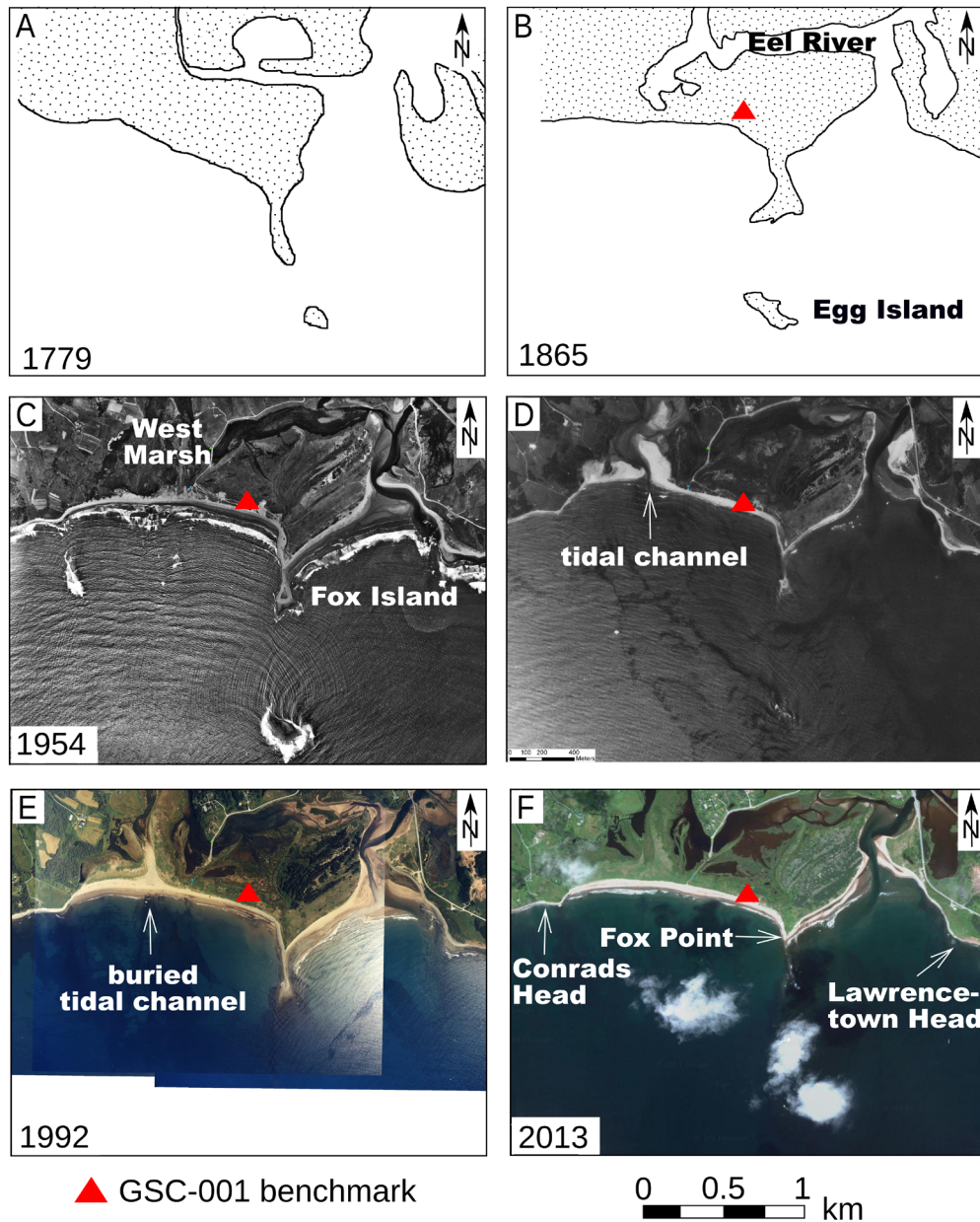


Figure 3.7 Topographic changes at Conrads Beach since 1779. Key events include the erosion of Egg Island (B) and Fox Island (C), the creation (D) and filling (E) of a tidal channel, and increased sedimentation in Eel River and West Marsh (E and F). The 1779 (A) map is taken from Taylor et al. (1985) and the 1865 (B) map is simplified from Church (1865). The 1954 (C) aerial photograph is from the National Air Photo Library; 1973 (D) and 1992 (E) from Nova Scotia Natural Resources; and 2013 (F) from Google Maps 2013 CNES/SPOT Image, Digital Globe. The 1865 to 2013 maps and photos were georectified in ArcGIS 9.2™ and referenced to the GSC-001 (Geological Survey of Canada) benchmark (red triangle).

system of trails east of the boardwalk and two bare areas (one east and one west of GSC-001) suggest continued anthropogenic change. In 1962 a tidal channel opened ~ 270 m west of the boardwalk (Taylor et al. 1985).

By 1973 (Nova Scotia Land Registry Service), Egg Island was completely submerged (Fig. 3.7D). The 1973 and 1992 (Nova Scotia Provincial Photographs) photographs (Figs. 3.7D, E) show an open tidal channel in the western part of the study area and closure and burial of the tidal channel (1989 (NRCan 2007)). The 1992 photo (Fig. 3.7E) shows a sandy zone 200 m wide covering the former position of the tidal channel and an increased beach width to the west. The West Marsh is considerably smaller than in earlier photos and some former marsh areas appear vegetated. East of Fox Point, Conrads Beach and Eel River also show evidence of increased sand deposition. The 1992 aerial video shows a large gravel/boulder shoal south of Fox Island (Taylor and Frobel 2001 [DVD]), which is the expected remnant of the planed-off drumlin platform.

The most recent photo showing the beach in a vegetated state is from 2013 (Fig. 3.7F) (Google Map Imagery 2013 CNES/SPOT, Digital Globe). After several major events over the previous decade (Table 3.5), Fox Island is submerged, and vegetation in the area of the buried tidal channel and reclaimed marsh is sufficiently dense to obscure surface traces of these features. During low tide, remnants of the Fox Island wharf are visible. Fox Island has continued to decrease in size, and Eel River has continued to narrow, with vegetation well established on the sand bars along the tidal inlet.

Vegetation lines were digitized from the georeferenced maps and aerial

photographs, facilitating identification of short- and long-term changes (Fig. 3.8). Vegetation changes due to the opening and closing of the tidal channel are apparent, and Hurricane Juan in 2003 resulted in a considerable reduction in vegetation on the western side of Conrads Beach (Fig. 3.8). West of Fox Point, the long-term trend is one of retrogradation and stasis (Fig. 3.8), with ~150 m of retrogradation between 1865 and 1945. West of the tidal channel, the vegetation retreated steadily until the channel opened in 1962. After the channel closed in 1989, the vegetation line was re-established just north of the 1972 vegetation line, and retrogradation has continued since. Between the tidal channel and Fox Point, the vegetation line has remained stable despite short periods of retrogradation and progradation.

East of Fox Point, long-term retrogradation was interrupted by periods of progradation (Fig. 3.8). There was significant deposition between 1865 and 1945, but the 1954 and 1960 vegetation lines overlap the 1945 line along the southeast-facing portion of the beach, suggesting stasis. The east-southeast-facing beach experienced retrogradation during this period. By 1974 the entire eastern beach was retrograding, but 1974 to 1992 was a period of progradation for the southeast-facing beach and a period of retrogradation for the east-southeast facing beach. Considerable retrogradation occurred between 1997 and 2002, and the entire eastern beach has exhibited retrogradation since then. At Fox Island, continued erosion since 1865 has resulted in the drowning of a boulder-retreat shoal.

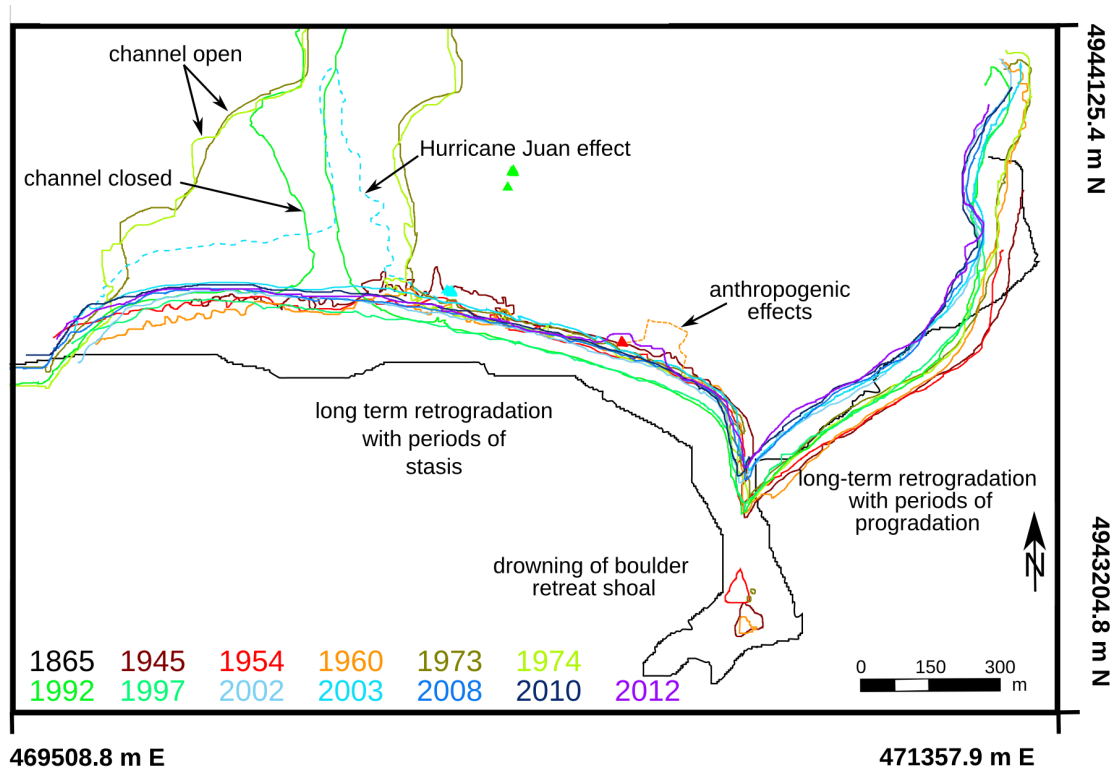


Figure 3.8 Conrads Beach seaward limit of vegetation. Long-term (centennial) changes in the vegetated area from 1865 to 2013. Anthropogenic changes in 1960 (dashed orange line) and the effects of Hurricane Juan in 2003 (dashed teal line) are also shown. The 1865 map and 1945 to 2012 photographs used to form this figure were georectified in ArcGIS 9.2™ and referenced to the GSC-001 benchmark (red triangle), center of the western gate post (green triangle) and center of the southernmost landing (blue triangle). The 1865 vegetation line was determined by first assuming that the map shows the location of the shoreline and then by removing the average distance from the shore to the vegetation line observed in the succeeding years.

3.5.4.2 Beach Profiles

As part of a long-term coastal monitoring program by the Geological Survey of Canada (Taylor et al. 2014), beach profiles have been surveyed repetitively along a number of transects at Conrads Beach since 1981 (Taylor et al. 1985, 2008, 2013). These profiles were compared to profiles obtained from the 2008 LiDAR data at three transects (western, central, eastern), as shown in Figure 3.9.

The temporal variability reflects a combination of short-term change due to storm events and decadal trends.

The western transect is oriented roughly north-south, approximately 500 m west of the present-day boardwalk and west of the buried channel. Six profiles were surveyed along this transect between April 1995 and March 2011 (Fig. 3.9A). From 1995 to 2002 approximately 1 m of new material appears to have been added to the beach-dune system, although this may be partly a result of aliasing seasonal variability. More significantly, the seaward dune crest advanced. Despite Hurricane Juan (Table 3.5), the September 2005 profile shows deposition of a high berm, although again this may be in part a seasonal (summer profile) effect. Between the 2005 and 2009 profiles, Post-Tropical Storm Noel, which caused flooding at Conrads Beach (Taylor et al. 2008), and Hurricane Bill affected Atlantic Canada (Table 3.5). Hurricane Earl in 2010 trimmed the upper beach face and dunes and produced waves with sufficient height to run up to the dune crest along the western beach (R. Taylor, pers. comm., 2011). Four storms in December 2010 also affected Conrads Beach (Table 3.5), and the March 2011 profile shows continued beach erosion and dune deposition (Taylor et al. 2013). Overall, there are fluctuations in the foreshore beach profile and variations in dune position and shape over a 16-year interval.

The central transect is oriented north-south midway between the boardwalk and Fox Point. Ten profiles were acquired between July 1981 and March 2011. Between July 1981 and March 1994, the beach was eroded by ~0.6 m, and the first dune crest increased in height by ~1 m and moved ~4 m seaward. The June

1997 profile shows 0.6 m of deposition on the beach and a slight seaward shift of the foredune (Fig. 3.9B). Hurricane Juan occurred before the next profile (September 2005) along this transect. Between June 1997 and September 2005, ~0.8 m of sand was deposited on the berm, while the dunes remained stable. The 2008 LiDAR-derived profile shows a 0.6 m reduction in dune height, but this may be a result of the LiDAR underestimating the dune crest heights as subsequent profiles show dunes of heights similar to those pre-2008. Overall there are vertical fluctuations in the foreshore beach level and variation in the dune crest position during this 30 year period.

The eastern transect is oriented northwest-southeast ~100 m east of Fox Point. Five GSC surveys and the 2008 LiDAR provide six profiles from October 1987 to September 2008 (Fig. 3.9C). During this period, eight storms are known to have caused damage at Conrads Beach or Lawrencetown Beach (Table 3.5). Sufficient time passed between storm events and profile collection that direct causal relationships can not be inferred. The profiles show ~50 m of overall retreat with ~1.5 m of beach erosion, dune-face steepening, and landward dune migration in a period of 21 years.

For each transect, between-profile changes are consistent with the changes in areal extent of vegetation seen in Figure 3.8. West of the buried channel, the foredunes have changed position while the established dunes have experienced changes in elevation (Fig. 3.9A). This subtle change in vegetation extent is reflected by the close spacing of the vegetation lines in Figure 3.8A. The

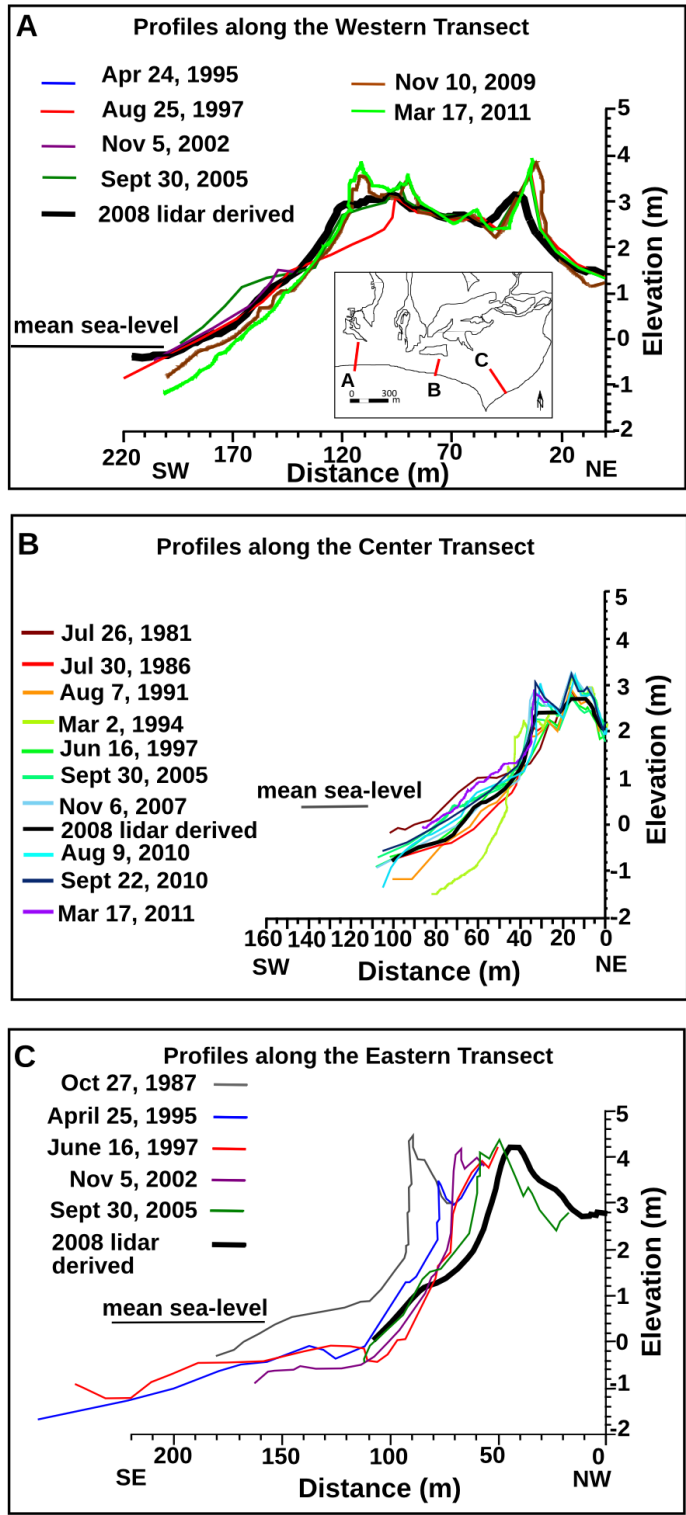


Figure 3.9 Selected profiles along three Conrads Beach transects. (A) Six Geological Survey of Canada (GSC) surveys and a profile derived from the 2008 LiDAR dataset along the western transect (B) Ten GSC surveys and a LiDAR profile along the central transect. (C) Five GSC surveys and a LiDAR profile along the eastern transect.

similarities between plan view (Fig. 3.8) and profiles (Fig. 3.9) are even more striking for the central transect. The 1994 profile (Fig. 3.9B) was collected between the 1992 and 1997 aerial photographs. The vegetation lines (Fig. 3.8) show relative stability during the 1990s, followed by retreat to the 2002 position and then relative stability again during the 2000s. The profiles (Fig. 3.9B) show a dramatic change between 1994 and 2005, with more subtle changes from 2005 to 2008. At the eastern transect (Fig. 3.9C), the landward dune migration is consistent with the long-term retrogradation illustrated in Figure 3.8. Here significant positional changes are observed in both profile (Fig. 3.9C) and plan view (Fig. 3.8).

3.6. Discussion

The oldest dated sample, on shell fragments in sand, near the base of core 9 (at ~2 m below modern sea level), yielded a date of 2876-2418 BP (Fig. 3.4; Table 3.4). Although the sample was located slightly below the depth of reliable GPR information at the site (Fig. 3.4), strata throughout the profile appear flat-lying and are attributed to radar facies 1, in accord with a beach or marsh setting (Fig. 3.3C). A beach setting is supported by the presence of shells, although sample 19 plots in the dune field (Fig. 3.6A). Three other cores (5, 7 and 8) are close to core 9 and extend to similar depths, but none yielded shell fragments in their lower parts. We provisionally suggest that the core site lay close to or below sea level at this time, perhaps in the littoral zone, whereas the present location is on land, 120 m south of the marsh, 150 m from the western shore, and 480 m

from the eastern shore (Fig. 3.4). The ocean or an open estuary may have covered the low-lying West Marsh-Eel River area and, perhaps, much of the Conrads Beach area at that time.

The next oldest date (2559-2185 BP) was obtained from core 5 at ~0.5 m below modern sea level (Fig. 3.4). The sample was collected from a thin organic layer, but the lack of roots below suggests that the material was reworked, rather than being an in situ peat. Shell fragments were not noted in the core, but the GPR profile shows good layering of radar facies 1. As inferred from core 9, the area may have been close to or below sea level at this time.

Cores 10 and 11 produced dates of 646-527 BP and 462-0 BP, respectively (Fig. 3.4; Table 3.4). In both cases dated materials were near the bottom of the cores and less than 50 cm above present sea-level. The two cores were drilled near the fringe of the beach-ridge area and ~50 m from the eastern shore (Fig. 3.4). For core 11, the date was from shell material in relatively coarse sediment with inclined reflections attributed to radar facies 3, and represents the lower strata of the beach-ridge system. Sample 22 from this level yielded equivocal grain-size results. For core 10, the dated sample was a wood fragment in finer sediment of radar facies 3 with shell fragments shortly above. Cores 12 and 13 were also drilled in the beach-ridge area but neither yielded material suitable for dating. The dates from cores 10 and 11 suggest that beach-ridge initiation took place ~600 years ago, and age/depth relations for the cores suggest rapid sediment buildup thereafter with average rates of 3.6 to 12.6 mm/year. Eroding drumlins at Fox Island and nearby Egg Island probably provided the sediment for

the beach ridges.

Peat samples from cores 5 and 9 near the Eel River marsh fringe yielded dates of 428-0 BP and Post 1950 AD at depths of 55 cm and 36 cm, respectively (Table 3.4). Along with shallow peats in two undated cores (7 and 8), these dates suggest extensive peat formation in this area within the past 400 years. Rooted zones at greater depth in all four cores suggest an earlier vegetation cover. These results suggest that Eel River has been a lagoon for a prolonged period, owing its isolation in part to the nearby beach ridges, over at least the past 600 years.

A wood sample at 374 cm depth (~1 m below sea level) was extracted from core 3, drilled through the buried tidal channel behind the western beach (Table 3.4). The tidal channel is known to have been active between 1962 and 1989 (NRCan 2007), but the date of 1998–1830 BP is considerably older than expected. The GPR profile (Fig. 3.2A) shows a well marked erosional cut below the base of the core, and grain-size analysis for samples 3 and 4 (above the dated material) and samples 5 to 7 (immediately below) lie in the river category of Figure 3.6 B and C (finer and more poorly sorted than beach or dune sands and positively skewed). As noted above, this attribution may be consistent with a channel-margin depositional setting. Three other cores (1, 2 and 4) were drilled through the channel fill, as confirmed from GPR lines and the 3D cube (Fig. 3.1B), and all four cores contain relatively coarse, pebbly sediment and shell fragments. These observations collectively suggest that the core has been correctly attributed to tidal-channel sediments. Although the dated wood may lie

within the fill of an older tidal channel cut by the younger channel, erosional surfaces are not apparent within the lower part of the cores and associated radargrams (Figs. 3.3A, 3.4). We suggest that the dated wood was reworked from older deposits, as suggested for material at depth in core 5.

Aerial photo, satellite photo and map analysis documents the past 235-year history of Conrads Beach, linking long-term shore development interpreted from sub-surface data with recent coastal dynamics. A map from 1779 (Fig 3.7A), shows little land east of Fox Point whereas the 1865 map (Fig. 3.7B) shows a considerable extension of the beach-ridge area, which may have prograded until relatively recent times. Rates of erosion and deposition are non-uniform but average rates can be calculated by comparing the vegetation lines (Fig. 3.8). The overall change from 1865 to 2012 has been retreat along the beach. The average rate of retreat was about 1.1 ± 0.1 m/year from 1865 to 2012 near the center of the western beach (south of the buried channel) and about 1.6 ± 0.1 m/year along the eastern beach (150 m northeast of Fox Point). Periods of progradation, stasis and retrogradation indicate that coastal evolution has been complex.

Profile analysis provides additional insight into recent short term (decadal) change. While changes to the western beach have been consistent (Fig. 3.9 A,B) with the changes seen in Fig. 3.8, the eastern transect (Fig 3.9C) shows ~ 2.4 m/year (50 m in 21 years) of beach ridge/dune retreat. At its widest, the distance from the shore to the lagoonward edge of the beach ridges on the eastern beach is ~ 430 m (Fig. 3.1B). If the eastern transect retreat rate is

applied to this value, it would take ~ 181 years for the beach ridges to be eroded. Eastern shore erosion does not happen in isolation. At Transect B on the western beach, ~160 m of mixed vegetation, dunes and beach lie between the shore and the marsh (Fig 3.1B, 3.9B). If erosion here continued at a rate of 1.1 ± 0.2 m/year, the western beach would be eroded in ~145 years, although the coastal system may maintain its form as it retreats. Accelerated sea-level rise will likely cause the water levels in Eel River and West Marsh to increase, potentially inundating the marshes. Additional anticipated effects of sea-level rise include more frequent overwashing of beaches and destabilization of coastal dunes (Shaw et al. 1998). This two-pronged attack (from the Atlantic Ocean and from the Eel River-West Marsh tidal channel) may result in the formation of new tidal channels along the west beach, further reducing its longevity.

Correlation between photo analysis and known recent events suggests that the shorelines eroded rapidly during extreme events, with short-term (decadal) changes on both sides of Fox Point as the barrier system adjusted to changing environmental conditions. The western beach showed steady retrogradation on a century scale, and was narrowing prior to the development of the tidal channel between 1954 and 1962. The eastern beach has alternately retreated and prograded, and the cliffed foredunes drop steeply to the beach as a result of recent erosive events. Similar variable advance and retreat on either side of a local sediment supply was documented by Walker and Barrie (2006) from a high-sensitivity area on the Pacific coast of Canada.

Maps confirm that the marsh was established by the 1800s, and coring

indicates that new sediments slowly accumulated over it with progressively rising sea level. Coarser sediments in the topmost parts of cores 5, 8 and 9 in this area suggest increased overwash from the present beach in recent times, in accord with landward migration of the barrier. The Egg Island-Fox Island drumlin complex has been progressively eroded through this period, leaving boulder-retreat shoals over the former drumlin footprint and trailing shoals in its lee (Boyd et al. 1987; Carter et al. 1990; Forbes 2012).

Examining changes on a scale of thousands of years, the coastal system is transgressive, in a state of barrier retreat, punctuated with short-term progradation as local sediment sources become available. Conrads Head drumlin currently anchors the western side of the beach and Lawrencetown Head (a much smaller drumlin) anchors the eastern side. Although the environmental setting can only be assessed provisionally, the oldest dated sediment in the cores yields evidence that the area was in a near-littoral position, and a barrier may have bridged the area between these two drumlins and the Fox Island-Egg Island drumlins some 2500 to 3000 years ago. After local southward progradation and beach-ridge formation over the past ~600 years, barrier retreat was underway by the 1950s and probably much earlier. Gradual retreat of Lawrencetown Head, the demise of the Egg Island headland, and removal of any earlier seaward barriers left the eastern beach progressively more exposed to the open ocean as sediment supply from Egg and Fox Islands was effectively switched off.

Scott et al. (1995) showed that 7000 years BP, sea level was ~ 21 m below

present higher high water at large tide (HHWLT) at Chezzetcook (Fig. 3.10). Relative sea-level (RSL) rise accelerated from ~ 5000 to 4000 years BP and then decelerated to approximately 1.6 mm/yr from 4000 to about 150 years ago (Scott et al. 1995; Gehrels et al. 2004). To plot the elevations of our dated samples (Table 3.4) relative to this sea-level curve based on HHWLT, we reduce the elevation by the height of HHWLT above our 'Mean Sea Level' (MSL) datum (CGVD28 = Canadian Geodetic Vertical Datum of 1928). Because MSL has been rising at ~3.2 mm/year in this region over the past century (Forbes et al. 2004, 2009), it is now about 27 cm above CGVD28. The elevation of HHWLT at Chezzetcook above CGVD28 was determined to be 1.14 m in 1964 (P. MacAulay, pers. comm., 2014) and sea level has risen about 15.4 cm since that time, so that HHWLT today is about 1.29 m above CGVD28. Subtracting this value from our sample elevations, we obtain the elevations relative to HHWLT at Chezzetcook (Fig 3.10).

The beach ridge samples (343156 and 343157) and shallow peat samples (343159 and 343161) are fairly young and their depth vs. age positions mostly plot along the Scott et al. (1995) sea-level curve (Fig. 3.10). This consistency with the sea-level curve was expected. The older samples that plot farthest from the RSL curve are 343158 (tidal channel), 343160 (deep shell) and 343162 (deep peat). We suspect the tidal channel sample to have been reworked and therefore not in its original stratigraphic position or geologic location. It is also possible that 343160 and 343162 are reworked, but in contrast to the tidal channel sample, this is difficult to determine from the GPR sections.

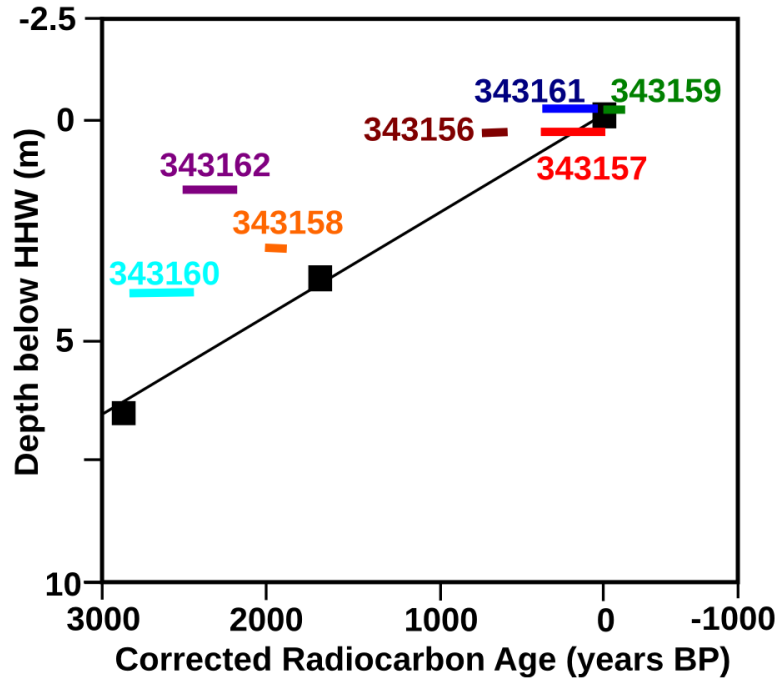


Figure 3.10 Comparison of results to Scott et al. (1995). See Table 3.4 for additional information regarding lab sample numbers 343156-343162.

Our results match well with those of Boyd and Honig (1992), who documented the history of Lawrencetown Lake, a lagoon situated behind the barrier at Lawrencetown Head just east of our study area. Cores in the lagoon terminated in brackish muds that were dated at 3220 ± 150 years BP. An upward passage into coarser flood-tide delta sediments by 1990 ± 130 years BP represents sediment entering the lagoon through tidal inlets in a barrier. This barrier system may have been a continuation of the littoral facies deposited at Conrads Beach by 2880 years BP. Erosion of Half Island Point drumlin to the east resulted in eastward longshore sediment transport, eventually closing an earlier inlet to Lawrencetown Lake east of Lawrencetown Head through the development of spits and beach ridges. Our results are also supported by

Hoskin (1983) who obtained a date of 700 years BP for beach-ridge formation at Lawrencetown Beach. Breaching of the barrier just east of Eel River (Fig. 3.1, northeast corner of study area) between 800 and 200 years ago led to the formation of a younger flood-tide delta in the lagoon.

As sea-level continues to rise and the current sediment supply diminishes, Conrads Beach will fail or be overtaken, as another discrete package of glacial sediment is used up (Boyd et al. 1987; Forbes 2012). The loss of the Egg Island drumlin has effectively shut off the sediment supply from that end of the beach. Conrads Head is sufficiently large that it will continue to provide the western anchor, and drumlins north of Conrads Beach may eventually be tapped to provide a new eastern anchor and sediment supply for a new barrier system in the West Marsh embayment. In the meantime, sediment eroded from the Eastern Beach may be largely reworked into the Eel River and Lawrencetown Lake estuaries, providing sand for future reworking and beach formation as the coast retreats.

3.7. Conclusions

The majority of the world's coastlines are transgressive (Boyd 2010) and more will become so with accelerated global sea-level rise (Rahmstorf et al. 2007; Church et al. 2013). Where present, rivers are an important sediment source for beach and dune building, acting to maintain coastal systems, but large sections of global coastlines lack river sediment input. This case study documents the history of barrier evolution on a transgressive, paraglacial coast

where episodic sediment supply is highly sensitive to geomorphic change. The results show that the magnitude and direction of coastal change is closely related to short-term sediment supply, as well as to oceanographic and atmospheric events. Eroding landforms such as drumlins may temporarily delay coastal retreat or even cause progradation over a period of centuries. This study has documented one such case in which there may have been a recent switch from progradation to erosion, highlighting the risks of assuming that recent rates of change are a guide to future rates in coastal planning. This study demonstrates the potential complexity of coastal systems and the need for holistic analysis for projection of future coastal development in such settings. This study may thereby serve as a cautionary tale and a model for approaches to the challenges of coastal transgression on other paraglacial or similarly complex coasts with limited sediment supply.

3.8. Acknowledgments

This research was funded by a Lew King Award to Forde, and by Natural Sciences and Engineering Research Council (NSERC) Discovery Grants to Gibling and Nedimović. The authors thank D. O'Connor, P. Regan, T. Duffet, J. Thibodeau, A. Farkas, F. Walsh, B. Louis, K. Landry, H. Kuehn, and J. Evangelatos for assistance in the field. Dalhousie University Earth Sciences 2270 students from 2007 and 2010-2012 assisted with GPR acquisition and refraction seismic acquisition and data processing. O. Brown (Geological Survey of Canada) and P. MacAulay (Canadian Hydrographic Service) provided advice

and assistance with grain-size analyses and tidal datum issues, respectively. R.B, Taylor and D. Frobel (Geological Survey of Canada) provided aerial photographs of Conrads Beach and were responsible for many of the beach surveys. A special thank you to Mr. & Mrs. Welch and Mr. Hood, nearby landowners, for their assistance and advice.

CHAPTER 4: DISCUSSION

4.1 Comparison to Other Sites in Atlantic Canada

The reconnaissance study sites are geographically distributed across Atlantic Canada (Fig 4.1) and represent three distinctive environments of coastal evolution: the Gulf of St. Lawrence, the Northumberland Strait, and the Atlantic Ocean.

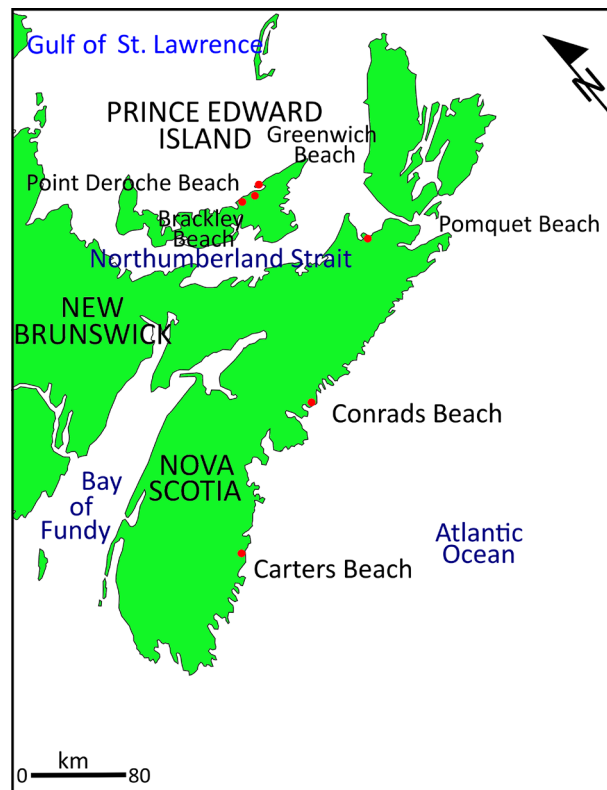


Figure 4.1 Locations of reconnaissance study sites in relation to Conrads Beach. Modified from Shaw et al. (1998).

Differences in precipitation, land temperatures and ocean temperatures in these three environments have been measured (Table 4.1). Seasonal variations in ocean and land temperatures contribute to storminess (Table 4.1). Due to its subdued relief and small size, the climate of PEI is fairly uniform across the

Table 4.1 Study site environments. Meteorological information from Phillips (1990).

Features	Coastal Environments		
	Atlantic Ocean	Northumberland Strait	Gulf of St. Lawrence
Precipitation	1500 mm / year	< 1000 mm / year	1100 mm / year
Summer ocean surface temperature	15.0 °C	17.9 °C	16.1 °C
Average summer temperature	17.4 °C	24.0 °C	18.5 °C
Winter ocean surface temperature	0.7 °C	-1.0 °C	0.0 °C
Average winter temperature	-3.0 °C	-6.0 °C	-7.0 °C

island. Fall and winter storms bring a variety of weather conditions including hurricane force winds, heavy precipitation (rain, snow, and/or freezing rain), high tides, storm surges, and winds up to 100 km/hour (Phillips 1990). NS has more storms per year than any other part of Canada and storms pass the Atlantic coast of the province frequently (Phillips 1990). Severe winter storms (nor'easters) often reach wind speeds of 150 km/hour and can generate 14 m waves (Phillips 1990). Winter storms are also known to bring freezing spray, snow, rain, sleet and/or fog, and subzero-wind-chill temperatures (Phillips 1990).

In addition to representing three coastal environments, the study sites were also selected to represent areas of moderate to high SI (Fig. 4.1) and easily accessible coastal systems for surveying. Table 4.2 lists the key features of the six study sites (Conrads Beach included).

Table 4.2 Features of coastal dune study sites. 1. White (2002, 2010). 2. Utting and Gallacher (2009). 3. Mathew et al. (2010). 4. Shaw et al. (1998)

Features	NS Study Sites			PEI Study Sites		
	Conrads Beach	Carters Beach	Pomquet Beach	Point Deroche Beach	Brackley Beach	Greenwich Beach
Coastal environment	Atlantic Ocean		Northumberland Strait	Gulf of St. Lawrence		
Degree of exposure	Exposed to open ocean	Partially sheltered by Spectacle Islands	Partially sheltered by Monks Head	Partially sheltered by North Rustico	Exposed to open ocean	Exposed to open ocean
Bedrock	Cambrian-Ordovician Meguma meta-sedimentary rocks ¹		Early Carboniferous marine sedimentary rocks ²	Pennsylvanian-Permian sandstone and shale ³		
Till	Yes	Yes	Yes	Yes	Yes	In subsurface
Beach length	1.5 km	1.4 km	3.8 km	4.6 km	7.5 km	5 km
Dune heights	1-2 m	2-4 m, up to 10 m at the ends	1-3 m	5+ m	12+ m	10+ m ³
Vegetation cover	Beach grass	Beach grass, trees	Beach grass, low shrubs	Beach grass, low shrubs	Beach grass, small shrubs, trees	Beach grass
Wetlands	Marsh, Eel River	Small river	Marsh	Marsh & pond	none	Marshes & ponds
Tidal Channel	Yes	No	No	No	No	No
Coastal sensitivity ⁴	High	High	Moderate	High	High	High

4.1.1 Carters Beach, NS

Carters Beach shares the same environment, bedrock, till, and coastal sensitivity as Conrads Beach, resulting in similar vegetation cover and water features (Table 4.1). Located on the South Shore of NS (Fig. 4.1), it is approximately 15 km from the town of Liverpool and is a popular recreational area. This beach consists of three crescent-shaped beaches (Fig. 4.2A). A

series of undulating foredunes, 2-4 m in height, is aligned parallel to the central 700 m long portion of the beach. They are vegetated with beach grass and the backdunes are densely vegetated with trees. At the southern end of the beach, the dunes are on the order of 10 m in height. A meandering river separates the northermost crescent from the rest of the beach. During this study, the river has been observed alternately on the eastern side and the western side of the small island at the channel mouth (Fig. 4.2A). Hales (1992) reported mean grain sizes of 2.42 phi, 2.48 phi, 2.44 phi, and 2.97 phi for the foreshore, backshore, ramp and crest, respectively. The southern end of the center beach appears to be prograding (Hales 1992).

During the spring/summer 2010 field season, 34 GPR/GPS lines were acquired parallel and perpendicular to the shore (Fig. 4.2A). User error resulted in the GPR data being spatially undersampled at this location, resulting in low resolution data for ~ 2/3 of the lines. It would be anticipated that seaward-sloping, sigmoidal, dipping subparallel, moderately continuous reflectors (radar facies 2) would be found where this beach is prograding. Traverse 32 (Fig. 4.2B) was acquired at the northwest section of the beach. In addition to the topography and internal dune/beach ridge fill, a strong, seaward dipping reflector is visible at depth. Traverse 5 was acquired near the center of the middle crescent. The radargram shows a series of seaward dipping, sigmoidal reflections at depth. The easternmost traverse (traverse 2, Fig 4.2A) was located several meters inland from the shore.. The radargram (Fig 4.2C) shows chaotic discontinuous facies (dune deposits), and a strong reflector crosscutting all other

signals (water table).

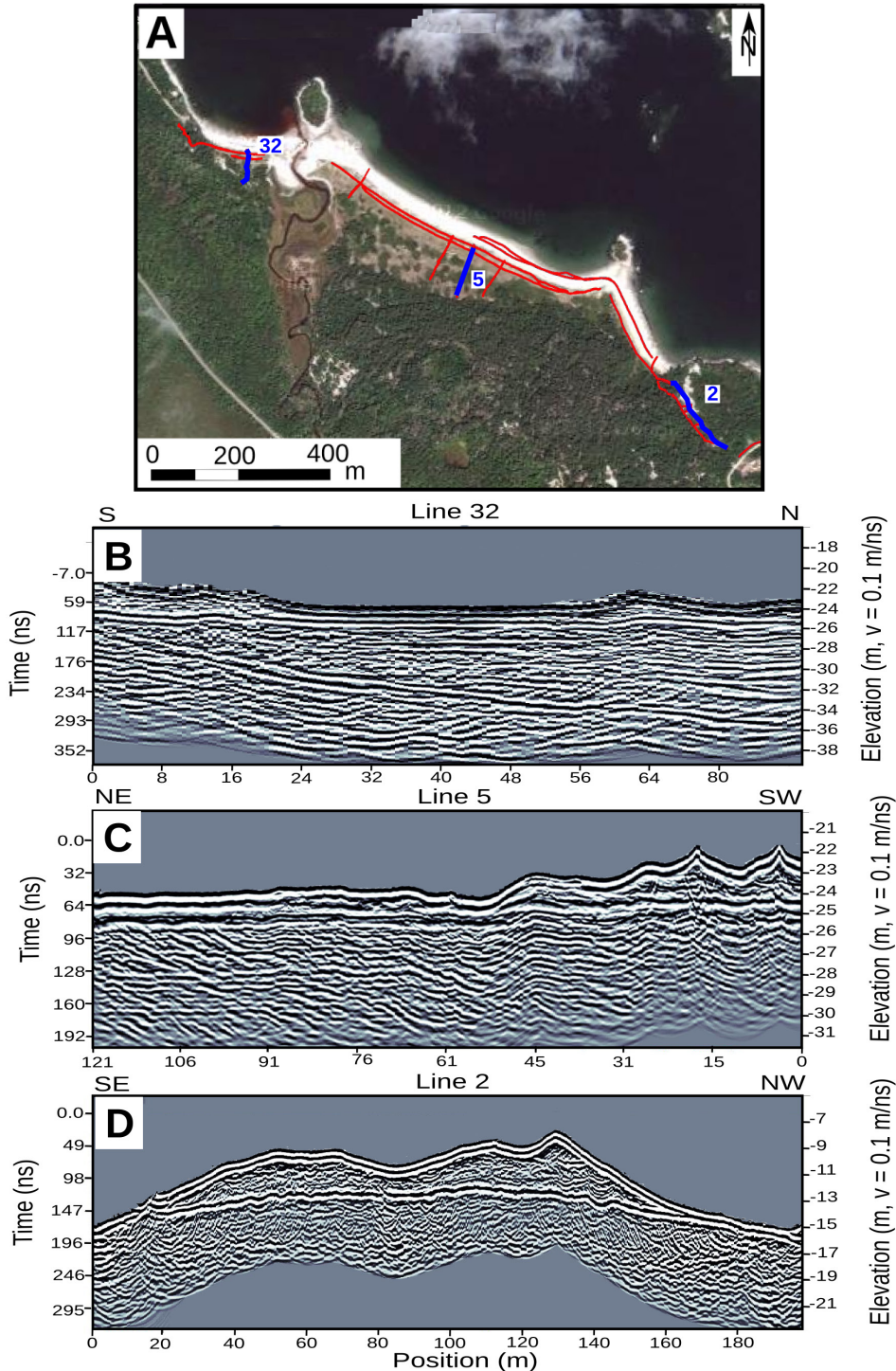


Figure 4.2 Carters Beach reconnaissance GPR/GPS lines and sample radargrams. (A) Carters Beach aerial photo (Google Maps 2012 CNES/SPOT Image, Digital Globe) with GPR/GPS traverses in red and blue. (B) Line 21 was acquired using 100 MHz antennas. (C) Line 16 was acquired using 200 MHz antennas. (D) Line 2 was acquired using 200 MHz antennas.

4.1.2. Pomquet Beach, NS

Pomquet Beach is located on the north shore of Nova Scotia, along the Northumberland Strait (Fig.4.1). Here the longshore transport is mainly to the east (Hales 1992; Utting and Gallacher 2009). An eroding till drumlin bluff is located west of Pomquet Beach and this material is deposited at the eastern end of Pomquet Beach (Utting and Gallacher 2009). Pomquet Beach is a well established prograding coastal system (Shore 1996) with foredunes vegetated with low shrubs and grasses, and heavily treed backdunes. The geomorphology of Pomquet Beach includes beaches, yellow dunes, grey dunes, heath and forest (McCann 1990). A network of boardwalks protects the marsh areas and delicate vegetation. Hales (1992) reported mean grain-sizes of 1.95 phi, 1.45 phi, 1.68 phi, and 1.70 phi for the foreshore, backshore, ramp and crest, respectively. An important difference between Pomquet Beach and the two beaches along the Atlantic Coast of NS is that St. Georges Bay (east of Pomquet Beach) freezes over during the winter (Atlas of Canada 2009). The resulting landfast ice protects the beach from coastal erosion that might otherwise occur during some winter storms (Utting and Gallacher 2009).

During the spring/summer 2010 field season, 46 GPR/GPS lines were acquired along the boardwalks, both perpendicular and parallel to the shoreline (Fig. 4.3A). User error resulted in the GPR data being spatially undersampled at this location, resulting in low resolution data. Given the history of prograding coastal systems at Pomquet Beach, a series of beach ridges with the oldest farthest from the current shore would be expected (similar to the eastern beach at Conrads Beach). Traverse 22 started in the backdunes and continued towards

the shore, near the center of the beach. The radargram (Fig. 4.3B) shows a series of crest and troughs (radar facies 1) with the largest ones closest to the beach. The internal stratigraphy of the largest troughs is similar to radar facies 4 at Conrads Beach. Below a strong reflector at 90 ns, there is a series of seaward dipping reflectors. While the radargram is inconclusive regarding the true nature of these reflectors, they may represent prograding beach ridges.

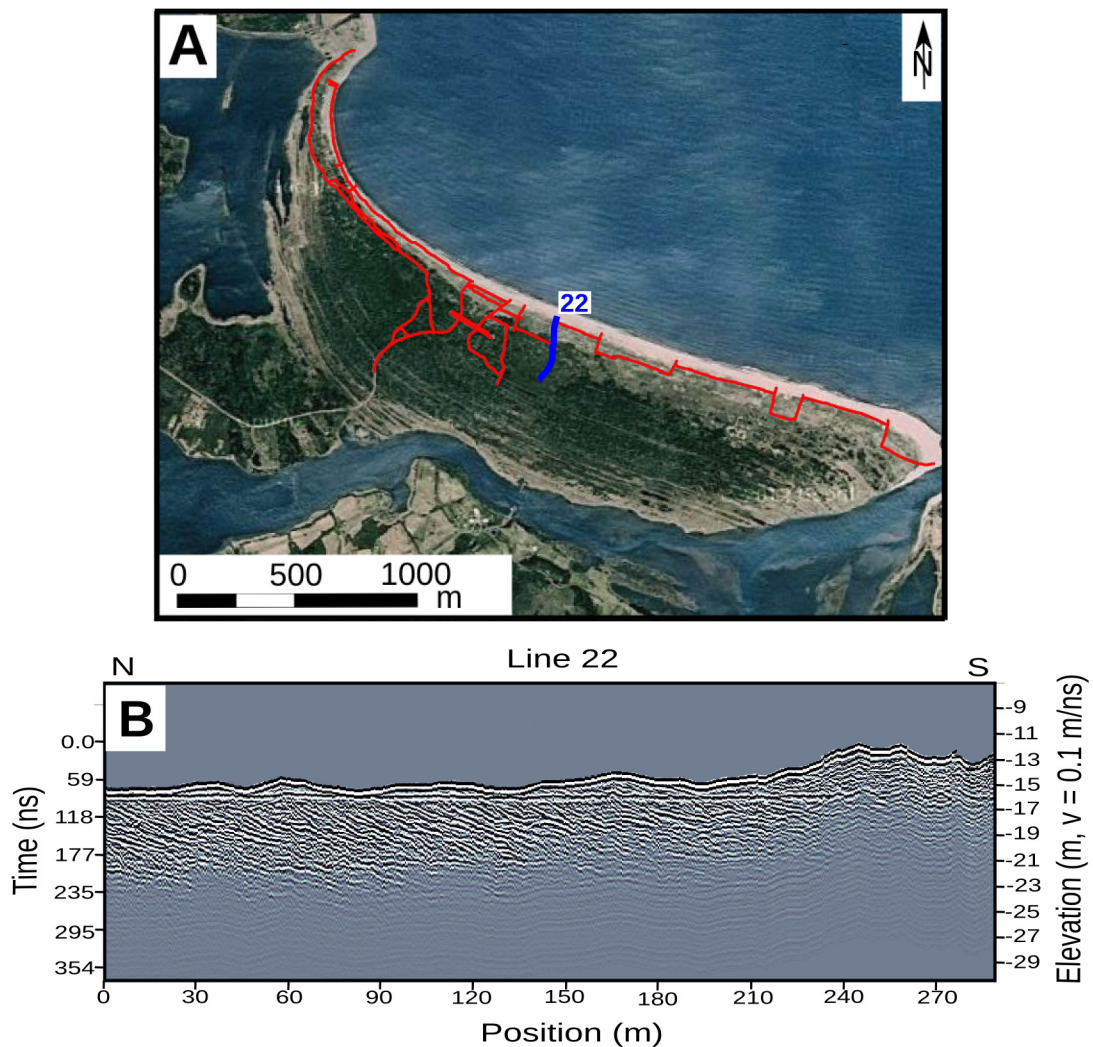


Figure 4.3 Pomquet Beach reconnaissance GPR lines and sample radargram. (A) Pomquet Beach aerial photo (Google Maps 2012 CNES/SPOT Image, Digital Globe) with GPR/GPS traverses in red and blue. (B) Line 22 was acquired using 200 MHz antennas.

4.1.3 Point Deroche Beach, PEI

Point Deroche Beach is located along the north shore of PEI, between the two parts of Prince Edward Island National Park (Fig. 4.1), both part of the island's central embayment (Shaw et al. 2008). This area is known to contain soft retreating bedrock cliffs and six estuary complexes (Shaw et al 2008). This microtidal, low wave energy environment experiences prevailing offshore winds from a westerly and southwesterly direction (Nutt and McCann 1991) and was subjected to sea-level rise on the order of 30 cm/century over the past 6000 years (Forbes et al. 2004). Approximately 50% of the northern shore of PEI has sandy spits, barriers and beaches, with dunes in the backshore zone (McCann 1990; Forbes et al. 2004). Maps from 1765 show continuous dune lines, lagoons, barrier islands, and channels along the north shore of PEI (Forbes et al. 2004). A series of major storms in the 1870s reworked these dune systems (McCulloch et al. 2002; Forbes et al. 2004). The majority of significant storms are extratropical and may result in high sediment transport rates and rapid profile changes (Forbes et al. 2004). In contrast, tropical storms that reach the northern shore of PEI tend to be weak and travel rapidly in an offshore direction, and as a result do not produce large storm surges (Mathew et al. 2009).

A 1935 air photo shows dune consolidation and recovery from the 1870 storm events (Forbes et al. 2004). Nutt and McCann (1991) reported that 80% of the dune frontage at Point Deroche Beach advanced seawards between 1938 and 1980 and 20% retreated landward during the same period. Forbes et al. (2004) reported that the overall coastal retreat ranged from <0.5 to 1.5 m/year

from 1935 to 1990 in the vicinity of Point Deroche Beach.

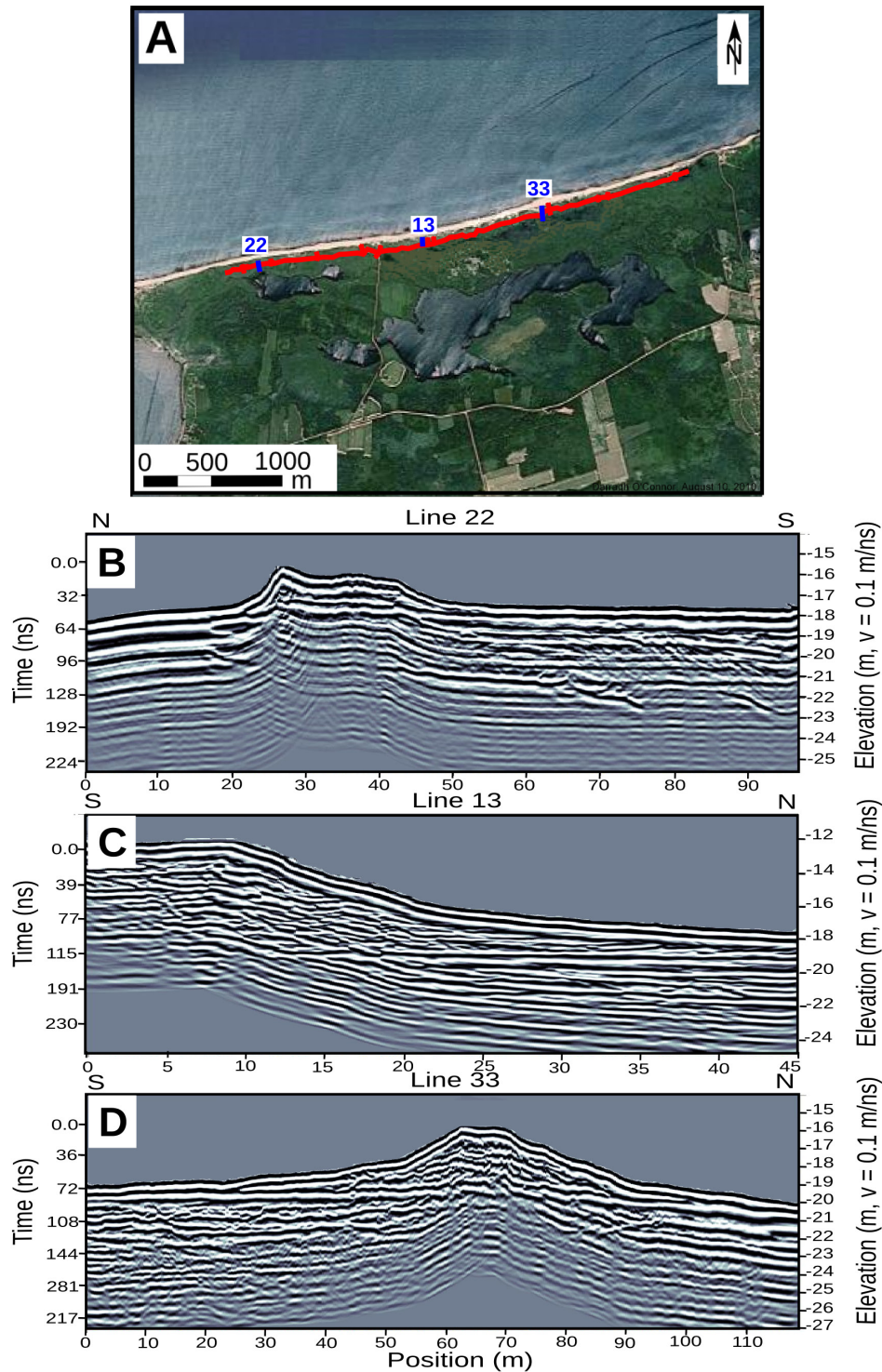


Figure 4.4 Point Deroche Beach reconnaissance GPR/GPS lines and sample radargrams. (A) Point Deroche Beach aerial photo (Google Maps 2012 CNES/SPOT Image, Digital Globe) with GPR/GPS traverses in red and blue. (B) Line 22 was acquired using 200 MHz antennas. (C) Line 13 was acquired using 200 MHz antennas. (D) Line 22 was acquired using 200 MHz antennas.

During the spring/summer 2010 field season, 33 GPR/GPS lines were acquired parallel and perpendicular to the shoreline (Fig 4.4A). User error resulted in the GPR data being spatially undersampled for approximately one third of the radargrams. The dunes were vegetated with beach grasses and shrubs but large blowouts were visible. The mid-dunes were densely vegetated with shrubs and the back-dunes included several marshy areas. Traverse 22 began near the shore at the western end of the beach. The radargram shows an internal dune stratigraphy which is similar to the topography (Fig. 4.4B). This stratigraphy does not resemble Conrads Beach radar facies 3 (beach ridges) or radar facies 4 (chaotic dune fill) (see Fig 3.2) but could be indicative of either landform. Given the predominant westerly and southwesterly wind direction, this stratigraphy could be the result of rather uniform aeolian deposition. Alternatively a series of washover events could have deposited uniform layers of sediment or it could be the result of aggradation (the vertical accumulation of sediment).

Traverse 13 is oriented perpendicular to the shore near the middle of the beach and continued from the backdune towards the shore (Fig.4.4A). The radargram (Fig. 4.4C) shows internal dune stratigraphy that tends towards the chaotic dune fill observed at Conrads Beach. Traverse 33 was acquired near the eastern end of the beach (Fig 4.4A) and covered the backdune, an isolated dune crest and the beach to the north. In addition to the topography, the radargram (Fig. 4.4D) shows a dune fill that is intermediate between the chaotic dune fill observed at Conrads Beach (Fig. 3.2) and the topography following dune fill of traverse 13 (Fig. 4.4C).

4.1.4 Brackley Beach, PEI

Brackley Beach is located in the western portion of Prince Edward Island National Park (Fig. 4.1). At the west end of the beach, eroded redbed bedrock is visible along the shore and in the steep cliff face. Given the open, linear beach shape and high SI, retrogradation might be expected. However, erosion of the soft bedrock and sandy glacial deposits provides an abundant sand supply to this microtidal, low-wave-energy environment (Armon and McCann 1979). As shown by the results from Conrads Beach, a plentiful sand supply can result in short-term stasis and/or progradation on a transgressive coast.

In 1765 Brackley Beach had high dunes and a channel behind the beach but by 1880 the channel had been filled (Forbes et al. 2004). A 1935 air photo shows washover flats in many former dune locations (Forbes et al. 2004). A subtropical storm on October 29, 2000 is known to have trimmed the dunes at Brackley Beach and a hybrid storm on November 7, 2001 breached the dunes (Forbes et al. 2004).

During the spring/summer 2010 field season 42 GPR/GPS lines were collected perpendicular and parallel to the shore (Fig.4.5A). Traverse 41 was oriented perpendicular to the shore and was located ~ 2.3 km from the eastern end of the beach. The associated radargram (Fig. 4.5B) is typical of the reconnaissance data obtained at this location during this study. While the internal dune stratigraphy was visible, the large size of the dunes (in excess of 12 m) meant the GPR penetration depth of 6-8 m was insufficient to determine the stratigraphy below the dunes.

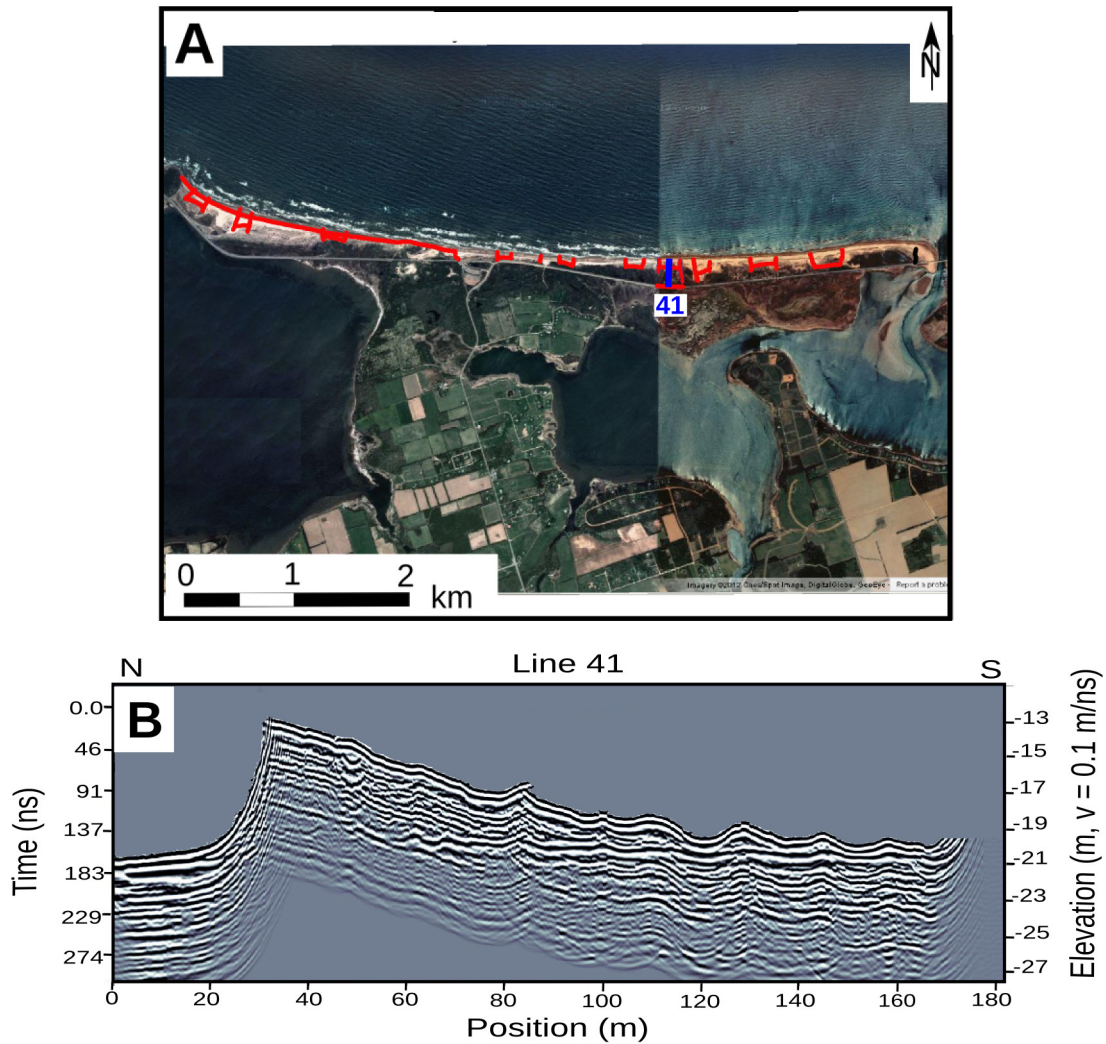


Figure 4.5 Brackley Beach reconnaissance GPR/GPS lines and sample radargram. (A) Brackley Beach aerial photo (Google Maps 2012 CNES/SPOT Image, Digital Globe) with GPR/GPS traverses in red and blue. (B) Line 41 was acquired using 200 MHz antennas.

4.1.5 Greenwich Beach, PEI

Greenwich Beach is located in the eastern portion of Prince Edward Island National Park (Fig. 4.1). While located farther east than Brackley Beach or Point Deroche Beach, Greenwich Beach is still in the area of relatively weak, rapidly eroding bedrock, which provides enough sediment to prevent rapid transgression

by the combination of sea-level rise and intense storm events (Mathew et al. 2009). This coastal dune system includes a large marsh in the backdunes, a series of large parabolic dunes, and three ponds. Older dunes form a transgressive dune field that overlies a shallow bedrock and till surface (Mathew et al. 2009). While the foredunes are vegetated with beach grasses, the mid-dunes and backdunes are densely vegetated with shrubs. Here the westerly winds tend to result in parabolic dune sand blowouts that are oriented towards the east (Mathew et al. 2009). In 1923 a storm surge resulted in catastrophic overwash at Greenwich Beach (Mathew et al. 2009). Thirteen years later, low transgressive dunes (dunes formed by the downwind movement of sand over vegetated and/or semi-vegetated ground (Hesp and Thom 1990)) were migrating landward, but the area remained extensively overwashed and re-vegetation of foredunes had not occurred (Mathew et al. 2009). By 2005, transgressive dunes were developing at the landward margins of the overwashed areas (Mathew et al. 2009). Mathew et al. (2009) also reported that the eastern half of Greenwich Beach is eroding while the western end is prograding.

During the spring/summer 2010 field season, 34 GPR/GPS lines, oriented approximately parallel or approximately perpendicular to the shore, were acquired at Greenwich Beach. Internal dune stratigraphy was imaged but sufficient evidence for dune migration was lacking because the GPR was unable to penetrate below the dunes. Line 21 (Fig. 4.6B) went across a low, flat area, up a small mound and then up the seaward face of a large parabolic dune. The internal stratigraphy has a slight seaward slope below the low flat area and

chaotic dune fill is visible in both the mound and parabolic dune (facies 4). Line 16 (Fig 4.6C) was oriented perpendicular to the shore, approximately 2 km from the west end of the beach. Line 2 (Fig 4.6D) was oriented perpendicular to the shore, near the eastern beach access. In both cases there is horizontal stratigraphy (facies 1) near the beach and chaotic dune fill (facies 4).

4.1.6 Reconnaissance Beach Summary

All six Atlantic Canada study areas are on transgressive coasts with either a high or moderate sensitivity index (Fig. 4.1). While the PEI sites share the same environment (Gulf of St. Lawrence) and bedrock geology, the three dune systems demonstrate great variability in dune size and form. The long-term tide-gauge records at Charlottetown, PEI show relative sea-level rise of 0.32 m/century over the past 100 years (Parkes et al. 2002) and the island is uniformly subsiding at a rate of 0.2 m per century (McCulloch et al. 2002). Under these conditions, it should be possible to obtain GPR/GPS evidence for seaward growth of the coastal systems. Due to the large size of the dunes and the 6-8 m GPR penetration depth, it was not possible to image below the dunes.

Both Carters Beach and Pomquet Beach are known to have prograding sections so it should be possible to find subsurface evidence of dune migration. Unfortunately spatially undersampled data resulted in a sufficiently high number of poor resolution radargrams as to make this a difficult task. At Carters Beach the presence of a river and a nearby bedrock islands (which partially protect the shoreline during high water events) may affect rates of sedimentation and

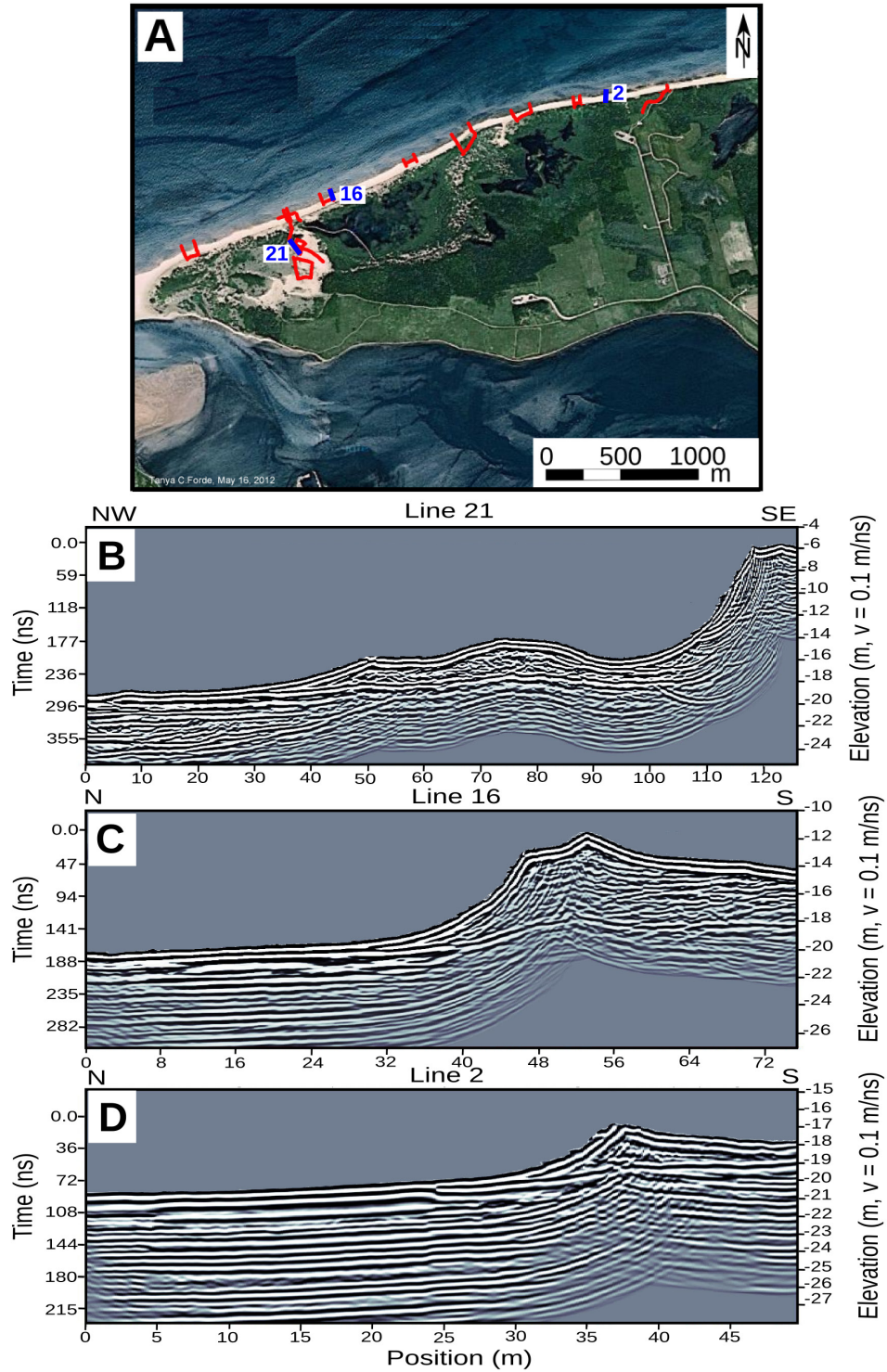


Figure 4.6 Greenwich Beach reconnaissance GPR/GPS lines and sample radargrams. (A) Greenwich Beach aerial photo (Google Maps 2012 CNES/SPOT Image, Digital Globe) with GPR/GPS traverses in red and blue. (B) Line 21 was acquired using 100 MHz antennas. (C) Line 16 was acquired using 200 MHz antennas. (D) Line 2 was acquired using 200 MHz antennas.

erosion by altering wind flow and mitigating high water events. Pomquet Beach is the only site in this study where the beach ridge/dune system was locked onto an island. Additionally its sediment supply comes from alongshore easterly sediment transport (Hales 1992; Utting and Gallacher 2009), suggesting a long history of progradation and/or stasis at the eastern end of the beach. Potentially the long-term history could show that the island was much smaller a thousand years ago.

4.2 Future Work

The history established here for Conrads Beach could be improved with additional work. Foraminiferal analysis would provide insight into the depositional environments of deeper layers and may assist in locating former mean high water levels in the cores (Boyd and Honig 1992; Scott et al. 1995; Gehrels et al. 1996). Acquiring additional vibracores in the beach ridges would provide additional sediment samples for comparison with existing beach ridge and dune samples, and aid in establishing the environment of deposition for existing samples. They may also provide suitable materials for radiocarbon dating, which could potentially determine the ages of the beach ridges more precisely and perhaps establish a higher resolution history of beach ridge progradation. Alternatively, the sands could be dated directly using optically stimulated luminescence dating.

To test the validity of using Conrads Beach as a model for coastal evolution on a transgressive coast in Atlantic Canada, similar studies at the other

five study sites could be carried out. Additional GPR/GPS surveying would provide improved coverage and increase the likelihood of imaging radar facies 2 (tidal channels), 3 (beach ridges) and/or 4 (chaotic dune fill) (Fig. 3.2). These facies are key indicators of stratigraphic change. While Carters Beach has a small river, none of the five reconnaissance sites had a tidal channel. Studying them and comparing the results to Conrads Beach could provide additional insight into the role of tidal channels in reworking barrier systems. Should the GPR/GPS surveying provide suitable targets, vibracoring would provide sediment samples for further analysis and may determine water table depths. Depth to the water table would provide additional constraints on the GPR data, which in turn would improve the interpretation. In addition to core logging and grain-size analysis, vibracoring may produce suitable samples for radiocarbon dating.

CHAPTER 5: CONCLUSIONS

Conrads Beach represents a coastal system along a transgressive drumlin shore bordering the Atlantic Ocean in NS. Similar coastal systems with barriers, dunes, tidal channels, and lagoons are distributed worldwide and play an important role in protecting inland areas from high-water events. Global sea-level rise is accelerating and consequences of this change include increases in high-water events and storminess. The Atlantic coast of Canada is highly susceptible to geomorphological change as a result of increased sea-level. In addition to a high SI, Conrads Beach is near Lawrencetown Beach (various features of which have been dated), Chezzetcook Inlet (the subject of many sea-level rise studies) and Halifax (with a tide-gauge record). It also has an abundant historical record providing in excess of 300 years of natural and anthropogenic events since the start of European settlement.

GPR/GPS surveying imaged the subsurface to depths of 6-8 m and four facies were identified. Radar facies 1 (continuous planar to sinuous, parallel to subparallel reflectors with a sheet to sheet-drape configuration) includes the air/wave ground wave and horizontal stratigraphy (Fig. 3.2A, B, C, F). Radar facies 2 (planar to sigmoidal, dipping, subparallel, moderately continuous reflectors with erosional boundaries) represent tidal channel deposits (Fig. 3.2A, D). Radar facies 3 (moderately continuous, sinuous, horizontal to dipping, parallel reflectors) represent beach ridges (Fig. 3.2 B, E). Radar facies 4 (low-amplitude, discontinuous reflectors) represents poorly stratified dune fill (Fig 3.2 F).

Refraction seismic surveying imaged the basement at depths of ~ 20 m along the foredune and beach ridges behind the eastern beach, as well as the foredune and lagoon areas behind the central beach, and ~ 10 m under the western beach. This suggests that most of the preserved thickness of the unconsolidated sediments has been imaged with the GPR near the western beach and approximately half in other investigated areas of the Conrads Beach coastal system.

The thirteen vibracores provided abundant materials for identifying core lithofacies, radiocarbon dating, and grain-size analysis. The eight core lithofacies range from gravel to silt and peat. Grain-size analysis showed distinctive signatures for tidal-channel deposits, and differentiated some beach sands from dune sands in other cores. Radiocarbon dating showed that peat formation occurred within the last 428 years BP and beach ridge formation began ~ 646-527 years BP. The deepest and oldest sample was in core 9 and had an age of 2878-2418 years BP. The depth of this sample puts it outside the confidence interval for this core and grain-size was inconclusive. The next oldest sample was peaty-material at depth in core 5. With an age of 2559-2185 years BP, it may be reworked. At 1998-1830 years BP the tidal channel sample was much older than expected and was likely reworked.

Map and photograph comparisons demonstrate both a reduction in land area at the Egg Island-Fox Point peninsula and an increase in land area at the eastern beach. The 1865 to 2012 vegetation lines reinforce a story of retrogradation and stasis along the western beach, drowning of a boulder retreat

shoal offshore of Fox Point and long-term retrogradation with periods of progradation along the eastern beach. Profiles from 1987 to 2008 show a steady landward retreat of the dunes along the eastern beach. The story is more complicated along the western beach where erosion due to storm/high water events, seasonal beach building (summer) and erosion (winter) cycles, and long-term retrogradation have all been documented.

The preliminary reconnaissance site data provided additional information regarding coastal barrier processes. While Conrads Beach and Carters Beach share many features (Table 4.2), the dunes are significantly larger at Carters Beach. This suggests a different depositional and/or erosional history. Pomquet Beach is more sheltered and less sensitive to geomorphological change than its Atlantic Ocean neighbours (Table 4.2). While this system lacks drumlins, longshore transport has provided material for progradation. While the PEI sites share many features, they are distinctly different from the NS sites (Table 4.2). The PEI dunes are more exposed, and they have been severely impacted by storms in the past 300 years. Their large size is a testament to an abundant sediment supply and efficient deposition.

Processes on transgressive coastlines are complex. Conrads Beach demonstrates that retrogradation, progradation and stasis are all possible responses to accelerating sea-level rise. The factor that may ultimately play the largest role in determining which of these shoreline states occurs and over what period is the sediment supply. As an example, beach ridges at Conrads Beach appear to have formed ~ 600 years ago, and prograded seaward until the

1980s, probably due to sediment supplied by the Egg Island-Fox Island drumlin. The dynamic nature of coastal processes also means that short-term changes such as storm effects are superimposed upon long-term trends such as millennial-scale cycles of barrier progradation, retreat, destruction and re-establishment. Conrads Beach in its present state will be destroyed as barrier retreat continues. Eventually, a new barrier will be established farther inland, anchored to drumlins or bedrock islands and perhaps maintained for a few centuries by sediment supplied from drumlin erosion or reworked coastal sand.

REFERENCES

Aadachi, 1954. On a proof of fundamental formula concerning refraction method of geophysical prospecting and some remarks. *Kumamoto Journal of Science Series A*, 18–23.

Annan, A.P., 2009. Electromagnetic principles of ground penetrating radar, in: Jol, H.M. (Ed.), *Ground Penetrating Radar: Theory and Applications*. Elsevier Science, New York, pp. 3–40.

Armon, J.W., McCann, S.B., 1979. Morphology and landward sediment transfer in a transgressive barrier island system, Southern Gulf of St. Lawrence, Canada. *Marine Geology* 31, 333–344.

Atlas of Canada 6th Edition Late Winter Sea Ice Conditions, 2009.
atlas.gc.ca/data/english/maps/thenorth/late_winter_sea_ice_conditions.pdf
Accessed 2014-04-04

Balsillie, J.H., Donoghue, J.F. 2004. High resolution sea-level history for the Gulf of Mexico since the Last Glacial Maximum: Florida Geological Survey, Report of Investigations 103, 65 p.

Bindoff, N.L., Willebrand, J., Artale, V., Cazenave, A., Gregory, J., Gulev, S., Hanawa, K., Le Quere, C., Levitus, S., Nojiri, Y., Shum, C.K., Talley, L.D., Unnikrishnan, A., 2007. Observations: Oceanic Climate Change and Sea Level., in: Solomon, S., Qin, D., Chen, Z., Marquis, M., Averty, K.B., Tignor, M., Miller, H.L. (Eds.), *Climate Change 2007: The Physical Science Basis. Contribution of Working Group I to the Fourth Assessment Report of the Intergovernmental Panel on Climate Change*. Cambridge University Press, United Kingdom and New York, pp. 385–432.

Bird, M., May 26, 1984. A new 1,500-acre provincial park will begin in July. *Chronicle Herald –Mail Star*, Halifax.

Bird, E., 2000. *Coastal Geomorphology: An Introduction*. John Wiley & Sons Ltd., Rexdale, ON.

Belknap, D.F., Anderson, B.G., Anderson, R.S., Anderson, W.A., Borns, H.W.J., Jacobson, G.L., Kelley, J.T., Shipp, R.C., Smith, D.C., Stuckenrath, R.J., Thompson, W.B., Tyler, D.A., n.d. Late Quaternary sea-level changes in Maine.

Blott, S.J., Pye, K., 2001. GRADISTAT: A grain size distribution and statistics package for the analysis of unconsolidated sediments. *Earth Surface Processes and Landforms* 26, 1237–1248.

Boyd, R., 2010. Transgressive wave-dominated coasts, in: James, N.P., Dalrymple, R.W. (Eds.), *Facies Models*. Geological Association of Canada, St. Johns, pp. 265–294.

Boyd, R., Bowen, A.J., Hall, R.K., 1987. An evolutionary model for transgressive sedimentation on the Eastern Shore of Nova Scotia, in: Fitzgerald, D.M., Rosen, P.S. (Eds.), *Glaciated Coasts*. Academic Press, San Diego, pp. 87–114.

Boyd, R., Honig, C., 1992. Estuarine sedimentation of the Eastern Shore of Nova Scotia. *Journal of Sedimentary Petrology* 62, 569–583.

Bristow, C.S., Chroston, P.N., Bailey, S.D., 2000. The structure and development of foredunes on a locally prograding coast: insights from ground-penetrating radar surveys, Norfolk, UK. *Sedimentology* 47, 923–944.

Brown, K.J., 1993. Holocene relative sea-level change in Nova Scotia. Unpublished B.Sc. honours thesis, Dalhousie University, Halifax.

Burger, H.R., Sheehan, A.F., Jones, C.H., 2006. *Introduction to Applied Geophysics: Exploring the Shallow Subsurface*. W.W. Norton and Company, Inc., New York.

Buynevich, I., Bitinas, A., Pupienis, D., 2007. Reactivation of coastal dunes documented by subsurface imaging of the Great Dune Ridge, Lithuania. *Journal of Coastal Research* 50, 226–230.

Carter, R.W.G., 1988. Coastal dunes, in: *Coastal Environments: An Introduction to the Physical, Ecological and Cultural Systems of Coastlines*. Academic Press, London, O.N., pp. 301–333.

Carter, R.W.G, Orford, J.D., Forbes, D.L., Taylor, R.B., 1990. Morphosedimentary development of drumlin-flank barriers with rapidly rising sea level, Story Head, Nova Scotia. *Sedimentary Geology* 69, 117-138.

Charman, D.J., Gehrels, W.R., Manning, C., Sharma, C., 2010. Reconstruction of recent sea-level change using testate amoebae. *Quaternary Research* 73, 208–219.

Church, A.E. 1865. Halifax County E-14-15. 1:11880. A.E. Church and Co. Nova Scotia Public Archives.

Church, J.A., White, N.J., 2006. A 20th century acceleration in global sea level rise. *Geophysical Research Letters* 33, L01602, doi:10.1029/2006GL024826.

Church, J.A., Clark, P.U., Cazenave, A., Gregory, J.M., Jevrejeva, S., Levermann, A., Merrifield, M.A., Milne, G.A., Nerem, R.S., Nunn, P.D., Payne, A.J., Pfeffer, W.T., Stammer, D., Unnikrishnan, A.S., 2013. Sea level change, in: Stocker, T.F., Qin, D., Plattner, G.-K., Tignor, M., Allen, S.K., Boschung, J., Nauels, A., Xia, Y., Bex V., Midgley, P.M. (Eds.), *Climate Change 2013: The Physical Science Basis. Contribution of Working Group I to the Fifth Assessment Report of the Intergovernmental Panel on Climate Change*. Cambridge University Press, Cambridge and New York, pp. 1137-1216.

- Costas, S., Alejo, I., Rial, F., Lorenzo, H., Nombela, M.A., 2006. Cyclical Evolution of a Modern Transgressive Sand Barrier in Northwestern Spain Elucidated by GPR and Aerial Photos. *Journal of Sedimentary Research* 76, 1077–1092. doi:10.2110/jsr.2006.094
- Creel, L., 2003. Ripple Effect: Population and Coastal Regions. Population Reference Bureau.
- Daigle, R. (Ed.), 2006. Impacts of Sea-level Rise and Climate Change on the Coastal Zone of Southeastern New Brunswick. Environment Canada, Ottawa.
- Davidson-Arnott, R.G.D., 2010. Introduction to Coastal Processes and Geomorphology. Cambridge University Press, New York.
- De Oliveira Caldas, L.H., de Oliveria, J.G.J., de Medeiros, W.E., Stattegger, K., Vital, H., 2006. Geometry and evolution of Holocene transgressive and regressive barrier on the semi-arid coast of NE Brazil. *Geo-Marine Letters* 26, 249–263. doi:10.1007/s00367-006-0034-2
- Defeo, O., McLachlan, A., Schoeman, D.S., Schlacher, T.A., Dugan, J., Jones, A., Lastra, M., Scapini, F., 2009. Threats to Sandy Beach Ecosystems: A Review. *Estuarine, Coastal and Shelf Science* 81, 1–12. doi:10.1016/j.ecss.2008.09.022
- Degen, T., 1979. The History of Lawrencetown. Unknown publisher.
- Delure, A., 1983. The effect of storms and sediment in Halifax inlet, Nova Scotia. Unpublished M.Sc. thesis, Department of Earth Sciences, Dalhousie University, Halifax.
- Dillenburg, S.R., Tomazelli, L.J., Hesp, P.A., Barboza, E.G., Clerot, L.C.P., da Silva, D.B., 2006. Stratigraphy and evolution of a prograded transgressive dunefield barrier in Southern Brazil. *Journal of Coastal Research, Special Issue* 39, 132–135.

Dubois, R.N., 1992. A re-evaluation of Bruun's rule and supporting evidence. *Journal of Coastal Research* 8, 618–628.

Faribault, E.R., 1906. Province of Nova Scotia, Halifax County, Lawrencetown Sheet, No 53. Geological Survey of Canada, Ottawa, Multicoloured Geological Map 700.

Folk, R., Ward, W.C., 1957. Brazos River bar: a study in the significance of grain size parameters. *Journal of Sedimentary Petrology* 27, 3–26.

Forbes, D.L., 2012. Glaciated coasts, in: Hansom J.D., Flemming, B. (Eds.), *Estuarine and Coastal Geology and Geomorphology*. Volume 3 in: McClusky, D., Wolanski, E. (Series Eds.), *Treatise on Estuarine and Coastal Science*. Academic Press, Waltham MA, pp. 223-243.

Forbes, D.L., Manson, G.K., Charles, J., Thompson, K.R., Taylor, R.B., 2009. Halifax Harbour Extreme Water Levels in the Context of Climate Change: Scenarios for a 100-year Planning Horizon. Geological Survey of Canada, Ottawa, Open File 6346.

Forbes, D.L., Parkes, G.S., Manson, G.K., Ketch, L.A., 2004. Storms and shoreline retreat in the southern Gulf of St. Lawrence. *Marine Geology* 210, 169–204.

Friedman, G.M., 1961. Distinction between dune, beach, and river sands from their textural characteristics. *Journal of Sedimentary Petrology* 31, 514–529.

Garrison, J.R., Williams, J., Potter Miller, S., Weber, E.T., McMechan, G., Zeng, X., 2010. Ground-penetrating radar study of North Padre Island: implications for barrier island internal architecture, model for growth of progradational microtidal barrier islands, and Gulf of Mexico sea-level cyclicity. *Journal of Sedimentary Research* 80, 303–319.

Gehrels, W.R., Kirby, J.R., Prokoph, A., Newnham, R.M., Achterberg, E.P., Evans, H., Black, S., Scott, D.B., 2005. Onset of recent rapid sea-level rise in the western Atlantic Ocean. *Quaternary Science Reviews* 24, 2083–2100.

Gehrels, W.R., Milne, G.A., Kirby, J.R., Patterson, R.T., Belknap, D.F., 2004. Late Holocene sea-level changes and isostatic crustal movements in Atlantic Canada. *Quaternary International* 120, 79–89.

González-Villanueva, R., Costas, S., Duarte, H., Pérez-Arlucea, M., Alejo, I., 2011. Blowout evolution in a coastal dune: using GPR, aerial imagery and core records. *Journal of Coastal Research, Special Issue* 64, 278–282.

Hales, W.J., 1992. Sand Dunes of Nova Scotia. Unpublished M.Sc. thesis, Department of Geography, McMaster University, Hamilton.

Hesp, P., 2002. Foredunes and blowouts: initiation, geomorphology and dynamics. *Geomorphology* 48, 245–268.

Harvey, N., 2006. Holocene Coastal Evolution: Barriers, Beach ridges, and Tidal flats of South Australia. *Journal of Coastal Research* 22, 90–99.

Harwood, R., 2014. Transgressive Facies. facweb.bhc.edu/academics/science/harwoodr/geol102/Study/Images/TransgressiveFacies.gif Accessed 2014-04-15

Hesp, P., 2002. Foredunes and blowouts: initiation, geomorphology and dynamics. *Geomorphology* 48, 245–268.

Hesp, P.A., Dillenburg, S.R., Barboza, E.G., Tomazelli, L.J., Ayup-Zouain, R.N., Esteves, L.S., Gruber, N.L.S., Toldo, E.E.J., Tabajara, L.L.C., Clerot, L.C.P., 2005. Beach ridges, foredunes or transgressive dunefields? Definitions and an examination of the Torres to Tramandaí barrier system, Southern Brazil. *Annals of the Brazilian Academy of Science* 77, 493–508.

Hesp, P.A., Thom, B.G., 1990. Geomorphology and evolution of active transgressive dunefields, in: Nordstrom, K.F., Psuty, N., Carter, B. (Eds.), *Coastal Dunes: Forms and Process*. John Wiley & Sons Ltd., Toronto, O.N., pp. 253–288.

Hoskin, K.S., 1983. Coastal Sedimentation at Lawrencetown Beach, Eastern Shore, Nova Scotia. Unpublished B.Sc. honours thesis, Dalhousie University, Halifax.

Hoyt, J.H., 1967. Barrier Island Formation. *Geological Society of America Bulletin* 78, 1118–1130.

Johnston, J.W., Thompson, T.A., Baedke, S.J., 2007. Systematic pattern of beach-ridge development and preservation: conceptual model and evidence from ground penetrating radar. *Geological Society of America, Special Paper* 432, 47–58.

Lessa, G.C., Angulo, R.J., Giannini, P.C., Araujo, A.D., 2000. Stratigraphy and Holocene evolution of a regressive barrier in south Brazil. *Marine Geology* 165, 87–108.

Martinez, M.L., Psuty, N.P., Lubke, R.A., 2008. A perspective on coastal dunes, in: Martinez, M.L., Psuty, N.P. (Eds.), *Coastal Dunes, Ecology and Conservation*. Springer, New York, , pp. 3–10.

Mathew, S., Davidson-Arnott, R.G.D., Ollerhead, J., 2010. Evolution of a beach-dune system following a catastrophic storm overwash event: Greenwich Dunes, Prince Edward Island, 1936–2005. *Canadian Journal of Earth Sciences* 47, 273–290. doi:10.1139/E09-078

McCann, S.B., 1990. An introduction to the coastal dunes of Atlantic Canada. in: Davidson-Arnott, R.G.D. (Ed.), *Proceedings of Canadian Symposium on Coastal Sand Dunes*, Guelph. Associate Committee on Shorelines, National Research Council Canada, Ottawa, pp. 89–107.

McCulloch, M., M., Forbes, D.L., Shaw, R.W., CCAF A041 Scientific Team, 2002. Synthesis report, in: Forbes, D.L. and Shaw, R.W. (Eds.), Coastal Impacts of Climate Change and Sea-level Rise on Prince Edward Island. Geological Survey of Canada, Ottawa, Open File 4261, pp. 1-62.

Morton, R.A., Paine, J.G., Blum, M.D., 2000. Responses of Stable Bay-Margin and Barrier-Island Systems to Holocene Sea-level Highstand, Western Gulf of Mexico. *Journal of Sedimentary Research* 70, 478–490.

Natural Resources Canada (NRCan), 2007. CoastWeb- Conrads Beach, Site 2035, Halifax County, Nova Scotia. www.nrcan.gc.ca/earth-sciences/geography-boundary/coastal-research/monitoring-coastal-change/9201.

Natural Resources Canada (NRCan), 2011. Impact of Storms [online]. www.nrcan.gc.ca/earth-sciences/natural-hazard/other-natural-hazards/storm-impact/8591. Accessed Dec 1, 2012.

Neal, A., Roberts, C.L., 2001. Internal structure of a trough blowout, determined from migrated ground-penetrating radar profiles. *Sedimentology* 48, 791–810.

Neal, A., 2004. Ground-penetrating radar and its use in sedimentology: principles, problems and progress. *Earth-Science Reviews* 66, 261–330. doi:10.1016/j.earscirev.2004.01.004

Nicholls, R.J., Wong, P.P., Burkett, V.R., Codignotto, J.O., Hay, J.E., McLean, R.F., Ragoonaden, S., Woodroffe, C.D., 2007. 2007:Coastal systems and low-lying areas., in: Parry, M.L., Canziani, O.F., Palutikof, J.P., van der Linden, P.J., Hanson, C.E. (Eds.), *Climate Change 2007: Impacts, Adaptation and Vulnerability*. Cambridge University Press, Cambridge, UK, pp. 315–356.

Nutt, L.A., McCann, S.B., 1991. Fore-dune evolution near Point Deroche on the north shore of Prince Edward Island.

Ollerhead, J., Davidson-Arnott, R.G., 1995. The evolution of Buctouche Spit, New Brunswick, Canada. *Marine Geology* 124, 215–236.

Orford, J.D., Carter, R.W.G., Jennings, S.C., 1996. Control domains and morphological phases in gravel-dominated coastal barriers of Nova Scotia. *Journal of Coastal Research* 589–604.

Orford, J.D., Jennings, S.C., Forbes, D.L., 2000. Origin, development, reworking and breakdown of gravel-dominated coastal barriers in Atlantic Canada: future scenarios for the British coast, in: Packham, J.R. (Ed.), *Ecology and Geomorphology of Coastal Shingle*. Smith-Settle, Otley, pp. 23-55.

Parkes, G.S., Forbes, D.L., Ketch, L.A., 2002. Sea-level rise, in: Forbes, D.L. and Shaw, R.W. (Eds.), *Coastal Impacts of Climate Change and Sea-level Rise on Prince Edward Island*. Geological Survey of Canada, Ottawa, Open File 4261, Supporting Document 1.

Pethick, J., 1984. Coastal sand dunes, in: *An Introduction to Coastal Geomorphology*. Edward Arnold, Baltimore, MD, pp. 127–143.

Phillips, D., 1990. *The climates of Canada*. Canadian Government Publishing Centre, Ottawa, O.N.

Quinlan, G., Beaumont, C., 1981. A Comparison of Observed and Theoretical Postglacial Relative Sea Level in Atlantic Canada. *Canadian Journal of Earth Sciences* 18, 1146–1163.

Quinlan, G., Beaumont, C., 1982. The deglaciation of Atlantic Canada as reconstructed from the postglacial relative sea-level record. *Canadian Journal of Earth Sciences* 19, 2232–2246.

Rahmstorf, S., Cazenave, A., Church, J.A., Hansen, J.E., Keeling, R.F., Parker, D.E., Somerville, R.C.J., 2007. Recent climate observations compared to projections. *Science* 316, 709.

Reed, D.J., Davidson-Arnott, R., Penillo, G.M.E., 2009. Estuaries, coastal marshes, tidal flats and coastal dunes, in: Slaymaker, O., Spencer, T., Embleton-Hamann, C. (Eds.), *Geomorphology and Global Environmental Change*. Cambridge University Press, Cambridge, UK, pp. 130–157.

Reimer, P.J., Bard, E., Baylissorford 1996, A., Beck, J.W., Blackwell, P.G., Ramsey, C.B., Buck, C.E., Cheng, H., Edwards, R.L., Freidrich, M., Grootes, P.M., Guilderson, T.P., Hafliason, H., Hajdas, I., Hatte, C., Heaton, T.J., Hoffmann, D.L., Hogg, A.G., Hughen, K.A., Kaiser, K.F., Kromer, B., Manning, S.W., Niu, M., Reimer, R.W., Richards, D.A., Scott, E.M., Southon, J.R., Staff, R.A., Turney, C.S.M., van der Plicht, J., 2013. INTCAL13 and MARINE13 radiocarbon age calibration curves 0-50,000 years cal BP. *Radiocarbon* 55, 1869–1887.

Reinson, G.E., 1992. Transgressive Barrier Islands and Estuarine Systems, in: Walker, R.G., James, N.P. (Eds.), *Facies Models: Response to Sea Level Change*. Geological Association of Canada, St. Johns, N.F., pp. 179–194.

Scheffers, A., Engel, M., Scheffers, S., Squire, P., Kelletat, D., 2012. Beach ridge systems—archives for Holocene coastal events? *Progress in Physical Geography* 36, 5–37.

Scott, D.B., 1977. Distribution and population dynamics of marsh-estuarine foraminifera with applications to relocating Holocene sea-level. (PhD.). Dalhousie University, Halifax, N.S.

Scott, D.B., Boyd, R., Medioli, F.S., 1987. Relative sea-level changes in Atlantic Canada: observed level and sedimentological changes vs. theoretical models, in: Nummedal, D., Pilkey, O.H., Howard, J.D. (Eds.), *Sea-Level Fluctuation and Coastal Evolution*, Special Publications. Society of Economic Paleontologist and Mineralogists, Tulsa, Oklahoma, pp. 87–96.

Scott, D.B., Brown, K., Collins, E.S., Medioli, F.S., 1995. A new sea-level curve from Nova Scotia: evidence for a rapid acceleration of sea-level rise in the late mid-Holocene. *Canadian Journal of Earth Sciences* 32, 2071–2080.

Sensors and Software Inc., 2006. Pulse EKKO Pro Users Guide. Sensors and Software Inc., Mississauga, ON.

Shaw, J., Piper, D.J.W., Fader, G.B.J., King, E.L., Todd, B.J., Bell, T., Batterson, M.J., Liverman, D.G.E., 2006. A conceptual model of the deglaciation of Atlantic Canada. *Quaternary Science Reviews* 25, 2059–2081.

Shaw, J., Duffy, G., Taylor, R.B., Chassé, J., Frobel, D., 2008. Role of a submarine bank in the long-term evolution of the Northeast coast of Prince Edward Island, Canada. *Journal of Coastal Research* 245, 1249–1259.
doi:10.2112/07-08607.1

Shaw, J., Taylor, R.B., Forbes, D.L., 1993. Impact of Holocene transgression on the Atlantic coastline of Nova Scotia. *Géographie physique et Quaternaire* 47, 221–238.

Shaw, J., Taylor, R.B., Forbes, D.L., Ruz, M.-H., Solomon, S., 1998. Sensitivity of the Coasts of Canada to Sea-level Rise. Geological Survey of Canada, Ottawa, Bulletin 505.

Shore, R., 1996. H2.6 Dune System, in: *Natural History of Nova Scotia*. Nova Scotia Museum of Natural History, Halifax, N.S., pp. 423–426.

Simms, A.R., Anderson, J.B., Blum, M., 2006. Barrier-island aggradation via inlet migration: Mustang Island, Texas. *Sedimentary Geology* 187, 105–125.
doi:10.1016/j.sedgeo.2005.12.023

Stea, R.R., Boyd, R., Fader, G.B.J., Courtney, R.C., Scott, D.B., Pecore, S.S., 1994. Morphology and seismic stratigraphy of the inner continental shelf of Nova Scotia, Canada: Evidence for a -65 m lowstand between 11,650 and 11,250 C¹⁴ yr B.P. *Marine Geology* 117, 135–154.

Stea, R.R., Piper, D.J.W., Fader, G.B.J., Boyd, R., 1998. Wisconsinan glacial and sea-level history of Maritime Canada and the adjacent continental shelf: A correlation of land and sea events. *Geological Society of America Bulletin* 110, 821–845. doi:10.1130/0016-7606(1998)110<0821:WGASLH>2.3.CO;2

Tanner, W.F., 1995. Origin of beach ridges and swales. *Marine Geology* 129, 149–161.

Tanner, W.F., 1992. Late Holocene sea-level changes from grain-size data: evidence from the Gulf of Mexico. *The Holocene* 2, 249–253.
doi:10.1177/095968369200200306

Taylor, R.B., Frobels, D., 1986. Aerial Video Surveys The Coastline of Nova Scotia Part 2: Atlantic Coast (Yarmouth to Halifax). Geological Survey of Canada, Ottawa, Open File 3301.

Taylor, R.B., Frobels, D., 2001. The Coastline of Nova Scotia Part 3: Atlantic Coast (Halifax to Cape North) (Open File No. 4020). Geological Survey of Canada, Nova Scotia.

Taylor, R.B., Frobels, D., 2001. The Coastline of Nova Scotia Part 3: Atlantic Coast (Halifax to Cape North). Geological Survey of Canada, Ottawa, Open File 4020.

Taylor, R.B., Forbes, D.L., Frobel, D., Manson, G.K., Shaw, J. 2014. Coastal geoscience studies at Bedford Institute of Oceanography, 1962-2012; in: Nettleship, D.N., Gordon, D.C., Lewis, C.F.M., Latremouille, M.P. (Eds.), *Voyage of Discovery: Fifty Years of Marine Research at Canada's Bedford Institute of Oceanography*, Bedford Institute of Oceanography – Oceans Association, Dartmouth, NS, pp. 197-204 (in press).

Taylor, R.B., Frobel, D., Forbes, D.L., Mercer, D., 2008. Impacts of Post-tropical Storm Noel (November, 2007) on the Atlantic Coastline of Nova Scotia. Geological Survey of Canada, Ottawa, Open File 5802.

Taylor, R.B., Frobel, D., Mercer, D., Fogarty, C., MacAulay, P., 2013. Impacts of Four Storms in December 2010 on the Eastern Shore of Nova Scotia. Geological Survey of Canada, Ottawa, Open File 7356.

Taylor, R.B., Wittmann, S.L., Milne, M.J., Kober, S.M., 1985. Beach Morphology and Coastal Changes at Selected Sites, Mainland Nova Scotia. Geological Survey of Canada. Ottawa, Paper 85-12.

Trenhaile, A.S., 1997. Sand dunes. Oxford University Press, Oxford, N.Y.

Utting, D.J., 2011. Surficial Geology Map, Part of the Cole Harbour Claim reference sheet 11D/11C, Halifax county, Nova Scotia. Open File Map ME 2011-010.

Utting, D., Gallacher, F., 2009. Coastal environments and erosion in Southwest St. Georges Bay, Antigonish County (Mineral Resources Branch No. ME 2009-1), Report of Activities. Nova Scotia Department of Natural Resources.

Walker, I.J., Barrie, J.V., 2004. Geomorphology and sea-level rise on one of Canada's most 'sensitive' coasts: northeast Graham Island, British Columbia. *Journal of Coastal Research Special Issue* 39, 220–226.

Webster, T.L., Forbes, D.L., 2005. Using airborne lidar to map exposure of coastal areas in Maritime Canada to flooding from storm-surge events: a review of recent experience. Presented at the Canadian Coastal Conference 2005.

Webster, T.L., Forbes, D.L., 2006. Airborne laser altimetry for predictive modelling of coastal storm-surge flooding, in: Richardson, L.L., LeDrew, E.F. (Eds.), *Remote Sensing of Aquatic Coastal Ecosystem Processes: Science and Management*. Springer, Dordrecht, pp. 157-182.

White, C.E., 2002. Preliminary Bedrock Geology of the Area Between Chebogue Point, Yarmouth County, and Cape Sable Island, Shelburne County, Southwestern Nova Scotia, Report of Activities. Nova Scotia Department of Natural Resources, Halifax, N.S.

White, C.E., 2010. Stratigraphy of the Lower Paleozoic Goldenville and Halifax groups in southwestern Nova Scotia. *Atlantic Geology* 46,136-154.

Widess, M.B., 1973. How thin is a thin bed? *Geophysics* 38, 1176–1180.

Zervas, D., Nichols, G.J., Hall, R., Smyth, H., Luthje, C., Murtagh, F., 2009. SedLog: A shareware program for drawing graphic logs and log data manipulation. *Computers & Geoscience* 35, 2151–2159.

APPENDIX 1: GPR and GPS Methodology

A1.1 GPR Surveying

Ground-penetrating radar (GPR) is an electromagnetic imaging method that utilizes radio waves to probe lossy (energy dissipative) dielectric materials (Annan 2002). The low conductivity and low magnetic permeability of sand makes GPR an effective tool for imaging the internal structure of sand dunes (Bristow 2009). This non-invasive technique can provide continuous, high-resolution images of the shallow subsurface quickly and efficiently (Bristow 2009; Møller and Anthony 2003) and has been used successfully to image a variety of coastal dune systems worldwide (Møller and Anthony 2003; Pedersen and Clemmensen 2005; Switzer et al. 2006). GPR surveying for this study was conducted using a PulseEKKO Pro Smart Cart™ GPR system and Leica GRX1200™ global positioning system (GPS). Both systems are owned by Dalhousie University.

Key components of any GPR system are the transmitting and receiving antennas. The PulseEKKO Pro Smart Cart™ GPR system mounts the antennas parallel to the ground surface and perpendicular to the direction of travel and, provides an easy method for selecting a fixed antenna spacing (Fig. A1.1). This transmitter-receiver direction-of-travel configuration is known as the perpendicular broadside orientation and reduces the likelihood of unwanted signals from offline features (Baker et al. 2007).

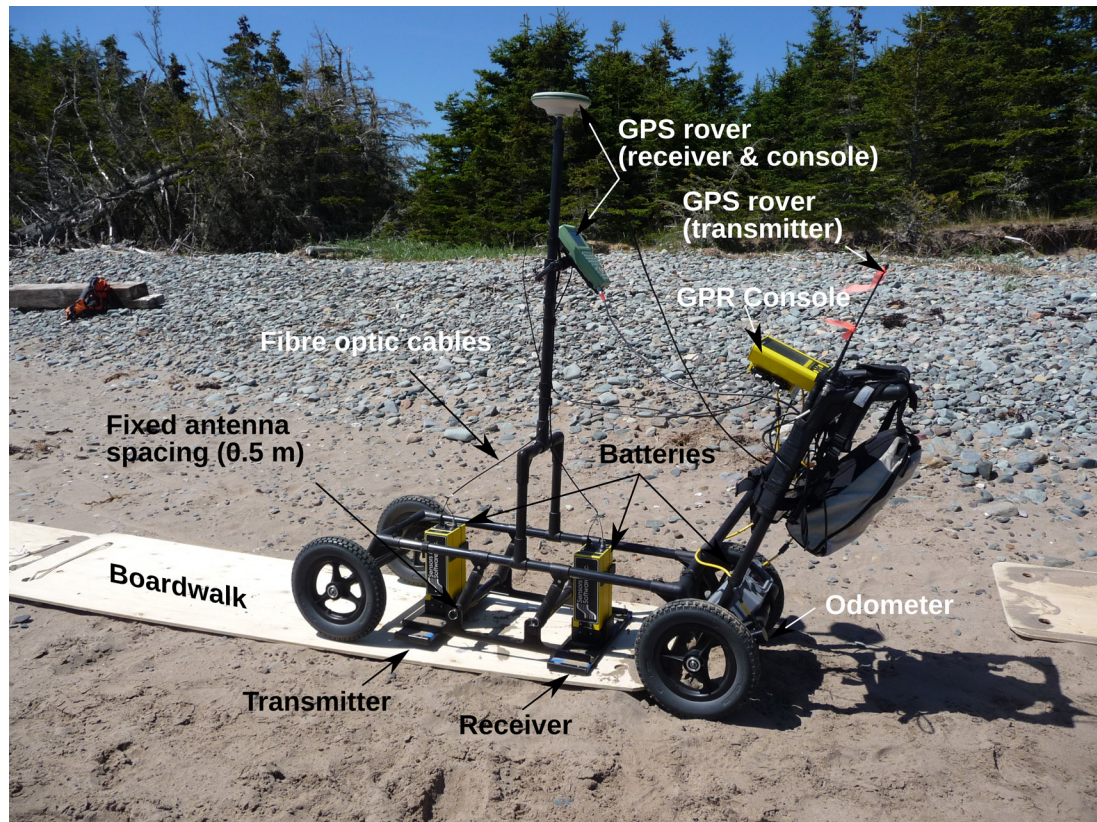


Figure A1.1 PulseEKKO Pro Smart Cart™ GPR with 200 MHz antennas and Leica GPX1200™ GPS Rover

Transmitting/receiving antenna pairs are available in a variety of radio frequencies from 50 MHz to 500 MHz. When triggered, the transmitting antenna emits an electromagnetic pulse centered about the selected radio frequency. The electromagnetic pulse travels to the receiving antenna through a variety of paths (Fig. A1.2). As a result of these combined signals, the receiving antenna records a complex combination of non-sinusoidal wavelets (Yelf and Yelf 2003) that vary in amplitude with time. As the cart is moved a series of pulses is transmitted and received and a radargram is generated.

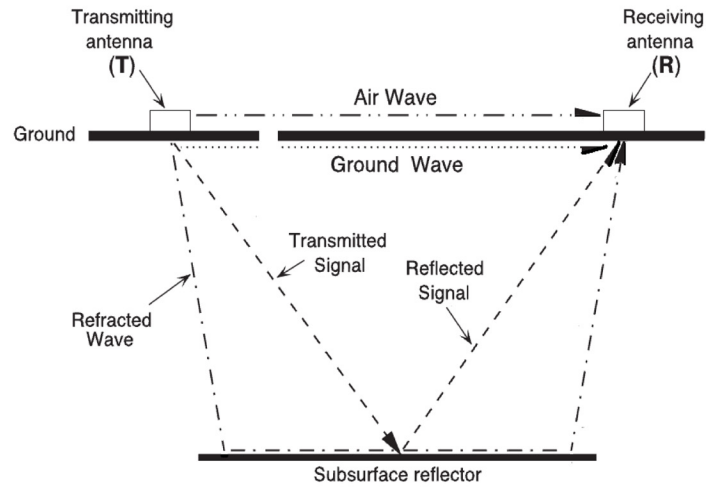


Figure A1.2 Electromagnetic wave ray paths (modified from Fisher et al. 1996).

While electromagnetic waves propagate through free space at a rate of 0.3 m/ns at or near sea-level (Davis and Annan 1989), they propagate through low loss materials at a rate of

$$v = \frac{c_0}{\sqrt{\epsilon_r}} \quad [1]$$

where (c_0) is the speed of light in a vacuum and (ϵ_r) is the medium's relative dielectric permittivity (Neal 2004). Electromagnetic waves with an initial amplitude (A_0) decay at a rate of

$$A = A_0 e^{-\alpha z} \quad [2]$$

as they travel distance (z) through low-loss materials with attenuation constant

$$\alpha = \frac{\sigma}{2} \sqrt{\mu/\epsilon} \quad [3]$$

where (σ), (μ), and (ϵ) are the material's electrical conductivity, magnetic permeability and dielectric permittivity respectively (Neal 2004). The attenuation constant is frequency independent and the fresh water content of geological

materials is the primary control over their dielectric properties (Davis and Annan 1989; Neal 2004). Additionally attenuation affects the penetration depth of electromagnetic waves (Van Heteran et al. 1998). Since maximum penetration depth is controlled by both the electromagnetic properties of stratigraphic units and the GPR system and antenna characteristics, higher frequencies give less penetration but better resolution (Van Heteren et al. 1998).

A subsurface reflector is an interface between materials with different dielectric permittivities, electrical conductivities, and/or magnetic permeabilities (Neal 2004). Material changes resulting in an interface include changes to the amount and type of fluid occupying pore spaces, porosity, and sediment grain type, shape, orientation and packing (Neal 2004).

In general subsurface layers are resolvable when their thicknesses and lengths are larger than the vertical resolution and lateral resolution respectively, but smaller units that cause changes in the GPR signal strength may also be resolvable (Yilmaz and Chambers 1984). GPR resolution has two components: depth resolution (Δl) and lateral resolution (Δr) (Annan 2009) (Fig. A1.3). In order to resolve an interface

$$\Delta r \geq \frac{\lambda_c}{4} \quad [4]$$

and

$$\Delta l \geq \sqrt{\frac{r \lambda_c}{2}} \quad [5]$$

where (r) is distance to the interface, (λ_c) is the wavelength of an electromagnetic pulse with central frequency (f_c) and

$$v = \lambda_c f_c \quad [6]$$

is the velocity of that pulse (Annan 2009).

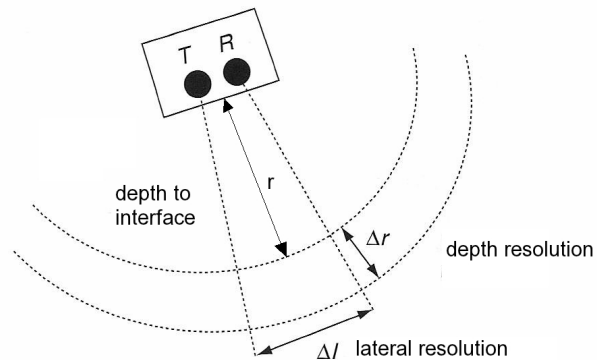


Figure A1.3 Depth resolution and lateral resolution of GPR data. Modified from Annan (2009).

GPR data is acquired using one of three survey designs: the common-midpoint survey (CMP), common offset survey, or transillumination survey (Baker et al. 2007). The PulseEKKO Pro Smart Cart™ is an example of the common offset survey design, in which the transmitter and receiver are kept at a fixed distance (or offset) at each measurement location (Annan 2009). The single-channel nature of GPR data make common offset surveying an efficient method for covering a large area in a short amount of time. During a CMP survey the transmitter and receiver separation is systematically varied while the point of reflection (midpoint) is kept constant (Annan 2009). This survey design is used to estimate radar signal velocity (Baker et al. 2007; Annan 2009) and dielectric properties (Baker et al. 2007) at depth. During a transillumination survey, the receiver and transmitter are placed on opposite sides of a target and the electromagnetic energy is transmitted between them (Baker et al. 2007) in order to measure the electromagnetic properties of the target medium. This study

utilized both common offset and CMP surveying techniques.

A1.2 GPS

The Leica GRX1200™ is a real-time kinematic global positioning system. The base station consists of a GPS transmitter and receiver on independent tripods (Fig.A1.4). The receiver is centered over a fixed or known location for the duration of the GPS survey. It is in contact with several satellites during surveying and is able to determine its position precisely. The second component of the system is the rover. The rover is an identical GPS receiver, carried in a backpack. It calculates its position in relation to both satellites and the base station.

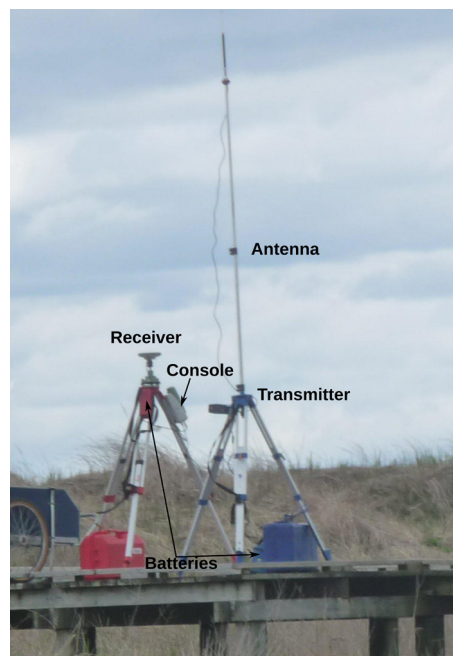


Figure A1.4 Leica GRX1200™ base station

A2.3 GPR Data Processing

GPR data processing makes the raw GPR data easier to interpret by transforming it into a more realistic representation of the barrier system. Sensors and Software Inc's EKKOView Deluxe (version 1 release 3)TM and Paradigm's Focus 5.4TM were used to process the GPR data. Dewow is a high-loss temporal filter used to suppress the low-frequency, slow, time-varying component resulting from the rapid decay of the electrostatic and inductive fields (Annan 2009). Bandpass filtering reduces the high and low frequency noise. The GPS data are utilized to conduct the topography correction. Topography corrected data resembles the topography of the survey area. Migration attempts to reduce the transmitter-receiver directionality (Annan 2009). A top-mute removes any migration artifacts that may occur prior to time zero. Once data processing has been applied, it becomes possible to identify erosional surfaces and depositional units on the radargram with increased reliability and to conduct radar facies analysis.

References

Annan, A.P., 2009. Electromagnetic principles of ground penetrating radar, in: Jol, H.M. (Ed.), *Ground Penetrating Radar: Theory and Applications*. Elsevier Science, New York, N.Y., pp. 3–40.

Baker, G.S., Jordan, T.E., Party, J., 2007. An introduction to ground penetrating radar (GPR). Geological Society of America, Special Paper 432, 1–18.

Bristow, C., 2009. Ground penetrating radar in aeolian dune sands, in: Jol, H.M. (Ed.), *Ground Penetrating Radar: Theory and Applications*. Elsevier Science, New York, N.Y., pp. 273–297.

Davis, J.L., Annan, A.P., 1989. Ground-penetrating radar for high-resolution mapping of soils and rock stratigraphy. *Geophysical Prospecting* 37, 531–551.

Fisher, S.C., Stewart, R.R., Jol, H.M., 1996. Ground penetrating radar (GPR) data enhancement using seismic techniques. *Journal of Environmental and Engineering Geophysics* 1, 89–96. doi:10.4133/JEEG1.2.89

Møller, I., Anthony, D., 2003. A GPR study of sedimentary structures within a transgressive coastal barrier along the Danish North Sea coast. *Geological Society, London, Special Publications* 211, 55–65.
doi:10.1144/GSL.SP.2001.211.01.05

Neal, A., 2004. Ground-penetrating radar and its use in sedimentology: principles, problems and progress. *Earth-Science Reviews* 66, 261–330.
doi:10.1016/j.earscirev.2004.01.004

Pedersen, K., Clemmensen, L.B., 2005. Unveiling past aeolian landscapes: a ground-penetrating radar survey of a Holocene coastal dunefield system, Thy, Denmark. *Sedimentary Geology* 177, 57–86.

Switzer, A.D., Bristow, C.S., Jones, B.G., 2006. Investigation of large-scale washover of a small barrier system on the southeast Australian coast using ground penetrating radar. *Sedimentary Geology* 183, 145–156.

Van Heteren, S., Fitzgerald, D.M., McKinlay, P.A., Buynevich, I.V., 1998. Radar facies of paraglacial barrier systems: coastal New England, USA. *Sedimentology* 45, 181–200.

Yelf, R., Yelf, D., 2003. Where is true rime zero [online].
http://www.emph.com.ua/18/pdf/yelf_03.pdf. Accessed 2011-11-15.

Yilmaz, O., Chambers, R., 1984. Migration velocity analysis by wave-field extrapolation. *Geophysics* 49, 1664–1674.

APPENDIX 2: VIBRACORE LOG SHEETS

The original vibracore core log sheets were letter-sized and reproduced the cores at a scale of 1:5, with each sheet representing 100 cm of core length. They are reproduced here. See Figure 3.4 for vibracore locations.

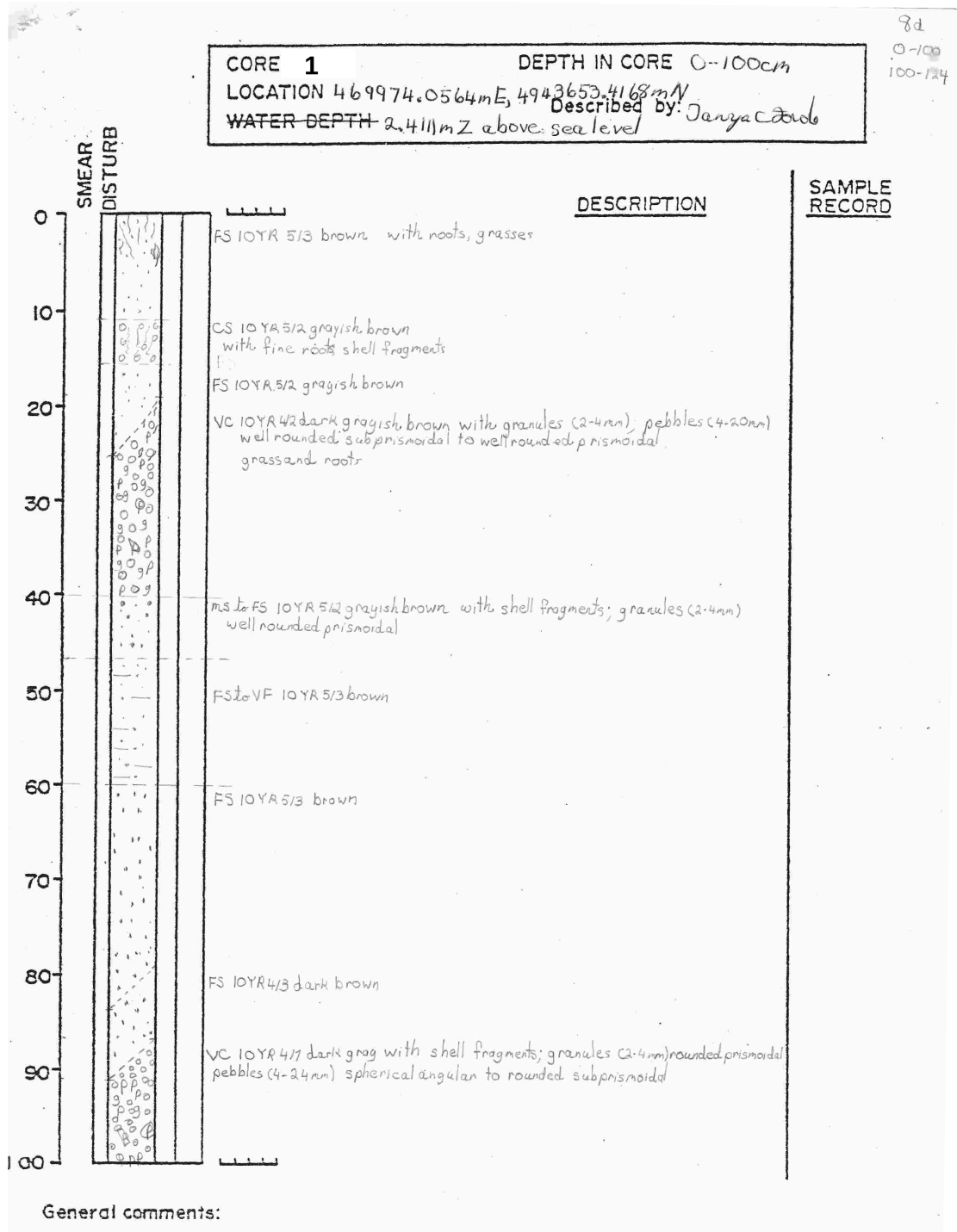
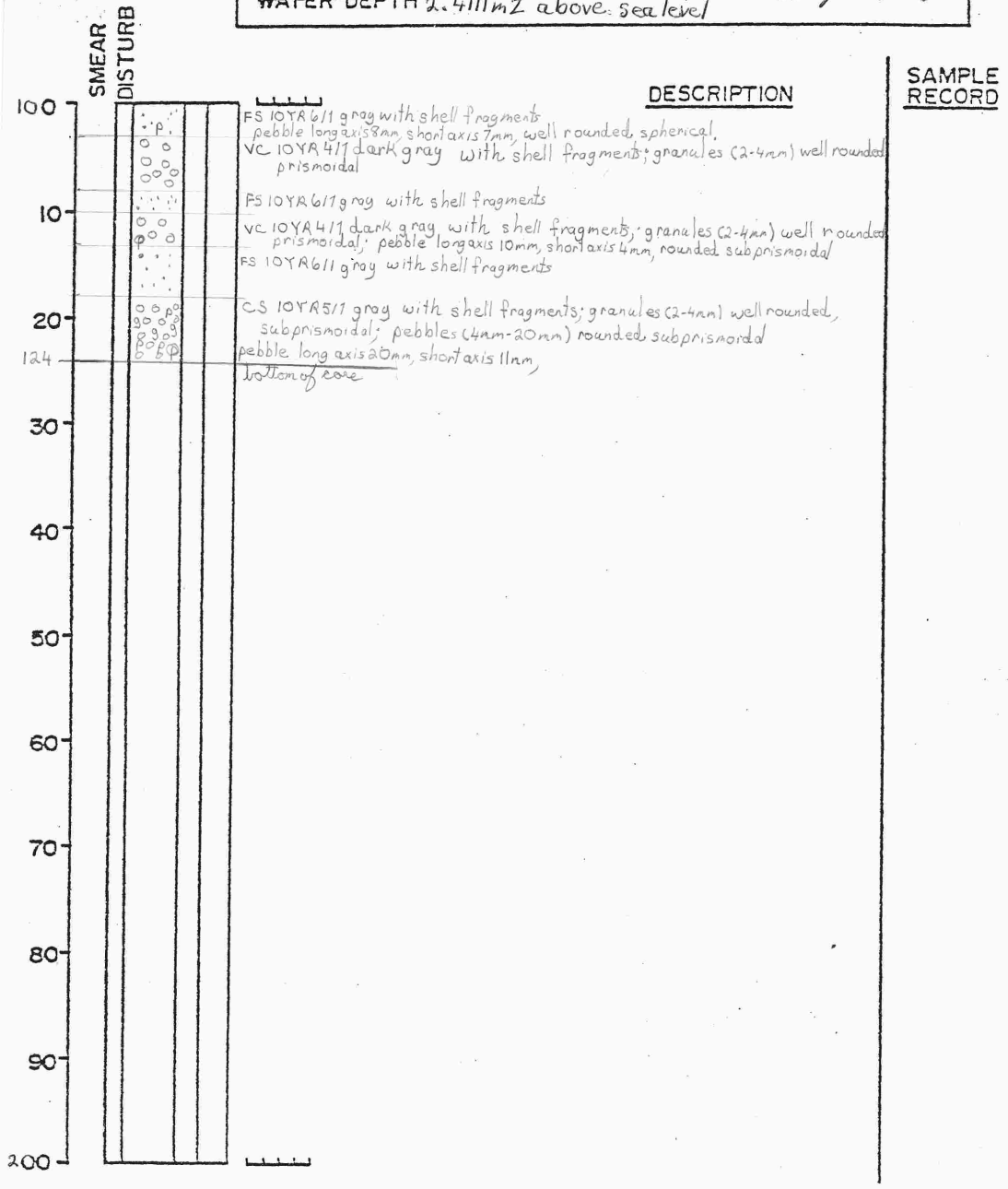


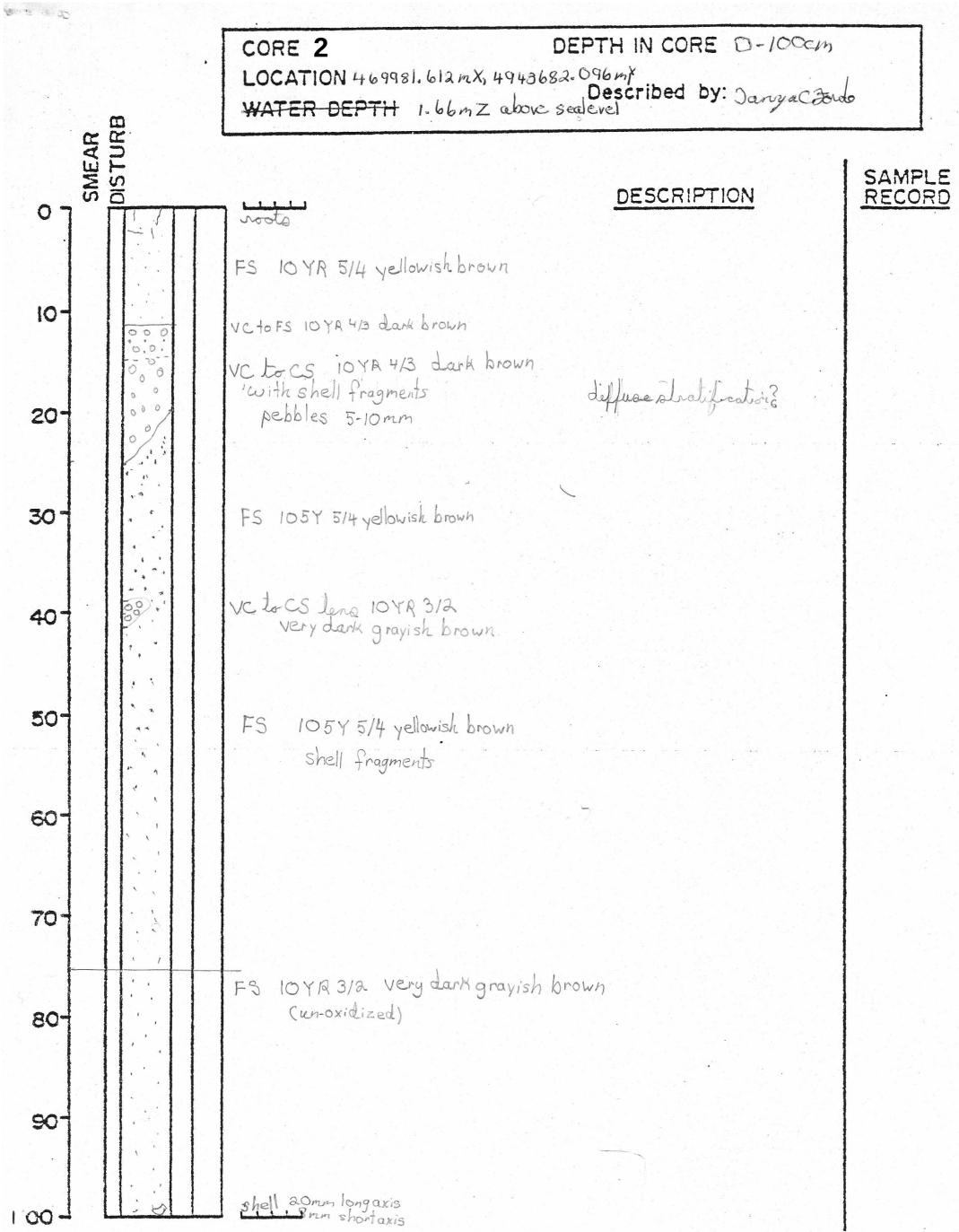
Figure A2.1 Vibracore log sheet 1, 0-100 cm.

CORE 1 DEPTH IN CORE 100-124 cm
 LOCATION 46 9974.0564mE, 4943653.4168mN
 WATER DEPTH 2.411mZ above sea level
 Described by: Janya C. Fido



General comments:

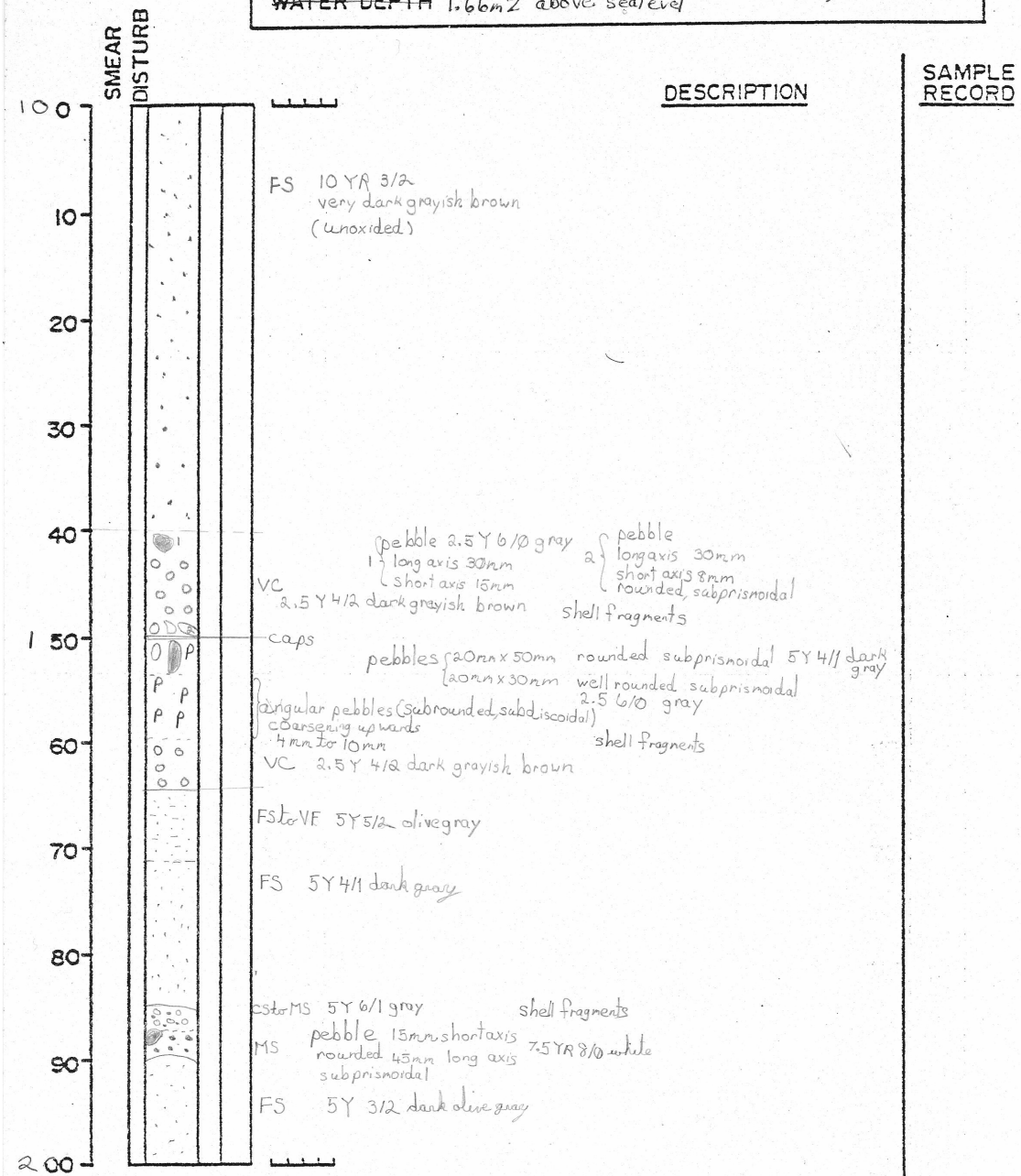
Figure A2.2 Vibracore log sheet 1, 0-124 cm.



General comments:

Figure A2.3 Vibracore log sheet 2, 0-100 cm.

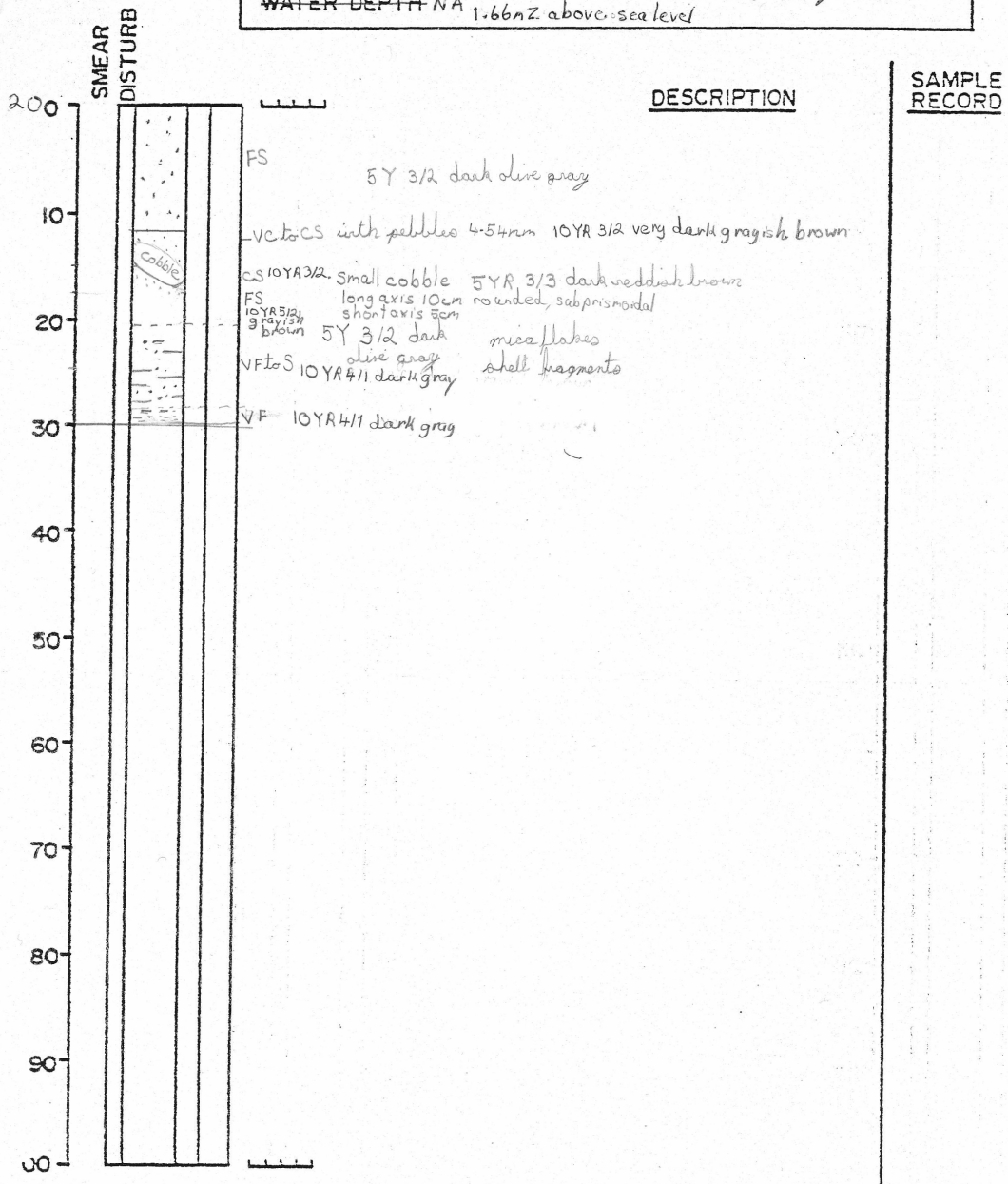
CORE 2 DEPTH IN CORE 100-200cm
 LOCATION 469981.612mX, 4943682.096mY Described by: Janyac Judo
 WATER DEPTH 1.66mZ above sea level



General comments:

Figure A2.4 Vibracore log sheet 2, 100-200 cm.

CORE 2 DEPTH IN CORE 200-230cm
 LOCATION 469981.612mX; 4943682.094mZ
 WATER DEPTH NA 1.66mZ above sea level
 Described by: Janya C Jorde



General comments:

Figure A2.5 Vibracore log sheet 2, 200-230 cm.

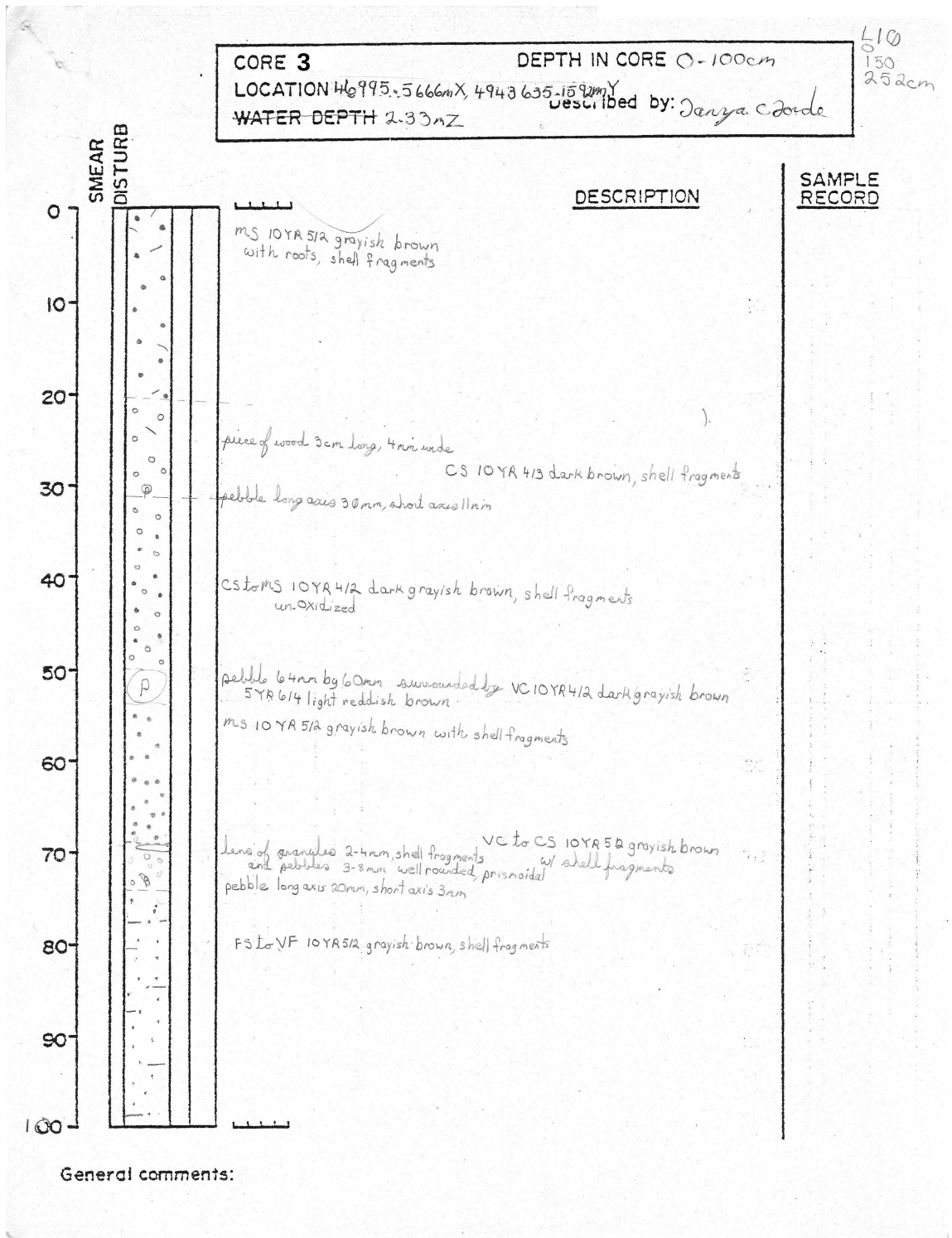
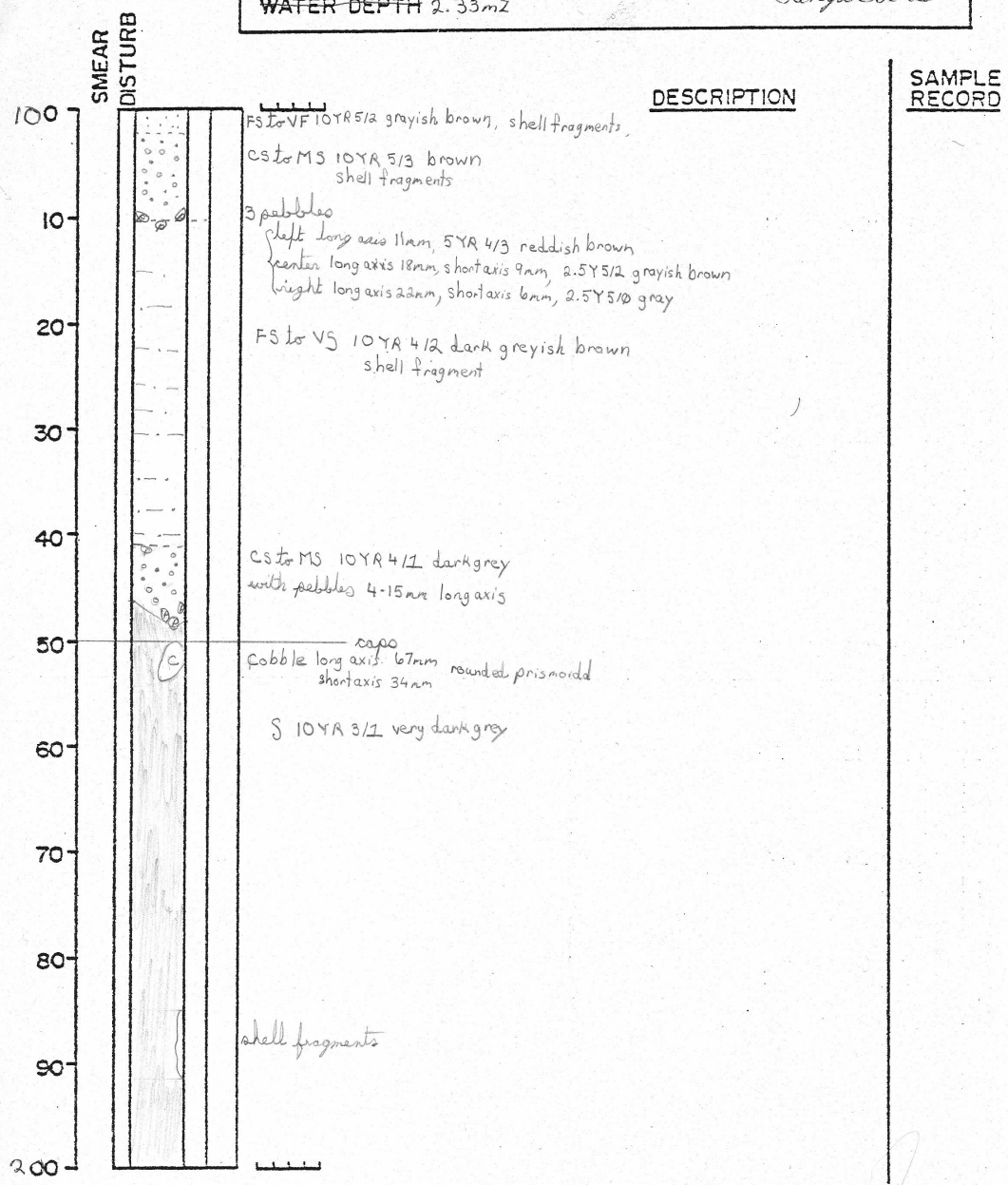


Figure A2.6 Vibracore log sheet 3, 0-100 cm.

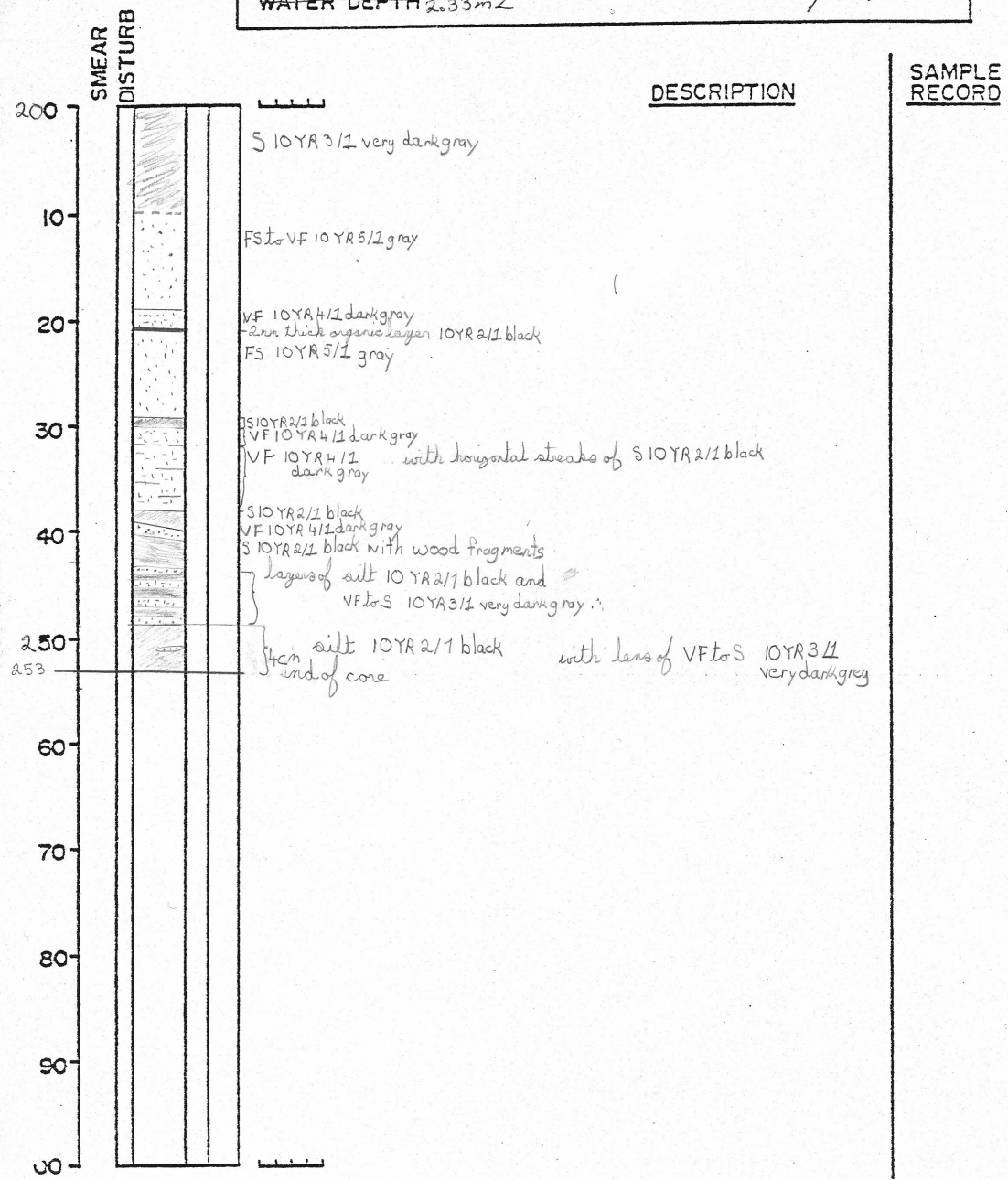
CORE 3 DEPTH IN CORE 100-200cm
 LOCATION 469995.5666N, 4943635.1592E
 WATER DEPTH 2.33mZ Described by: Janya C. Jorda



General comments:

Figure A2.7 Vibracore log sheet 3, 100-200 cm.

CORE 3 DEPTH IN CORE 200-253cm
 LOCATION 469995.5666mX, 4943635.1592mY
 WATER DEPTH 2.33mZ Described by: Janya C Jade



General comments:

Figure A2.8 Vibracore log sheet 3, 200-253 cm.

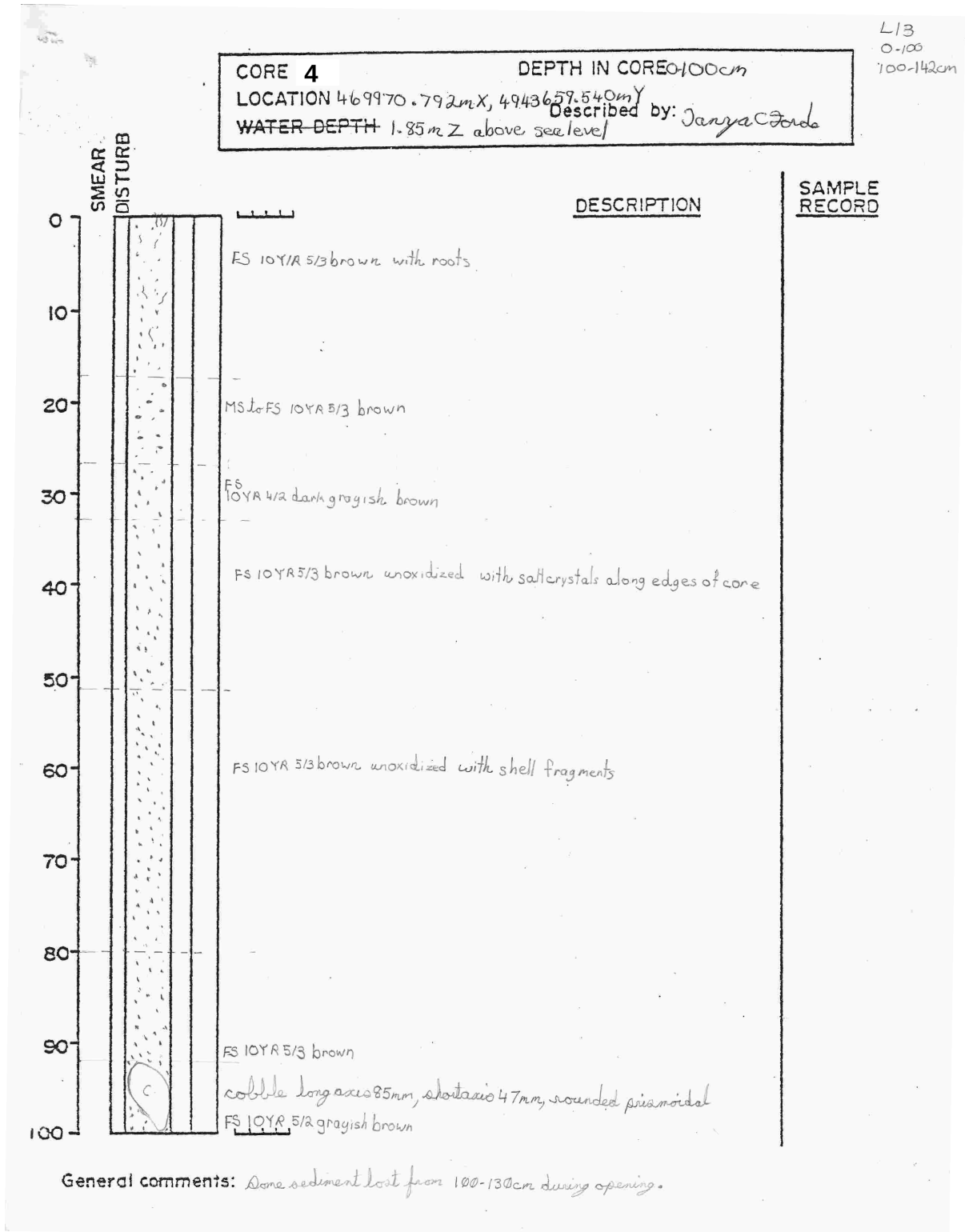
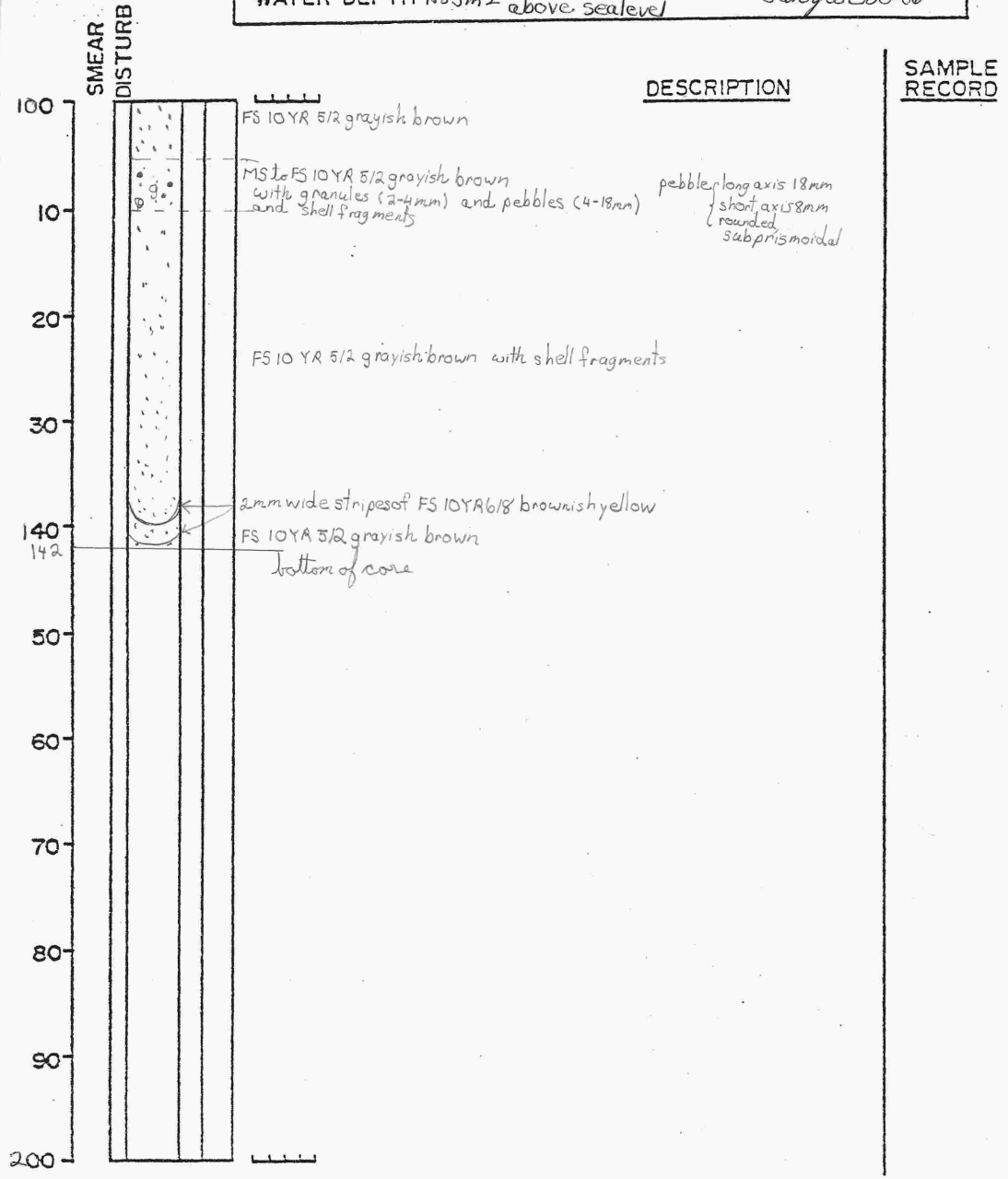


Figure A2.9 Vibracore log sheet 4, 0-100 cm.

CORE 4 DEPTH IN CORE 100-142cm
 LOCATION 469970.792mX, 4943659.540mY
 WATER DEPTH 1.85mZ above sea level
 Described by: *Janya C. Doro*



General comments:

Figure A2.10 Vibracore log sheet 4, 100-142 cm.

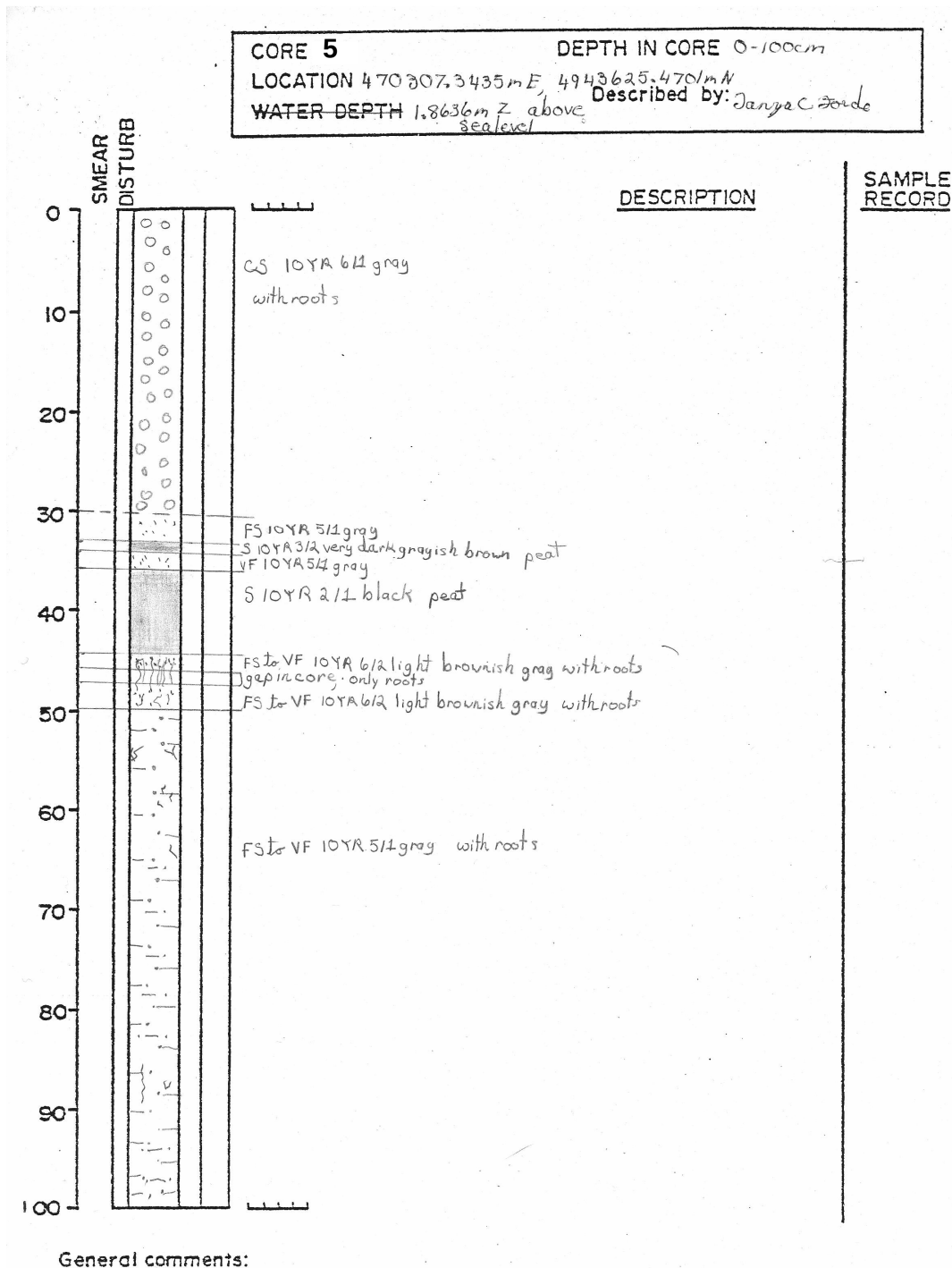
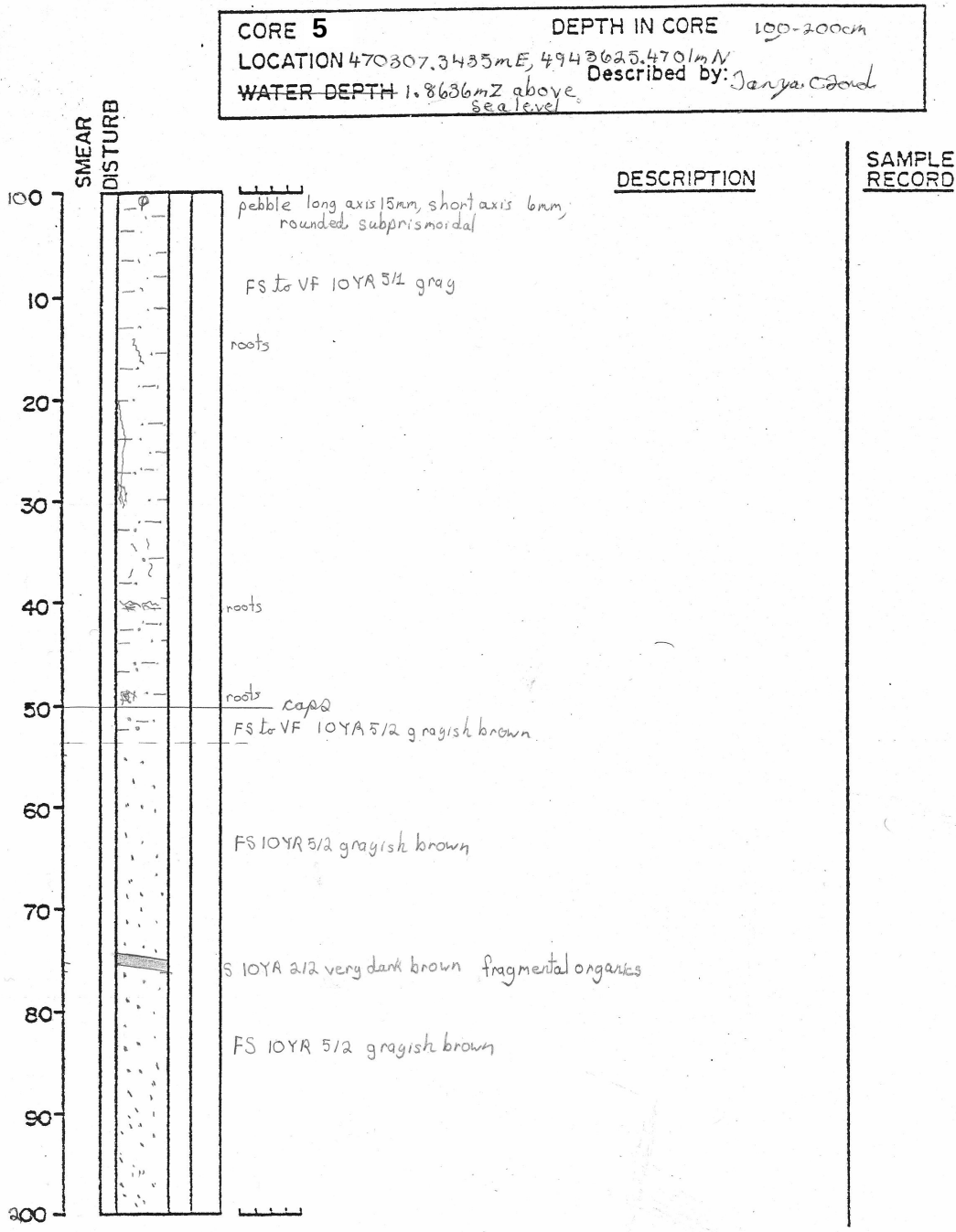


Figure A2.11 Vibracore log sheet 5, 0-100 cm.



General comments:

Figure A2.12 Vibracore log sheet 5, 100-200 cm.

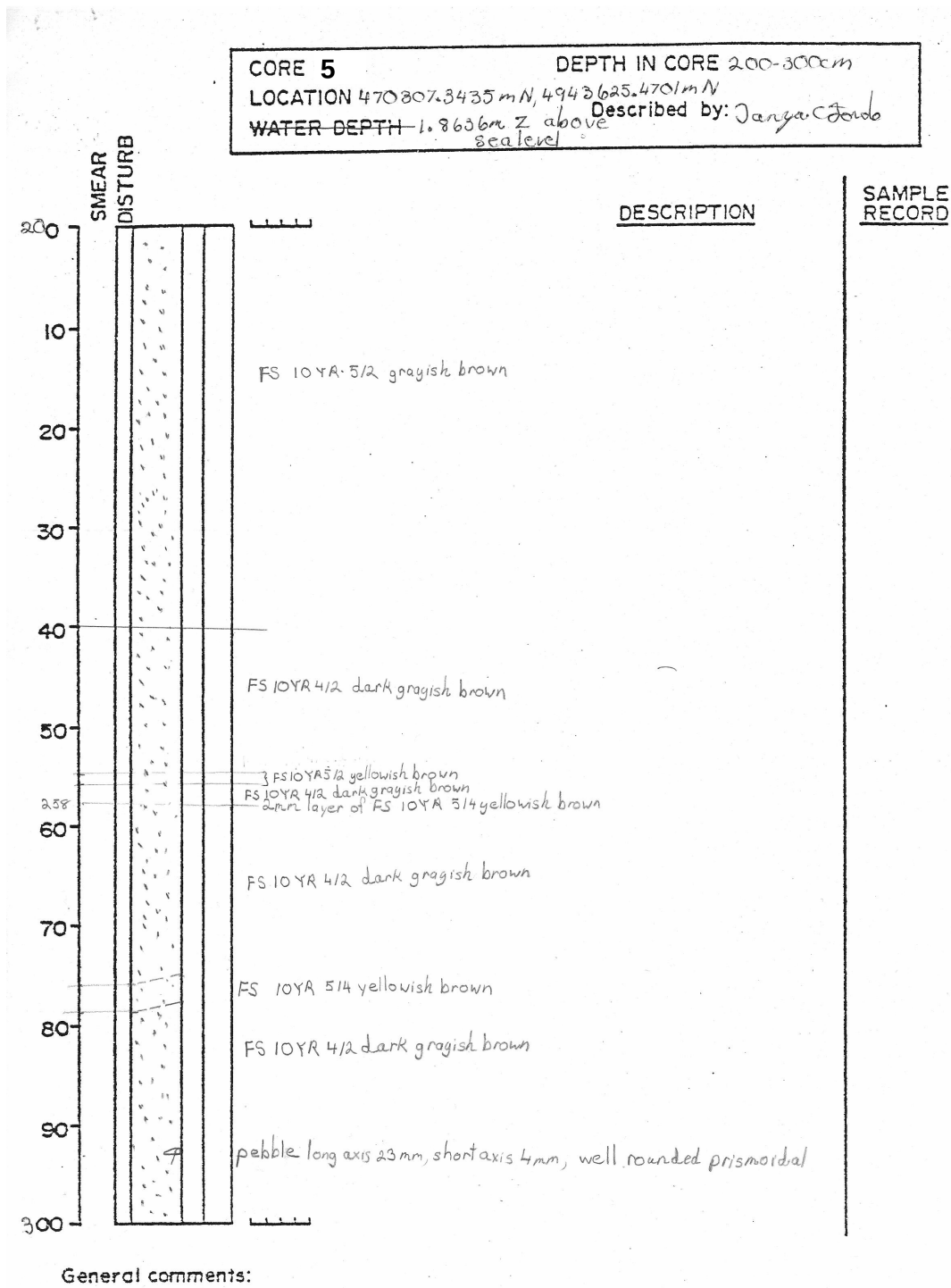


Figure A2.13 Vibracore log sheet 5, 200-300 cm.

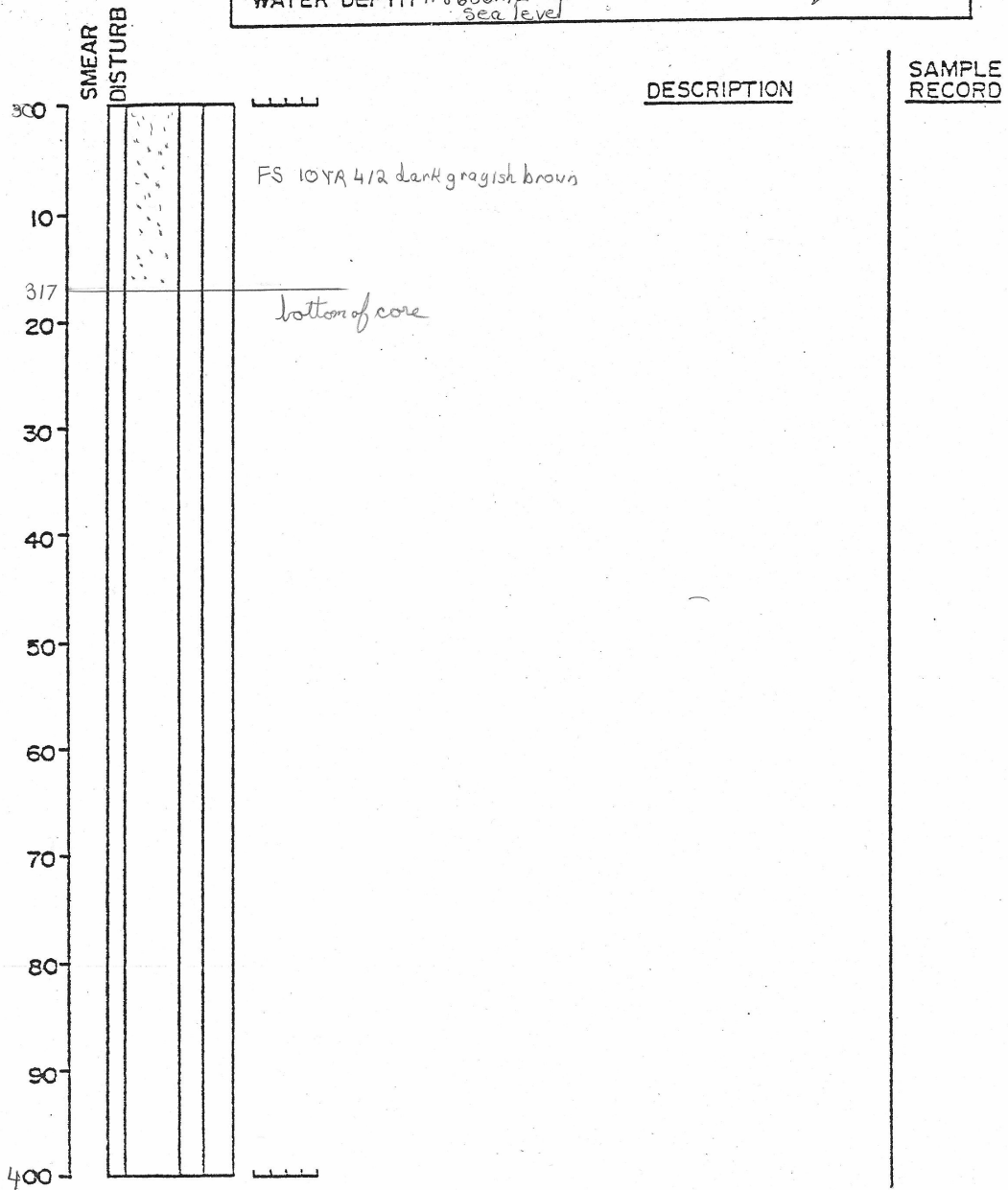
CORE 5

DEPTH IN CORE 300-317m

LOCATION 47°30' 34.35"N, 49°43' 25.4701"W

WATER DEPTH 1.8636m ² above sea level

Described by: Janya C. Jorda



General comments:

Figure A2.14 Vibracore log sheet 5, 300-317 cm.

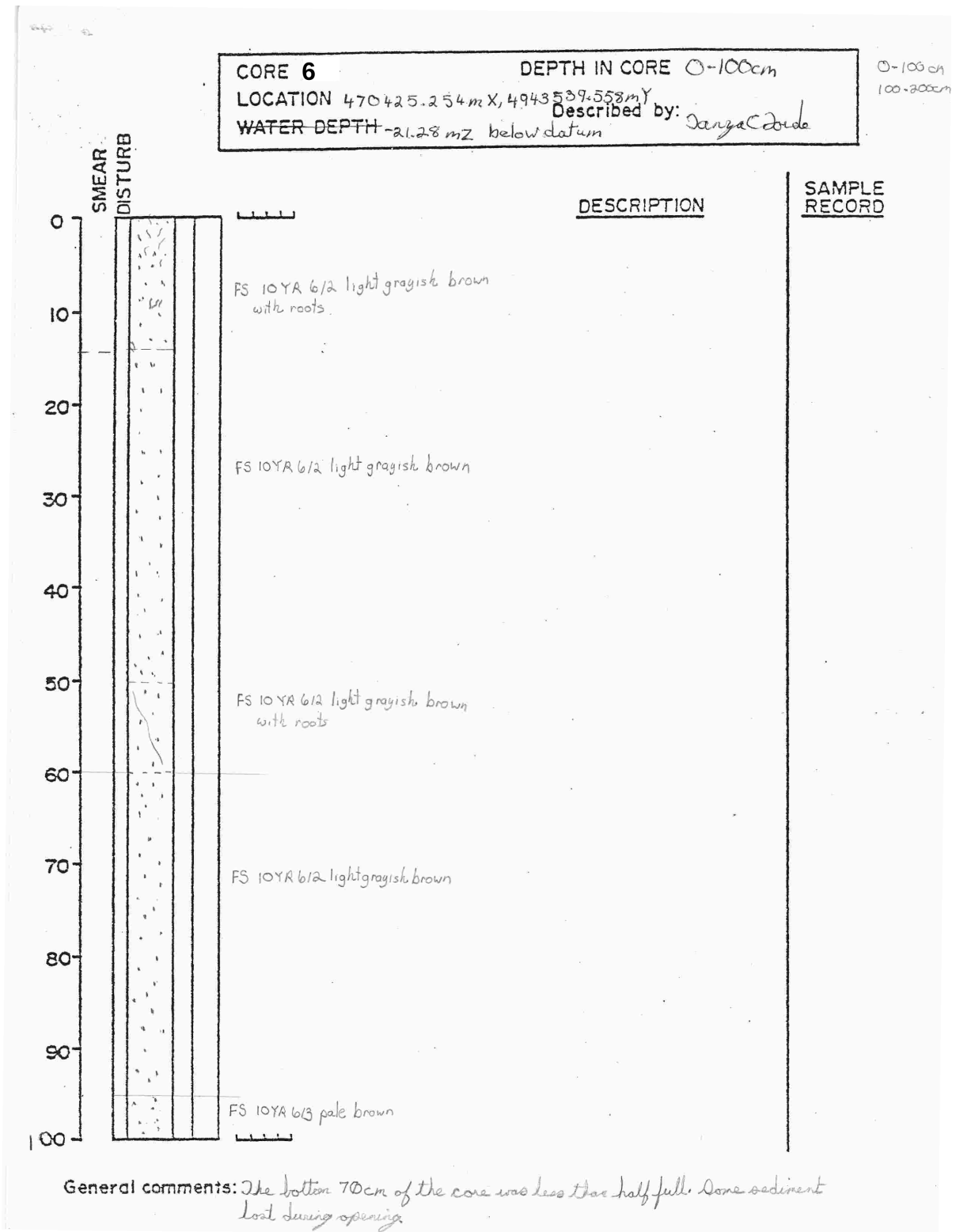


Figure A2.15 Vibracore log sheet 6, 0-100 cm.

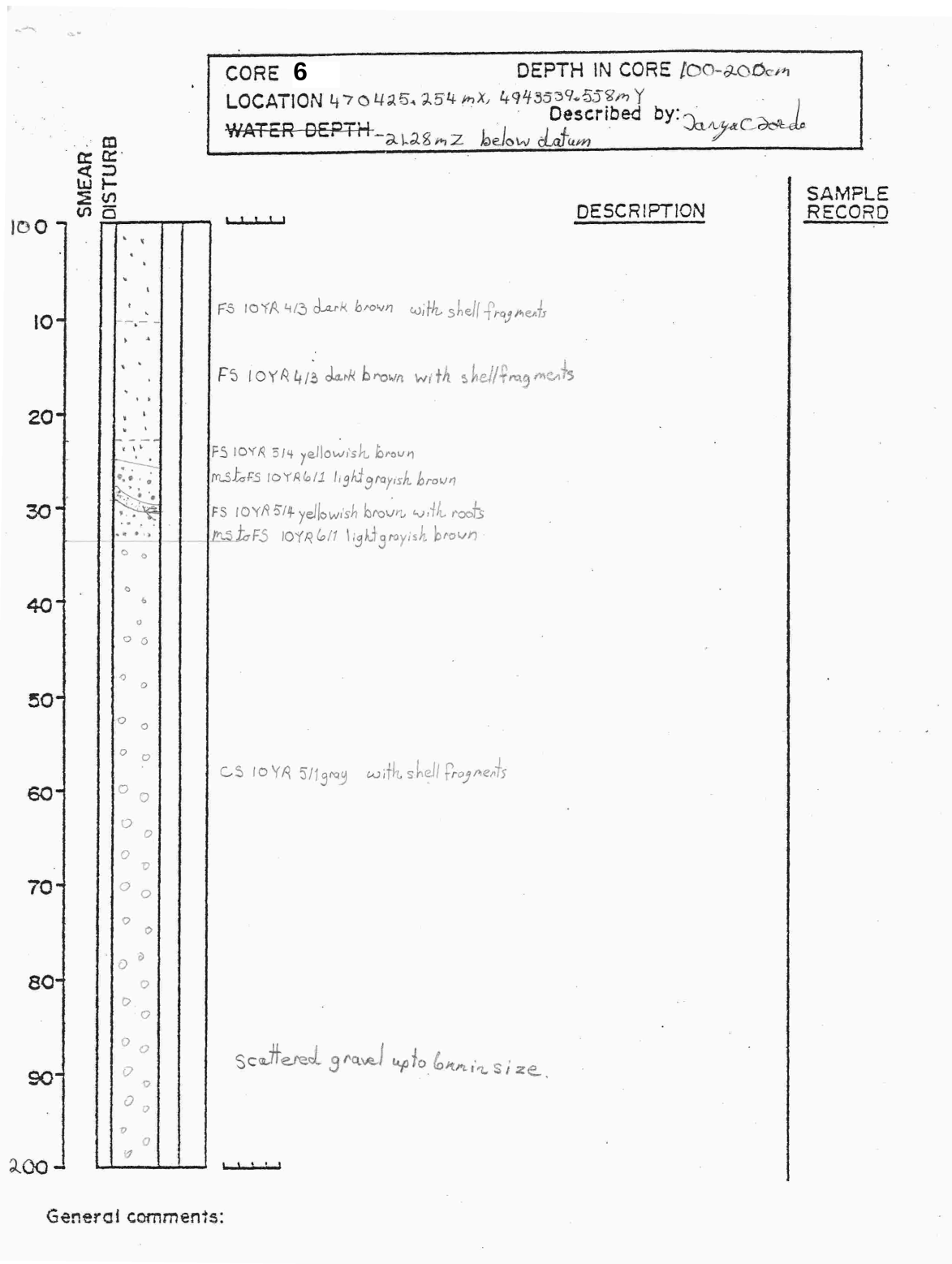


Figure A2.16 Vibracore log sheet 6, 100-200 cm.

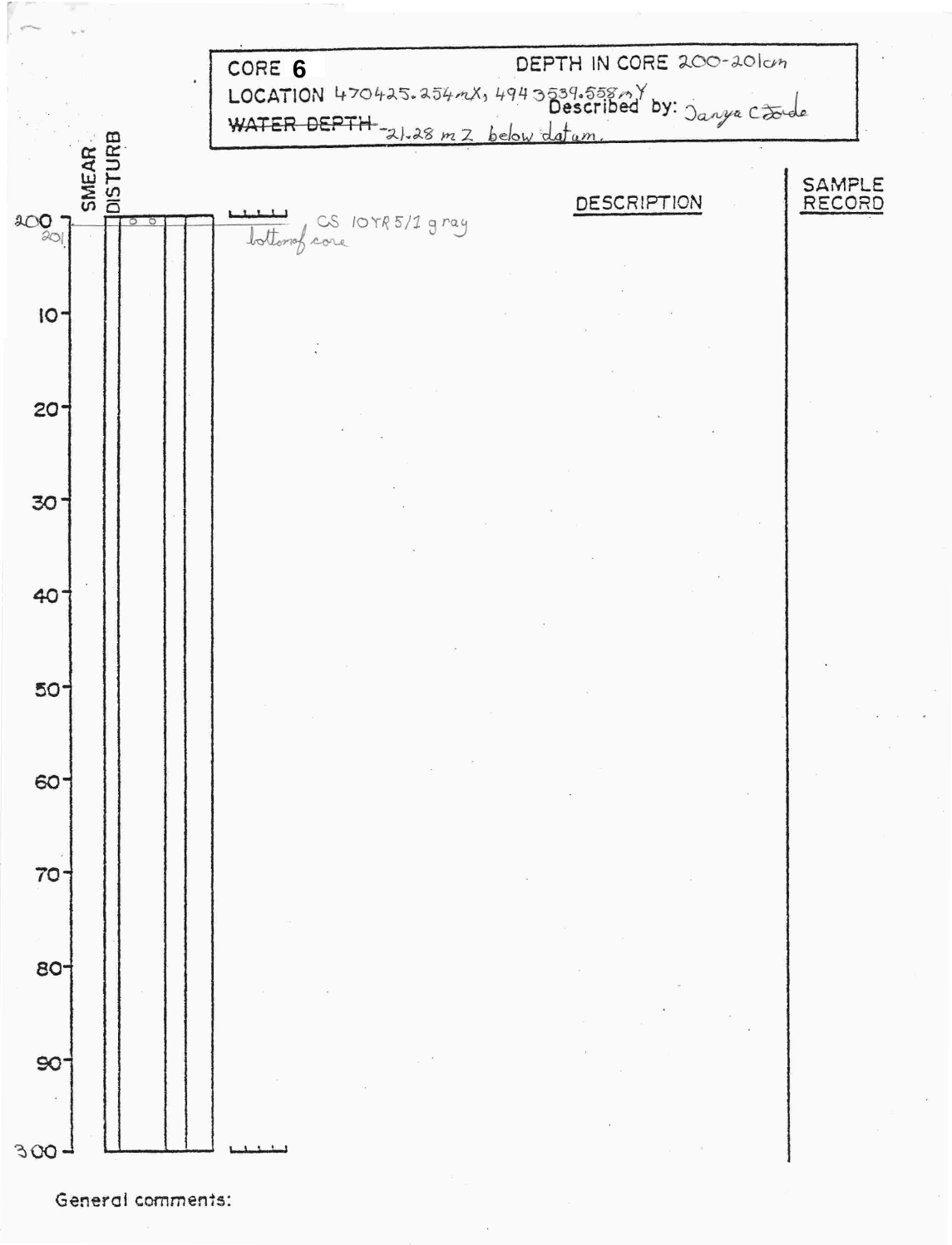
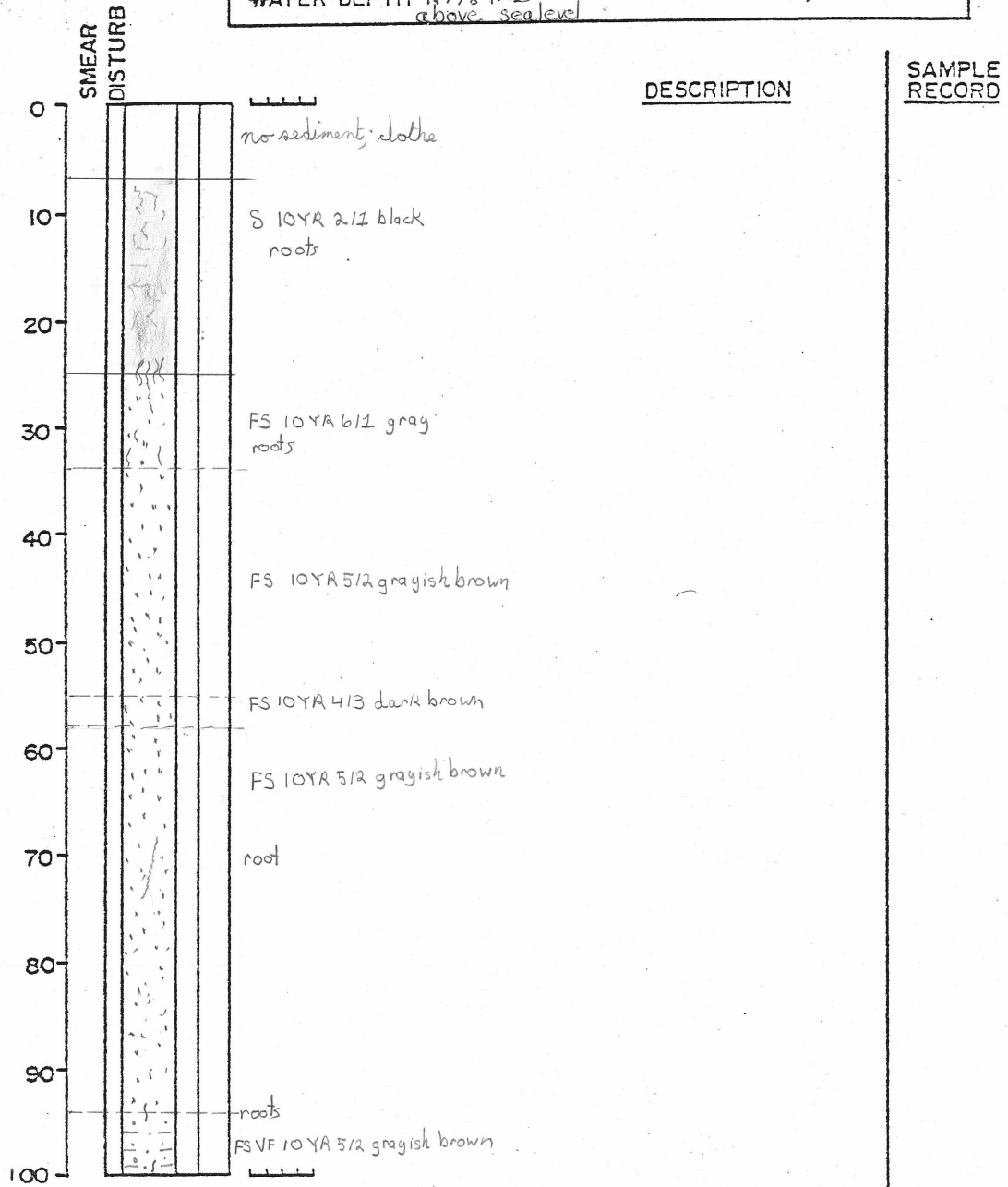


Figure A2.17 Vibracore log sheet 6, 200-201 cm.

CORE 7 DEPTH IN CORE 0-100cm
 LOCATION 4 70475.3509mE 4943594.4515mN
 WATER DEPTH 1.7789mZ above sea level
 Described by: *Danya C. Fido*

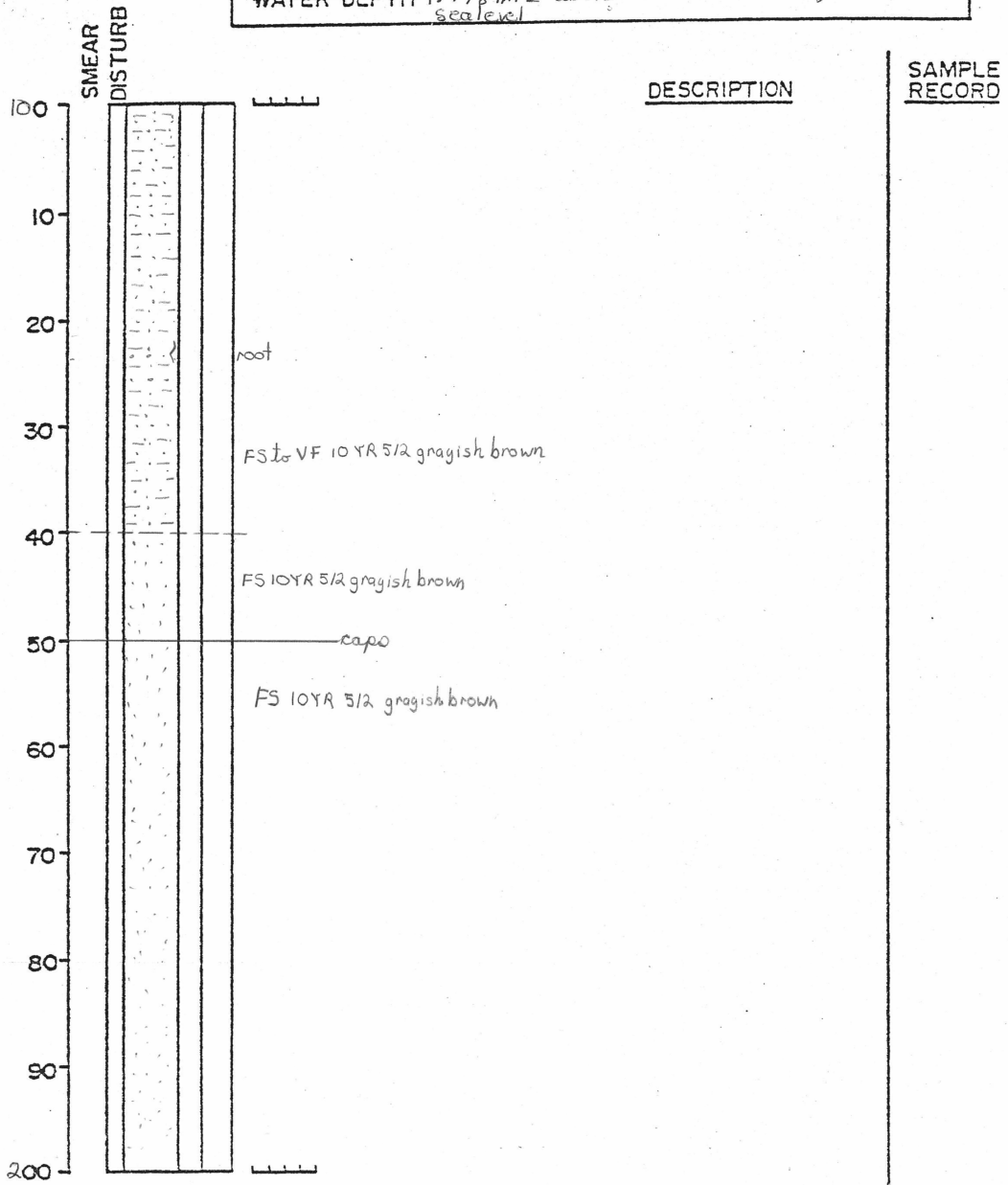
L23
 0-100
 100-200
 200-300
 300-347



General comments:

Figure A2.18 Vibracore log sheet 7, 0-100 cm.

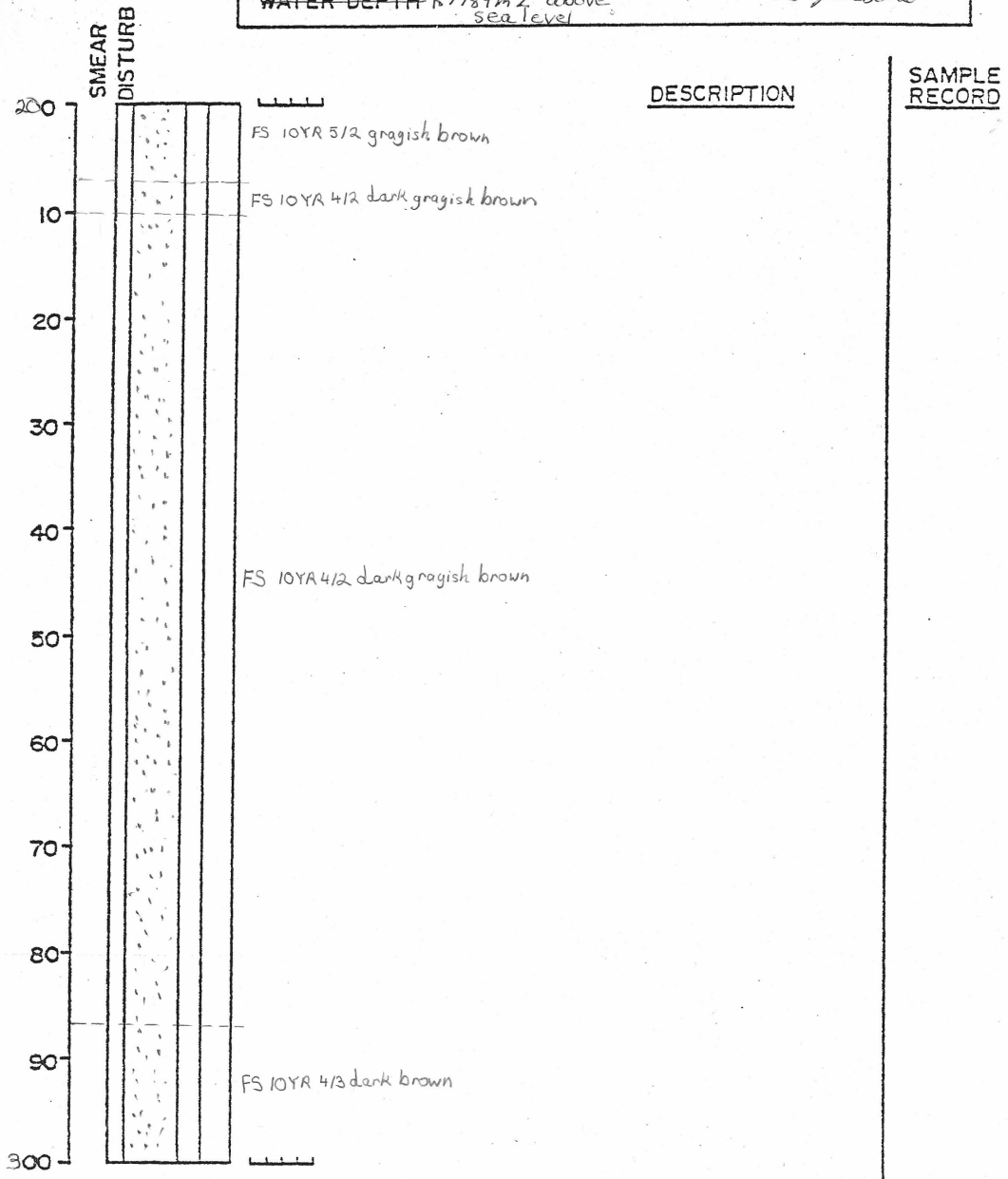
CORE 7 DEPTH IN CORE 100-200cm
 LOCATION 470475.3509mE, 4943594.4515mN
 WATER DEPTH 1.7789m \pm above sea level Described by: Janya C Zende



General comments:

Figure A2.19 Vibracore log sheet 7, 100-200 cm.

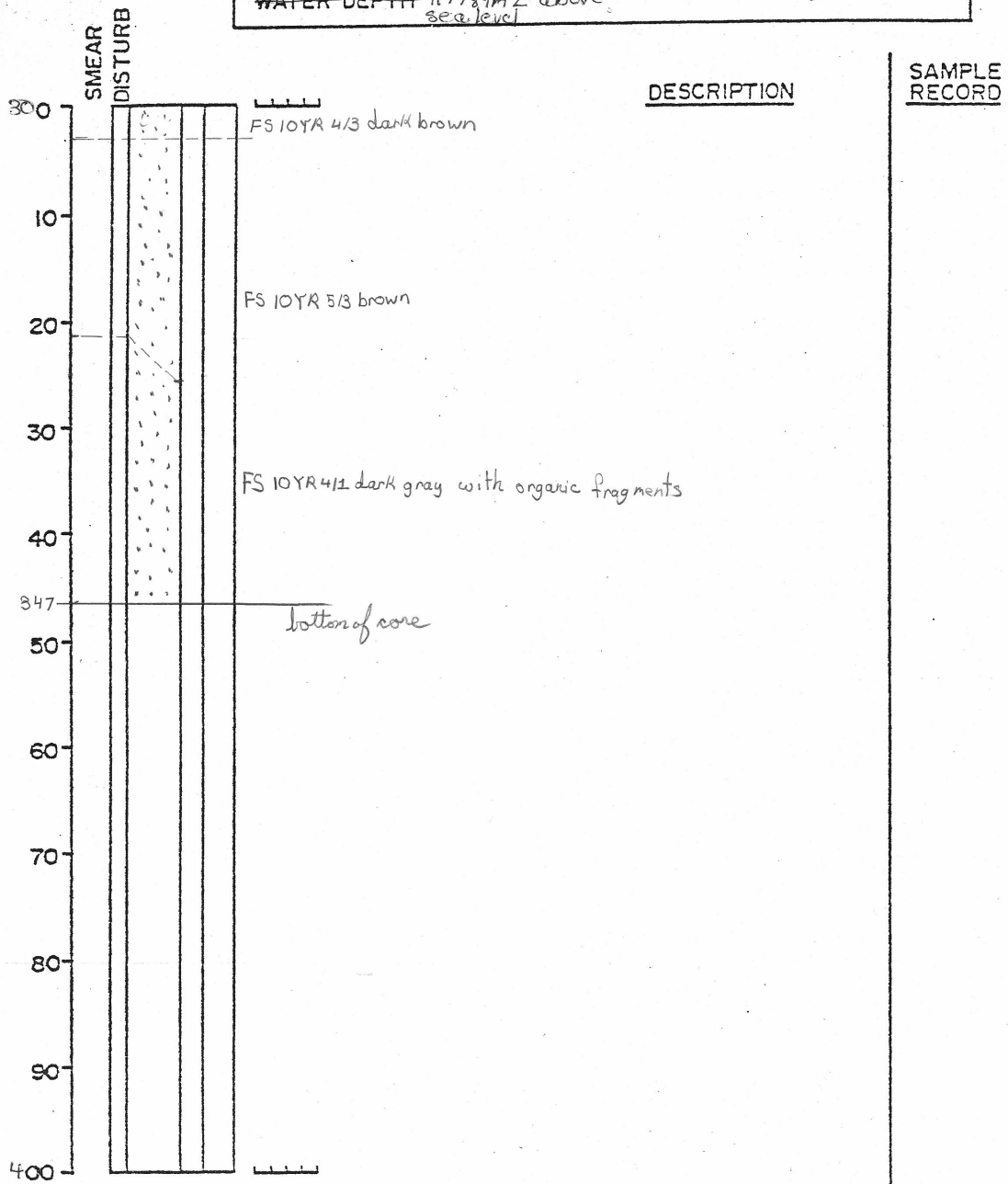
CORE 7	DEPTH IN CORE 200-300cm
LOCATION 470475.3509mE, 4943594.4515mN	Described by: <i>Janya C. Jando</i>
WATER DEPTH 1.7789m Z above sea level	



General comments:

Figure A2.20 Vibracore log sheet 7, 200-300 cm.

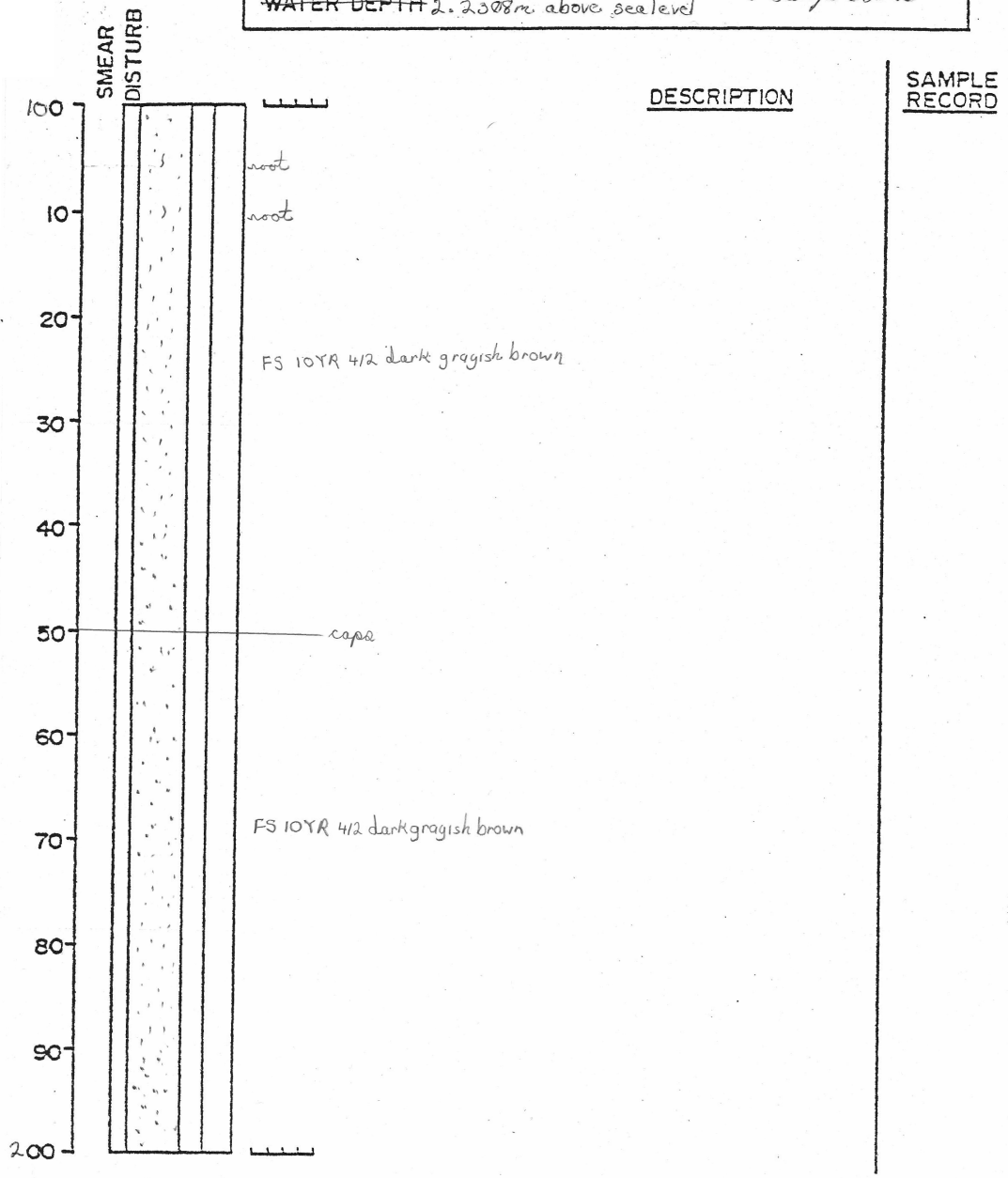
CORE 7 DEPTH IN CORE 300-347cm
 LOCATION 470475.3509mE, 4943594.4515mN
 WATER DEPTH 1.7799mZ above sea level Described by: Danya C. Jando



General comments:

Figure A2.21 Vibracore log sheet 7, 300-347 cm.

CORE 8 DEPTH IN CORE 100-200cm
 LOCATION 47055.8112mE, 4943555.0209mN
 WATER DEPTH 2.2308m above sea level
 Described by: Danya C. Jorda



General comments:

Figure A2.23 Vibracore log sheet 8, 100-200 cm.

CORE 8 DEPTH IN CORE 200-300cm
 LOCATION 47055.3112m E, 4943555.0209m N Described by: *Danya C. Fardo*
 WATER DEPTH 2.2308m above sea level

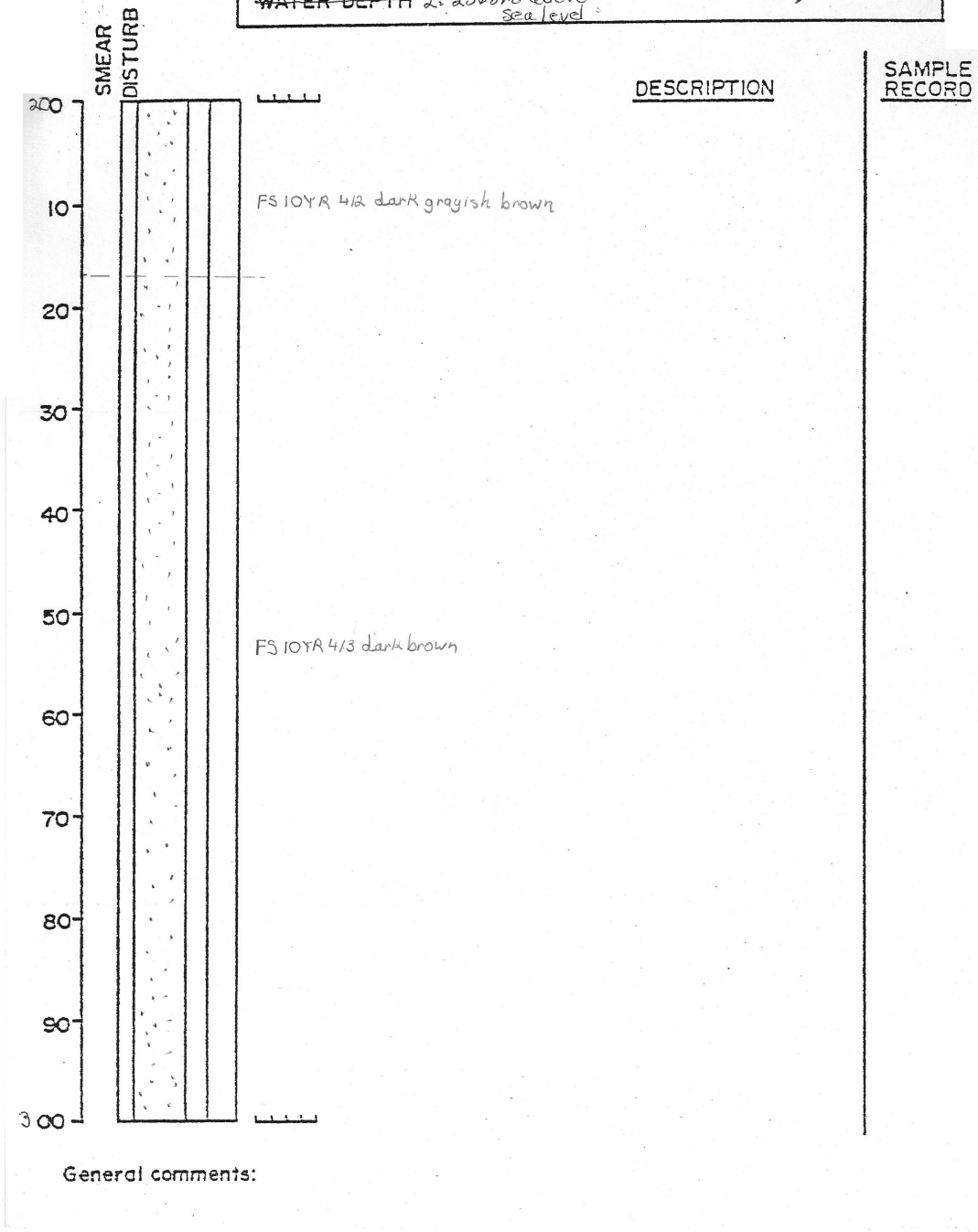
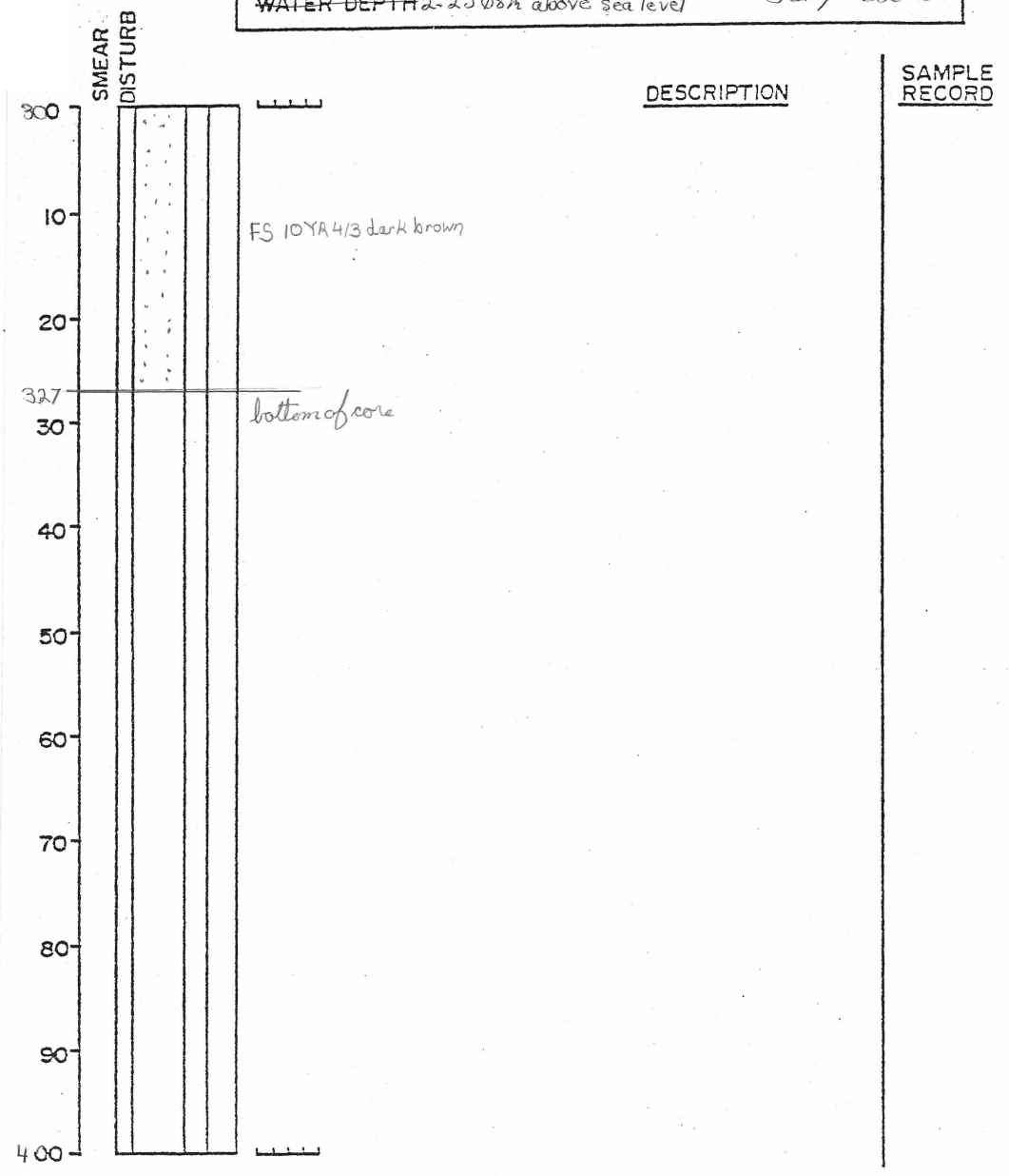


Figure A2.24 Vibracore log sheet 8, 200-300 cm.

CORE 8 DEPTH IN CORE 300-327cm
 LOCATION 47055.312mE, 494,8555.0209mN
 WATER DEPTH 2.2308m above sea level
 Described by: Janya Cando



General comments:

Figure A2.25 Vibracore log sheet 8, 300-327 cm.

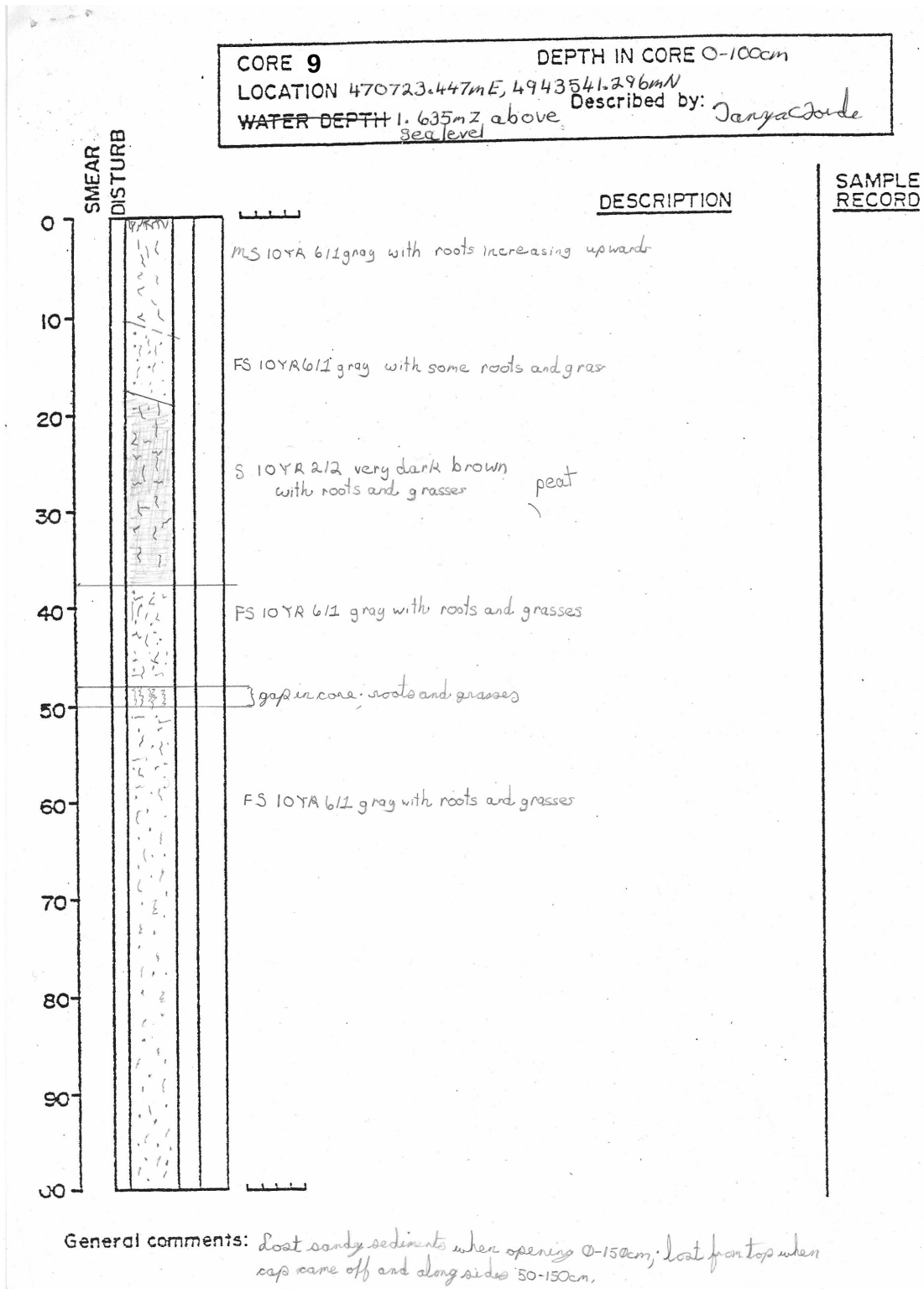


Figure A2.26 Vibracore log sheet 9, 0-100 cm.

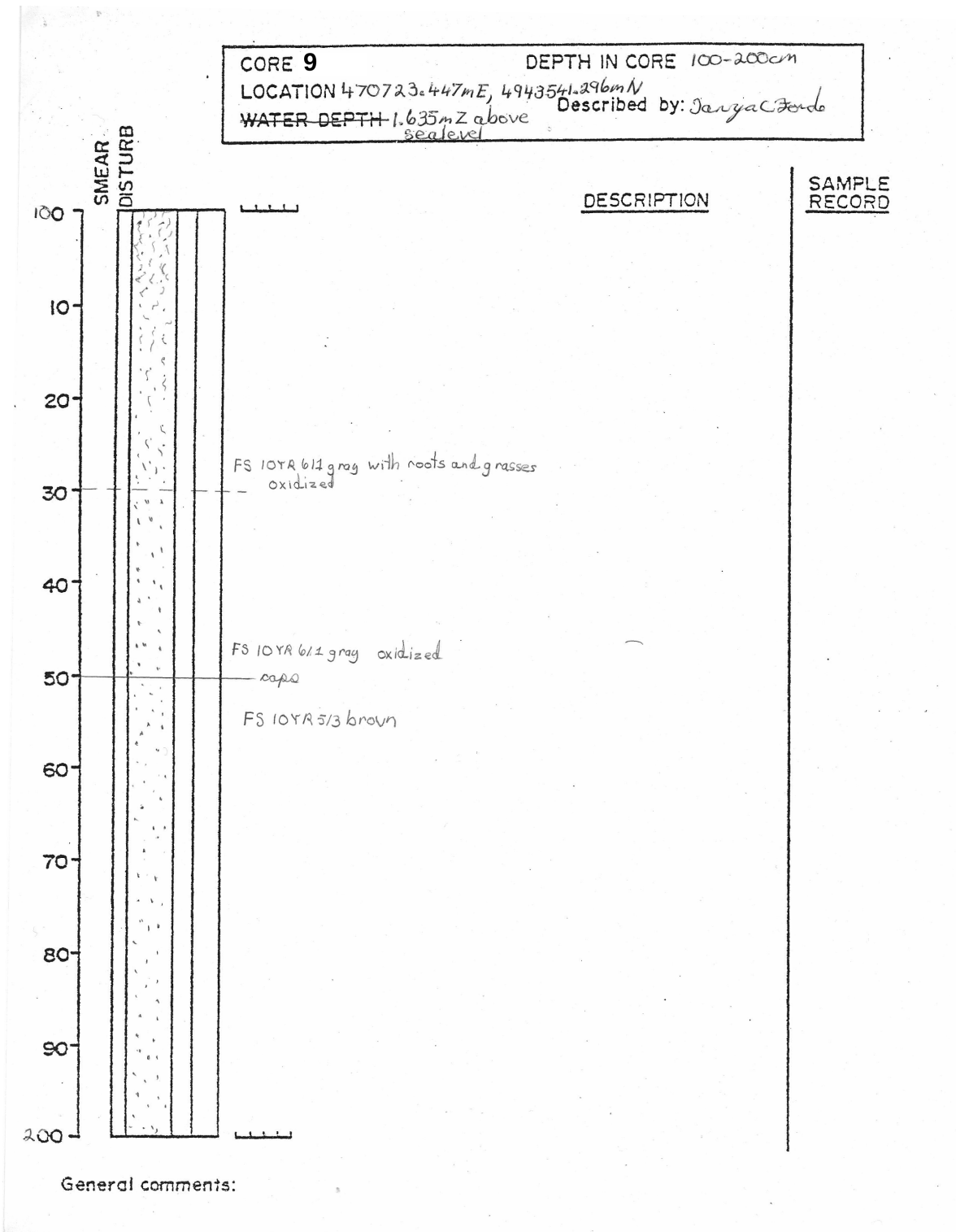
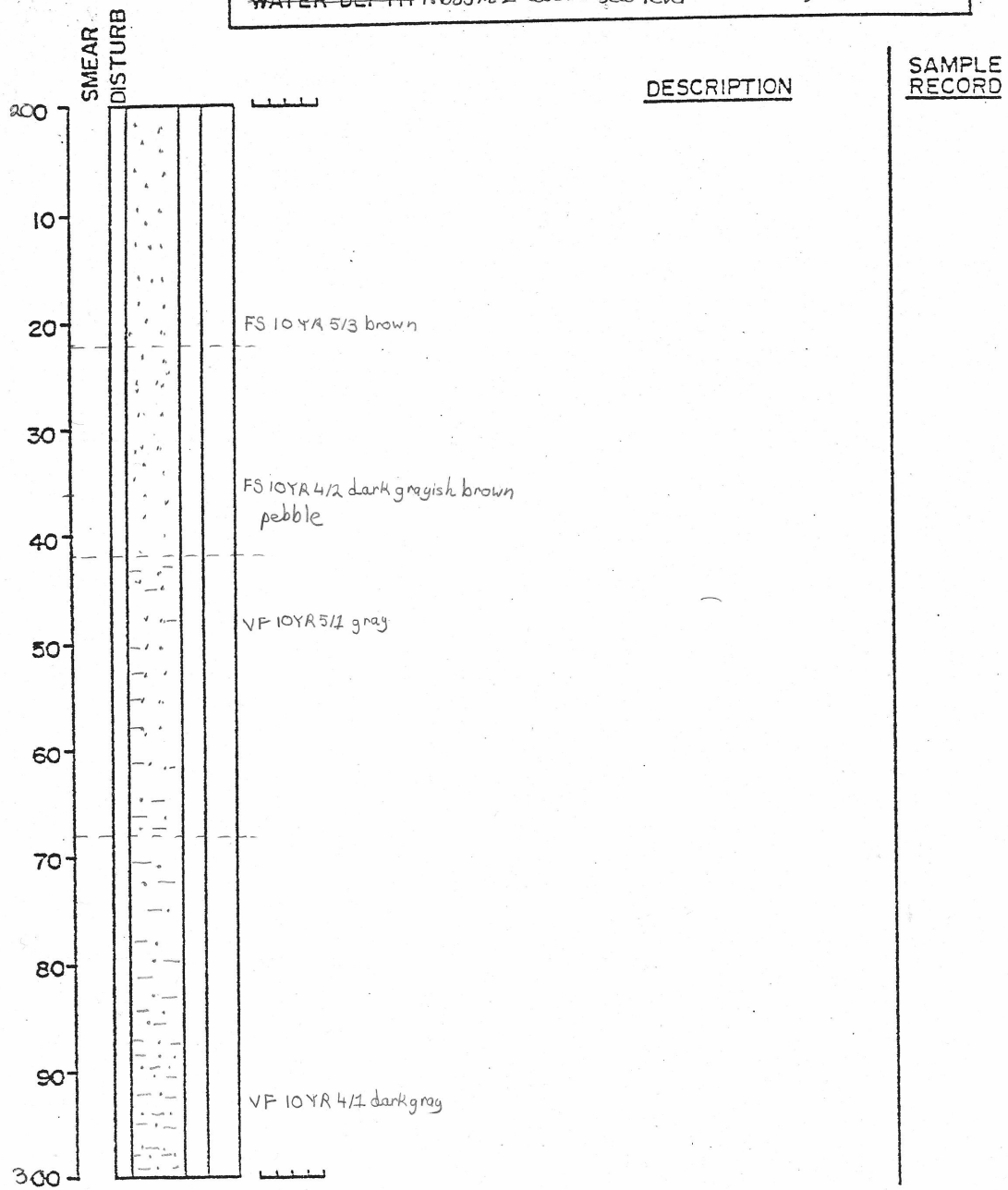


Figure A2.27 Vibracore log sheet 9, 100-200 cm.

CORE 9 DEPTH IN CORE 200-300cm
 LOCATION 470723.447mE, 4943541.296mN
 WATER DEPTH 1.635m Z above sea level
 Described by: Danye C. Jardo



General comments:

Figure A2.28 Vibracore log sheet 9, 200-300 cm.

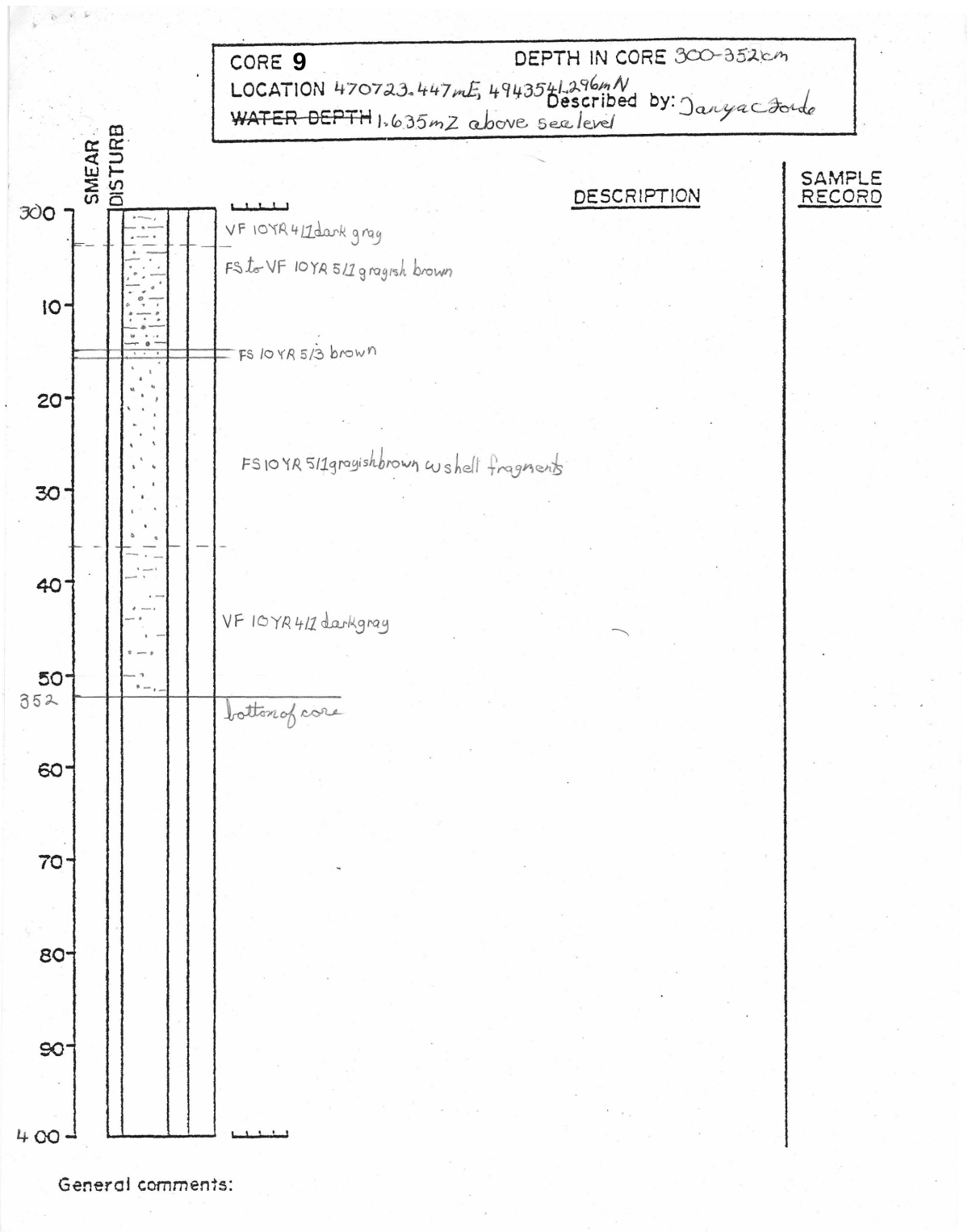
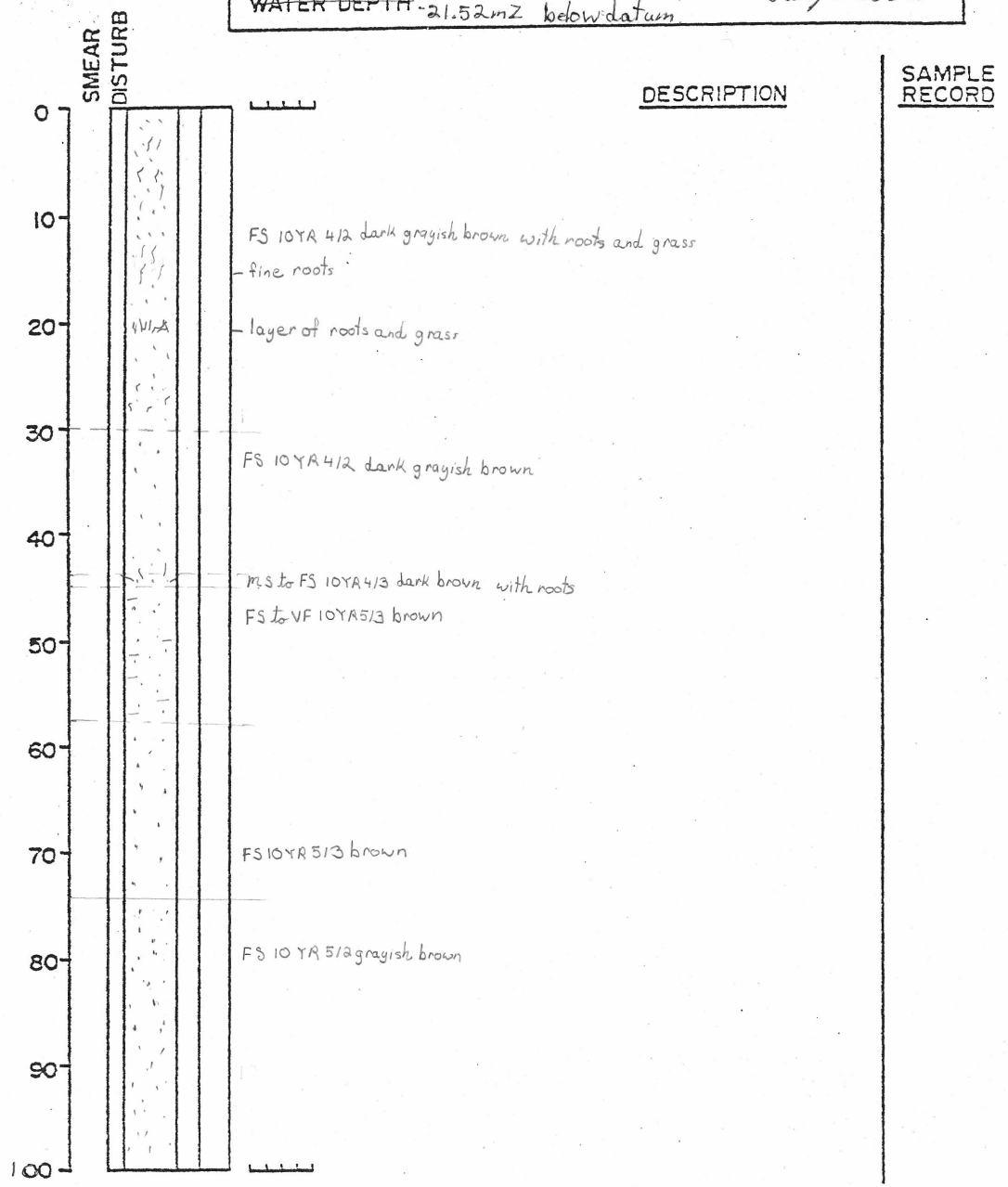


Figure A2.29 Vibracore log sheet 9, 300-352 cm.

L15A
0-15cm

CORE 10 DEPTH IN CORE 0-100cm
 LOCATION 470854.648672mX, 4943354.739852mY
 Described by: Janya C. Jorde
 WATER DEPTH -21.52mZ below datum



General comments:

Figure A2.30 Vibracore log sheet 10, 0-100 cm.

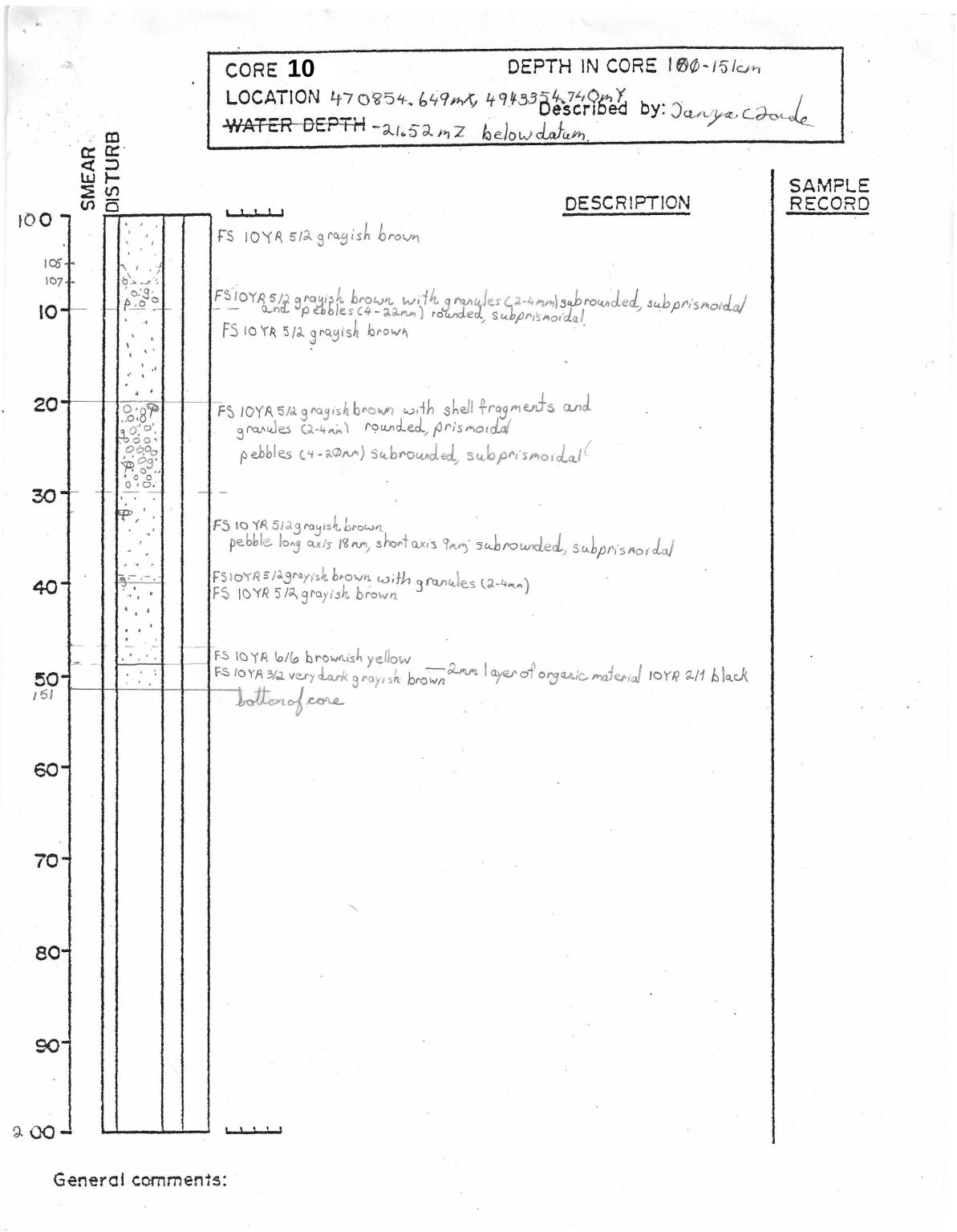
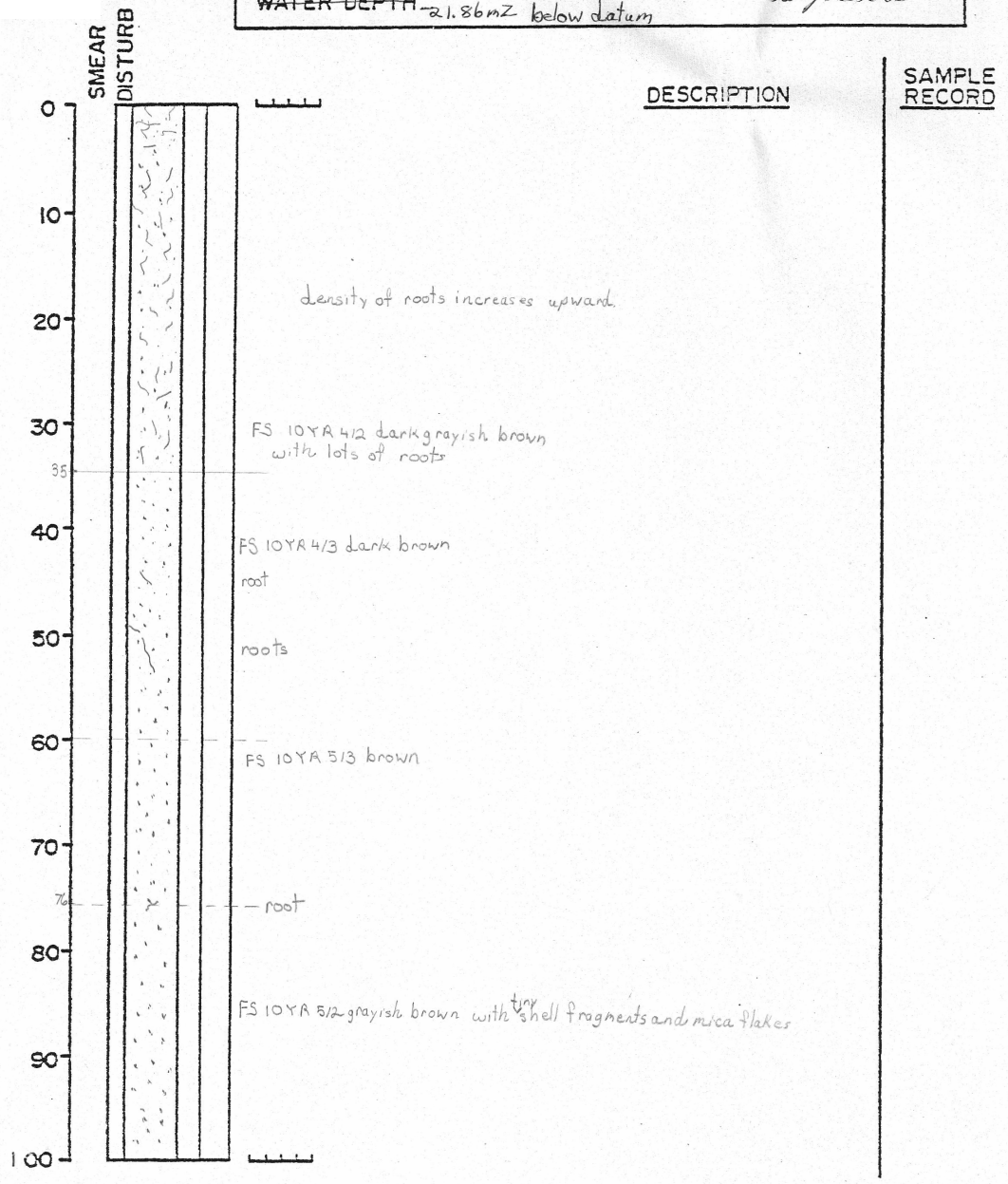


Figure A2.31 Vibracore log sheet 10, 100-151 cm.

CORE 11 DEPTH IN CORE 0-100cm
 LOCATION 470952.295m X, 494 3396.542m Y
 WATER DEPTH 21.86mZ below datum
 Described by: *Janyce C. Zide*

L1
 0-150
 150-267



General comments: the top 30cm of the core tube appeared empty; when opened it was less than half full. This sandy core was difficult to open without sand loss, but did not split evenly.

Figure A2.32 Vibracore log sheet 11, 0-100 cm.

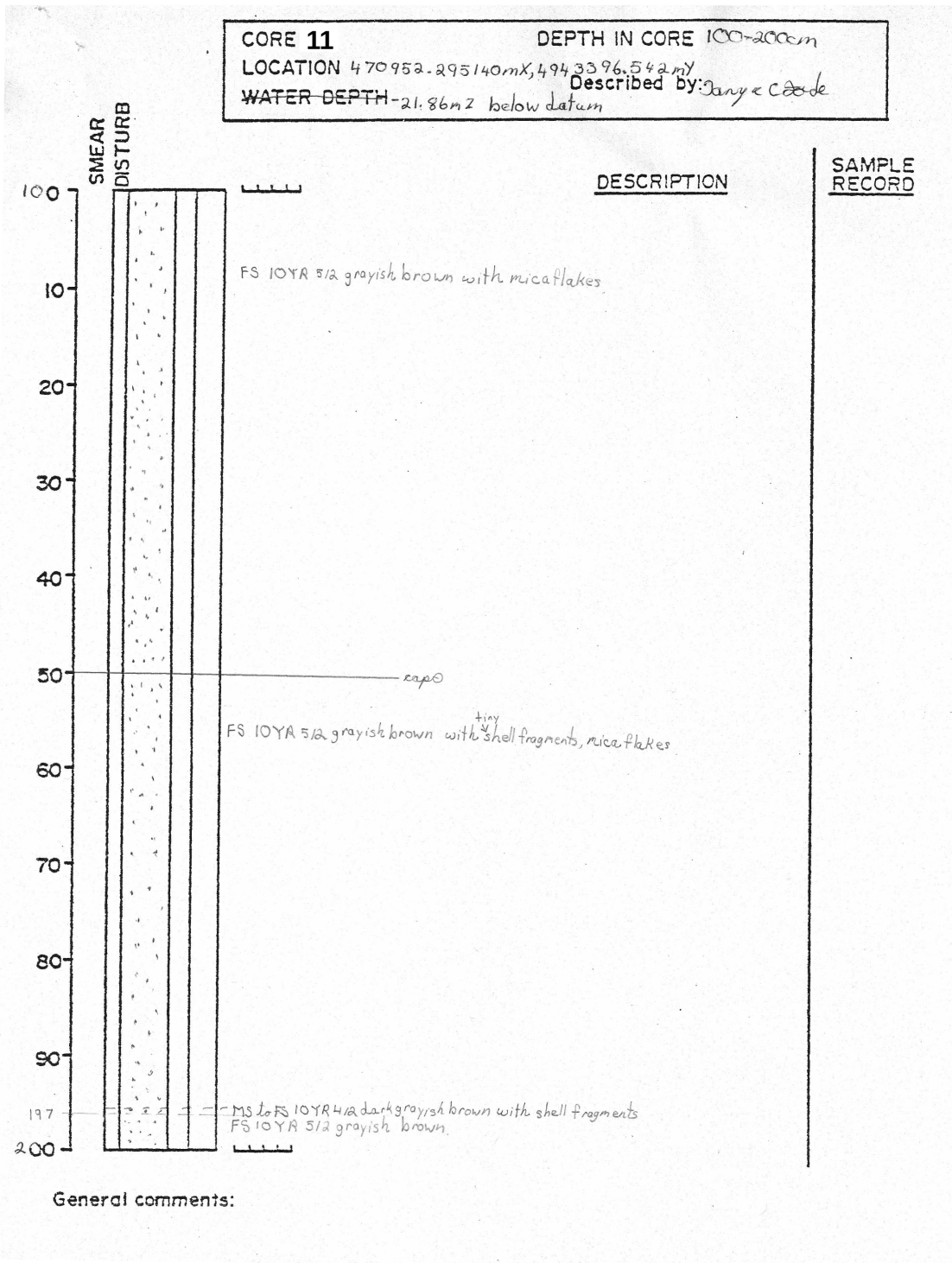
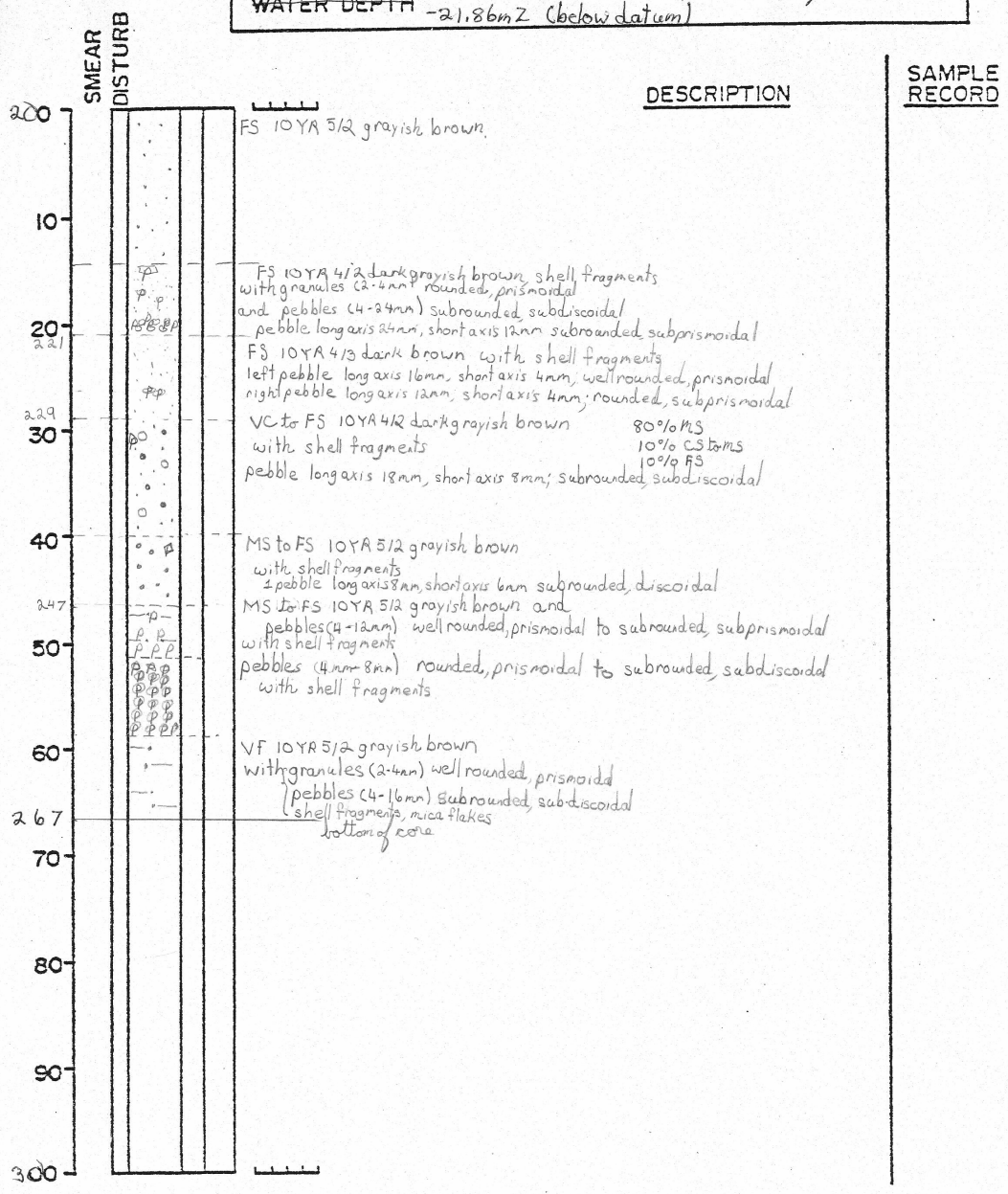


Figure A2.33 Vibracore log sheet 11, 100-200 cm.

CORE 11 DEPTH IN CORE 200-267cm
 LOCATION 47095.295mX, 4943396.542mY Described by: Janyz C. Jorde
 WATER DEPTH -21.86mZ (below datum)

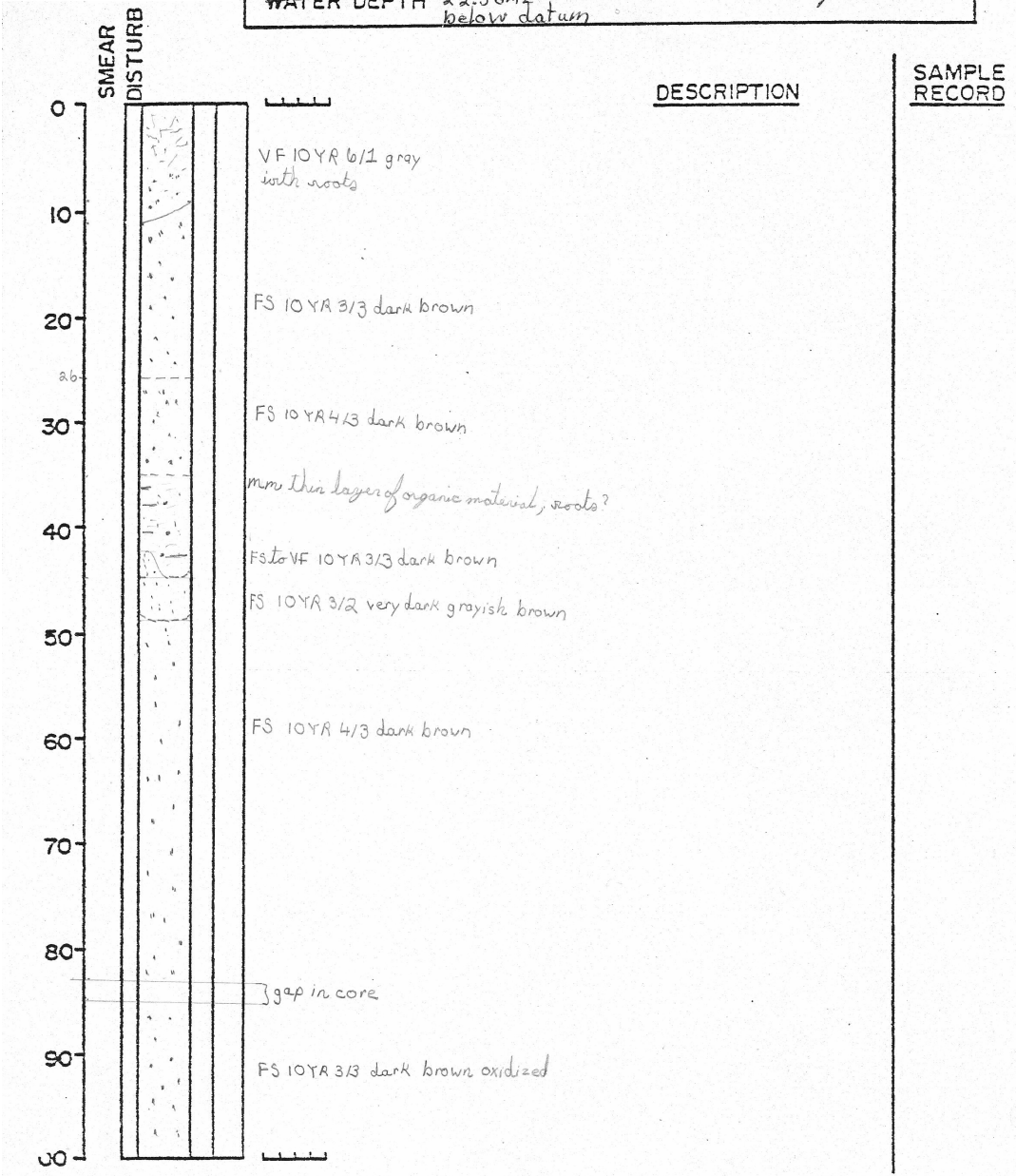


General comments:

Figure A2.34 Vibracore log sheet 11, 200-267 cm.

CORE 12 DEPTH IN CORE 0-100cm
 LOCATION 471001.569mX, 4943692.701mY
 WATER DEPTH 22.56mZ
 below datum Described by: Janya C Jorde

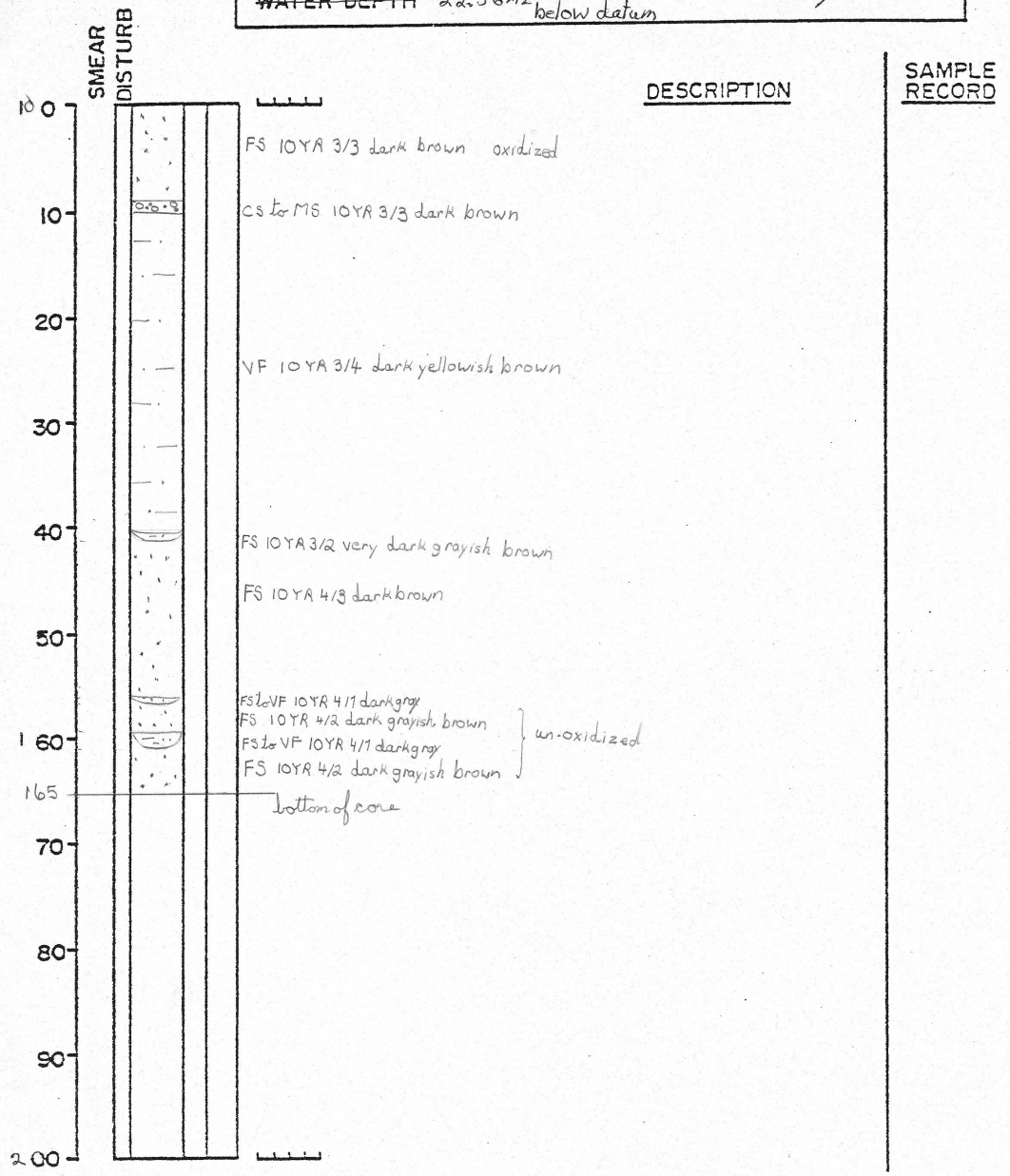
L5
 165cm



General comments:

Figure A2.35 Vibracore log sheet 12, 0-100 cm.

CORE 12 DEPTH IN CORE 100-165cm
 LOCATION 471001.569mX, 4943692.701mY
 Described by: Janya C. Jorda
 WATER DEPTH -22.56mZ below datum

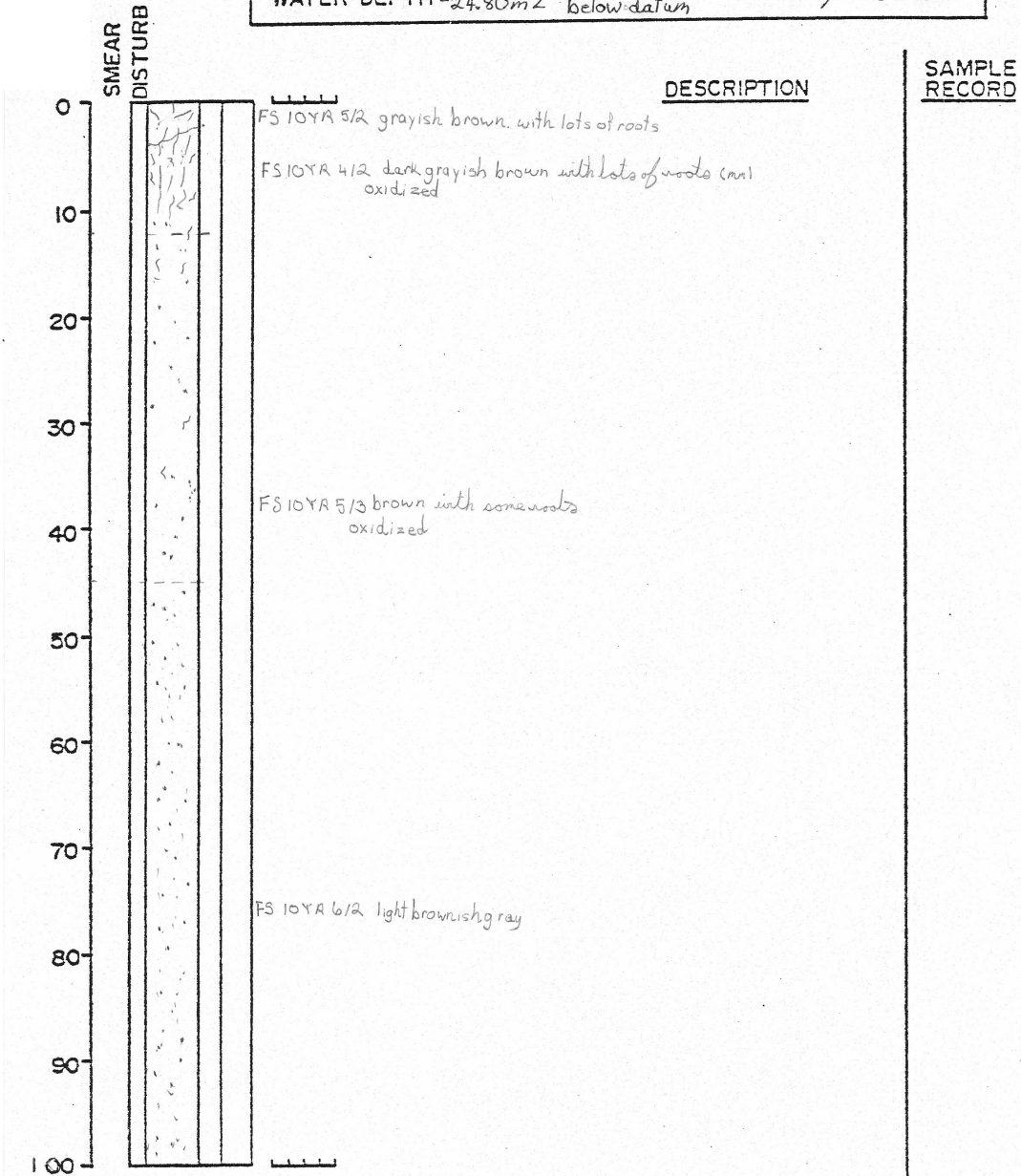


General comments:

Figure A2.36 Vibracore log sheet 12, 100-165 cm.

La
0-150
150.242

CORE 13 DEPTH IN CORE 0-100cm
LOCATION 471167.262mX, 4943542.291mY
WATER DEPTH -24.80mZ below datum
Described by: *Janya C. Jorda*



General comments: *lost lots of sand when moving and opening core.
top of core cut off in the field and saved in a bag* FS 10YA 3/2 very dark grayish brown
with roots up to 3mm in diameter

Figure A2.37 Vibracore log sheet 13, 0-100 cm.

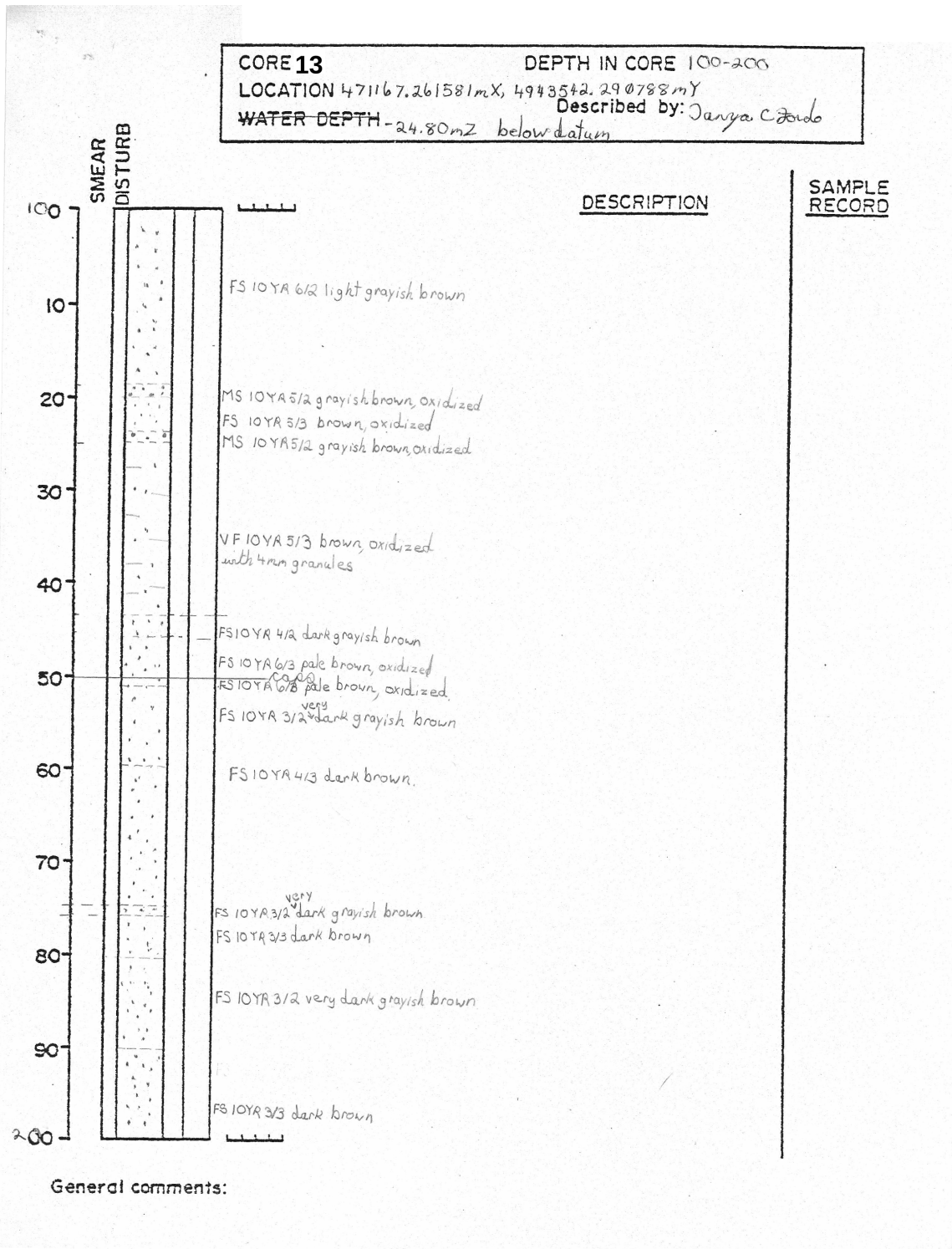
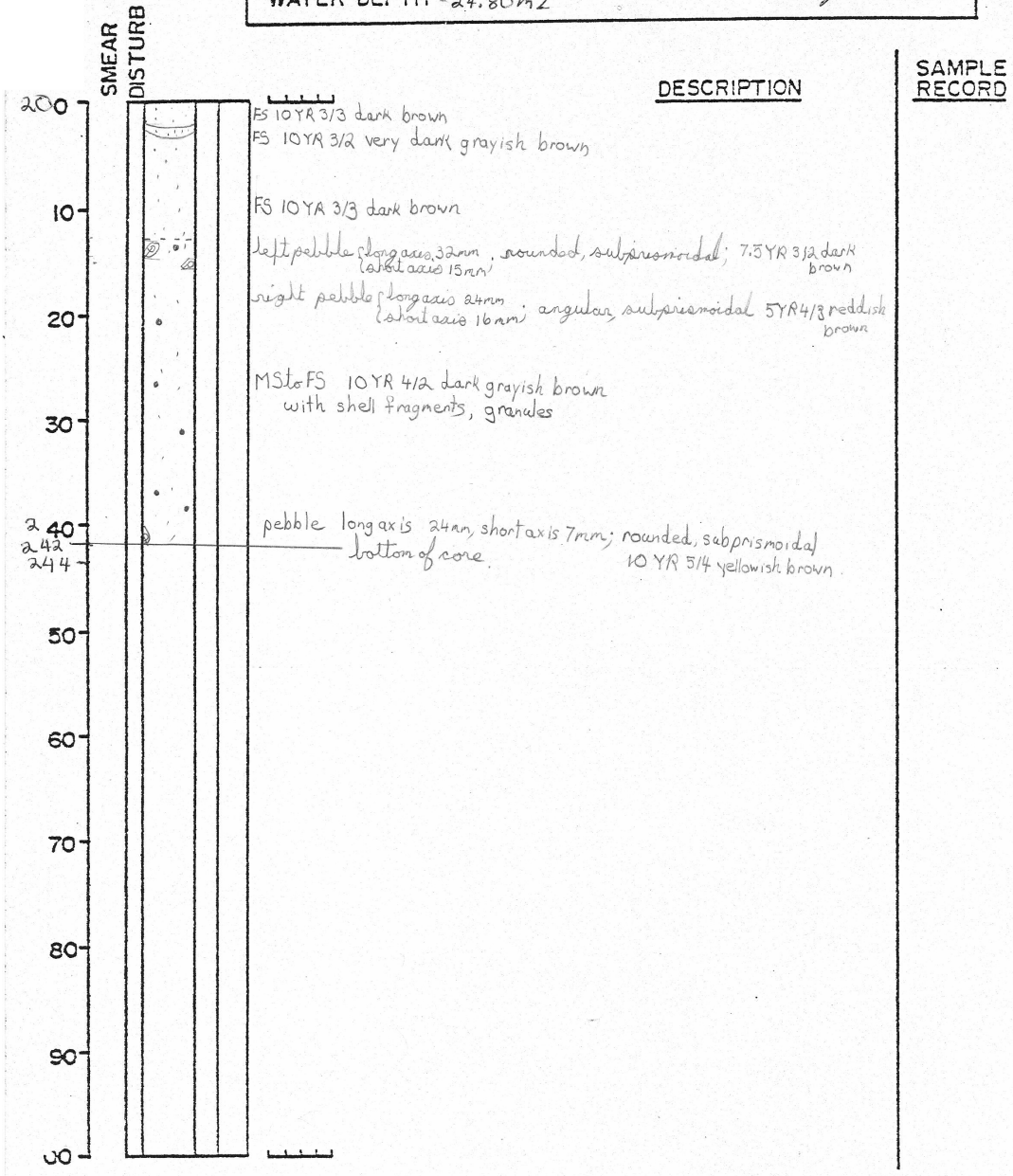


Figure A2.38 Vibracore log sheet 13, 100-200 cm.

CORE 13 DEPTH IN CORE 200-242 cm
 LOCATION 471167.261581mX, 4943542.290788mY
 WATER DEPTH -24.80mZ Described by: Janya C. Jorde



General comments:

Figure A2.39 Vibracore log sheet 13, 200-242 cm.

APPENDIX 3: GRADISTAT Grain-size Analysis Statistics

Twenty-three sediment samples from the vibracores (Fig. 3.4) were analysed for grain-size. The GRADISTAT printouts are reproduced here.

SAMPLE STATISTICS						
SAMPLE IDENTITY: 01			ANALYST & DATE: TCF, 4/16/2013			
SAMPLE TYPE: Unimodal, Moderately Well Sorted			TEXTURAL GROUP: Slightly Gravelly Sand			
SEDIMENT NAME: Slightly Medium Gravelly Fine Sand						
	μm	ϕ	GRAIN SIZE DISTRIBUTION			
MODE 1:	185.5	2.432	GRAVEL: 0.3%		COARSE SAND: 4.5%	
MODE 2:			SAND: 99.6%		MEDIUM SAND: 17.3%	
MODE 3:			MUD: 0.1%		FINE SAND: 68.6%	
D ₁₀ :	126.2	1.598			V FINE SAND: 9.3%	
MEDIAN or D ₅₀ :	188.8	2.405	V COARSE GRAVEL: 0.0%		V COARSE SILT: 0.1%	
D ₉₀ :	330.4	2.986	COARSE GRAVEL: 0.0%		COARSE SILT: 0.0%	
(D ₉₀ / D ₁₀):	2.618	1.869	MEDIUM GRAVEL: 0.3%		MEDIUM SILT: 0.0%	
(D ₉₀ - D ₁₀):	204.1	1.388	FINE GRAVEL: 0.0%		FINE SILT: 0.0%	
(D ₇₅ / D ₂₅):	1.583	1.322	V FINE GRAVEL: 0.0%		V FINE SILT: 0.0%	
(D ₇₅ - D ₂₅):	88.59	0.663	V COARSE SAND: 0.0%		CLAY: 0.0%	
	METHOD OF MOMENTS			FOLK & WARD METHOD		
	Arithmetic	Geometric	Logarithmic	Geometric	Logarithmic	Description
	μm	μm	ϕ	μm	ϕ	
MEAN (\bar{x}):	255.7	200.5	2.318	192.9	2.374	Fine Sand
SORTING (σ):	716.9	1.593	0.672	1.485	0.571	Moderately Well Sorted
SKEWNESS (Sk):	18.10	2.592	-2.592	0.198	-0.198	Coarse Skewed
KURTOSIS (K):	336.8	21.13	21.13	1.304	1.304	Leptokurtic

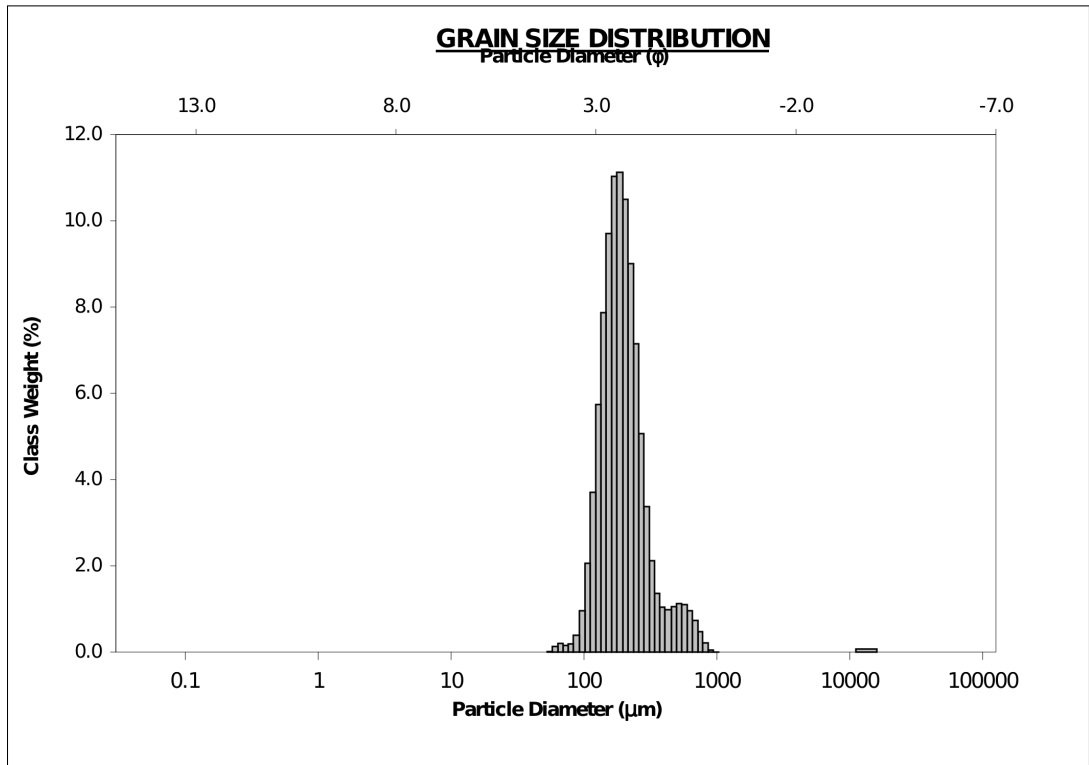


Figure A3.1 GRADISTAT printout with logarithmic frequency plot for grain-size sample 1.

SAMPLE STATISTICS						
SAMPLE IDENTITY: 02			ANALYST & DATE: TCF, 4/16/2013			
SAMPLE TYPE: Unimodal, Moderately Well Sorted			TEXTURAL GROUP: Sand			
SEDIMENT NAME: Moderately Well Sorted Fine Sand						
	μm	ϕ	GRAIN SIZE DISTRIBUTION			
MODE 1:	223.7	2.162	GRAVEL: 0.0%		COARSE SAND: 6.4%	
MODE 2:			SAND: 100.0%		MEDIUM SAND: 32.4%	
MODE 3:			MUD: 0.0%		FINE SAND: 58.4%	
D ₁₀ :	152.1	1.345			V FINE SAND: 2.6%	
MEDIAN or D ₅₀ :	227.3	2.137	V COARSE GRAVEL: 0.0%		V COARSE SILT: 0.0%	
D ₉₀ :	393.8	2.717	COARSE GRAVEL: 0.0%		COARSE SILT: 0.0%	
(D ₉₀ / D ₁₀):	2.589	2.021	MEDIUM GRAVEL: 0.0%		MEDIUM SILT: 0.0%	
(D ₉₀ - D ₁₀):	241.7	1.373	FINE GRAVEL: 0.0%		FINE SILT: 0.0%	
(D ₇₅ / D ₂₅):	1.581	1.369	V FINE GRAVEL: 0.0%		V FINE SILT: 0.0%	
(D ₇₅ - D ₂₅):	106.2	0.661	V COARSE SAND: 0.1%		CLAY: 0.0%	
	METHOD OF MOMENTS			FOLK & WARD METHOD		
	Arithmetic	Geometric	Logarithmic	Geometric	Logarithmic	Description
	μm	μm	ϕ	μm	ϕ	
MEAN (\bar{x}):	262.9	238.8	2.066	232.0	2.108	Fine Sand
SORTING (σ):	137.3	1.506	0.591	1.479	0.564	Moderately Well Sorted
SKEWNESS (Sk):	2.482	0.870	-0.870	0.191	-0.191	Coarse Skewed
KURTOSIS (K):	10.36	4.342	4.342	1.288	1.288	Leptokurtic

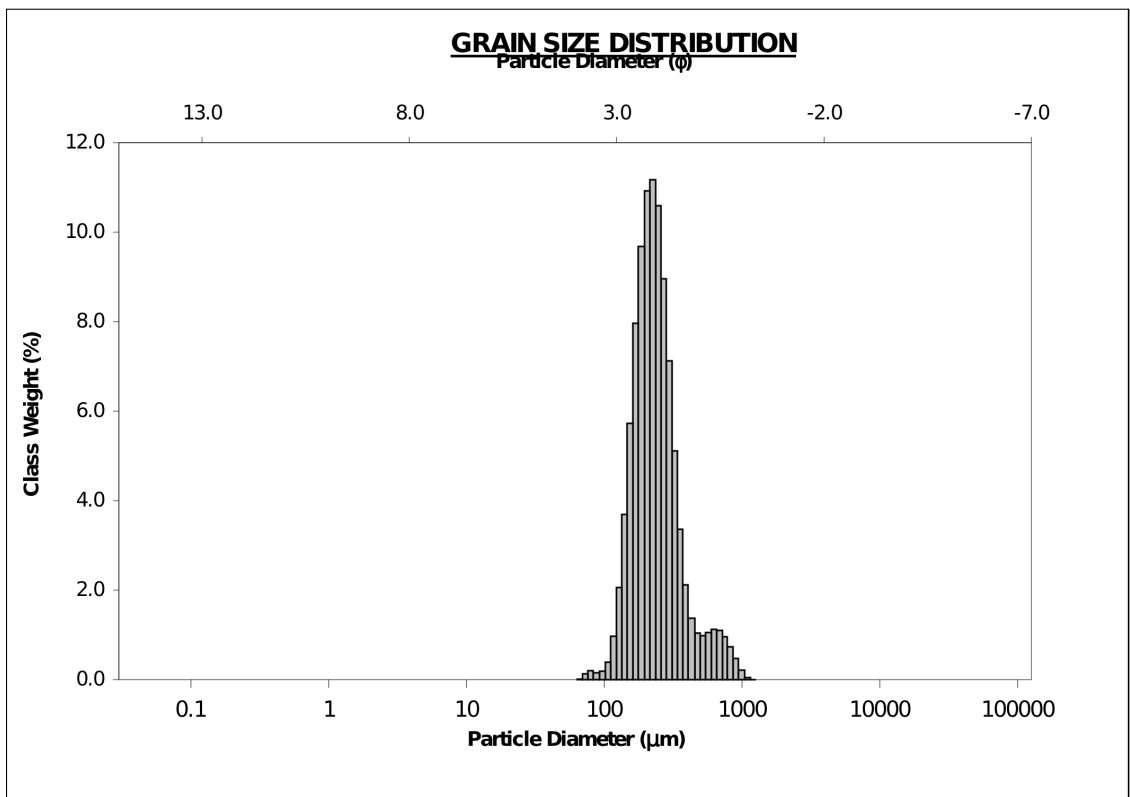


Figure A3.2 GRADISTAT printout with logarithmic frequency plot for grain-size sample 2.

SAMPLE STATISTICS						
SAMPLE IDENTITY: 03			ANALYST & DATE: TCF, 4/16/2013			
SAMPLE TYPE: Bimodal, Very Poorly Sorted			TEXTURAL GROUP: Sandy Mud			
SEDIMENT NAME: Fine Sandy Coarse Silt						
	μm	ϕ	GRAIN SIZE DISTRIBUTION			
MODE 1:	31.54	4.988	GRAVEL: 0.0%		COARSE SAND: 0.6%	
MODE 2:	169.0	2.566	SAND: 20.5%		MEDIUM SAND: 2.3%	
MODE 3:			MUD: 79.5%		FINE SAND: 10.1%	
D ₁₀ :	3.015	2.686			V FINE SAND: 7.6%	
MEDIAN or D ₅₀ :	27.05	5.208	V COARSE GRAVEL: 0.0%		V COARSE SILT: 22.9%	
D ₉₀ :	155.4	8.374	COARSE GRAVEL: 0.0%		COARSE SILT: 26.1%	
(D ₉₀ / D ₁₀):	51.55	3.118	MEDIUM GRAVEL: 0.0%		MEDIUM SILT: 12.1%	
(D ₉₀ - D ₁₀):	152.4	5.688	FINE GRAVEL: 0.0%		FINE SILT: 6.6%	
(D ₇₅ / D ₂₅):	4.153	1.477	V FINE GRAVEL: 0.0%		V FINE SILT: 4.5%	
(D ₇₅ - D ₂₅):	38.31	2.054	V COARSE SAND: 0.0%		CLAY: 7.4%	
	METHOD OF MOMENTS			FOLK & WARD METHOD		
	Arithmetic	Geometric	Logarithmic	Geometric	Logarithmic	Description
	μm	μm	ϕ	μm	ϕ	
MEAN (\bar{x}):	53.64	23.38	5.419	24.84	5.331	Coarse Silt
SORTING (σ):	81.10	4.144	2.051	4.214	2.075	Very Poorly Sorted
SKEWNESS (Sk):	3.710	-0.518	0.518	-0.147	0.147	Fine Skewed
KURTOSIS (K):	22.71	3.319	3.319	1.468	1.468	Leptokurtic

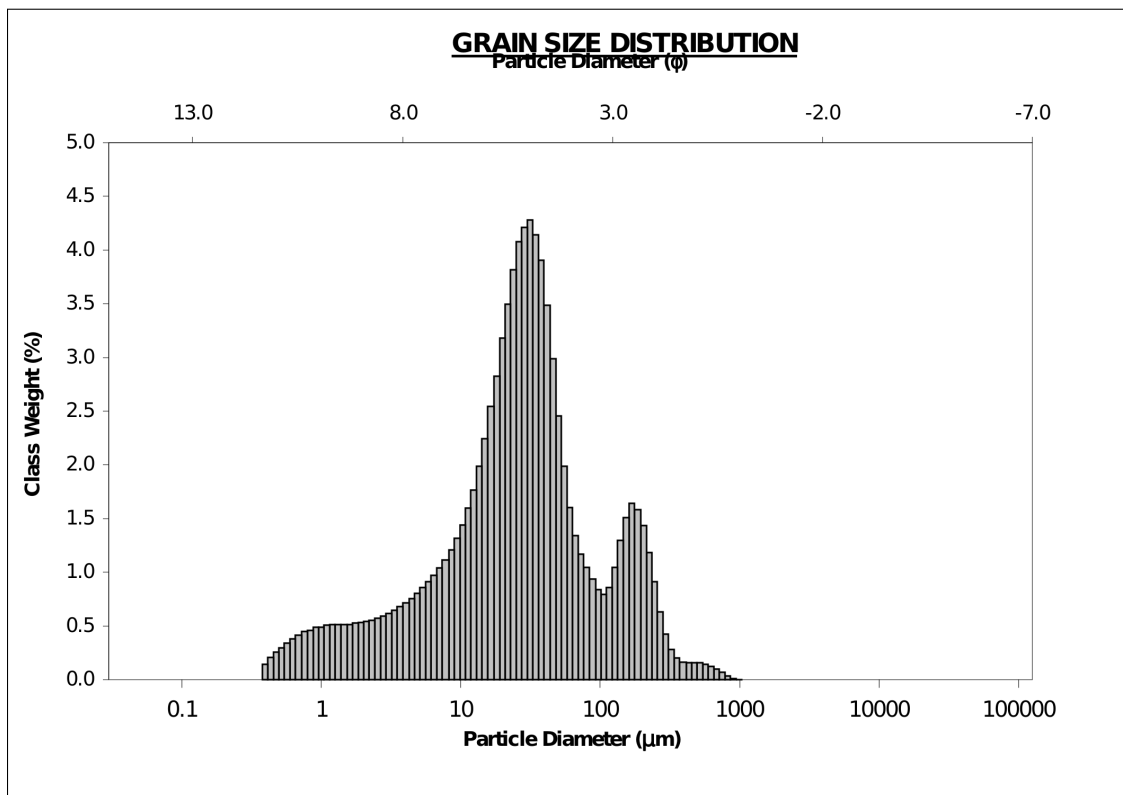


Figure A3.3 GRADISTAT printout with logarithmic frequency plot for grain-size sample 3.

SAMPLE STATISTICS						
SAMPLE IDENTITY: 04			ANALYST & DATE: TCF, 4/16/2013			
SAMPLE TYPE: Bimodal, Very Poorly Sorted			TEXTURAL GROUP: Sandy Mud			
SEDIMENT NAME: Very Fine Sandy Coarse Silt						
	μm	ϕ	GRAIN SIZE DISTRIBUTION			
MODE 1:	38.01	4.719	GRAVEL: 0.0%		COARSE SAND: 0.4%	
MODE 2:	185.5	2.432	SAND: 14.5%		MEDIUM SAND: 1.9%	
MODE 3:			MUD: 85.5%		FINE SAND: 6.1%	
D ₁₀ :	2.192	3.462			V FINE SAND: 6.1%	
MEDIAN or D ₅₀ :	19.49	5.681	V COARSE GRAVEL: 0.0%		V COARSE SILT: 20.8%	
D ₉₀ :	90.77	8.833	COARSE GRAVEL: 0.0%		COARSE SILT: 20.8%	
(D ₉₀ / D ₁₀):	41.40	2.552	MEDIUM GRAVEL: 0.0%		MEDIUM SILT: 15.7%	
(D ₉₀ - D ₁₀):	88.58	5.372	FINE GRAVEL: 0.0%		FINE SILT: 11.7%	
(D ₇₅ / D ₂₅):	6.413	1.587	V FINE GRAVEL: 0.0%		V FINE SILT: 7.6%	
(D ₇₅ - D ₂₅):	35.65	2.681	V COARSE SAND: 0.0%		CLAY: 9.0%	
	METHOD OF MOMENTS			FOLK & WARD METHOD		
	Arithmetic	Geometric	Logarithmic	Geometric	Logarithmic	Description
	μm	μm	ϕ	μm	ϕ	
MEAN (\bar{x}):	41.05	16.55	5.917	16.16	5.951	Coarse Silt
SORTING (σ):	69.36	4.209	2.073	4.282	2.098	Very Poorly Sorted
SKEWNESS (Sk):	4.236	-0.255	0.255	-0.160	0.160	Fine Skewed
KURTOSIS (K):	28.16	2.825	2.825	1.120	1.120	Leptokurtic

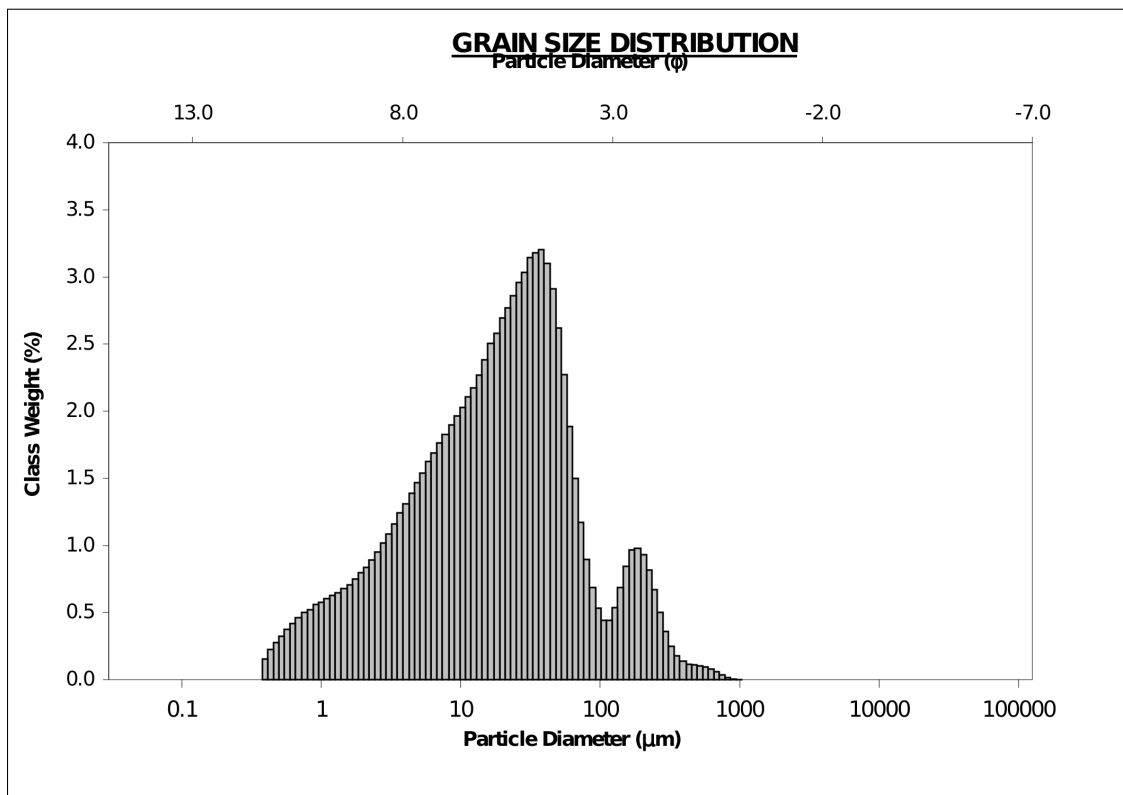


Figure A3.4 GRADISTAT printout with logarithmic frequency plot for grain-size sample 4.

SAMPLE STATISTICS						
SAMPLE IDENTITY: 05			ANALYST & DATE: TCF, 4/16/2013			
SAMPLE TYPE: Unimodal, Moderately Well Sorted			TEXTURAL GROUP: Sand			
SEDIMENT NAME: Moderately Well Sorted Fine Sand						
	μm	ϕ	GRAIN SIZE DISTRIBUTION			
MODE 1:	223.7	2.162	GRAVEL: 0.0%		COARSE SAND: 6.0%	
MODE 2:			SAND: 97.0%		MEDIUM SAND: 32.6%	
MODE 3:			MUD: 3.0%		FINE SAND: 52.5%	
D ₁₀ :	131.5	1.321			V FINE SAND: 5.8%	
MEDIAN or D ₅₀ :	224.5	2.155	V COARSE GRAVEL: 0.0%		V COARSE SILT: 1.1%	
D ₉₀ :	400.3	2.927	COARSE GRAVEL: 0.0%		COARSE SILT: 0.5%	
(D ₉₀ / D ₁₀):	3.044	2.216	MEDIUM GRAVEL: 0.0%		MEDIUM SILT: 0.3%	
(D ₉₀ - D ₁₀):	268.8	1.606	FINE GRAVEL: 0.0%		FINE SILT: 0.3%	
(D ₇₅ / D ₂₅):	1.674	1.419	V FINE GRAVEL: 0.0%		V FINE SILT: 0.3%	
(D ₇₅ - D ₂₅):	117.6	0.743	V COARSE SAND: 0.1%		CLAY: 0.6%	
	METHOD OF MOMENTS			FOLK & WARD METHOD		
	Arithmetic	Geometric	Logarithmic	Geometric	Logarithmic	Description
	μm	μm	ϕ	μm	ϕ	
MEAN (\bar{x}):	253.0	213.7	2.227	226.1	2.145	Fine Sand
SORTING (σ):	139.5	2.055	1.039	1.603	0.681	Moderately Well Sorted
SKEWNESS (Sk):	1.925	-3.371	3.371	0.003	-0.003	Symmetrical
KURTOSIS (K):	8.444	23.45	23.45	1.436	1.436	Leptokurtic

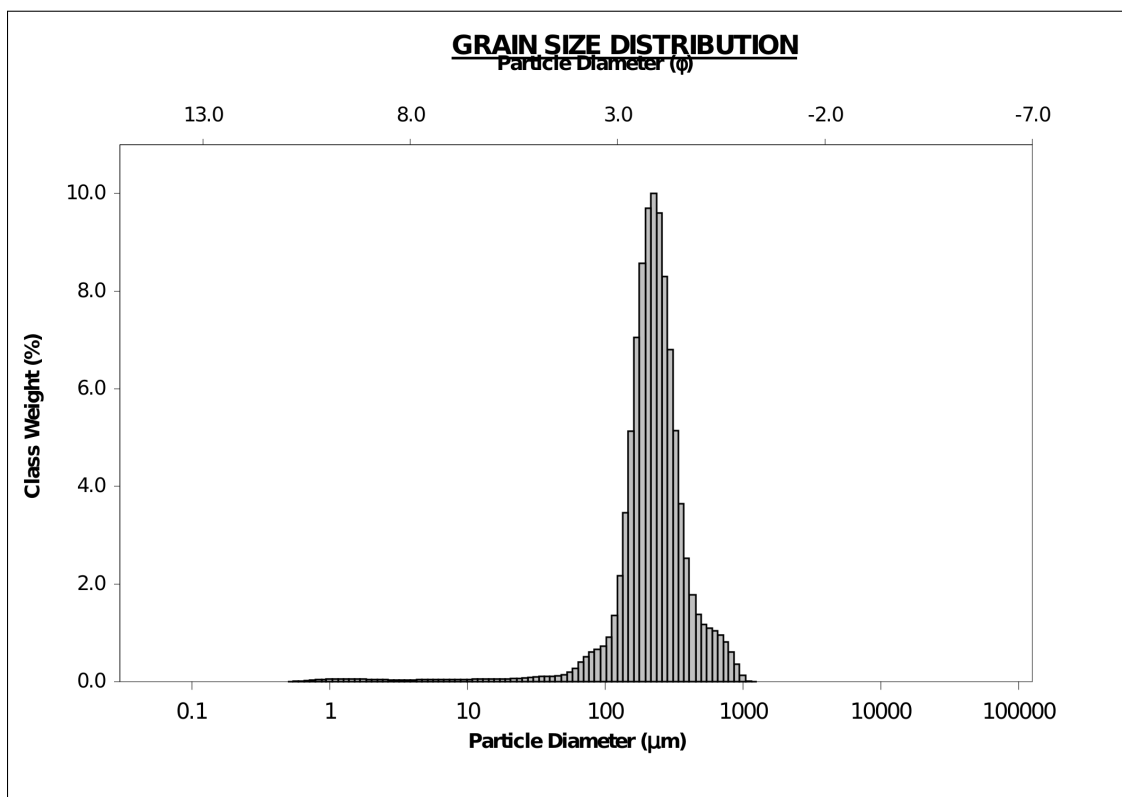


Figure A3.5 GRADISTAT printout with logarithmic frequency plot for grain-size sample 5.

SAMPLE STATISTICS						
SAMPLE IDENTITY: 06			ANALYST & DATE: TCF, 4/16/2013			
SAMPLE TYPE: Unimodal, Very Poorly Sorted			TEXTURAL GROUP: Muddy Sand			
SEDIMENT NAME: Coarse Silty Fine Sand						
	μm	ϕ	GRAIN SIZE DISTRIBUTION			
MODE 1:	185.5	2.432	GRAVEL: 0.0%		COARSE SAND: 2.2%	
MODE 2:			SAND: 70.6%		MEDIUM SAND: 11.4%	
MODE 3:			MUD: 29.4%		FINE SAND: 47.8%	
D ₁₀ :	6.670	1.882			V FINE SAND: 9.2%	
MEDIAN or D ₅₀ :	153.3	2.706	V COARSE GRAVEL: 0.0%		V COARSE SILT: 5.7%	
D ₉₀ :	271.3	7.228	COARSE GRAVEL: 0.0%		COARSE SILT: 6.4%	
(D ₉₀ / D ₁₀):	40.67	3.840	MEDIUM GRAVEL: 0.0%		MEDIUM SILT: 6.1%	
(D ₉₀ - D ₁₀):	264.6	5.346	FINE GRAVEL: 0.0%		FINE SILT: 4.8%	
(D ₇₅ / D ₂₅):	5.768	2.120	V FINE GRAVEL: 0.0%		V FINE SILT: 3.1%	
(D ₇₅ - D ₂₅):	173.0	2.528	V COARSE SAND: 0.0%		CLAY: 3.3%	
	METHOD OF MOMENTS			FOLK & WARD METHOD		
	Arithmetic	Geometric	Logarithmic	Geometric	Logarithmic	Description
	μm	μm	ϕ	μm	ϕ	
MEAN (\bar{x}):	150.3	79.22	3.658	79.14	3.659	Very Fine Sand
SORTING (σ):	121.5	4.585	2.197	4.192	2.068	Very Poorly Sorted
SKEWNESS (Sk):	1.372	-1.323	1.323	-0.680	0.680	Very Fine Skewed
KURTOSIS (K):	6.957	3.882	3.882	1.104	1.104	Mesokurtic

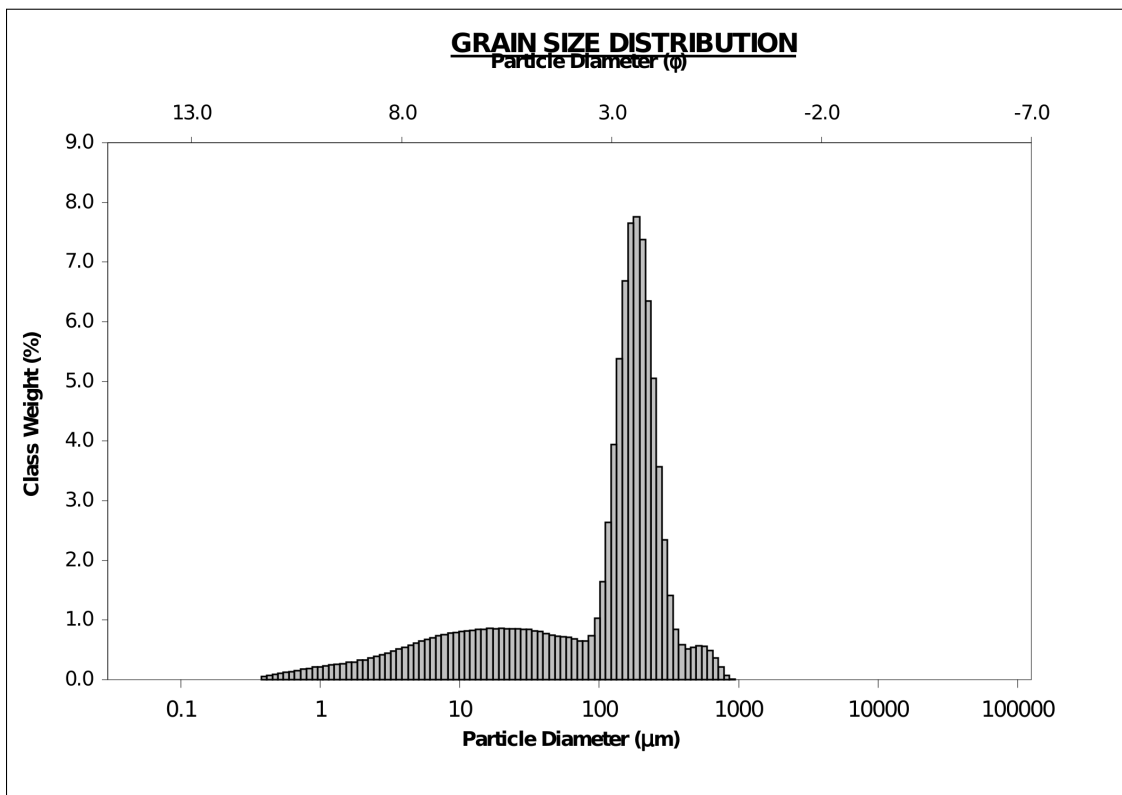


Figure A3.6 GRADISTAT printout with logarithmic frequency plot for grain-size sample 6.

SAMPLE STATISTICS						
SAMPLE IDENTITY: 07			ANALYST & DATE: TCF, 4/16/2013			
SAMPLE TYPE: Unimodal, Moderately Well Sorted			TEXTURAL GROUP: Sand			
SEDIMENT NAME: Moderately Well Sorted Fine Sand						
	μm	ϕ	GRAIN SIZE DISTRIBUTION			
MODE 1:	203.7	2.297	GRAVEL: 0.0%		COARSE SAND: 10.6%	
MODE 2:			SAND: 98.9%		MEDIUM SAND: 34.3%	
MODE 3:			MUD: 1.1%		FINE SAND: 50.8%	
D ₁₀ :	147.1	0.965			V FINE SAND: 3.2%	
MEDIAN or D ₅₀ :	236.5	2.080	V COARSE GRAVEL: 0.0%		V COARSE SILT: 0.4%	
D ₉₀ :	512.1	2.765	COARSE GRAVEL: 0.0%		COARSE SILT: 0.1%	
(D ₉₀ / D ₁₀):	3.482	2.864	MEDIUM GRAVEL: 0.0%		MEDIUM SILT: 0.1%	
(D ₉₀ - D ₁₀):	365.0	1.800	FINE GRAVEL: 0.0%		FINE SILT: 0.1%	
(D ₇₅ / D ₂₅):	1.846	1.561	V FINE GRAVEL: 0.0%		V FINE SILT: 0.1%	
(D ₇₅ - D ₂₅):	153.6	0.885	V COARSE SAND: 0.0%		CLAY: 0.3%	
	METHOD OF MOMENTS			FOLK & WARD METHOD		
	Arithmetic	Geometric	Logarithmic	Geometric	Logarithmic	Description
	μm	μm	ϕ	μm	ϕ	
MEAN (\bar{x}):	283.8	246.3	2.021	252.8	1.984	Medium Sand
SORTING (σ):	153.4	1.817	0.861	1.611	0.688	Moderately Well Sorted
SKEWNESS (Sk):	1.501	-2.712	2.712	0.218	-0.218	Coarse Skewed
KURTOSIS (K):	5.254	25.79	25.79	1.051	1.051	Mesokurtic

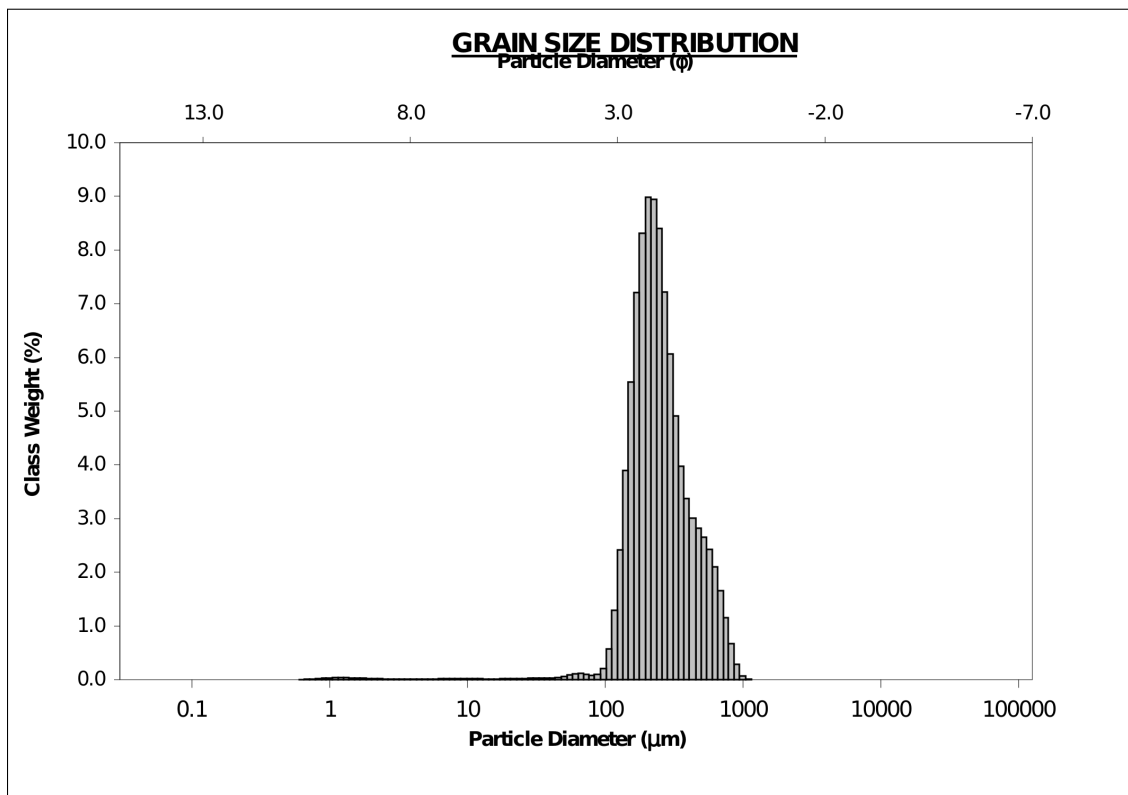


Figure A3.7 GRADISTAT printout with logarithmic frequency plot for grain-size sample 7.

SAMPLE STATISTICS						
SAMPLE IDENTITY: 08			ANALYST & DATE: TCF, 4/16/2013			
SAMPLE TYPE: Unimodal, Moderately Well Sorted			TEXTURAL GROUP: Sand			
SEDIMENT NAME: Moderately Well Sorted Medium Sand						
	μm	ϕ	GRAIN SIZE DISTRIBUTION			
MODE 1:	245.5	2.028	GRAVEL: 0.0%		COARSE SAND: 15.8%	
MODE 2:			SAND: 99.1%		MEDIUM SAND: 46.1%	
MODE 3:			MUD: 0.9%		FINE SAND: 35.6%	
D ₁₀ :	177.1	0.696			V FINE SAND: 1.0%	
MEDIAN or D ₅₀ :	285.0	1.811	V COARSE GRAVEL: 0.0%		V COARSE SILT: 0.2%	
D ₉₀ :	617.2	2.497	COARSE GRAVEL: 0.0%		COARSE SILT: 0.1%	
(D ₉₀ / D ₁₀):	3.484	3.586	MEDIUM GRAVEL: 0.0%		MEDIUM SILT: 0.1%	
(D ₉₀ - D ₁₀):	440.0	1.801	FINE GRAVEL: 0.0%		FINE SILT: 0.1%	
(D ₇₅ / D ₂₅):	1.846	1.676	V FINE GRAVEL: 0.0%		V FINE SILT: 0.1%	
(D ₇₅ - D ₂₅):	185.1	0.884	V COARSE SAND: 0.6%		CLAY: 0.2%	
	METHOD OF MOMENTS			FOLK & WARD METHOD		
	Arithmetic	Geometric	Logarithmic	Geometric	Logarithmic	Description
	μm	μm	ϕ	μm	ϕ	
MEAN (\bar{x}):	342.0	296.9	1.752	304.7	1.715	Medium Sand
SORTING (σ):	184.8	1.817	0.861	1.611	0.688	Moderately Well Sorted
SKEWNESS (Sk):	1.501	-2.712	2.712	0.218	-0.218	Coarse Skewed
KURTOSIS (K):	5.254	25.79	25.79	1.051	1.051	Mesokurtic

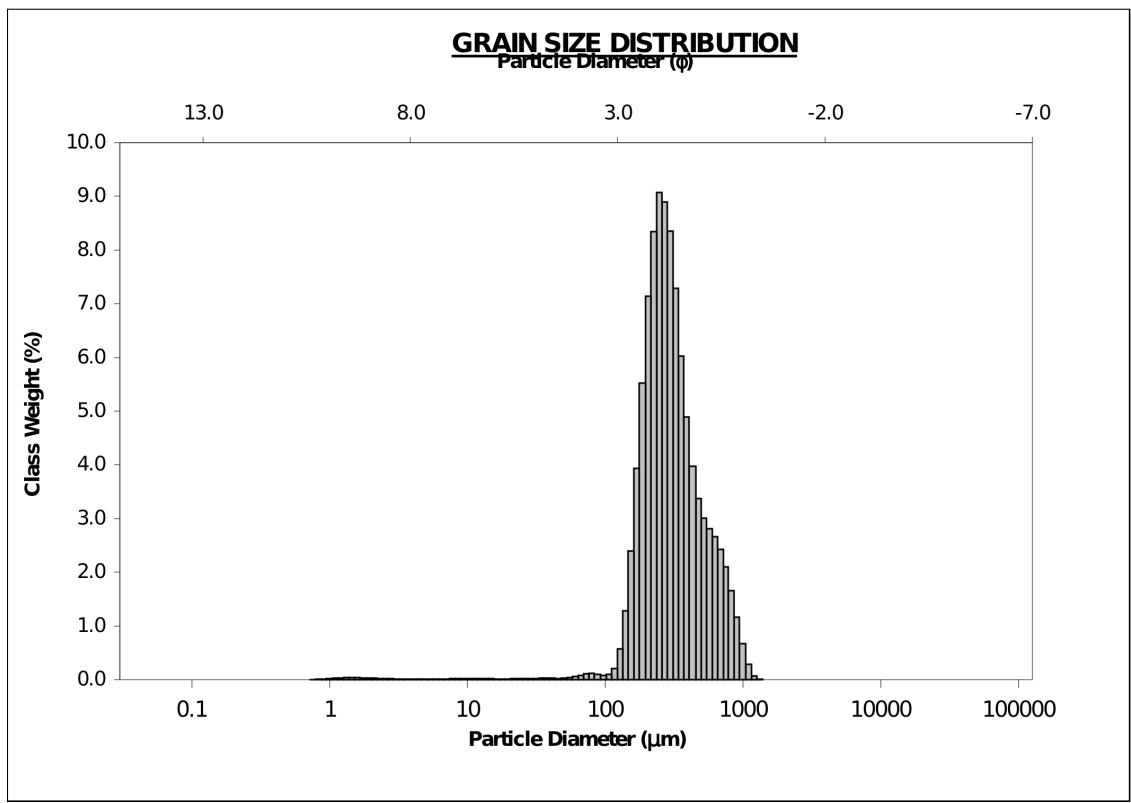


Figure A3.8 GRADISTAT printout with logarithmic frequency plot for grain-size sample 8.

SAMPLE STATISTICS						
SAMPLE IDENTITY: 09			ANALYST & DATE: TCF, 4/16/2013			
SAMPLE TYPE: Unimodal, Moderately Well Sorted			TEXTURAL GROUP: Sand			
SEDIMENT NAME: Moderately Well Sorted Medium Sand						
	μm	ϕ	GRAIN SIZE DISTRIBUTION			
MODE 1:	269.5	1.894	GRAVEL: 0.0%		COARSE SAND: 17.0%	
MODE 2:			SAND: 100.0%		MEDIUM SAND: 50.0%	
MODE 3:			MUD: 0.0%		FINE SAND: 32.2%	
D ₁₀ :	189.7	0.674			V FINE SAND: 0.1%	
MEDIAN or D ₅₀ :	299.7	1.738	V COARSE GRAVEL: 0.0%		V COARSE SILT: 0.0%	
D ₉₀ :	626.7	2.398	COARSE GRAVEL: 0.0%		COARSE SILT: 0.0%	
(D ₉₀ / D ₁₀):	3.303	3.557	MEDIUM GRAVEL: 0.0%		MEDIUM SILT: 0.0%	
(D ₉₀ - D ₁₀):	436.9	1.724	FINE GRAVEL: 0.0%		FINE SILT: 0.0%	
(D ₇₅ / D ₂₅):	1.825	1.699	V FINE GRAVEL: 0.0%		V FINE SILT: 0.0%	
(D ₇₅ - D ₂₅):	191.1	0.868	V COARSE SAND: 0.7%		CLAY: 0.0%	
	METHOD OF MOMENTS			FOLK & WARD METHOD		
	Arithmetic	Geometric	Logarithmic	Geometric	Logarithmic	Description
	μm	μm	ϕ	μm	ϕ	
MEAN (\bar{x}):	357.1	320.9	1.640	319.2	1.647	Medium Sand
SORTING (σ):	181.0	1.559	0.641	1.578	0.658	Moderately Well Sorted
SKEWNESS (Sk):	1.526	0.536	-0.536	0.223	-0.223	Coarse Skewed
KURTOSIS (K):	5.188	2.715	2.715	1.012	1.012	Mesokurtic

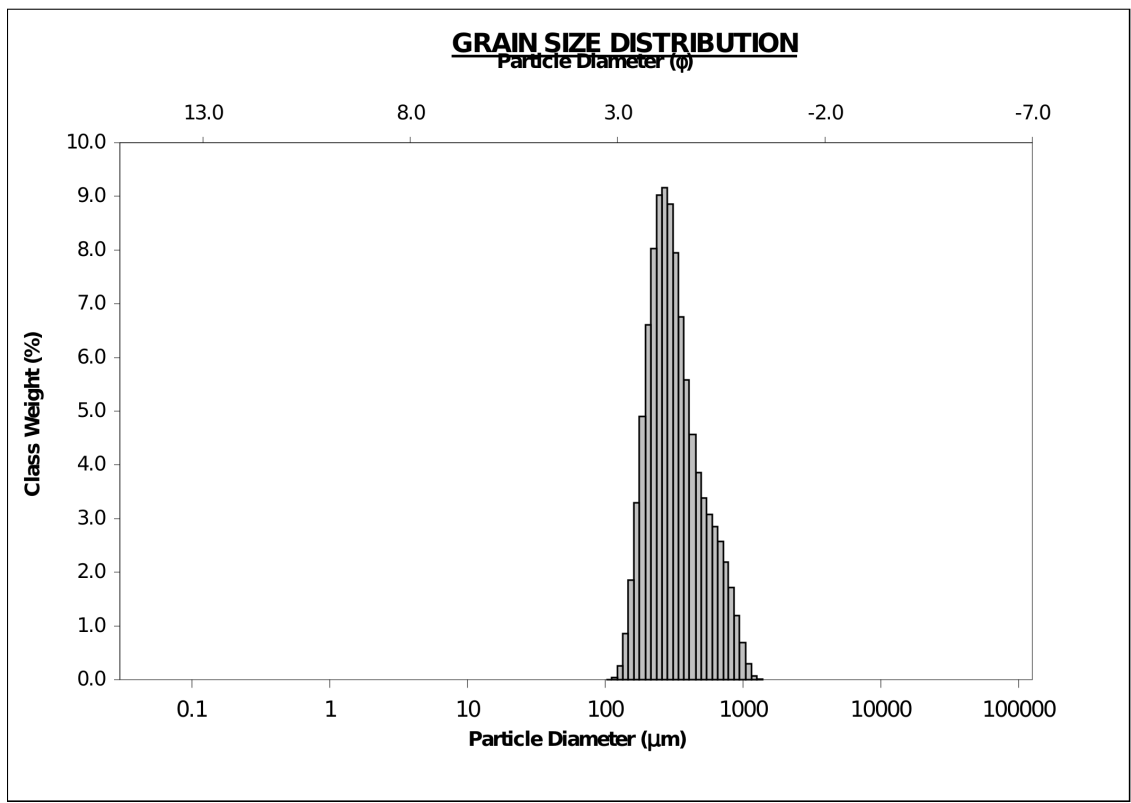


Figure A3.9 GRADISTAT printout with logarithmic frequency plot for grain-size sample 9.

SAMPLE STATISTICS						
SAMPLE IDENTITY: 10			ANALYST & DATE: TCF, 4/16/2013			
SAMPLE TYPE: Unimodal, Well Sorted			TEXTURAL GROUP: Slightly Gravelly Sand			
SEDIMENT NAME: Slightly Fine Gravelly Fine Sand						
	μm	ϕ	GRAIN SIZE DISTRIBUTION			
MODE 1:	203.7	2.297	GRAVEL: 0.6%		COARSE SAND: 2.6%	
MODE 2:			SAND: 99.4%		MEDIUM SAND: 25.3%	
MODE 3:			MUD: 0.0%		FINE SAND: 68.2%	
D ₁₀ :	143.4	1.628			V FINE SAND: 3.3%	
MEDIAN or D ₅₀ :	208.4	2.262	V COARSE GRAVEL: 0.0%		V COARSE SILT: 0.0%	
D ₉₀ :	323.5	2.802	COARSE GRAVEL: 0.0%		COARSE SILT: 0.0%	
(D ₉₀ / D ₁₀):	2.256	1.721	MEDIUM GRAVEL: 0.0%		MEDIUM SILT: 0.0%	
(D ₉₀ - D ₁₀):	180.1	1.174	FINE GRAVEL: 0.6%		FINE SILT: 0.0%	
(D ₇₅ / D ₂₅):	1.523	1.311	V FINE GRAVEL: 0.0%		V FINE SILT: 0.0%	
(D ₇₅ - D ₂₅):	88.74	0.607	V COARSE SAND: 0.0%		CLAY: 0.0%	
	METHOD OF MOMENTS			FOLK & WARD METHOD		
	Arithmetic	Geometric	Logarithmic	Geometric	Logarithmic	Description
	μm	μm	ϕ	μm	ϕ	
MEAN (\bar{x}):	256.3	217.8	2.199	210.6	2.247	Fine Sand
SORTING (σ):	372.7	1.514	0.598	1.383	0.467	Well Sorted
SKEWNESS (Sk):	11.39	2.896	-2.896	0.105	-0.105	Coarse Skewed
KURTOSIS (K):	138.7	20.83	20.83	1.081	1.081	Mesokurtic

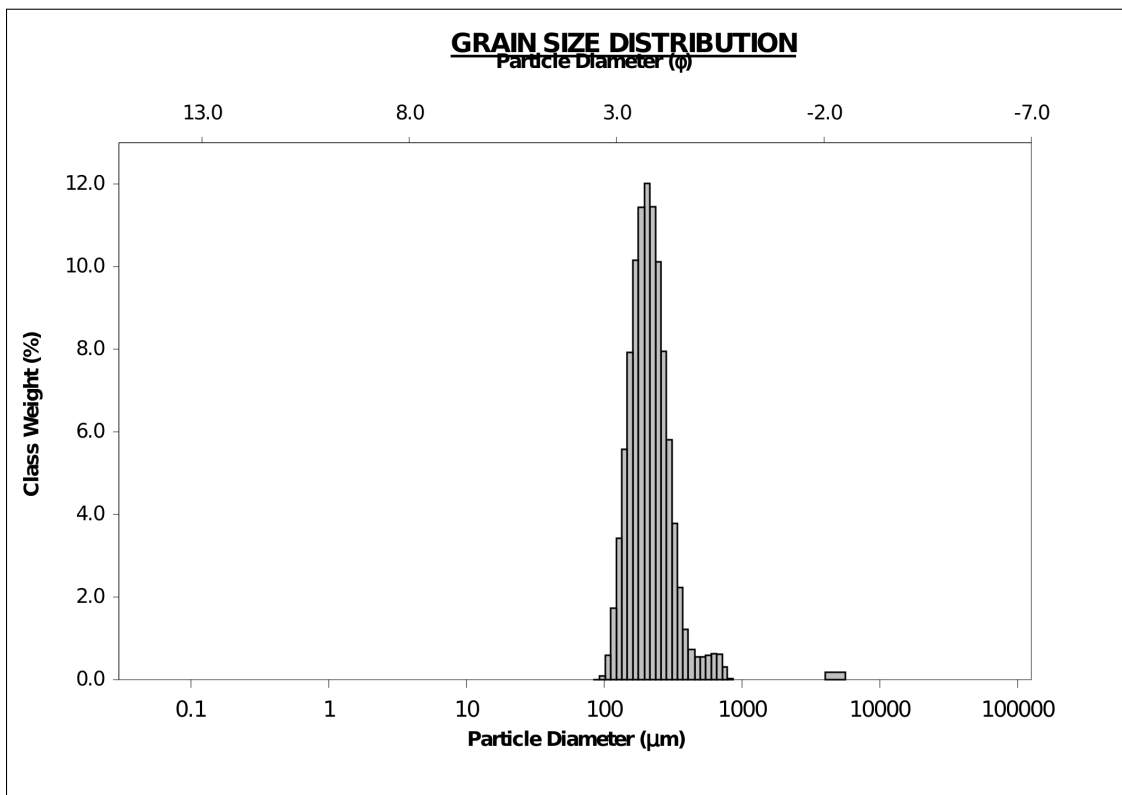


Figure A3.10 GRADISTAT printout with logarithmic frequency plot for grain-size sample 10.

SAMPLE STATISTICS

SAMPLE IDENTITY: **11**

ANALYST & DATE: TCF, 4/16/2013

SAMPLE TYPE: Unimodal, Well Sorted

TEXTURAL GROUP: Slightly Gravelly Sand

SEDIMENT NAME: Slightly Fine Gravelly Fine Sand

	μm ϕ		GRAIN SIZE DISTRIBUTION			
	MODE 1:	245.5	2.028	GRAVEL: 0.0%	COARSE SAND: 3.8%	
MODE 2:			SAND: 100.0%	MEDIUM SAND: 46.4%		
MODE 3:			MUD: 0.0%	FINE SAND: 49.5%		
D ₁₀ :	172.6	1.378		V FINE SAND: 0.3%		
MEDIAN or D ₅₀ :	250.5	1.997	V COARSE GRAVEL: 0.0%	V COARSE SILT: 0.0%		
D ₉₀ :	384.8	2.535	COARSE GRAVEL: 0.0%	COARSE SILT: 0.0%		
(D ₉₀ / D ₁₀):	2.230	1.840	MEDIUM GRAVEL: 0.0%	MEDIUM SILT: 0.0%		
(D ₉₀ - D ₁₀):	212.2	1.157	FINE GRAVEL: 0.0%	FINE SILT: 0.0%		
(D ₇₅ / D ₂₅):	1.517	1.356	V FINE GRAVEL: 0.0%	V FINE SILT: 0.0%		
(D ₇₅ - D ₂₅):	105.7	0.601	V COARSE SAND: 0.0%	CLAY: 0.0%		
	METHOD OF MOMENTS			FOLK & WARD METHOD		
	Arithmetic	Geometric	Logarithmic	Geometric	Logarithmic	Description
	μm	μm	ϕ	μm	ϕ	
MEAN (\bar{x}):	275.6	257.7	1.957	252.8	1.984	Medium Sand
SORTING (σ):	136.5	1.405	0.490	1.371	0.456	Well Sorted
SKEWNESS (SK):	12.26	0.953	-0.953	0.086	-0.086	Symmetrical
KURTOSIS (K):	367.6	5.761	5.761	1.048	1.048	Mesokurtic

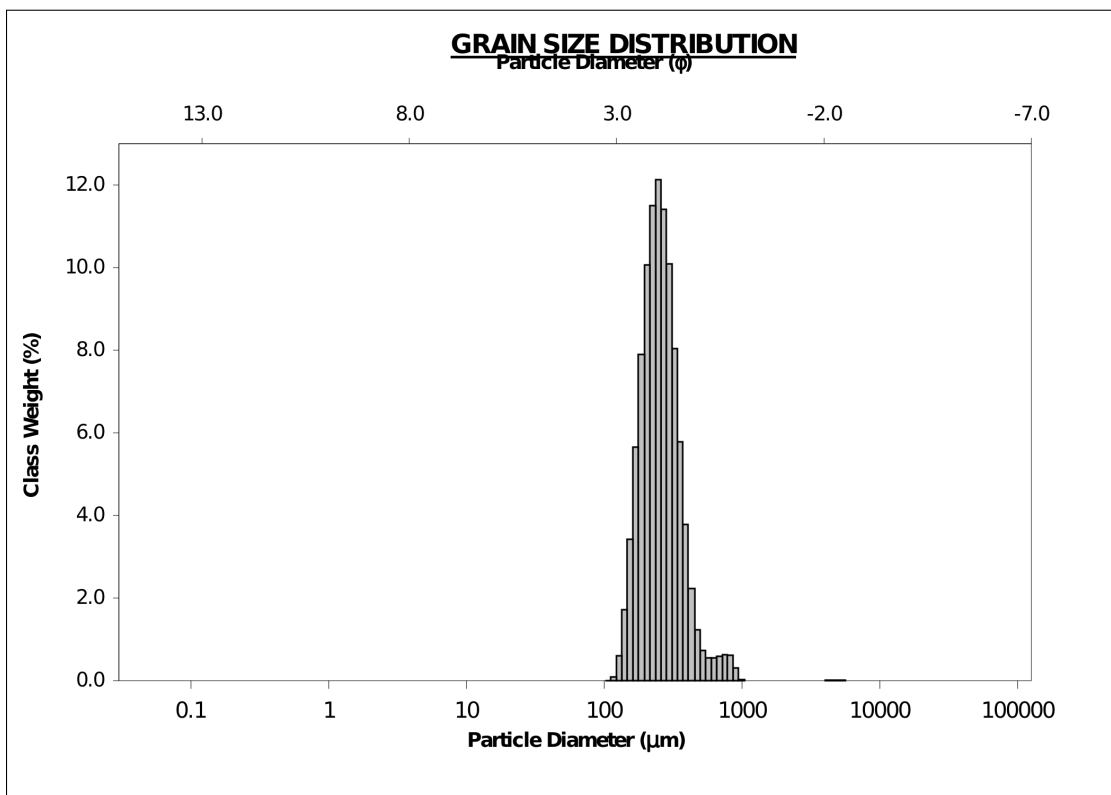


Figure A3.11 GRADISTAT printout with logarithmic frequency plot for grain-size sample 11.

SAMPLE STATISTICS						
SAMPLE IDENTITY: 12			ANALYST & DATE: TCF, 4/16/2013			
SAMPLE TYPE: Bimodal, Moderately Sorted			TEXTURAL GROUP: Slightly Gravelly Sand			
SEDIMENT NAME: Slightly Medium Gravelly Fine Sand						
	μm	ϕ	GRAIN SIZE DISTRIBUTION			
MODE 1:	203.7	2.297	GRAVEL: 0.0%		COARSE SAND: 11.0%	
MODE 2:	568.4	0.817	SAND: 100.0%		MEDIUM SAND: 28.3%	
MODE 3:			MUD: 0.0%		FINE SAND: 56.7%	
D ₁₀ :	149.4	0.821			V FINE SAND: 2.4%	
MEDIAN or D ₅₀ :	227.5	2.136	V COARSE GRAVEL: 0.0%		V COARSE SILT: 0.0%	
D ₉₀ :	565.9	2.743	COARSE GRAVEL: 0.0%		COARSE SILT: 0.0%	
(D ₉₀ / D ₁₀):	3.788	3.339	MEDIUM GRAVEL: 0.0%		MEDIUM SILT: 0.0%	
(D ₉₀ - D ₁₀):	416.5	1.921	FINE GRAVEL: 0.0%		FINE SILT: 0.0%	
(D ₇₅ / D ₂₅):	1.758	1.489	V FINE GRAVEL: 0.0%		V FINE SILT: 0.0%	
(D ₇₅ - D ₂₅):	136.0	0.814	V COARSE SAND: 1.5%		CLAY: 0.0%	
	METHOD OF MOMENTS			FOLK & WARD METHOD		
	Arithmetic	Geometric	Logarithmic	Geometric	Logarithmic	Description
	μm	μm	ϕ	μm	ϕ	
MEAN (\bar{x}):	300.3	254.9	1.972	250.1	1.999	Medium Sand
SORTING (σ):	312.9	1.663	0.734	1.640	0.714	Moderately Sorted
SKEWNESS (Sk):	27.99	1.148	-1.148	0.342	-0.342	Very Coarse Skewed
KURTOSIS (K):	1358.5	4.750	4.750	1.227	1.227	Leptokurtic

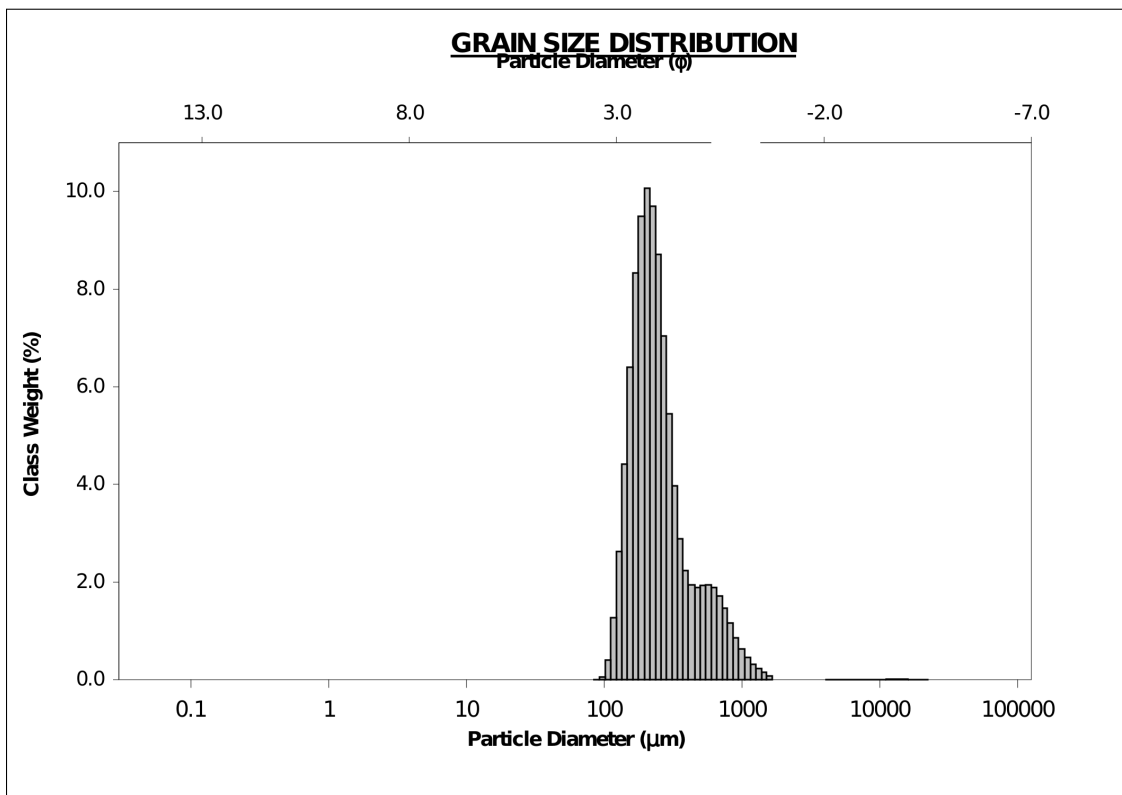


Figure A3.12 GRADISTAT printout with logarithmic frequency plot for grain-size sample 12.

SAMPLE STATISTICS						
SAMPLE IDENTITY: 13			ANALYST & DATE: TCF, 4/16/2013			
SAMPLE TYPE: Bimodal, Moderately Sorted			TEXTURAL GROUP: Slightly Gravelly Sand			
SEDIMENT NAME: Slightly Fine Gravelly Fine Sand						
	μm	ϕ	GRAIN SIZE DISTRIBUTION			
MODE 1:	223.7	2.162	GRAVEL: 1.0%		COARSE SAND: 19.9%	
MODE 2:	517.8	0.951	SAND: 98.0%		MEDIUM SAND: 34.6%	
MODE 3:			MUD: 1.0%		FINE SAND: 39.3%	
D ₁₀ :	160.6	0.455			V FINE SAND: 1.5%	
MEDIAN or D ₅₀ :	281.0	1.831	V COARSE GRAVEL: 0.0%		V COARSE SILT: 0.4%	
D ₉₀ :	729.7	2.638	COARSE GRAVEL: 0.0%		COARSE SILT: 0.2%	
(D ₉₀ / D ₁₀):	4.543	5.802	MEDIUM GRAVEL: 0.4%		MEDIUM SILT: 0.1%	
(D ₉₀ - D ₁₀):	569.0	2.184	FINE GRAVEL: 0.6%		FINE SILT: 0.0%	
(D ₇₅ / D ₂₅):	2.393	2.199	V FINE GRAVEL: 0.0%		V FINE SILT: 0.0%	
(D ₇₅ - D ₂₅):	281.1	1.259	V COARSE SAND: 2.7%		CLAY: 0.2%	
	METHOD OF MOMENTS			FOLK & WARD METHOD		
	Arithmetic	Geometric	Logarithmic	Geometric	Logarithmic	Description
	μm	μm	ϕ	μm	ϕ	
MEAN (\bar{x}):	433.0	313.4	1.674	312.4	1.678	Medium Sand
SORTING (σ):	718.7	2.059	1.042	1.805	0.852	Moderately Sorted
SKEWNESS (Sk):	9.693	-0.442	0.442	0.259	-0.259	Coarse Skewed
KURTOSIS (K):	113.8	13.84	13.84	0.877	0.877	Platykurtic

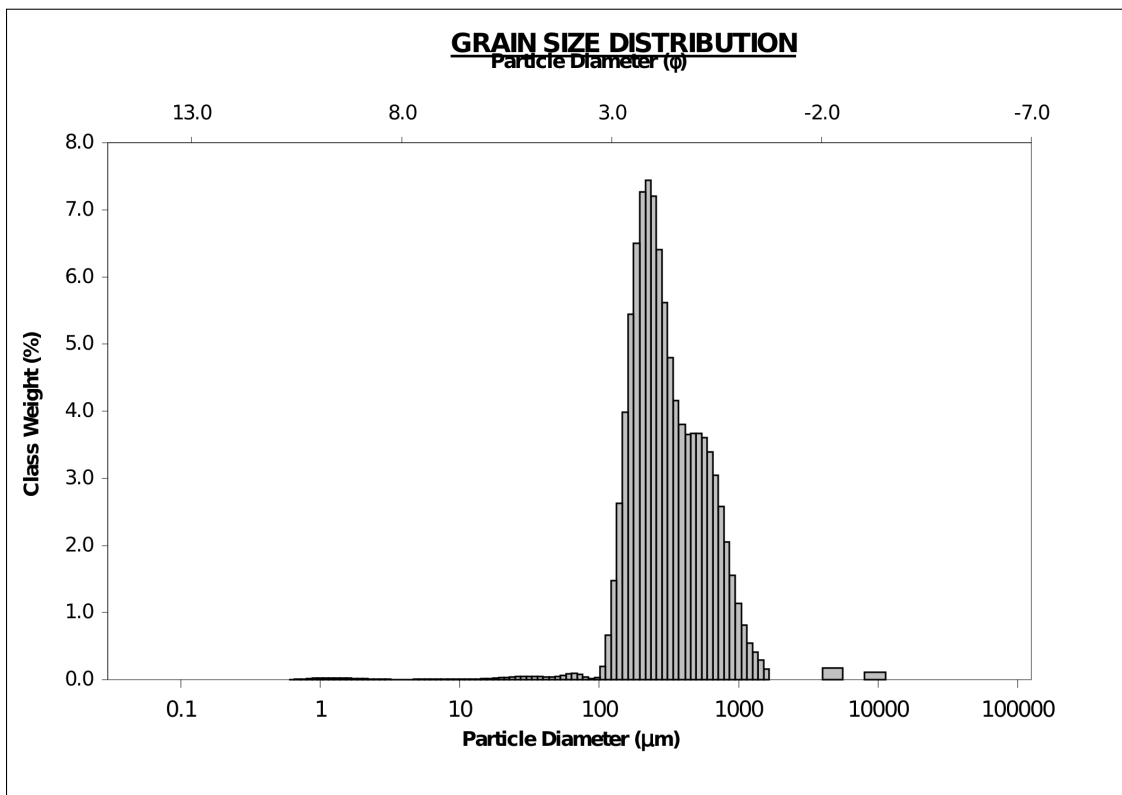


Figure A3.13 GRADISTAT printout with logarithmic frequency plot for grain-size sample 13.

SAMPLE STATISTICS						
SAMPLE IDENTITY: 14			ANALYST & DATE: TCF, 4/16/2013			
SAMPLE TYPE: Bimodal, Moderately Sorted			TEXTURAL GROUP: Sand			
SEDIMENT NAME: Moderately Sorted Medium Sand						
	μm	ϕ	GRAIN SIZE DISTRIBUTION			
MODE 1:	269.5	1.894	GRAVEL: 0.0%		COARSE SAND: 24.4%	
MODE 2:	624.0	0.682	SAND: 99.2%		MEDIUM SAND: 42.3%	
MODE 3:			MUD: 0.8%		FINE SAND: 26.2%	
D ₁₀ :	193.0	0.231			V FINE SAND: 0.5%	
MEDIAN or D ₅₀ :	336.0	1.574	V COARSE GRAVEL: 0.0%		V COARSE SILT: 0.3%	
D ₉₀ :	852.2	2.373	COARSE GRAVEL: 0.0%		COARSE SILT: 0.2%	
(D ₉₀ / D ₁₀):	4.415	10.28	MEDIUM GRAVEL: 0.0%		MEDIUM SILT: 0.0%	
(D ₉₀ - D ₁₀):	659.2	2.142	FINE GRAVEL: 0.0%		FINE SILT: 0.0%	
(D ₇₅ / D ₂₅):	2.354	2.526	V FINE GRAVEL: 0.0%		V FINE SILT: 0.1%	
(D ₇₅ - D ₂₅):	328.2	1.235	V COARSE SAND: 5.8%		CLAY: 0.2%	
	METHOD OF MOMENTS			FOLK & WARD METHOD		
	Arithmetic	Geometric	Logarithmic	Geometric	Logarithmic	Description
	μm	μm	ϕ	μm	ϕ	
MEAN (\bar{x}):	443.8	366.1	1.450	372.3	1.425	Medium Sand
SORTING (σ):	291.4	1.930	0.949	1.780	0.832	Moderately Sorted
SKEWNESS (Sk):	1.659	-1.459	1.459	0.249	-0.249	Coarse Skewed
KURTOSIS (K):	6.123	15.32	15.32	0.867	0.867	Platykurtic

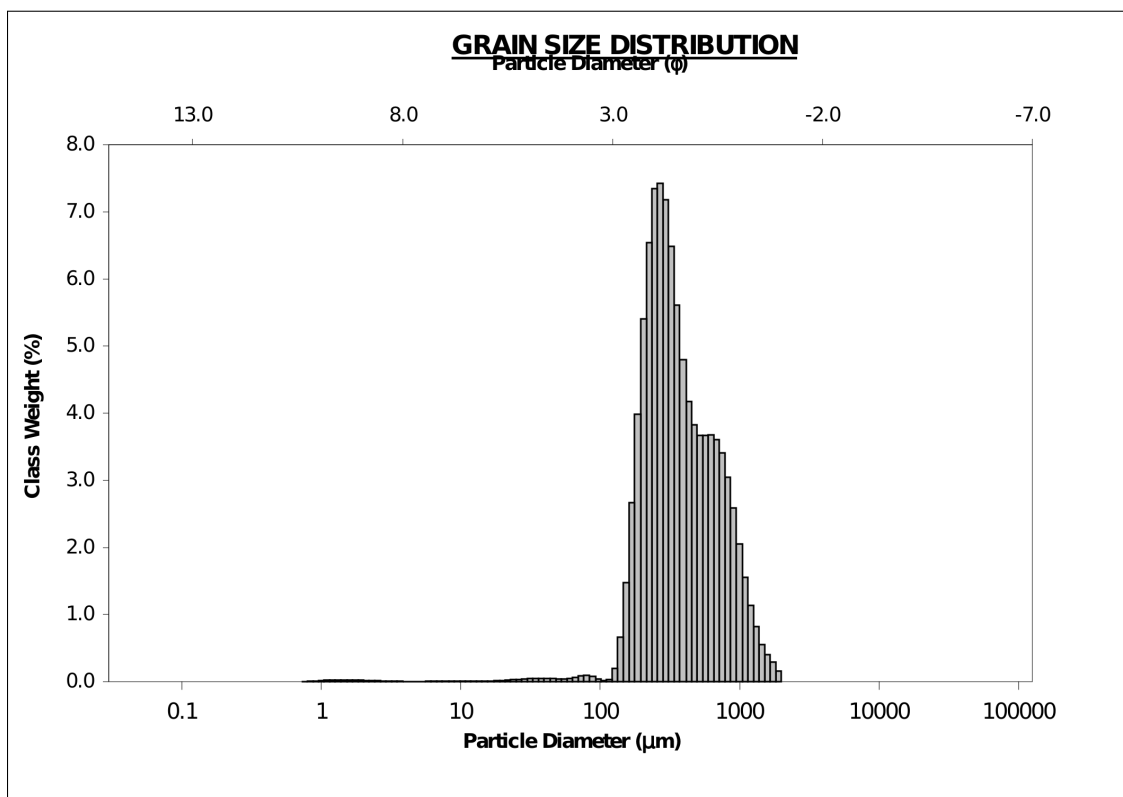


Figure A3.14 GRADISTAT printout with logarithmic frequency plot for grain-size sample 14.

SAMPLE STATISTICS						
SAMPLE IDENTITY: 15			ANALYST & DATE: TCF, 4/16/2013			
SAMPLE TYPE: Unimodal, Moderately Well Sorted			TEXTURAL GROUP: Slightly Gravelly Sand			
SEDIMENT NAME: Slightly Medium Gravelly Fine Sand						
	μm	ϕ	GRAIN SIZE DISTRIBUTION			
MODE 1:	203.7	2.297	GRAVEL: 0.1%		COARSE SAND: 10.6%	
MODE 2:			SAND: 99.9%		MEDIUM SAND: 29.2%	
MODE 3:			MUD: 0.0%		FINE SAND: 56.4%	
D ₁₀ :	144.0	0.958			V FINE SAND: 3.6%	
MEDIAN or D ₅₀ :	223.4	2.162	V COARSE GRAVEL: 0.0%		V COARSE SILT: 0.0%	
D ₉₀ :	514.8	2.796	COARSE GRAVEL: 0.0%		COARSE SILT: 0.0%	
(D ₉₀ / D ₁₀):	3.575	2.919	MEDIUM GRAVEL: 0.1%		MEDIUM SILT: 0.0%	
(D ₉₀ - D ₁₀):	370.8	1.838	FINE GRAVEL: 0.0%		FINE SILT: 0.0%	
(D ₇₅ / D ₂₅):	1.838	1.534	V FINE GRAVEL: 0.0%		V FINE SILT: 0.0%	
(D ₇₅ - D ₂₅):	145.7	0.878	V COARSE SAND: 0.1%		CLAY: 0.0%	
	METHOD OF MOMENTS			FOLK & WARD METHOD		
	Arithmetic	Geometric	Logarithmic	Geometric	Logarithmic	Description
	μm	μm	ϕ	μm	ϕ	
MEAN (\bar{x}):	285.4	246.0	2.024	244.1	2.035	Fine Sand
SORTING (σ):	308.6	1.622	0.697	1.620	0.696	Moderately Well Sorted
SKEWNESS (Sk):	22.24	1.009	-1.009	0.294	-0.294	Coarse Skewed
KURTOSIS (K):	660.1	5.330	5.330	1.064	1.064	Mesokurtic

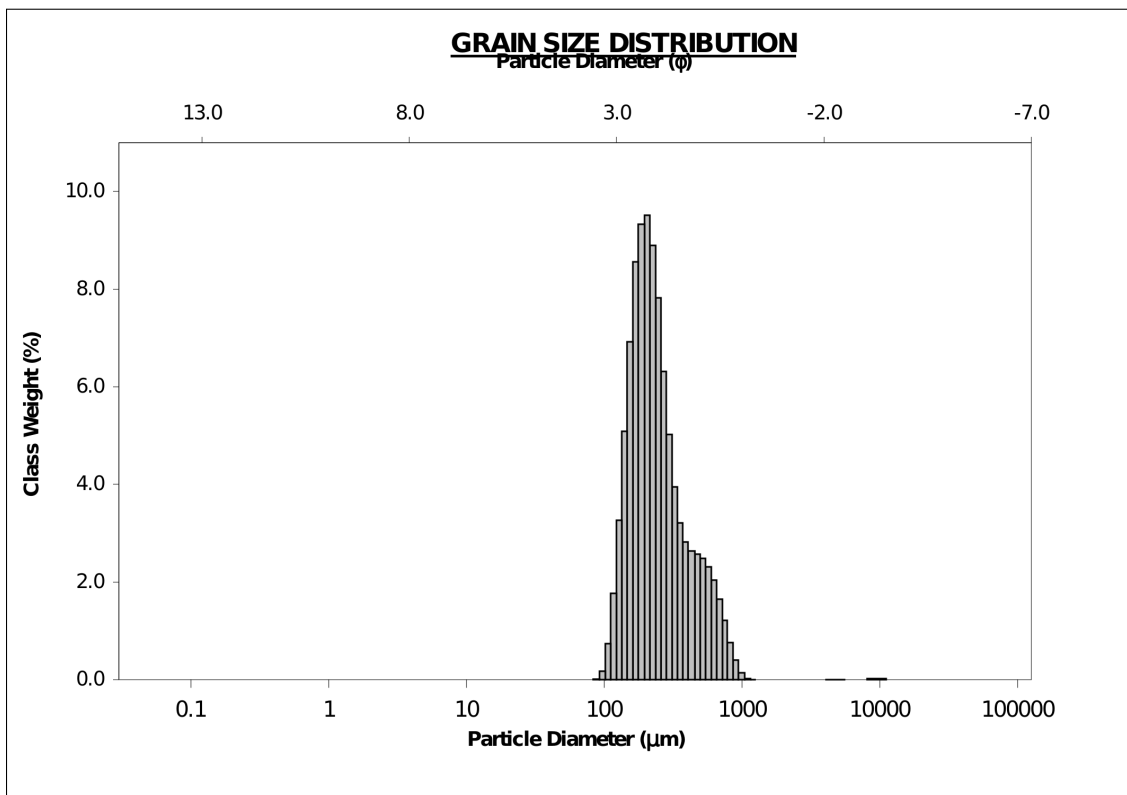


Figure A3.15 GRADISTAT printout with logarithmic frequency plot for grain-size sample 15.

SAMPLE STATISTICS						
SAMPLE IDENTITY: 16			ANALYST & DATE: TCF, 4/16/2013			
SAMPLE TYPE: Unimodal, Moderately Well Sorted			TEXTURAL GROUP: Sand			
SEDIMENT NAME: Moderately Well Sorted Fine Sand						
	μm	ϕ	GRAIN SIZE DISTRIBUTION			
MODE 1:	245.5	2.028	GRAVEL: 0.0%		COARSE SAND: 15.0%	
MODE 2:			SAND: 100.0%		MEDIUM SAND: 41.3%	
MODE 3:			MUD: 0.0%		FINE SAND: 42.4%	
D ₁₀ :	173.4	0.693			V FINE SAND: 0.4%	
MEDIAN or D ₅₀ :	269.1	1.894	V COARSE GRAVEL: 0.0%		V COARSE SILT: 0.0%	
D ₉₀ :	618.5	2.528	COARSE GRAVEL: 0.0%		COARSE SILT: 0.0%	
(D ₉₀ / D ₁₀):	3.567	3.647	MEDIUM GRAVEL: 0.0%		MEDIUM SILT: 0.0%	
(D ₉₀ - D ₁₀):	445.1	1.835	FINE GRAVEL: 0.0%		FINE SILT: 0.0%	
(D ₇₅ / D ₂₅):	1.835	1.635	V FINE GRAVEL: 0.0%		V FINE SILT: 0.0%	
(D ₇₅ - D ₂₅):	175.0	0.876	V COARSE SAND: 0.9%		CLAY: 0.0%	
	METHOD OF MOMENTS			FOLK & WARD METHOD		
	Arithmetic	Geometric	Logarithmic	Geometric	Logarithmic	Description
	μm	μm	ϕ	μm	ϕ	
MEAN (\bar{x}):	334.4	295.4	1.759	293.7	1.767	Medium Sand
SORTING (σ):	188.6	1.602	0.680	1.618	0.694	Moderately Well Sorted
SKEWNESS (Sk):	1.744	0.714	-0.714	0.293	-0.293	Coarse Skewed
KURTOSIS (K):	5.919	2.903	2.903	1.064	1.064	Mesokurtic

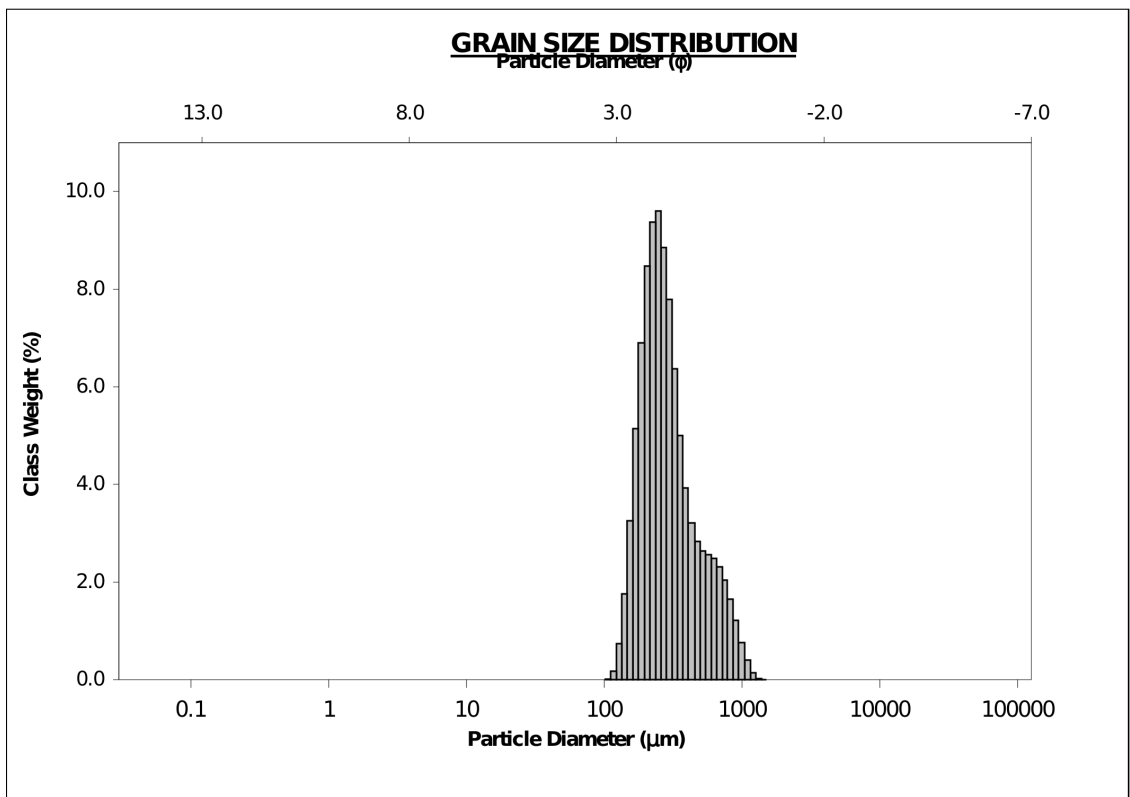


Figure A3.16 GRADISTAT printout with logarithmic frequency plot for grain-size sample 16.

SAMPLE STATISTICS						
SAMPLE IDENTITY: 17			ANALYST & DATE: TCF, 4/16/2013			
SAMPLE TYPE: Unimodal, Moderately Well Sorted			TEXTURAL GROUP: Sand			
SEDIMENT NAME: Moderately Well Sorted Fine Sand						
	μm	ϕ	GRAIN SIZE DISTRIBUTION			
MODE 1:	203.7	2.297	GRAVEL: 0.0%	COARSE SAND: 4.3%		
MODE 2:			SAND: 100.0%	MEDIUM SAND: 28.7%		
MODE 3:			MUD: 0.0%	FINE SAND: 64.1%		
D ₁₀ :	148.1	1.518	V COARSE GRAVEL: 0.0%	V FINE SAND: 2.9%		
MEDIAN or D ₅₀ :	216.7	2.206	COARSE GRAVEL: 0.0%	V COARSE SILT: 0.0%		
D ₉₀ :	349.1	2.755	MEDIUM GRAVEL: 0.0%	COARSE SILT: 0.0%		
(D ₉₀ / D ₁₀):	2.357	1.815	FINE GRAVEL: 0.0%	MEDIUM SILT: 0.0%		
(D ₉₀ - D ₁₀):	201.0	1.237	V FINE GRAVEL: 0.0%	FINE SILT: 0.0%		
(D ₇₅ / D ₂₅):	1.541	1.332	V COARSE SAND: 0.0%	V FINE SILT: 0.0%		
(D ₇₅ - D ₂₅):	95.36	0.624		CLAY: 0.0%		
	METHOD OF MOMENTS			FOLK & WARD METHOD		
	Arithmetic	Geometric	Logarithmic	Geometric	Logarithmic	Description
	μm	μm	ϕ	μm	ϕ	
MEAN (\bar{x}):	243.5	225.0	2.152	220.0	2.185	Fine Sand
SORTING (σ):	113.6	1.451	0.537	1.418	0.504	Moderately Well Sorted
SKEWNESS (sk):	2.563	0.848	-0.848	0.151	-0.151	Coarse Skewed
KURTOSIS (K):	11.64	4.514	4.514	1.179	1.179	Leptokurtic

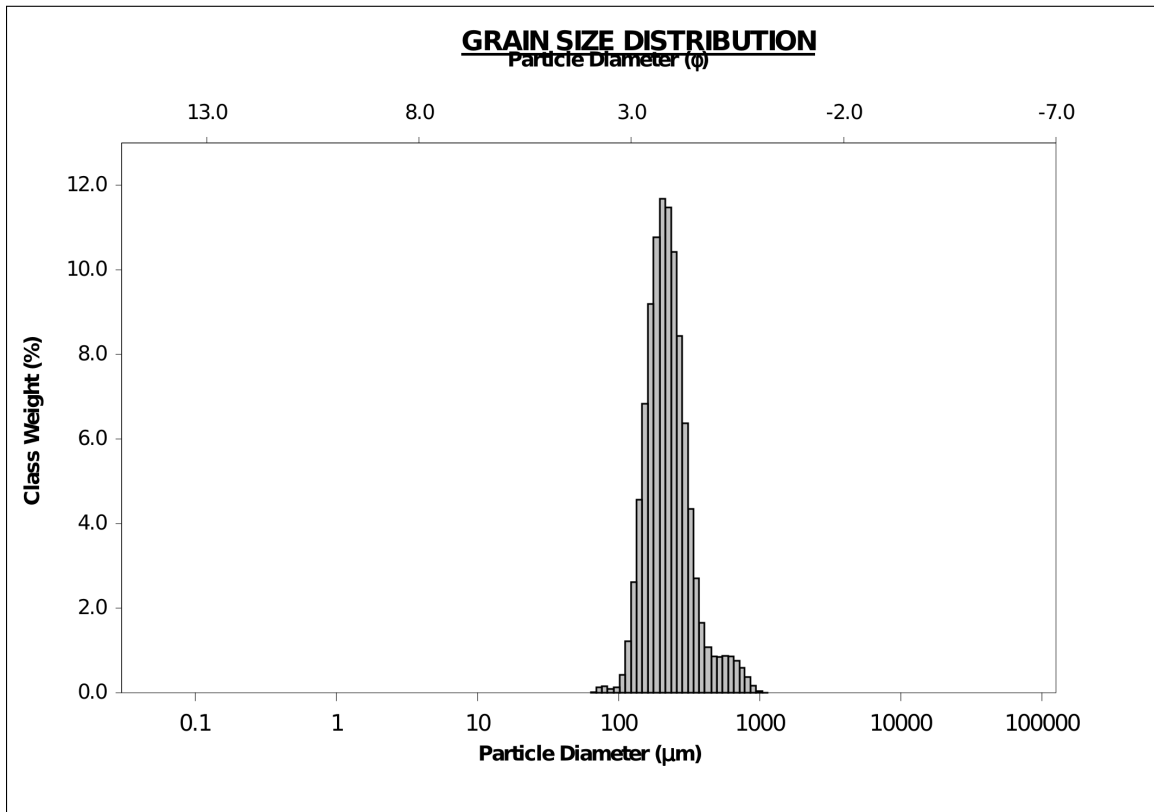


Figure A3.17 GRADISTAT printout with logarithmic frequency plot for grain-size sample 17.

SAMPLE STATISTICS						
SAMPLE IDENTITY: 18			ANALYST & DATE: TCF, 4/16/2013			
SAMPLE TYPE: Unimodal, Well Sorted			TEXTURAL GROUP: Sand			
SEDIMENT NAME: Well Sorted Fine Sand						
	μm	ϕ	GRAIN SIZE DISTRIBUTION			
MODE 1:	169.0	2.566	GRAVEL: 0.0%		COARSE SAND: 0.0%	
MODE 2:			SAND: 97.0%		MEDIUM SAND: 2.1%	
MODE 3:			MUD: 3.0%		FINE SAND: 77.4%	
D ₁₀ :	108.0	2.206			V FINE SAND: 17.5%	
MEDIAN or D ₅₀ :	157.9	2.663	V COARSE GRAVEL: 0.0%		V COARSE SILT: 1.0%	
D ₉₀ :	216.8	3.211	COARSE GRAVEL: 0.0%		COARSE SILT: 0.4%	
(D ₉₀ / D ₁₀):	2.007	1.456	MEDIUM GRAVEL: 0.0%		MEDIUM SILT: 0.3%	
(D ₉₀ - D ₁₀):	108.8	1.005	FINE GRAVEL: 0.0%		FINE SILT: 0.3%	
(D ₇₅ / D ₂₅):	1.442	1.219	V FINE GRAVEL: 0.0%		V FINE SILT: 0.3%	
(D ₇₅ - D ₂₅):	57.70	0.528	V COARSE SAND: 0.0%		CLAY: 0.7%	
	METHOD OF MOMENTS			FOLK & WARD METHOD		
	Arithmetic	Geometric	Logarithmic	Geometric	Logarithmic	Description
	μm	μm	ϕ	μm	ϕ	
MEAN (\bar{x}):	158.7	145.0	2.786	156.3	2.678	Fine Sand
SORTING (σ):	46.04	1.836	0.877	1.317	0.397	Well Sorted
SKEWNESS (Sk):	-0.430	-5.701	5.701	-0.110	0.110	Fine Skewed
KURTOSIS (K):	4.206	43.82	43.82	1.036	1.036	Mesokurtic

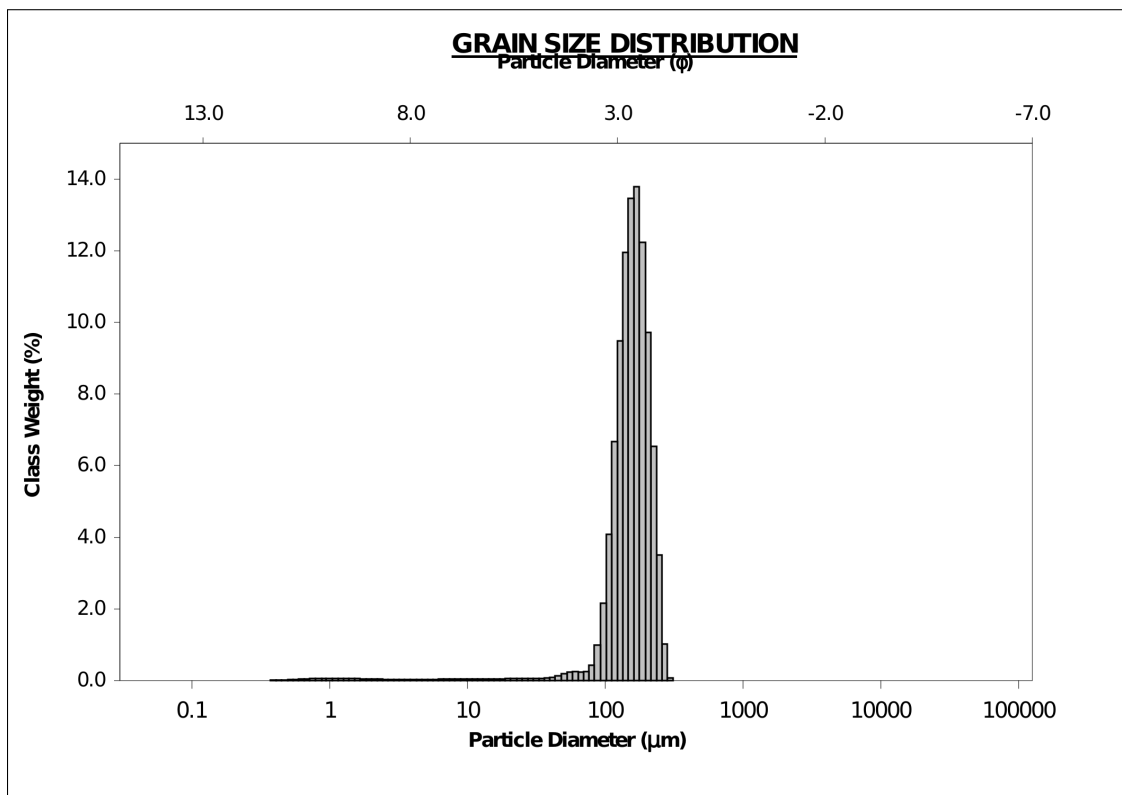


Figure A3.18 GRADISTAT printout with logarithmic frequency plot for grain-size sample 18.

SAMPLE STATISTICS						
SAMPLE IDENTITY: 19			ANALYST & DATE: TCF, 4/16/2013			
SAMPLE TYPE: Unimodal, Moderately Well Sorted			TEXTURAL GROUP: Slightly Gravelly Sand			
SEDIMENT NAME: Slightly Fine Gravelly Fine Sand						
	μm	ϕ	GRAIN SIZE DISTRIBUTION			
MODE 1:	185.5	2.432	GRAVEL: 0.1%		COARSE SAND: 4.2%	
MODE 2:			SAND: 97.9%		MEDIUM SAND: 14.1%	
MODE 3:			MUD: 1.9%		FINE SAND: 72.9%	
D ₁₀ :	128.1	1.789			V FINE SAND: 6.7%	
MEDIAN or D ₅₀ :	188.6	2.407	V COARSE GRAVEL: 0.0%		V COARSE SILT: 0.6%	
D ₉₀ :	289.5	2.964	COARSE GRAVEL: 0.0%		COARSE SILT: 0.3%	
(D ₉₀ / D ₁₀):	2.259	1.657	MEDIUM GRAVEL: 0.0%		MEDIUM SILT: 0.2%	
(D ₉₀ - D ₁₀):	161.3	1.176	FINE GRAVEL: 0.0%		FINE SILT: 0.2%	
(D ₇₅ / D ₂₅):	1.504	1.279	V FINE GRAVEL: 0.0%		V FINE SILT: 0.2%	
(D ₇₅ - D ₂₅):	77.75	0.589	V COARSE SAND: 0.0%		CLAY: 0.5%	
	METHOD OF MOMENTS			FOLK & WARD METHOD		
	Arithmetic	Geometric	Logarithmic	Geometric	Logarithmic	Description
	μm	μm	ϕ	μm	ϕ	
MEAN (\bar{x}):	246.9	187.1	2.418	189.4	2.400	Fine Sand
SORTING (σ):	1388.1	1.882	0.912	1.437	0.523	Moderately Well Sorted
SKEWNESS (Sk):	46.13	-3.133	3.133	0.143	-0.143	Coarse Skewed
KURTOSIS (K):	2238.2	34.54	34.54	1.392	1.392	Leptokurtic

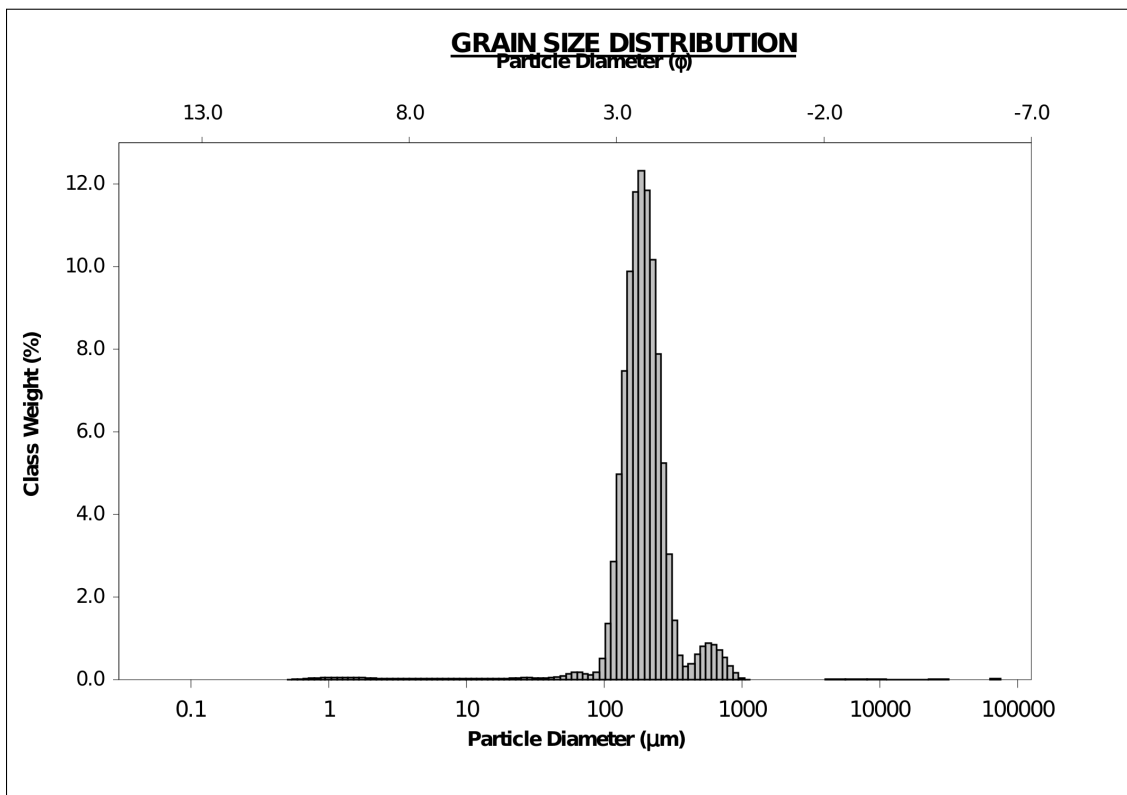


Figure A3.19 GRADISTAT printout with logarithmic frequency plot for grain-size sample 19.

SAMPLE STATISTICS						
SAMPLE IDENTITY: 20			ANALYST & DATE: TCF, 4/16/2013			
SAMPLE TYPE: Unimodal, Well Sorted			TEXTURAL GROUP: Sand			
SEDIMENT NAME: Well Sorted Fine Sand						
	μm	ϕ	GRAIN SIZE DISTRIBUTION			
MODE 1:	245.5	2.028	GRAVEL: 0.0%		COARSE SAND: 3.9%	
MODE 2:			SAND: 97.9%		MEDIUM SAND: 40.1%	
MODE 3:			MUD: 2.1%		FINE SAND: 52.3%	
D ₁₀ :	160.3	1.466	V COARSE GRAVEL: 0.0%		V FINE SAND: 1.6%	
MEDIAN or D ₅₀ :	238.8	2.066	COARSE GRAVEL: 0.0%		V COARSE SILT: 0.5%	
D ₉₀ :	362.0	2.641	MEDIUM GRAVEL: 0.0%		COARSE SILT: 0.4%	
(D ₉₀ / D ₁₀):	2.258	1.802	FINE GRAVEL: 0.0%		MEDIUM SILT: 0.3%	
(D ₉₀ - D ₁₀):	201.7	1.175	V FINE GRAVEL: 0.0%		FINE SILT: 0.2%	
(D ₇₅ / D ₂₅):	1.515	1.340	V COARSE SAND: 0.1%		V FINE SILT: 0.2%	
(D ₇₅ - D ₂₅):	100.2	0.600			CLAY: 0.4%	
	METHOD OF MOMENTS			FOLK & WARD METHOD		
	Arithmetic	Geometric	Logarithmic	Geometric	Logarithmic	Description
	μm	μm	ϕ	μm	ϕ	
MEAN (\bar{x}):	258.8	229.9	2.121	239.5	2.062	Fine Sand
SORTING (σ):	119.1	1.848	0.886	1.391	0.476	Well Sorted
SKEWNESS (Sk):	2.325	-4.383	4.383	0.030	-0.030	Symmetrical
KURTOSIS (K):	12.00	35.60	35.60	1.138	1.138	Leptokurtic

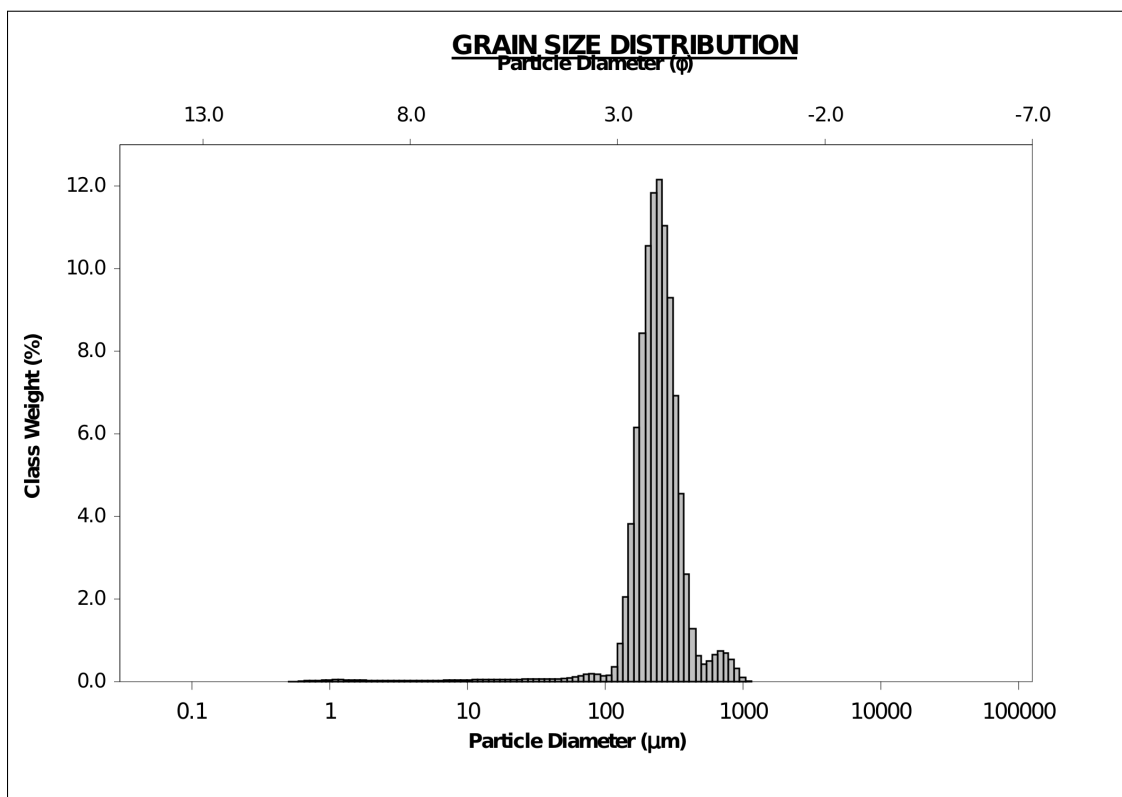


Figure A3.20 GRADISTAT printout with logarithmic frequency plot for grain-size sample 20.

SAMPLE STATISTICS						
SAMPLE IDENTITY: 21			ANALYST & DATE: TCF, 4/16/2013			
SAMPLE TYPE: Unimodal, Well Sorted			TEXTURAL GROUP: Sand			
SEDIMENT NAME: Well Sorted Fine Sand						
	μm	ϕ	GRAIN SIZE DISTRIBUTION			
MODE 1:	245.5	2.028	GRAVEL: 0.0%		COARSE SAND: 5.3%	
MODE 2:			SAND: 100.0%		MEDIUM SAND: 46.8%	
MODE 3:			MUD: 0.0%		FINE SAND: 47.5%	
D ₁₀ :	174.1	1.300			V FINE SAND: 0.3%	
MEDIAN or D ₅₀ :	254.4	1.975	V COARSE GRAVEL: 0.0%		V COARSE SILT: 0.0%	
D ₉₀ :	406.1	2.522	COARSE GRAVEL: 0.0%		COARSE SILT: 0.0%	
(D ₉₀ / D ₁₀):	2.333	1.940	MEDIUM GRAVEL: 0.0%		MEDIUM SILT: 0.0%	
(D ₉₀ - D ₁₀):	232.0	1.222	FINE GRAVEL: 0.0%		FINE SILT: 0.0%	
(D ₇₅ / D ₂₅):	1.543	1.380	V FINE GRAVEL: 0.0%		V FINE SILT: 0.0%	
(D ₇₅ - D ₂₅):	112.2	0.626	V COARSE SAND: 0.1%		CLAY: 0.0%	
	METHOD OF MOMENTS			FOLK & WARD METHOD		
	Arithmetic	Geometric	Logarithmic	Geometric	Logarithmic	Description
	μm	μm	ϕ	μm	ϕ	
MEAN (\bar{x}):	283.6	263.9	1.922	258.2	1.954	Medium Sand
SORTING (σ):	124.9	1.430	0.516	1.406	0.492	Well Sorted
SKEWNESS (Sk):	2.454	0.853	-0.853	0.135	-0.135	Coarse Skewed
KURTOSIS (K):	11.21	4.250	4.250	1.119	1.119	Leptokurtic

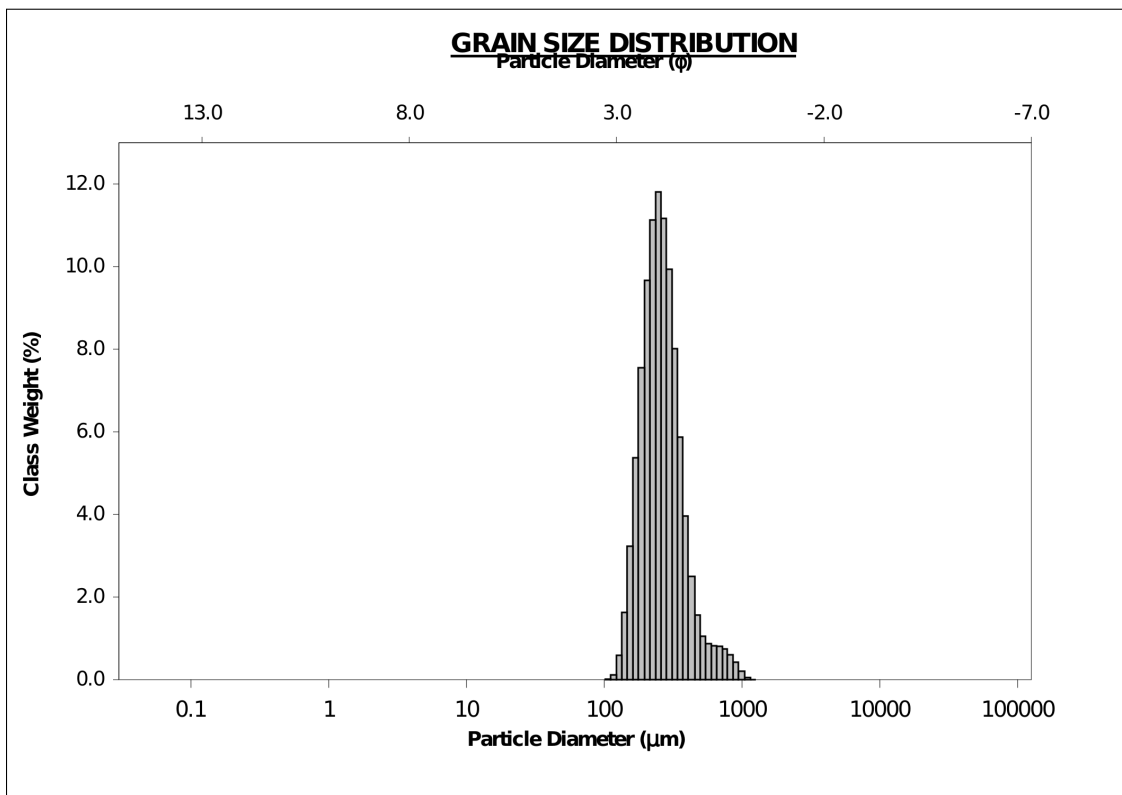


Figure A3.21 GRADISTAT printout with logarithmic frequency plot for grain-size sample 21.

SAMPLE STATISTICS						
SAMPLE IDENTITY: 22			ANALYST & DATE: TCF, 4/16/2013			
SAMPLE TYPE: Bimodal, Poorly Sorted			TEXTURAL GROUP: Slightly Gravelly Sand			
SEDIMENT NAME: Slightly Fine Gravelly Very Coarse Sand						
	μm	ϕ	GRAIN SIZE DISTRIBUTION			
MODE 1:	1316.0	-0.395	GRAVEL: 2.9%	COARSE SAND: 28.0%		
MODE 2:	169.0	2.566	SAND: 95.6%	MEDIUM SAND: 6.0%		
MODE 3:			MUD: 1.4%	FINE SAND: 20.1%		
D ₁₀ :	146.8	-0.589		V FINE SAND: 4.1%		
MEDIAN or D ₅₀ :	860.9	0.216	V COARSE GRAVEL: 0.7%	V COARSE SILT: 0.4%		
D ₉₀ :	1504.1	2.768	COARSE GRAVEL: 0.7%	COARSE SILT: 0.3%		
(D ₉₀ / D ₁₀):	10.24	-4.700	MEDIUM GRAVEL: 0.7%	MEDIUM SILT: 0.2%		
(D ₉₀ - D ₁₀):	1357.2	3.357	FINE GRAVEL: 0.9%	FINE SILT: 0.2%		
(D ₇₅ / D ₂₅):	5.146	-6.846	V FINE GRAVEL: 0.0%	V FINE SILT: 0.1%		
(D ₇₅ - D ₂₅):	992.7	2.363	V COARSE SAND: 37.3%	CLAY: 0.3%		
	METHOD OF MOMENTS			FOLK & WARD METHOD		
	Arithmetic	Geometric	Logarithmic	Geometric	Logarithmic	Description
	μm	μm	ϕ	μm	ϕ	
MEAN (\bar{x}):	1318.3	614.4	0.690	592.3	0.756	Coarse Sand
SORTING (σ):	4284.6	3.161	1.628	2.486	1.314	Poorly Sorted
SKEWNESS (sk):	10.86	-0.749	0.586	-0.527	0.527	Very Fine Skewed
KURTOSIS (K):	139.0	8.037	7.397	0.646	0.646	Very Platykurtic

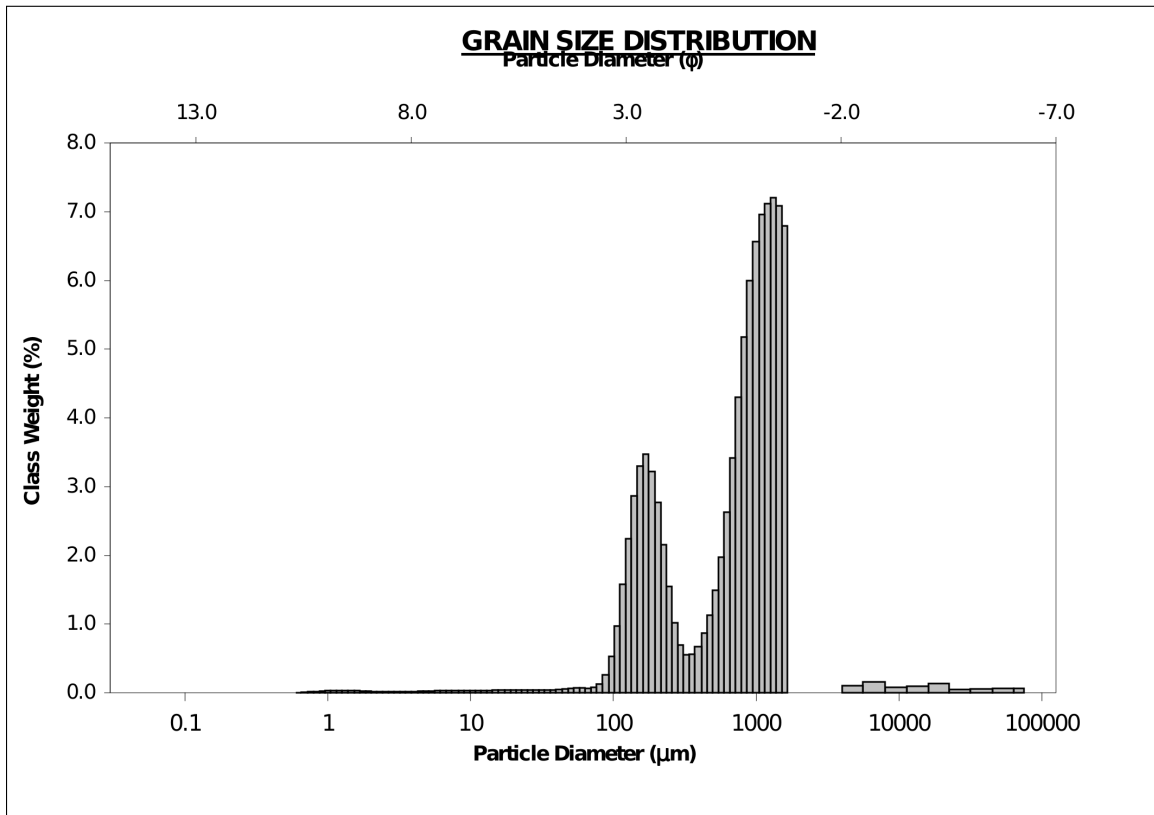


Figure A3.22 GRADISTAT printout with logarithmic frequency plot for grain-size sample 22

SAMPLE STATISTICS						
SAMPLE IDENTITY: 23			ANALYST & DATE: TCF, 4/16/2013			
SAMPLE TYPE: Polymodal, Very Poorly Sorted			TEXTURAL GROUP: Sandy Gravel			
SEDIMENT NAME: Sandy Very Fine Gravel						
	μm	ϕ	GRAIN SIZE DISTRIBUTION			
MODE 1:	1586.0	-0.664	GRAVEL: 46.0%		COARSE SAND: 10.2%	
MODE 2:	3400.0	-1.743	SAND: 53.3%		MEDIUM SAND: 4.4%	
MODE 3:	9600.0	-3.243	MUD: 0.7%		FINE SAND: 10.6%	
D ₁₀ :	222.0	-4.723			V FINE SAND: 0.8%	
MEDIAN or D ₅₀ :	1810.5	-0.856	V COARSE GRAVEL: 8.3%		V COARSE SILT: 0.2%	
D ₉₀ :	26404.8	2.172	COARSE GRAVEL: 5.9%		COARSE SILT: 0.1%	
(D ₉₀ / D ₁₀):	119.0	-0.460	MEDIUM GRAVEL: 9.2%		MEDIUM SILT: 0.1%	
(D ₉₀ - D ₁₀):	26182.9	6.894	FINE GRAVEL: 9.3%		FINE SILT: 0.1%	
(D ₇₅ / D ₂₅):	7.612	-0.028	V FINE GRAVEL: 13.3%		V FINE SILT: 0.1%	
(D ₇₅ - D ₂₅):	6250.5	2.928	V COARSE SAND: 27.3%		CLAY: 0.1%	
	METHOD OF MOMENTS			FOLK & WARD METHOD		
	Arithmetic	Geometric	Logarithmic	Geometric	Logarithmic	Description
	μm	μm	ϕ	μm	ϕ	
MEAN (\bar{x}):	8814.8	2309.4	-1.207	2128.6	-1.090	Very Fine Gravel
SORTING (σ):	16808.4	5.371	2.425	5.605	2.487	Very Poorly Sorted
SKEWNESS (Sk):	2.689	0.022	-0.022	0.173	-0.173	Coarse Skewed
KURTOSIS (K):	9.292	3.267	3.267	1.191	1.191	Leptokurtic

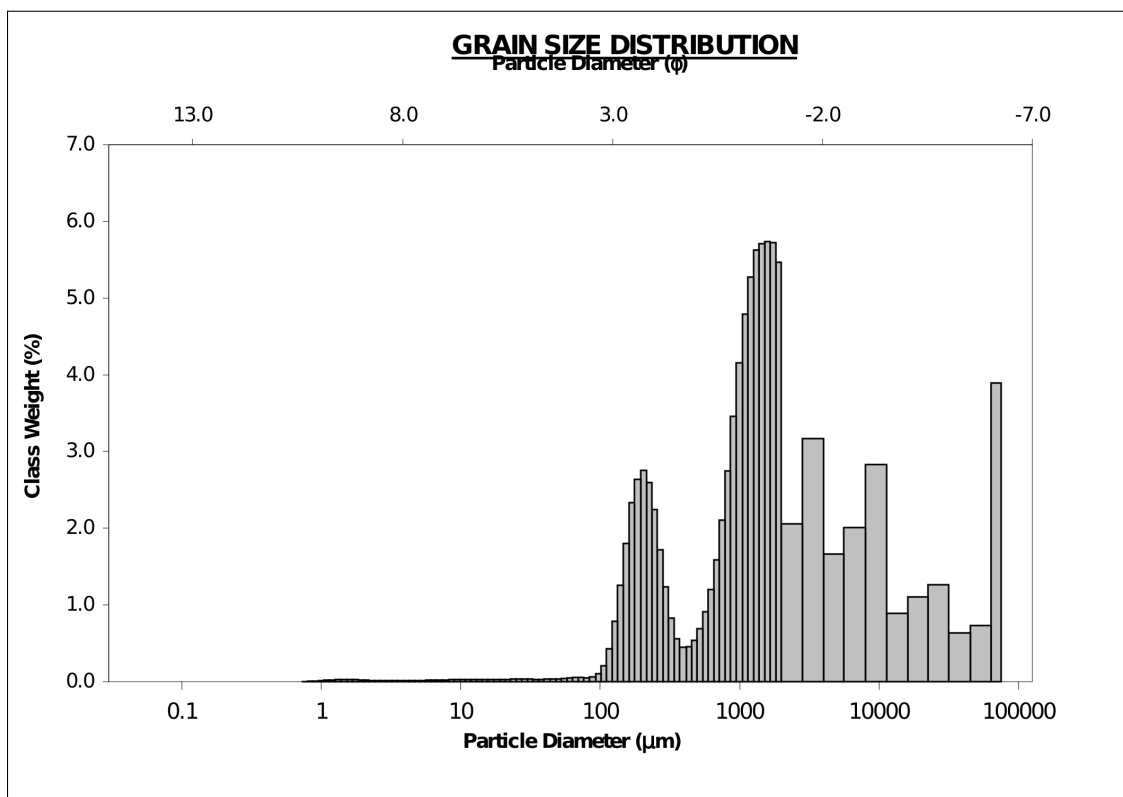


Figure A3.23 GRADISTAT printout with logarithmic frequency plot for grain-size sample 23.

APPENDIX 4: BETA Analytic Inc. Radiocarbon Dating Report



*Consistent Accuracy . . .
... Delivered On-time*

Beta Analytic Inc.
4985 SW 74 Court
Miami, Florida 33155 USA
Tel: 305 667 5167
Fax: 305 663 0964
Beta@radiocarbon.com
www.radiocarbon.com

Darden Hood
President

Ronald Hatfield
Christopher Patrick
Deputy Directors

March 7, 2013

Ms. Tanya C. Forde
Dalhousie University
Department of Earth Sciences
Life Sciences Center
1459 Oxford Street, Room 3006
Halifax, NS B3H 4R2
Canada

RE: Radiocarbon Dating Results For Samples L15A148WA, L01240SA, L10240WA, L20030PA,
L20324SA, L24041PA, L24175PA

Dear Ms. Forde:

Enclosed are the radiocarbon dating results for seven samples recently sent to us. They each provided plenty of carbon for accurate measurements and all the analyses proceeded normally. The report sheet contains the dating result, method used, material type, applied pretreatment and two-sigma calendar calibration result (where applicable) for each sample.

This report has been both mailed and sent electronically, along with a separate publication quality calendar calibration page. This is useful for incorporating directly into your reports. It is also digitally available in Windows metafile (.wmf) format upon request. Calibrations are calculated using the newest (2009) calibration database. References are quoted on the bottom of each calibration page. Multiple probability ranges may appear in some cases, due to short-term variations in the atmospheric ¹⁴C contents at certain time periods. Examining the calibration graphs will help you understand this phenomenon. Calibrations may not be included with all analyses. The upper limit is about 42,000 years, the lower limit is about 250 years and some material types are not suitable for calibration (e.g. water).

We analyzed these samples on a sole priority basis. No students or intern researchers who would necessarily be distracted with other obligations and priorities were used in the analyses. We analyzed them with the combined attention of our entire professional staff.

Information pages are enclosed with the mailed copy of this report. They should answer most of questions you may have. If they do not, or if you have specific questions about the analyses, please do not hesitate to contact us. Someone is always available to answer your questions.

Our invoice will be emailed separately. Please, forward it to the appropriate officer or send VISA charge authorization. Thank you. As always, if you have any questions or would like to discuss the results, don't hesitate to contact me.

Sincerely,



BETA ANALYTIC INC.

DR. M.A. TAMERS and MR. D.G. HOOD

4985 S.W. 74 COURT
MIAMI, FLORIDA, USA 33155
PH: 305-667-5167 FAX:305-663-0964
beta@radiocarbon.com

REPORT OF RADIOCARBON DATING ANALYSES

Ms. Tanya C. Forde

Report Date: 3/7/2013

Dalhousie University

Material Received: 2/20/2013

Sample Data	Measured Radiocarbon Age	13C/12C Ratio	Conventional Radiocarbon Age(*)
Beta - 343156 SAMPLE : L15A148WA ANALYSIS : AMS-Standard delivery MATERIAL/PRETREATMENT : (wood): acid/alkali/acid 2 SIGMA CALIBRATION : Cal AD 1300 to 1360 (Cal BP 640 to 590) AND Cal AD 1380 to 1420 (Cal BP 570 to 530)	580 +/- 30 BP	-25.9 o/oo	570 +/- 30 BP
Beta - 343157 SAMPLE : L01240SA ANALYSIS : AMS-Standard delivery MATERIAL/PRETREATMENT : (shell): acid etch	180 +/- 30 BP	+0.4 o/oo	600 +/- 30 BP
Beta - 343158 SAMPLE : L10240WA ANALYSIS : AMS-Standard delivery MATERIAL/PRETREATMENT : (wood): acid/alkali/acid 2 SIGMA CALIBRATION : Cal BC 40 to 10 (Cal BP 1990 to 1960) AND Cal BC 0 Cal AD 80 (Cal BP 1950 to 1860)	1990 +/- 30 BP	-26.6 o/oo	1960 +/- 30 BP
Beta - 343159 SAMPLE : L20030PA ANALYSIS : AMS-Standard delivery MATERIAL/PRETREATMENT : (plant material): acid/alkali/acid 2 SIGMA CALIBRATION : Cal AD 1690 to 1730 (Cal BP 260 to 220) AND Cal AD 1810 to 1840 (Cal BP 140 to 110) Cal AD 1840 to 1850 (Cal BP 110 to 100) AND Cal AD 1860 to 1860 (Cal BP 90 to 90) AND Cal AD 1870 to 1920 (Cal BP 80 to 30) AND Cal AD Post 1950	60 +/- 30 BP	-24.8 o/oo	60 +/- 30 BP

Dates are reported as RCYBP (radiocarbon years before present, "present" = AD 1950). By international convention, the modern reference standard was 95% the 14C activity of the National Institute of Standards and Technology (NIST) Oxalic Acid (SRM 4990C) and calculated using the Libby 14C half-life (5568 years). Quoted errors represent 1 relative standard deviation statistics (68% probability) counting errors based on the combined measurements of the sample, background, and modern reference standards. Measured 13C/12C ratios (delta 13C) were calculated relative to the PDB-1 standard.

The Conventional Radiocarbon Age represents the Measured Radiocarbon Age corrected for isotopic fractionation, calculated using the delta 13C. On rare occasion where the Conventional Radiocarbon Age was calculated using an assumed delta 13C, the ratio and the Conventional Radiocarbon Age will be followed by "ass". The Conventional Radiocarbon Age is not calendar calibrated. When available, the Calendar Calibrated result is calculated from the Conventional Radiocarbon Age and is listed as the "Two Sigma Calibrated Result" for each sample.



BETA ANALYTIC INC.

DR. M.A. TAMERS and MR. D.G. HOOD

4985 S.W. 74 COURT
MIAMI, FLORIDA, USA 33155
PH: 305-667-5167 FAX:305-663-0964
beta@radiocarbon.com

REPORT OF RADIOCARBON DATING ANALYSES

Ms. Tanya C. Forde

Report Date: 3/7/2013

Sample Data	Measured Radiocarbon Age	¹³ C/ ¹² C Ratio	Conventional Radiocarbon Age(*)
Beta - 343160 SAMPLE : L20324SA ANALYSIS : AMS-Standard delivery MATERIAL/PRETREATMENT : (shell): acid etch 2 SIGMA CALIBRATION : Cal BC 790 to 410 (Cal BP 2740 to 2360)	2450 +/- 30 BP	+1.0 o/oo	2880 +/- 30 BP
Beta - 343161 SAMPLE : L24041PA ANALYSIS : AMS-Standard delivery MATERIAL/PRETREATMENT : (charred material): acid/alkali/acid 2 SIGMA CALIBRATION : Cal AD 1530 to 1540 (Cal BP 420 to 410) AND Cal AD 1550 to 1550 (Cal BP 400 to 400) Cal AD 1630 to 1670 (Cal BP 320 to 280) AND Cal AD 1780 to 1800 (Cal BP 170 to 150) AND Cal AD 1940 to 1950 (Cal BP 0 to 0)	250 +/- 30 BP	-25.3 o/oo	250 +/- 30 BP
Beta - 343162 SAMPLE : L24175PA ANALYSIS : AMS-Standard delivery MATERIAL/PRETREATMENT : (plant material): acid/alkali/acid 2 SIGMA CALIBRATION : Cal BC 400 to 370 (Cal BP 2350 to 2320)	2270 +/- 30 BP	-22.4 o/oo	2310 +/- 30 BP

Dates are reported as RCYBP (radiocarbon years before present, "present" = AD 1950). By international convention, the modern reference standard was 95% the ¹⁴C activity of the National Institute of Standards and Technology (NIST) Oxalic Acid (SRM 4990C) and calculated using the Libby ¹⁴C half-life (5568 years). Quoted errors represent 1 relative standard deviation statistics (68% probability) counting errors based on the combined measurements of the sample, background, and modern reference standards. Measured ¹³C/¹²C ratios (delta ¹³C) were calculated relative to the PDB-1 standard.

The Conventional Radiocarbon Age represents the Measured Radiocarbon Age corrected for isotopic fractionation, calculated using the delta ¹³C. On rare occasion where the Conventional Radiocarbon Age was calculated using an assumed delta ¹³C, the ratio and the Conventional Radiocarbon Age will be followed by "****". The Conventional Radiocarbon Age is not calendar calibrated. When available, the Calendar Calibrated result is calculated from the Conventional Radiocarbon Age and is listed as the "Two Sigma Calibrated Result" for each sample.

CALIBRATION OF RADIOCARBON AGE TO CALENDAR YEARS

(Variables: C13/C12=-25.9:lab. mult=1)

Laboratory number: **Beta-343156**

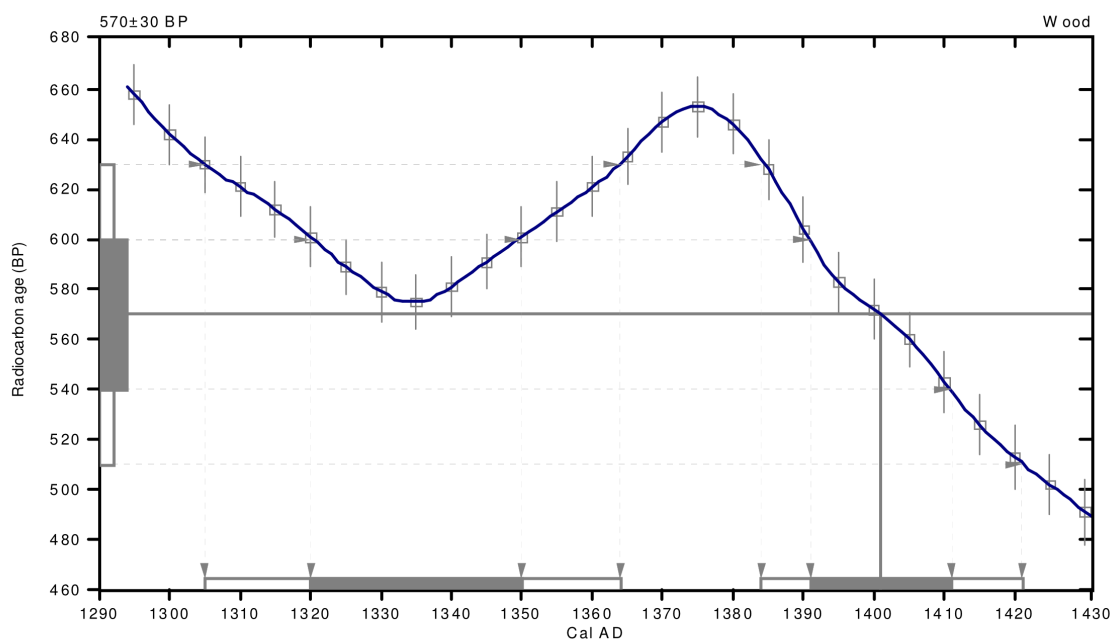
Conventional radiocarbon age: **570±30 BP**

2 Sigma calibrated results: Cal AD 1300 to 1360 (Cal BP 640 to 590) and
(95% probability) Cal AD 1380 to 1420 (Cal BP 570 to 530)

Intercept data

Intercept of radiocarbon age
with calibration curve: Cal AD 1400 (Cal BP 550)

1 Sigma calibrated results: Cal AD 1320 to 1350 (Cal BP 630 to 600) and
(68% probability) Cal AD 1390 to 1410 (Cal BP 560 to 540)



References:

Database used

INTCAL09

References to INTCAL09 database

Heaton, et al., 2009, *Radiocarbon* 51(4):1151-1164, Reimer, et al., 2009, *Radiocarbon* 51(4):1111-1150,

Stuiver, et al., 1993, *Radiocarbon* 35(1):1-244, Oeschger, et al., 1975, *Tellus* 27:168-192

Mathematics used for calibration scenario

A Simplified Approach to Calibrating C14 Dates

Talma, A. S., Vogel, J. C., 1993, *Radiocarbon* 35(2):317-322

Beta Analytic Radiocarbon Dating Laboratory

4985 S.W. 74th Court, Miami, Florida 33155 • Tel: (305)667-5167 • Fax: (305)663-0964 • E-Mail: beta@radiocarbon.com

CALIBRATION OF RADIOCARBON AGE TO CALENDAR YEARS

(Variables: C13/C12=0.4:Delta-R=30±60:Glob res=-200 to 500:lab. mult=1)

Laboratory number: **Beta-343157**

Conventional radiocarbon age: **600±30 BP**

(570±690 adjusted for local reservoir correction)

**2 Sigma calibrated result²: Cal AD 440 to post 1950 (Cal BP 1510 to post 1950)
(95% probability)**

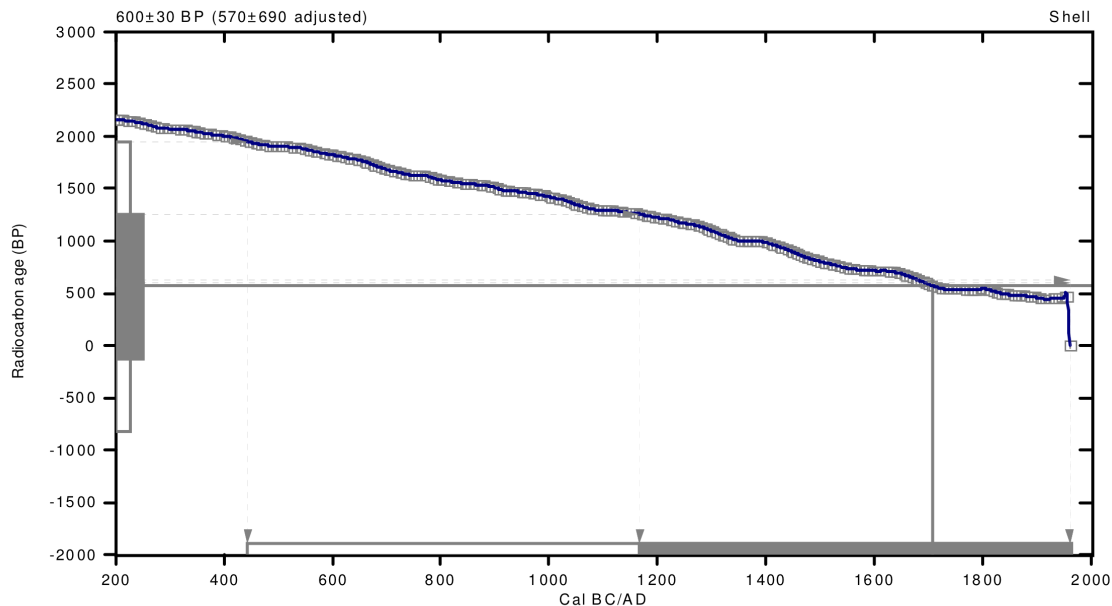
² 2 Sigma range being quoted is the maximum antiquity based on the minus 2 Sigma range

Intercept data

Intercept of radiocarbon age
with calibration curve: Cal AD 1710 (Cal BP 240)

**1 Sigma calibrated result³: Cal AD 1170 to post 1950 (Cal BP 780 to post 1950)
(68% probability)**

³ 1 Sigma range being quoted is the maximum antiquity based on the minus 1 Sigma range



References:

Database used

MARINE09

References to INTCAL09 database

Heaton, et al., 2009, Radiocarbon 51(4):1151-1164, Reimer, et al., 2009, Radiocarbon 51(4):1111-1150,

Stuiver, et al., 1993, Radiocarbon 35(1):1-244, Oeschger, et al., 1975, Tellus 27:168-192

Mathematics used for calibration scenario

A Simplified Approach to Calibrating C14 Dates

Talma, A. S., Vogel, J. C., 1993, Radiocarbon 35(2):317-322

Beta Analytic Radiocarbon Dating Laboratory

4985 S.W. 74th Court, Miami, Florida 33155 • Tel: (305)667-5167 • Fax: (305)663-0964 • E-Mail: beta@radiocarbon.com

CALIBRATION OF RADIOCARBON AGE TO CALENDAR YEARS

(Variables: C13/C12=-26.6;lab. mult=1)

Laboratory number: **Beta-343158**

Conventional radiocarbon age: **1960±30 BP**

2 Sigma calibrated results: **Cal BC 40 to 10 (Cal BP 1990 to 1960) and
(95% probability) Cal BC 0 Cal AD 80 (Cal BP 1950 to 1860)**

Intercept data

Intercepts of radiocarbon age

with calibration curve:

Cal AD 30 (Cal BP 1920) and

Cal AD 40 (Cal BP 1920) and

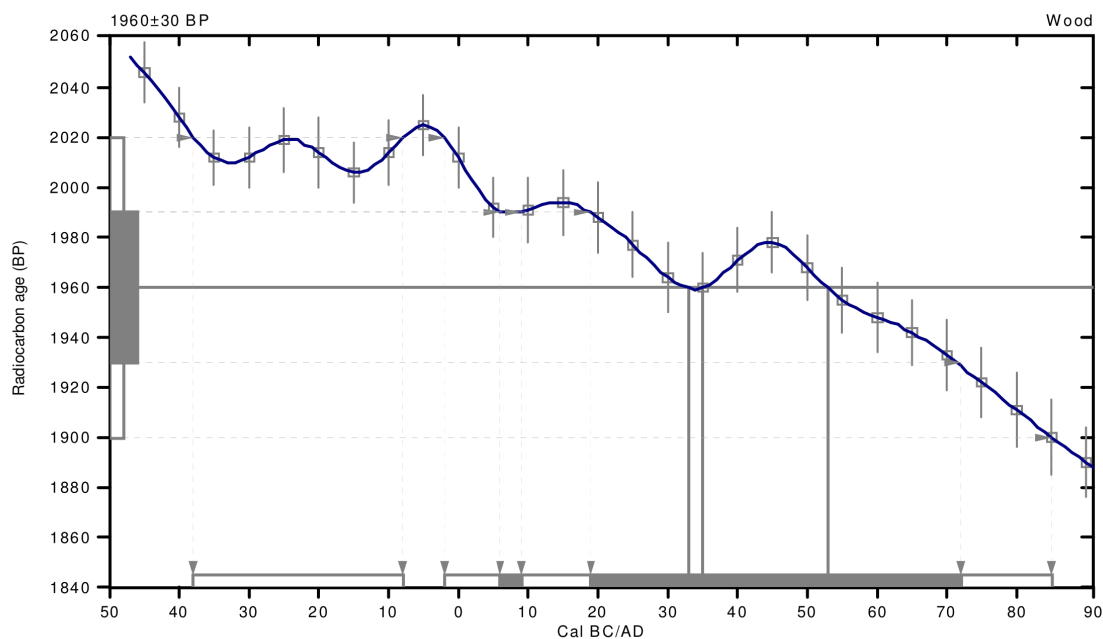
Cal AD 50 (Cal BP 1900)

1 Sigma calibrated results:

Cal AD 10 to 10 (Cal BP 1940 to 1940) and

(68% probability)

Cal AD 20 to 70 (Cal BP 1930 to 1880)



References:

Database used

INTCAL09

References to INTCAL09 database

Heaton, et al., 2009, *Radiocarbon* 51(4):1151-1164, Reimer, et al., 2009, *Radiocarbon* 51(4):1111-1150,

Stuiver, et al., 1993, *Radiocarbon* 35(1):137-189, Oeschger, et al., 1975, *Tellus* 27:168-192

Mathematics used for calibration scenario

A Simplified Approach to Calibrating C14 Dates

Talma, A. S., Vogel, J. C., 1993, *Radiocarbon* 35(2):317-322

Beta Analytic Radiocarbon Dating Laboratory

4985 S.W. 74th Court, Miami, Florida 33155 • Tel: (305)667-5167 • Fax: (305)663-0964 • E-Mail: beta@radiocarbon.com

CALIBRATION OF RADIOCARBON AGE TO CALENDAR YEARS

(Variables: C13/C12=-24.8;lab. mult=1)

Laboratory number: Beta-343159

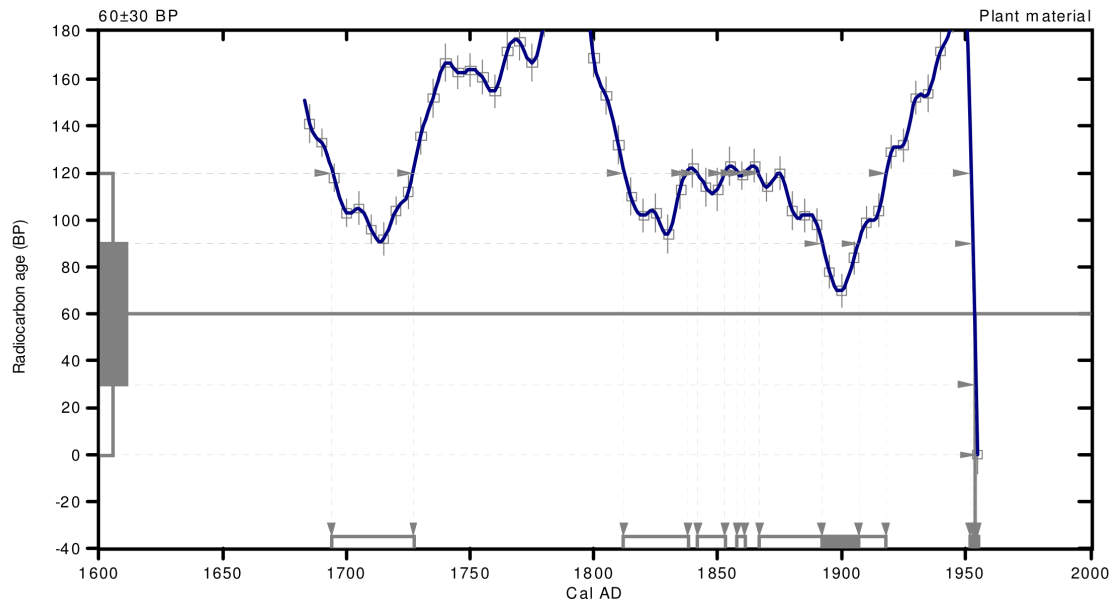
Conventional radiocarbon age: 60 ± 30 BP

2 Sigma calibrated results: Cal AD 1690 to 1730 (Cal BP 260 to 220) and
(95% probability) Cal AD 1810 to 1840 (Cal BP 140 to 110) and
Cal AD 1840 to 1850 (Cal BP 110 to 100) and
Cal AD 1860 to 1860 (Cal BP 90 to 90) and
Cal AD 1870 to 1920 (Cal BP 80 to 30) and
Cal AD Post 1950

Intercept data

Intercept of radiocarbon age
with calibration curve: Cal AD Post 1950

1 Sigma calibrated results: Cal AD 1890 to 1910 (Cal BP 60 to 40) and
(68% probability) Cal AD Post 1950



References:

Database used

INTCAL09

References to INTCAL09 database

Heaton, et al., 2009, *Radiocarbon* 51(4):1151-1164, Reimer, et al., 2009, *Radiocarbon* 51(4):1111-1150, Stuiver, et al., 1993, *Radiocarbon* 35(1):137-189, Oeschger, et al., 1975, *Tellus* 27:168-192

Mathematics used for calibration scenario

A Simplified Approach to Calibrating C14 Dates

Talma, A. S., Vogel, J. C., 1993, *Radiocarbon* 35(2):317-322

Beta Analytic Radiocarbon Dating Laboratory

4985 S.W. 74th Court, Miami, Florida 33155 • Tel: (305)667-5167 • Fax: (305)663-0964 • E-Mail: beta@radiocarbon.com

CALIBRATION OF RADIOCARBON AGE TO CALENDAR YEARS

(Variables: C13/C12=1:Delta-R=30±60:Glob res=-200 to 500:lab. mult=1)

Laboratory number: **Beta-343160**

Conventional radiocarbon age: **2880±30 BP**

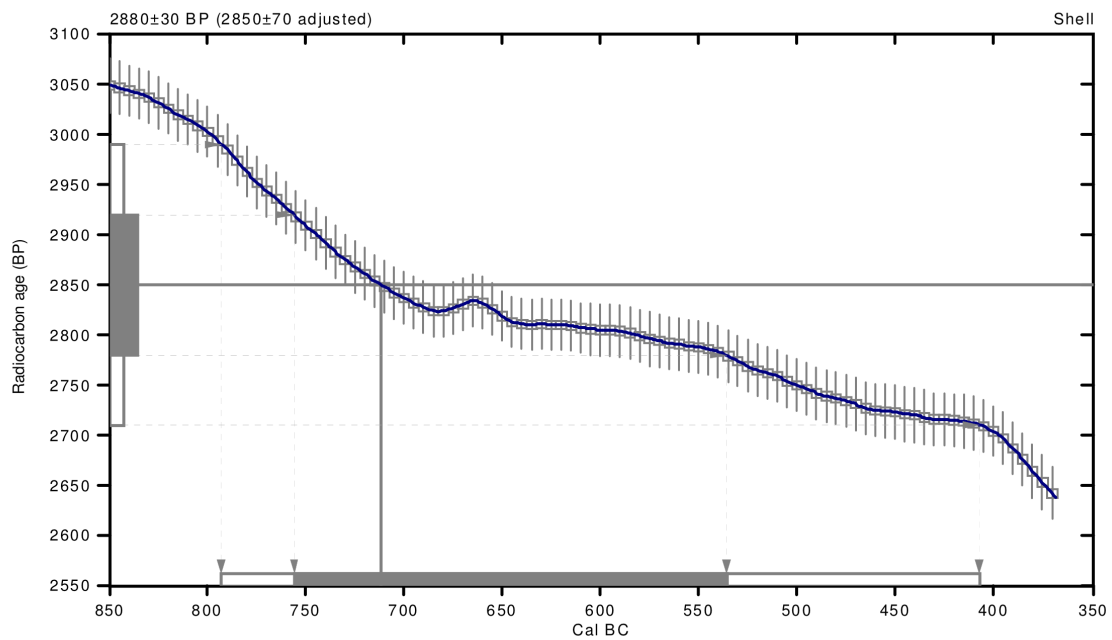
(2850±70 adjusted for local reservoir correction)

2 Sigma calibrated result: Cal BC 790 to 410 (Cal BP 2740 to 2360)
(95% probability)

Intercept data

Intercept of radiocarbon age
with calibration curve: Cal BC 710 (Cal BP 2660)

1 Sigma calibrated result: Cal BC 760 to 540 (Cal BP 2710 to 2490)
(68% probability)



References:

Database used

MARINE09

References to INTCAL09 database

Heaton, et al., 2009, Radiocarbon 51(4):1151-1164, Reimer, et al., 2009, Radiocarbon 51(4):1111-1150,

Stuiver, et al., 1993, Radiocarbon 35(1):137-189, Oeschger, et al., 1975, Tellus 27:168-192

Mathematics used for calibration scenario

A Simplified Approach to Calibrating C14 Dates

Talma, A. S., Vogel, J. C., 1993, Radiocarbon 35(2):317-322

Beta Analytic Radiocarbon Dating Laboratory

4985 S.W. 74th Court, Miami, Florida 33155 • Tel: (305)667-5167 • Fax: (305)663-0964 • E-Mail: beta@radiocarbon.com

CALIBRATION OF RADIOCARBON AGE TO CALENDAR YEARS

(Variables: C13/C12=-25.3:lab. mult=1)

Laboratory number: **Beta-343161**

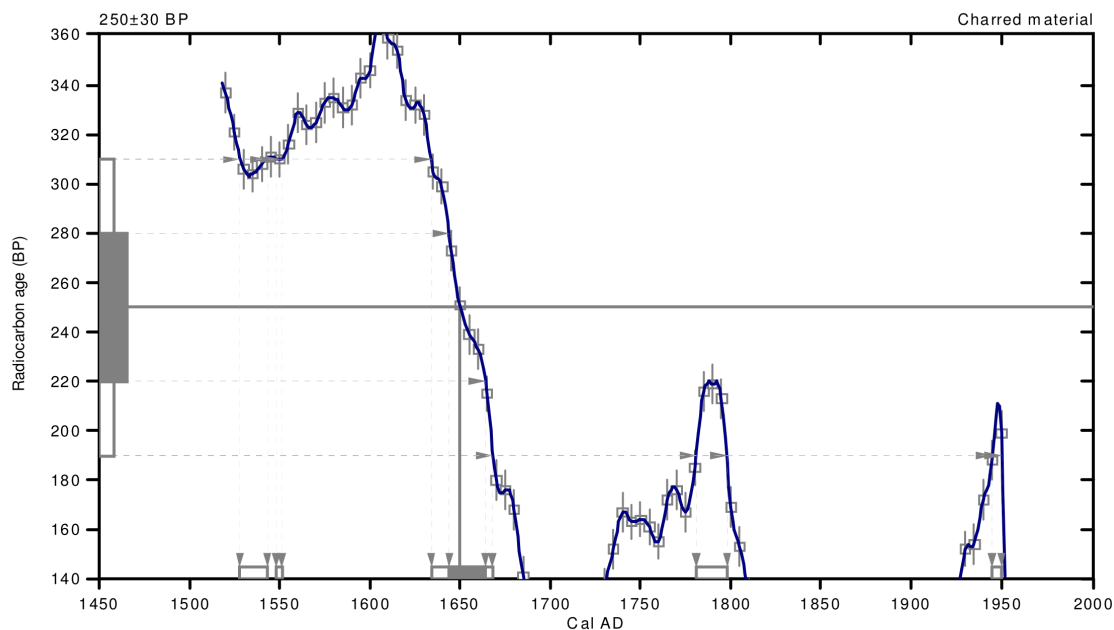
Conventional radiocarbon age: **250±30 BP**

**2 Sigma calibrated results: Cal AD 1530 to 1540 (Cal BP 420 to 410) and
(95% probability) Cal AD 1550 to 1550 (Cal BP 400 to 400) and
Cal AD 1630 to 1670 (Cal BP 320 to 280) and
Cal AD 1780 to 1800 (Cal BP 170 to 150) and
Cal AD 1940 to 1950 (Cal BP 0 to 0)**

Intercept data

Intercept of radiocarbon age
with calibration curve: Cal AD 1650 (Cal BP 300)

1 Sigma calibrated result: Cal AD 1640 to 1660 (Cal BP 310 to 290)
(68% probability)



References:

Database used

INTCAL09

References to INTCAL09 database

Heaton, et al., 2009, *Radiocarbon* 51(4):1151-1164, Reimer, et al., 2009, *Radiocarbon* 51(4):1111-1150, Stuiver, et al., 1993, *Radiocarbon* 35(1):137-189, Oeschger, et al., 1975, *Tellus* 27:168-192

Mathematics used for calibration scenario

A Simplified Approach to Calibrating C14 Dates

Talma, A. S., Vogel, J. C., 1993, *Radiocarbon* 35(2):317-322

Beta Analytic Radiocarbon Dating Laboratory

4985 S.W. 74th Court, Miami, Florida 33155 • Tel: (305)667-5167 • Fax: (305)663-0964 • E-Mail: beta@radiocarbon.com

CALIBRATION OF RADIOCARBON AGE TO CALENDAR YEARS

(Variables: C13/C12=-22.4;lab. mult=1)

Laboratory number: **Beta-343162**

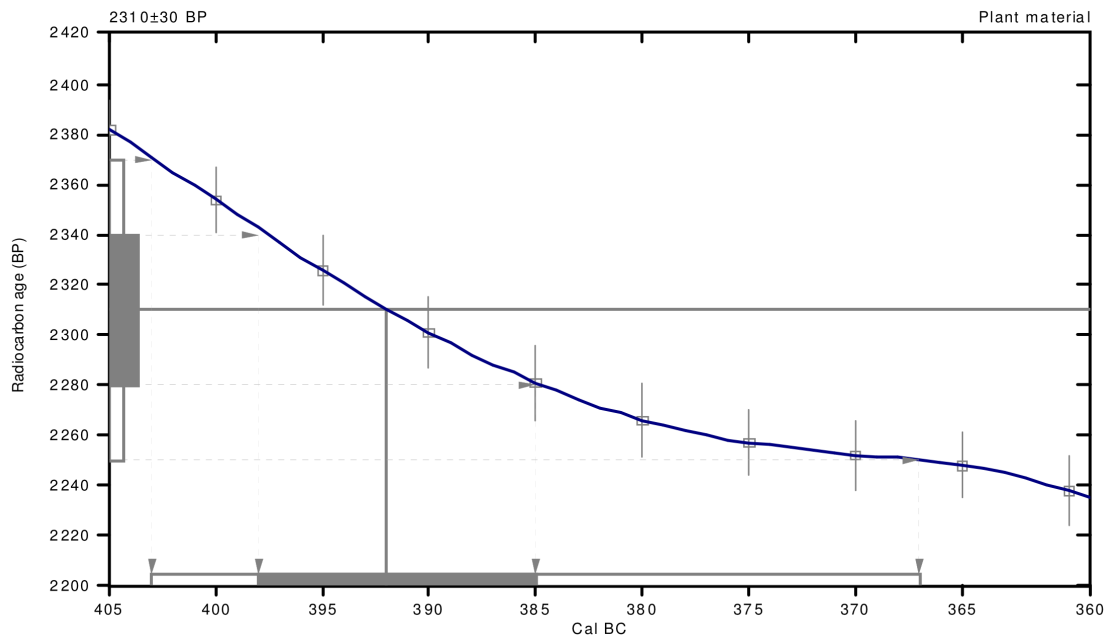
Conventional radiocarbon age: **2310±30 BP**

2 Sigma calibrated result: Cal BC 400 to 370 (Cal BP 2350 to 2320)
(95% probability)

Intercept data

Intercept of radiocarbon age
with calibration curve: Cal BC 390 (Cal BP 2340)

1 Sigma calibrated result: Cal BC 400 to 380 (Cal BP 2350 to 2340)
(68% probability)



References:

Database used

INTCAL09

References to INTCAL09 database

Heaton, et al., 2009, *Radiocarbon* 51(4):1151-1164, Reimer, et al., 2009, *Radiocarbon* 51(4):1111-1150,

Stuiver, et al., 1993, *Radiocarbon* 35(1):137-189, Oeschger, et al., 1975, *Tellus* 27:168-192

Mathematics used for calibration scenario

A Simplified Approach to Calibrating C14 Dates

Talma, A. S., Vogel, J. C., 1993, *Radiocarbon* 35(2):317-322

Beta Analytic Radiocarbon Dating Laboratory

4985 S.W. 74th Court, Miami, Florida 33155 • Tel: (305)667-5167 • Fax: (305)663-0964 • E-Mail: beta@radiocarbon.com